Universidad Autónoma de Madrid
Facultad de Ciencias Físicas
Departamento de Física Teórica

Disk Evolution at the Ages of Planet Formation

Dirigido por el **Dr. Lee W. Hartmann**

Memoria presentada por
Aurora Sicilia-Aguilar
para aspirar al título de
Doctor en Ciencias Físicas

Tutor:
Dr. Carlos Eiroa de San Francisco

Cambridge, Abril de 2005

A mis padres y abuelos.

Abstract

This thesis comprises the multiwavelength study of young stars and protoplanetary disks through the ages of 1-10 Myr, when disk dissipation and planet formation are supposed to occur. The epoch from 3 to 10 Myr is particularly interesting, since there is a lack of research on young stars in this age range, due to the fact that most clusters and associations aged 3-10 Myr are more distant, so obtaining good observations is more complicated. The new generation of instruments, including the multi-fiber spectrographs Hectospec and Hectochelle, operating on the 6.5m Multiple Mirror Telescope (MMT)[1] in Mount Hopkins, AZ, and the Spitzer Space Telescope, have opened a window to the study of more distant regions. Here I present one of the first studies of stars aged 3-10 Myr, one of the first results obtained with Hectospec and Hectochelle, and one of the first Spitzer results on disk evolution. This work is part of a program to follow the evolution of protoplanetary disks through the ages thought to be crucial to understanding disk dissipation and the formation of planetary systems (∼1-10 Myr).

First, I present the results of the optical and JHK observations of young stars in two young clusters in the Cep OB2 Association, Tr37 (embedded in the H II region IC 1396) and NGC 7160. Using low resolution optical spectra from the Hectospec multifiber spectrograph, a total of ∼165 and ∼50 low-mass members have been identified in Tr37 and in NGC 7160, respectively. Indicators of youth (Li absorption at 6707 Å) and accretion/chromospheric activity (Hα emission) are used to identify and to classify the low-mass cluster members. Spectral types for all the low-mass candidates are derived, together with the individual extinction and its average over the clusters. The estimated accretion disk fraction in the clusters is ∼40-45% for the low-mass stars in Tr 37, whereas only 1 star out of the NGC 7160 sample shows indications of active accretion. Optical photometry and theoretical isochrones are used to determine the age of the cluster members, confirming the estimates of 4 Myr for Tr 37 and 10 Myr for NGC 7160. Accretion rates in Tr 37 ($\sim 10^{-8} M_{\odot} yr^{-1}$ in average) are derived from U band photometry. Only ∼50% of the accreting stars have near-IR JHK excesses (from 2MASS), which could be due to the geometry and orientation of their disks or be an indication dust settling/grain growth.

The presence of protoplanetary disks in Cep OB2 is determined using the data from a Guaranteed Time Observing (GTO) program to study disk evolution with Spitzer. The data, from the IRAC and MIPS instruments on Spitzer, cover the wavelength range from 3.6 to 24 μm, and allows to study the characteristics and presence of disks at distances from ∼0.1-20 AU in accreting and non-accreting stars. The IR colors and spectral energy distributions of the low, intermediate, and high mass members of the clusters, which had been identified in our optical survey, are presented. The characteristics of disks and spectral energy distributions (SEDs) of the stars in NGC 7160 and Tr 37 are compared, as well as those obtained for younger

[1]Observations reported here were obtained at the MMT Observatory, a joint facility of the Smithsonian Institution and the University of Arizona.

regions (Taurus), finding significant evidence of disk evolution. The most striking differences between the 4 Myr old Tr 37 and younger regions (Taurus, the globule in Tr 37), appear as the color excesses for the shorter wavelengths (up to 5.8 μm) are significantly smaller. The comparison with models suggests that a noticeable amount of dust settling/grain growth and perhaps even disk clearing has occurred in the inner disk by the age of $\sim$4 Myr. Most of the IR emission from disks has disappeared by the age of $\sim$10 Myr, and the few remaining disks have suffered a more dramatic grain growth, settling and/or flattening affecting the emission at wavelengths from 3.6 to 24.0 μm. The data supports the picture that disk evolution starts in the inner part of the disks (fractions of AU) and proceeds to the outside with time. A small fraction of "transition objects", or non-accreting stars with disks evacuated in their innermost part (with excess emission only at wavelengths similar or longer than 5.8 μm), is also found in the cluster, suggesting a rapid evolution/dissipation of the disk once the inner part has been cleared or agglomerated into planets. The small fraction of these disks (a few percent of the total) suggests lifetimes of the order of several times 10^5yr, at most, so the outer disk does not seem to survive for a long time once the inner disk has been dissipated or coagulated into planets (see Figure 0.1).

The high- and intermediate-mass stars in the regions are also considered in the study. The membership of the B,A, and F-type stars in the regions is established through spectral types and extinction. The IRAC and MIPS data from Spitzer reveal a total of 7 disks around BAF stars in Tr 37, of which 4 of them are optically thin, debris disks, plus 3 more debris disks in NGC 7160. These are among the youngest debris disks known, and one of the few examples of debris disks with well-determined ages (by using the low-mass, pre-Main Sequence stars). The presence of these disks raises the question of whether they correspond to the remnants of optically thick, protoplanetary disks, or whether they are produced by reprocessed dust after the formation of planetesimals. In any of the two cases, considerable disk evolution and planet formation must have occurred by the early ages of 4-10 Myr.

Finally, well-known members of the younger Orion Nebula Cluster were observed with high-resolution optical spectra with the Hectochelle spectrograph operating on the MMT in order to determine accretion disk fraction, and to set the best procedures for the detection of accretion in cases where the use of near-IR excesses and/or low-resolution spectra may present problems.

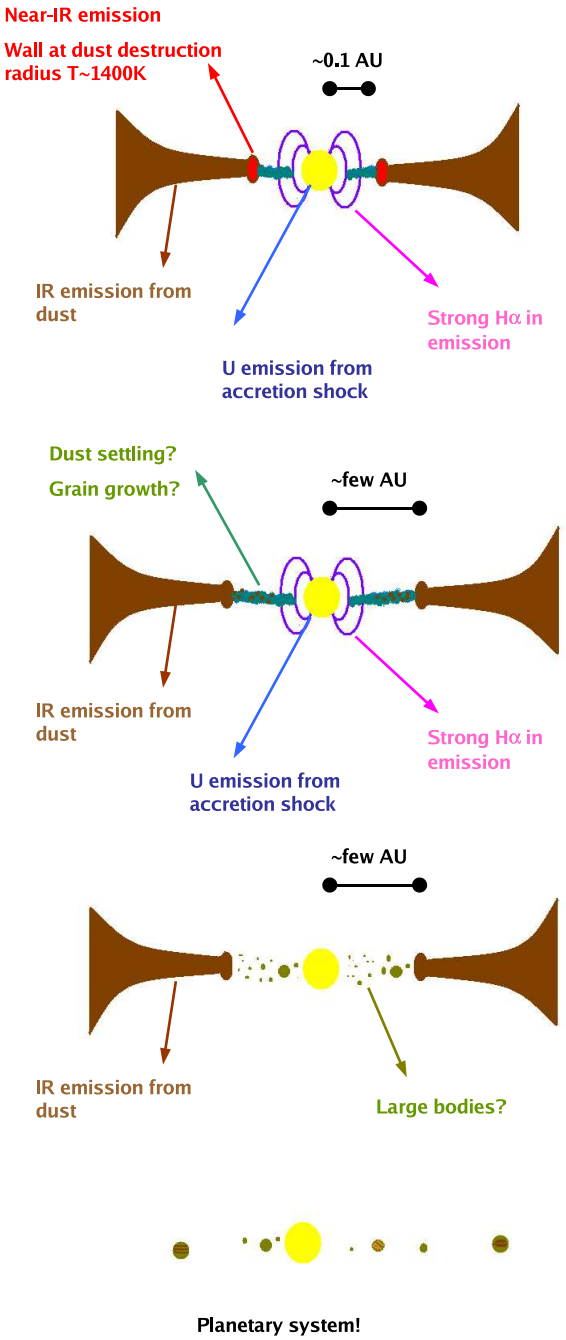

Figure 0.1 Scheme of the Evolution of Protoplanetary Disks in Cep OB2: Starting with a classical, accreting T Tauri star (upper figure), the inner disk can evolve, due to grain growth and dust settling, decreasing the emission at the shorter IR wavelengths (second figure). If the bodies in the inner disk reach large sizes, the flux of gas from the outer disk may stop, stopping accretion while the outer disk still remains, producing what we call here a "transition object" (third figure). The remaining outer disk could agglomerate and dissipate in about 10^5 years, producing a planetary system (fourth figure).

Resumen

Este trabajo comprende el estudio de poblaciones de estrellas jóvenes y de sus discos protoplanetarios, con edades entre 1 y 10 millones de años, pertenecientes a la etapa en la cual los discos circumestelares se disipan, probablemente tras formar sistemas planetarios. La época entre los 3 y los 10 millones de años presenta un interés particular, puesto que, debido a la ausencia de cúmulos y regiones cercanas en este rango de edades, existe una carencia sistemática de datos acerca de los procesos que tienen lugar en los discos durante la misma. Los instrumentos de nueva generación, que incluyen los espectrógrafos multifibra Hectospec y Hectochelle, operativos en el telescopio de 6.5m MMT (Multiple Mirror Telescope, Mount Hopkins, Arizona), y el Telescopio Espacial Spitzer, han abierto recientemente una nueva ventana para la investigación de estas regiones más distantes. Este estudio forma parte de un programa para trazar la evolución de los discos protoplanetarios durante las etapas cruciales (de 1 a 10 millones de años) para entender los procesos que llevan a la disipación de los discos y a la formación de sistemas planetarios.

En primer lugar, se presentan los resultados de las observaciones en longitudes de onda ópticas y JHK en dos cúmulos jóvenes en la Asociación de Cep OB2: Tr 37 (el cual está embebido en la región H II denominada IC 1396), y NGC 7160. Usando espectros ópticos de baja resolución tomados con el espectrógrafo Hectospec, se ha identificado un total de $\sim$165 y $\sim$50 estrellas de baja masa pertenecientes a Tr 37 y NGC 7160, respectivamente. Dicha identificación se basa en la presencia de rasgos de juventud (la línea de Li a 6707 Å) y de acrecimiento y/o actividad cromosférica (emisión en Hα). Esta última permite asimismo la distinción entre sistemas con y sin acrecimiento. Además, se obtienen tipos espectrales y extinciones para cada una de las estrellas, así como la extinción promedio en los cúmulos. La fracción de estrellas de baja masa con discos es de $\sim$40-45% en Tr 37, mientras que sólo una estrella en NGC 7160 presenta indicadores de acrecimiento activo. La fotometría en el óptico, junto con las correspondientes isocronas teóricas, permite la estimación de las edades de Tr 37 y NGC 7160, que son 4 y 10 millones de años, respectivamente. Para Tr 37, se obtienen tasas de acrecimiento basadas en los excesos de luminosidad en la banda U, obteniendo valores de $\sim 10^{-8} M_{\odot} yr^{-1}$ en promedio. Examinando la fotometría JHK (del estudio de 2MASS), se encuentra que sólo el 50% de las estrellas con acrecimiento activo presentan excesos en JHK, lo cual podría deberse a la geometría y orientación de los discos, o ser una indicación de evolución (tal como crecimiento de los granos, o asentamiento del polvo en el plano medio del disco) en la parte mas interna de los mismos.

La presencia de discos protoplanetarios en Cep OB2 se puede inferir a través de los datos del Spitzer, pertenecientes a un programa con Tiempo de Observación Garantizado (GTO) destinado al estudio de la evolución de los discos. Las observaciones del Spitzer, que cubren el rango de 3.6 a 24.0 μm usando los intrumentos IRAC y MIPS, permiten determinar la presencia y las características de los discos en el rango de distancias de $\sim$0.1 a 20 unidades astronómicas, en estrellas con acrecimiento y sin él. Los colores en IR y las distribuciones

espectrales de energía (SEDs) de las estrellas poco masivas (clasificación que incluye las estrellas de tipo solar y las de masa inferior al Sol), cuya pertenencia a los cúmulos se establece mediante el estudio en óptico, se presentan y describen, comparándolos con los de las regiones más jóvenes. La principal diferencia entre Tr 37 y Tauro radica en que los excesos de color para las longitudes de onda inferiores o iguales a 5.8 μm son substancialmente menores en Tr 37. De acuerdo con los modelos de discos, este efecto sugiere que la parte más interna del disco ha sufrido una importante aglomeración del polvo, y/o un destacado asentamiento del mismo en el plano medio (aplanando la región del disco responsable de esta emisión), e incluso parte del disco puede haberse eliminado, al cabo de 4 millones de años. Al cabo de 10 millones de años (NGC 7160), cuando la mayoría de los excesos IR de los discos ha desaparecido, el efecto de la coagulación y asentamiento del polvo es aún más evidente en los discos que quedan, viéndose afectada la emisión entre 3.6 y 24.0 μm. Estas observaciones sugieren, entonces, que la evolución (coagulación, asentamiento, y/o aplanamiento) en el disco comienza en la parte interna del mismo, propagándose hacia el exterior. También se ha encontrado una pequeña fracción de "objetos de transición", consistentes en estrellas que no están acretando, y, aunque la parte interna de sus discos se ha evacuado o ha evolucionado, ya que no se detecta exceso de emisión (quizá dando lugar a planetesimales o planetas), aún conservan la parte más externa del disco (detectable como un exceso a longitudes de onda de 5.8 μm o más largas). La escasez de estos objetos sugiere que sus tiempos de vida son del orden de cientos de miles de años como mucho, luego el disco externo no tardaría en disiparse una vez que el disco interno ha desaparecido o se ha aglomerado (Figura 0.2).

También se consideran las estrellas de alta masa y de masa intermedia (tipos espectrales B,A,F, o masas entre 2 y 7 $M_{\odot}$), cuya pertenencia a los cúmulos se establece a través de sus tipos espectrales y extinciones. Los datos de IRAC y MIPS en Spitzer revelan un total de 7 discos en Tr 37, y otros 3 en NGC 7160. De los discos en Tr 37, 4 son ópticamente delgados y presentan exceso de emisión sólo a 24 μm, al igual que los 3 discos en NGC 7160. Esto los convierte en unos de los discos residuales o de escombros (*debris disks*) más jóvenes que se conocen, así como uno de los casos en los que las edades de los discos están claramente determinadas (a través de las estrellas de baja masa pre-secuencia principal). La juventud de estos objetos plantea la pregunta de si estos discos son los remanentes de discos protoplanetarios ópticamente gruesos, que han evolucionado, o si se han producido debido a la colisión de planetesimales recién formados. En cualquier caso, la presencia de estos discos apoya la idea de que, a las edades de 4-10 millones de años, la evolucion de los discos y probablemente, la formación de planetas y/o planetesimales, está muy avanzada.

Por último, se estudian miembros bien conocidos en el Cúmulo de la Nebulosa de Orión (ONC), utilizando espectros ópticos de alta resolución, tomados con el espectrógrafo multi-fibra Hectochelle en el telescopio MMT. Los espectros de la región de Hα se emplean para determinar la fracción de discos que están acretando, comparándose la efectividad de este procedimiento con los resultados obtenidos a través de los excesos en IR y los espectros ópticos de baja resolución.

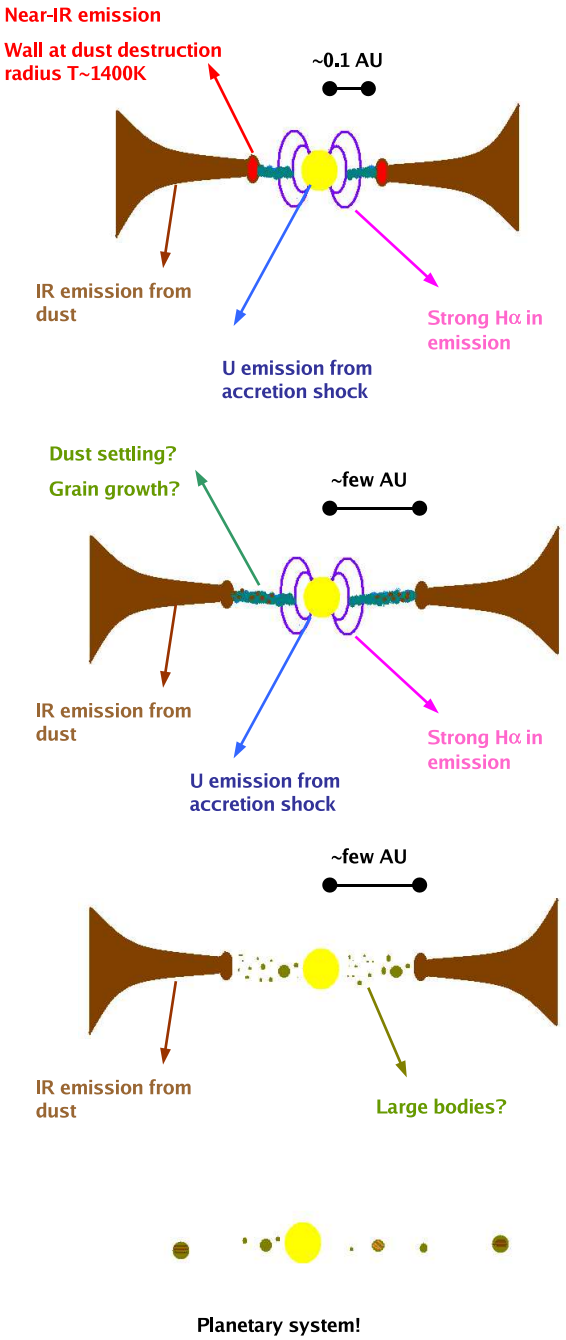

Figure 0.2 Esquema de la evolución de los discos protoplanetarios en Cep OB2: Comenzando con una estrella T Tauri clásica, acretando (figura superior), la evolución del disco interno, debido al asentamiento del polvo y al crecimiento de los granos, daría lugar a una disminución de la emisión en IR (segunda figura). Si los granulos se aglomeran en cuerpos de grandes dimensiones, el flujo de gas del disco externo al disco interno puede detenerse, así como el acrecimiento, aunque el disco externo aún sobreviviría durante un tiempo, dando lugar a un "objeto de transición" (tercera figura). El resto del disco externo se aglomeraría y disiparía en unos 10^5 años, produciendo un sistema planetario (cuarta figura).

Agradecimientos

Cuando finalmente me acerco a este primer "final de etapa", que parecía que nunca iba a llegar, me gustaría dar las gracias a todas las personas que han formado parte de esta gran experiencia en mi vida que ha sido venir a los EE.UU. para hacer la tesis, y que la han hecho posible.

Gracias a mi familia, por su apoyo y su ayuda en todo momento y, en especial, a mis hermanas Isa y Conchi, por no dudar ni en ir a la Autónoma a resolverme los papeleos, ni en venir aquí a echarme una mano, ni en pelear horas y horas con la impresora para conseguir que esta tesis pudiera imprimirse. Gracias a mi madre por todo su apoyo, su ayuda, su venida aquí y sus idas a la Autónoma. Gracias a mi padre por su ayuda en la búsqueda de información y de becas. Gracias también a mi hermano, por los secretos de la música irlandesa, y por sus dibujos y mensajes en élfico. Gracias a mi abuelo por sus cartas cada mes, y a mis tíos Gema, Mercedes, Lola, Mari, Pepe, Paco, Antonio, Juan y Kety por acordarse de mí.

Gracias a Carlos por la idea de mandarme al otro lado del océano para que aprendiera lo más posible, y por ayudarme a solucionar todos los asuntos burocráticos que me surgieron en la Autónoma. Y, por supuesto, gracias a Lee, sin cuyas ideas, enseñanzas y ayuda, nada de lo que hay en esta tesis hubiera sido posible. Y muchísimas gracias a todas las personas que me han ayudado y apoyado en el CfA: a Nuria, por preocuparse de los asuntos científicos y humanos, a Martina, Maru, Mayra, Alicia, María, Pedro y familia, y Nimesh, por ser mucho más que simples compañeros de trabajo y de edificio, y a Lori y Tom porque, sin su ayuda, aún seguiría luchando con la reducción de los datos del Spitzer (y con los dichosos errores). Muchas gracias a Manami, Paula, Esther, Sridharan, David, Hans Jakob, Marijke, Bruno, Robert, Ramiro, Guillem, Yang, Estel, José Luis, Mari Paz, Charlie, Chris, Sunil, y todos los que alguna vez estuvieron y/o pasaron por el CfA. En especial, muchas gracias a Bruno y Benja por el tiempo que pasaron en el CfA y en Boston y lo que me han ayudado después. Muchas gracias a César por toda la ayuda y los ánimos en los momentos de observación y de desesperación, y a Jesús por tener siempre en mente comentarios graciosos. Gracias a Kathy por su ayuda con la variabilidad. Muchas gracias a Alicia por la ayuda con Mopex, los ositos de goma, y las discusiones gramático-semánticas. Muchas gracias a Subu por las discusiones pre-Journal Club y por su ayuda en la búsqueda de postdocs. Gracias a Nimesh, Phil y Scott por la ayuda del "Predoc Committee". Muchas gracias a Paola por las discusiones y las charlas. Y muchas gracias a Muriel y a Tom, por toda su ayuda deslindando los problemas burocráticos que me surgieron durante mi estancia en el CfA. Gracias a Muriel también por los caramelos en el correo y las felicitaciones de cumpleaños, y por venir a defenderme de los médicos inútiles.

Muchas gracias también a todas las personas que conocí en mis viajes a Arizona y en las observaciones. Gracias a James, a Amaya , a Serena y a Mike, a los que siempre me encontré por allí. Gracias en especial a James, por su ayuda en el trabajo y en las observaciones. Muchas gracias a Perry a Emilio, y a Mike por su ayuda con el 1.2m y la expulsión de las

tarántulas, ratones, escorpiones y sapos que se aparecían por la noche en el pasillo. Muchas gracias a Nelson, a Dan, a Andy y a Gabor en el MMT, así como al resto de personal de los telescopios y a la gente de distintos lugares con quien tuve la suerte de encontrarme en Mount Hopkins y en Kitt Peak. Muchas gracias también por todo el tiempo que pasé por allí, por el paisaje impresionante, las tormentas sobre el desierto, los osos, las serpientes y los colibríes.

Muchas gracias también a mis amigos "de siempre", por no olvidarse de mi a pesar de que las comunciaciones no fueran siempre muy constantes. Muchas gracias a Alicia, que me conoce desde que jugábamos a las gomas, y a Elena, quien dice que yo soy responsable de haberla metido donde ella está... Muchas gracias a Mari-Ángeles, que se atrevió incluso a venir a verme a estos lugares, y a Esther y Fernando, que se pasarán justo a tiempo antes de que yo me vaya. Muchas gracias también a Parra, Conchi, Óscar, Maya, Silvia, Gema, Mayte y los demás por los e-mails multitudinarios y los cafés y las horchatas en mis visitas esporádicas por Tres Cantos. Gracias a Nina, Maribel, Vicky y Álex por no perder el contacto. Muchísimas gracias a todos por las felicitaciones y las llamadas de cumpleaños, y por los ánimos en todo momento.

Muchas gracias a mis compañeros de Universidad, con los cuales compartí experiencias en la carrera y en el doctorado e historias ocurridas en algún lugar del extranjero. Gracias a Miguel Ángel, Sara, Marta, María, Juan Pedro, Álex, y todos los demás. Muchas gracias también por la ayuda con los trámites burocráticos. Gracias a Bruno, Alcione e Itziar por su ayuda con las burocracias de la tesis y tesina.

Y, cómo no, muchas gracias a todos los amigos que me han acompañado durante mi estancia en Boston. Sin ellos creo que me hubiera muerto de desesperación en los primeros meses, y hubiera dejado de aprender todas las cosas de la vida que me han enseñado durante todos estos años.

Muchas gracias a Martina y a Hugh por llevarme a conocer todos los rincones de Boston, por incluirme en sus veladas internacionales, por enseñarme los lugares donde se puede comprar desde miel de azahar a allozas, por llevarme en sus excursiones, y enseñarme el Jordan Hall, las White Mountains y Walden Pond.

Muchas gracias a Maru, por recogerme en cuanto llegué, y por acompañarme en mis primeros meses bostonianos. Muchas gracias a Maite, por revelarme los secretos de la vida de los predocs. Muchas gracias a Mayra, por no dejarse asustar por mí y por acompañarme a tomar tantos chocolates calientes y al hospital, y por ayudarme a transportar las cajas de fruta que comprabamos en el Haymarket.

Muchísimas gracias a An, con quien he compartido casi todo el tiempo de mi estancia en Boston, mientras mirábamos juntas cómo el resto de los amigos iba y venía. Muchas gracias por las excursiones a Chinatown, por las cabalgadas en bici, las patinadas y patinazos, las zambullidas en el gélido Atlántico, por ayudarme con el ordenador portátil, por enseñarme a bailar el cha-cha-cha, y a preparar los rollos de primavera vietnamitas, el sorbete de aguacate, y el pastel de yuca.

Muchas gracias a mis compañeros de casa. Gracias a Ásdís y a Kæja, por demostrarme que el invierno de aquí se sobrevive tan bien como el de Reykjavík. Muchas gracias por recibirme las dos veces que he ido a vuestra tierra, y por no perder el contacto. Gracias también a Brynhildur, Hrafnkell, Erla e Idunn por incluirme en vuestras celebraciones de familia. Gracias a Kæja, Erla e Idunn por jugar conmigo a los niños-leones de la selva y tratar de enseñarme a cantar canciones de Disney en islandés.

Muchas gracias a mis compas del 4 Beacon Street, durante los años que viví allí. Gracias a Ans, por los paseos al atardecer y las largas charlas y el apoyo que siempre me prestaste.

Gracias a Johannes y a Sebastian, por hacer de esta etapa una de las mejores de mi vida, por las historias del "horrible hombre del baño", por las fiestas de galletas hasta las 4 de la madrugada, los cumpleaños, Halloween, carnaval y todo lo que celebramos juntos, y por los huevos de pascua que aún sigo encontrando entre mis calcetines. Gracias a Diego por su cariño, a Markus, a Dèlia, y a todos los que pasaron por esta casa y a los que seguí viendo una vez que ya no vivían allí. Y gracias a Bernd, que empezó siendo uno más del clan del 4 Beacon Street. Muchas gracias a Manami, por estar siempre (siempre) ahí, dentro y fuera del CfA, por ser casi una más en el 4 de Beacon Street, por las cenas internacionales y por tantas otras cosas.

Muchas gracias a todo el resto de amigos con los que me crucé en estos años, a Christian H. por su música y por estar siempre preocupándose de la gente. Muchas gracias a Heike por su compañía y por toda su ayuda, y por ser la inventora de la "Cabin Fever" del fin de semana de Acción de Gracias. Muchísimas gracias a Karen por estar siempre amable y sonriente. Gracias a Sophie, a Marjorie, a Alexis, a Cédric, a Anna, a Anya. Gracias a Wolfgang, a Myrto, a Conny, a Carsten y a Walter por las excursiones a la playa y las carreras a nado hasta la boya. Gracias a Georg, el "salsameister", a An, Wolfgang, Yuchi, Johannes, Karen y tantos otros con los que nos entró la fiebre del baile y acabamos como asiduos clientes de "Sophia's" y del "Ryles". Muchas gracias a María, por las largas conversaciones y cotilleos, la información sobre lo que ocurría en España, las compras y las cenas multitudinarias. Gracias a Yuchi por la subida a Mount Laffayete, a Eugènia por hacer que me subiera por las paredes (eso sí, con cuerdas y arneses), y a Karen, Catia, Ans, Frauke, Markus, Johannes y Bernd por hacer que bajara por las pistas azules (de momento).

Muchas gracias a todos los que participaron en la "Cabin Fever" de cada año: a Heike, Ursula, Ans, Wolfgang, Peter, Tanya, Johannes, Sebastian, Bernd, Alicia, An, Manami, Megumi, Christian S., Karen, Stephanie, Yuchi, Dèlia, Steve, Christine, Thomas, David, Conny. Gracias por las subidas a pie, las bajadas en trineo, la danza del amanecer, los conciertos para sartén, botella y orquesta, el "bubble-soccer", y las veladas con 17 personas de 12 nacionalidades distintas.

Gracias a Kierann, Doris, Wendy y Alex por enseñarme la vuelta con pincho, el salto de vals, las espirales y cómo ponerlo todo junto en una coreografía sobre hielo. Gracias a Sara, Helen, Rebecca y Francesca por estar allí siempre, practicando.

Gracias a Irmgard y a Cornelia por enseñarme lo que sé de alemán, que me va a venir tan bien en el futuro próximo. Y gracias a toda la gente con la que coincidí en el Goethe Institut.

Muchas gracias a todos los que no me dejaron abandonar la música. Gracias a Na'ama y a Todd por los programas en la Mather House. Gracias a Christian H. y a Edwin por la genial idea de mandar un e-mail recolectando músicos. Gracias a Sophie, Johannes y Cody, a quienes conocí a través de la música. Gracias a Ursula, Jenni, Kobey, Mike, Larry, Sheera, Bernd, Markus, Helen, Nathalie, Beth, Diego, Aron y a todos los que me han acompañado en el sentido musical de la palabra. Gracias a Wolfgang, Jan, Dinah y Oliver por las noches de "Follia" y cena internacional y las búsquedas de instrumentos y partituras. Gracias a Annette por atreverse a organizar un coro, y a Kimball por inventar la combinación de música, acampada y excursiones. Gracias a los músicos callejeros de Harvard Square, y a Isa y Bernd por atreverse a tocar conmigo en la calle. Y gracias a Bach, Corelli, Ortiz, Marais, Landini, Marcello, van Eyck, Sor, Vivaldi, Telemann, Belinzani, Narváez y tantos otros por componer una música tan maravillosa.

Gracias a los Dres. Rubenstein y Sullivan por "recomponerme" las partes del cuerpo que no funcionaban del todo bien, y a Heike por ayudarme a encontrarlos.

Y muchas gracias a Bernd por su música, y por tantísimas otras cosas. Muchas gracias por haberme dado todo el apoyo del mundo, por estar conmigo para cuidarme tanto si tenía la gripe como si estaba muy agobiada, por levantarme los ánimos sólo con estar ahí, por inventar conmigo un lenguaje nuevo, por ser capaz de leerse mi tesis y mis "proto-papers" para ver si se entendían, por arreglarme el ordenador cada vez que se encabritaba, y por conseguir que las figuras de esta tesis aparecieran donde se suponía que debían estar. Sin él, muchas de todas estas cosas no hubieran sido posibles, y con él, todo lo que ya era posible no pudo sino ser mejor.

Contents

1 Introduction and Motivation

1.1 Protoplanetary Disks at the Ages of Planet Formation

The evolution of accretion disks through the ages of planet formation is still an open question. Accretion disks form as a consequence of the collapse of giant molecular cloud cores, involving a contraction of the initial cloud over six orders of magnitude. In order to preserve angular momentum, the infalling material is deposited in a larger structure, a disk, rather than directly falling onto the protostar (Lynden-Bell & Pringle, 1974; Shu et al., 1987). This disk evolves with time as it drives the angular momentum, and finally disappears, probably forming planets, through some mechanisms that are not fully understood yet. Two possibilities to stop accretion onto the central star and to form planets are: grain coagulation, evolving from dust particles to protoplanets and planets (Weidenschilling, 1977; Weidenschilling & Cuzzi, 1993); and formation of protoplanetary clumps via gravitational instability (Goldreich & Ward, 1973). One of the main problems with grain coagulation is that it seems to require rather long timescales: ∼1-16 Myr for Jupiter-Saturn like planets (Pollack et al., 1996), or even ∼10-50 Myr for giant planets and maybe longer for terrestrial planets (Boss, 2003). On the other hand, the timescales for gravitational instability require very massive disks and involve extremely short timescales comparable to a certain number of orbital periods (about thousand of years, $<<$1 Myr) that would not account for the long lives of most disks. None of the theories can fully explain the process of planet formation yet. There is a strong dependence of several parameters, mainly, the disk surface density and the initial conditions (angular momentum, mass), but such other factors as the influence of the environment (close encounters, photoevaporation) may also play an important role. Moreover, planet formation is likely to proceed on different timescales in different systems; existing observations indicate considerable disk dissipation even at ages of 1-2 Myr (Hillenbrand, 1997; Hillenbrand et al., 1998; Lada et al., 2000; Muzerolle et al., 2000). But, due to the lack of observations, what happens in between the ages of 3-10 Myr is still unclear. This points out the importance of studying the evolution of protoplanetary disks at intermediate stages.

So far, observations indicate that accretion disks are common at the ages of 1 Myr (Strom et al., 1993; Hillenbrand, 1997; Hillenbrand et al., 1998; Lada et al., 2000; Muzerolle et al., 2000; Briceño et al., 2001), but the accretion processes become very rare in objects over 10 Myr of age (Muzerolle et al., 2000; Calvet et al., 2002), and no optically thick disks have been identified around solar-type stars older than 30 Myr (Strom et al., 1993). Together with the fact that the study of meteorites in our Solar System suggests a timescale for the accretion phase of ∼10 Myr (Podosek & Cassen, 1994), the data available strongly point out that most disks disappear between the ages of 3-10 Myr, perhaps due to the formation of planets. The long survival time of some protoplanetary disks suggests different disk/angular momentum properties (Bouvier et al., 1997; Hueso & Guillot, 2005, in preparation). Hence, taking into account the probable dependence of disk evolution with mass (Hartmann et al., 1998), the

study of disk characteristics and disk removal requires statistically significant samples of stars in different mass ranges (Hartmann et al., 1998).

This leads to search for young open clusters in the appropriate age range. The study of clusters minimizes the errors due to distance, and provides reasonably large samples of stars that share metallicity, distance, and age. The main drawback of this approach is that there are no nearby clusters aged 3-10 Myr, so that a strong method and powerful instruments are required in order to identify members and to study their properties. Instruments such as the Hectospec multifiber spectrograph, and the Spitzer Space Telescope, need to be used in order to identify the low mass members of more distant clusters with published ages (from high mass members and kinematical signatures) in the range were disk dissipation is expected to occur. Once a large sample of young stars has been identified, the objective is to determine the characteristics of the stars (ages, spectral types, accretion) and the presence of disks (accreting or non-accreting). Finally, the comparison of large samples of stars with different ages reveals the different stages of disk evolution.

1.2 The Cep OB2 Association

The clusters Tr 37 and NGC 7160, both of them in the Cep OB2 Association (Platais et al., 1998), are two promising candidates to look for evolved disks and transition objects as indications of active planet formation. The Cep OB2 association contains stars spanning the ages of ∼1 to ∼10-15 Myr (Garrison & Kormendy, 1976; Simonson & van Someren Greve, 1976; Marschall & van Altena, 1987), and IRAS sky maps have revealed several point sources consistent with young stellar objects (Schwartz et al., 1991).

The older cluster, NGC 7160, lies near the center of a bubble of atomic and molecular gas, which has been mapped in H I (Simonson & van Someren Greve, 1976; Patel et al., 1994, 1998) and CO emission (Patel et al., 1998). These observations reveal a large bubble-shaped structure of approximate diameter of 3 degrees. The presence of several B stars in NGC 7160 (Daflon et al., 1999) makes plausible the hypothesis of a stellar wind-driven bubble, in which a supernova took place a few Myr ago, triggering star formation processes at the edge of the bubble (Balázs & Kun, 1989; Duvert et al., 1990; Patel et al., 1995, 1998; Codella et al., 2001). Tr 37 is placed at the edge of this bubble (See Figure 1.1) and could be bubble-shaped itself, containing the bright O6 star HD 206267 (Garrison & Kormendy, 1976; Ábrahám et al., 2000). It also shows an inhomogeneous H II region (IC1396) with numerous globules and gas illuminated rims (Patel et al., 1998; Clayton & Fitzpatrick, 1987), powered by HD 206267.

Kinetic and stellar ages (Patel et al., 1998) have been derived for the massive stars in the association and the expanding gas in the H II region. The stellar winds of the massive stars and maybe a supernova have produced an expanding molecular ring around NGC 7160, with an expansion age ∼7-10 Myr (Patel et al., 1995, 1998), which gives an age estimate of ∼10 Myr for NGC 7160 and ∼3 Myr for Tr 37, corroborated by the presence of several B stars in NGC 7160 and O and B stars in Tr 37. The study of the upper Main Sequence stars in Tr 37 provides a distance of around 900 pc and, extrapolating from the high mass population, a populous cluster with numerous (hundreds) low mass members is expected (Contreras et al., 2002).

Therefore, Tr 37 and NGC 7160 constitute a pair of clusters with age estimates in the range when disk dissipation is expected to occur, and they are located at a well determined distance, which makes the Cep OB2 Association an ideal place for this study. Because of

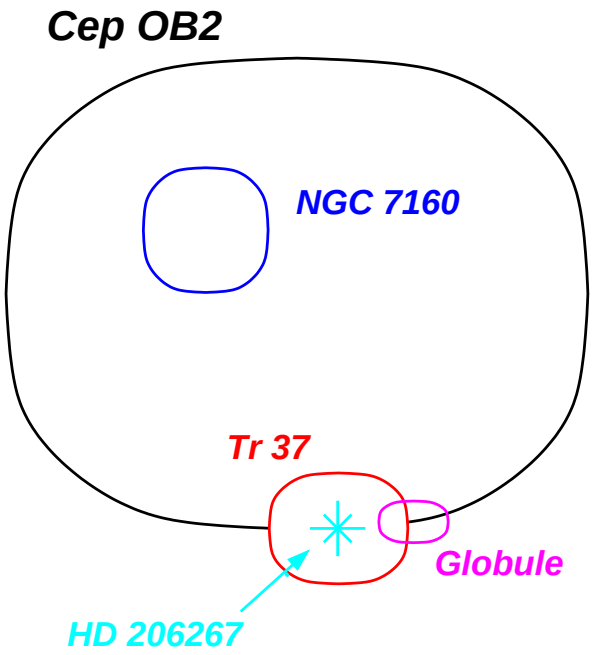

Figure 1.1 Scheme of the Cep OB2 Association: The large Cep OB2 gas bubble is symbolized by a black ellipse. Numerous IRAS sources and dark globules are located all around the Cep OB2 rim. NGC 7160 (blue ellipse) is located near its center, and Tr 37 (red) is at the rim of the bubble. The O6 star HD 206267 is located inside Tr 37, producing an inhomogeneous H II region around it, A gas and dust globule, blown away and illuminated by the bright stars, is found to the West of HD 206267.

their optimal characteristics, the clusters were included in a GTO program with the Spitzer Space Telescope to study disk evolution, the results of which are presented here.

1.3 Method and Organization

The strength of the method used here for the identification of the young stars and their disks is based on the combination of several independent observations covering a very large wavelength range (from U band to 24 μm), and using both photometric and spectroscopic data. The multiple observations allow to check the self-consistency of the scheme, as well as to understand how the different characteristics of accreting and non-accreting stars may be correlated.

Optical (VRI) photometry and the appropriate isochrones (Siess et al., 2000) are used for a preliminary selection of the possible young stars in the region. Optical variability is measured to refine the pre-selection (Herbst et al., 1994; Briceño et al., 2001; Rhode et al., 2001). Then, we took optical spectra to determine the membership of our candidates, based on spectral signatures characteristic of youth, like Lithium absorption at 6707 Å, (Randich et al., 2001; Hartmann, 2003); and of accretion, and intense chromospheric activity, like the Balmer series in emission (Hartmann, 1998; Muzerolle et al., 1998a). In the standard model of T Tauri accretion, the disk is truncated by the stellar magnetic field, and material falling

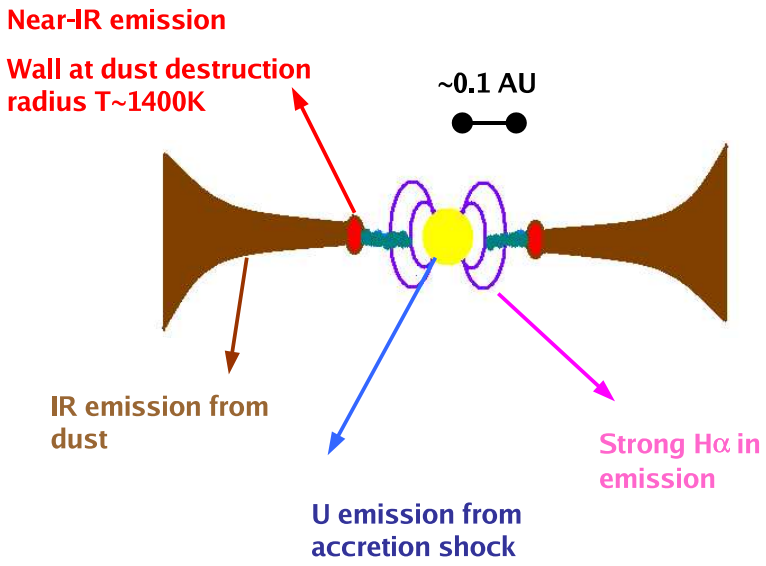

Figure 1.2 Scheme of a Classical T Tauri Star and Magnetospheric Accretion: The disk of well-mixed gas and dust is truncated at the dust destruction radius (T∼1400 K). The dust in the disk produces IR emission, and most of the near-IR emission is originated in the wall at the dust destruction radius. Inside this radius, there is only gas, which is taken from the disk by the magnetic field of the star, and channelized onto the star. The channelized gas produces strong Hα emission because of the large velocities of the accreted material, and the hot shock onto the star produces and excess in U luminosity.

onto the stellar surface is channeled along magnetic field lines (Bertout, Basri, & Bouvier, 1988; Königl, 1991; Hartmann, Hewett, & Calvet, 1994). The motions of the infalling gas produce broad emission line profiles, with velocity widths typically $> 100\,\mathrm{km\,s^{-1}}$, as explained in Muzerolle et al. (1998a, 2001, 2003a). These strong emission can be translated into larger equivalent widths (EW) of Hα in emission for CTTS (in general, larger than 10Å, although there is a dependence with the spectral type, see White and Basri, 2003, and the following sections in this work). In contrast, the non-accreting or weak T Tauri stars (WTTS) have only chromospheric emission, and thus exhibit lower levels of line emission and much smaller line velocity widths (Hartmann, 1998) and EW. Although Hα is one of the most sensitive indicators of accretion in the low-mass, classical T Tauri stars (CTTS) (see Muzerolle, Hartmann & Calvet 1998, Muzerolle et al. 2003a), it is also the brightest *nebular* emission line, and it is highly variable spatially, so a very careful background subtraction is required in most of the young regions with strong nebular emission from H II regions. However, precisely because CTTS generally exhibit such broad Hα emission profiles, it is possible to find the Hα signature of accretion using optical spectra with low and high spectral resolution to measure the EW and to detect the broad wings at velocities widely different from those characteristic of the H II region. Furthermore, through the analysis of the spectral types of the stars and their extinction, we can remove background and foreground contaminating objects.

Once membership is established for the low-mass stars, the presence of accretion disks can be inferred using Hα emission line (through its equivalent width, EW, and following the

criterion by White and Basri 2003) as a strong indicator of accretion processes (Hartmann, 1998; Muzerolle et al., 1998a). Finally, the near-IR counterparts of the cluster members are drawn from the 2MASS survey (released in March 2003, Cutri et al. (2003)), and the the Spitzer GTO data from IRAC and MIPS is used to determine the presence of the IR excesses caused by emission of the heated disk, in a large range of wavelengths or distances to the star (from J to 24 μm, or $\sim$0.1 to 10-20 AU). U band photometry yields a measure of accretion rates (Gullbring et al., 1998). The distribution and extinction of the low-mass objects are considered to revise the previous work done on the determination of the high- and intermediate-mass members (spectral types BAF).

Finally, the information for individual stars can be put together and the different characteristics (accretion, disks, spectral energy distribution) are analyzed to determine how they correlate with each other and with different parameters of the stars (mass, environment), as well as how they evolve with time.

This report is organized in the following way:

- In Chapter 2, the different observations are described, together with the data reduction procedures, and the available data sets are presented.
- In Chapter 3, cluster Tr 37 is analyzed, determining its members, their properties (ages, accretion, spectral types, extinctions, disks), and the characteristics of the cluster and its environment (ongoing or triggered star formation, presence of photoevaporation).
- In Chapter 4, a similar analysis is done for the cluster NGC 7160.
- In Chapter 5, the characteristics of stars and disks in Tr 37 and NGC 7160 are compared, finding evidence of disk evolution (dust settling and/or grain growth) starting in the inner disk and propagating outward.
- In Chapter 6, some well-known members of the Orion Nebula Cluster are analyzed using high-resolution spectra, in order to set the best tools for the determination of the accretion processes that could be applied to the Cep OB2 Association and other regions of relevant ages for planet formation.
- Finally, Chapter 7 summarizes the results of this work, together with the prospective projects for the future.

A small glossary is added at the end, in order to clarify the terms and acronyms which are widely used in this work.

2 Observations and Data Reduction

Published in "Low Mass Stars and Accretion at the Ages of Planet Formation in the Cep OB2 Region" by Sicilia-Aguilar, A., Hartmann, L., Briceño, C., Muzerolle, J., & Calvet, N., 2004, AJ128, 805; "Cep OB2: Disk Evolution and Accretion at 3-10 Myr", by Sicilia-Aguilar, A., Hartmann, L., Hernández, J., Briceño, C., & Calvet, N., 2005, AJ in press; and "Disk Evolution in Cep OB2: Results from Spitzer Space Telescope", by Sicilia-Aguilar, A., Hartmann, L., Calvet,N., Megeath, S.T., Muzerolle, J., Allen, L., D'Alessio, P., Merín B., and Stauffer, J., 2005, in preparation.

The strongest point in this study of the evolution of accretion disks at the ages of planet formation is the combination of multi-wavelength (optical and IR) photometry and spectroscopy, in order to determine with accuracy the members of the young clusters and their ages, their photometric characteristics (variability), the spectral types, extinction, the presence of accretion, the accretion rates, and the presence of a disk at distances from 0.1 to 20 AU (depending on the spectral type). The combination of multiple independent observations allows to check the self-consistency of the work, to reach great completeness, and to study how the different properties of stars and disks may be correlated.

Using low resolution optical spectra from the Hydra multifiber spectrograph, the FAST slit spectrograph, and the Hectospec multifiber spectrograph, a total of ∼165 low-mass members in Tr37, and ∼55 in NGC 7160 have been identified. Optical photometry and theoretical isochrones are used to determine the age of the cluster members, confirming the estimates of ∼4 Myr for Tr 37 and ∼10 Myr for NGC 7160. Accretion rates are derived from U band photometry. The data from the IRAC and MIPS instruments on Spitzer cover the wavelength range from 3.6 to 24 μm, and allow to study the characteristics and presence of disks in accreting and non-accreting stars spanning the age range 1-10 Myr, which had been identified in the optical survey. The coverage at different wavelengths of the two clusters is summarized in Figures 2.1 and 2.2, and the different observations are listed in Table 2.1.

Finally, with the high-resolution Hectochelle spectra, we were able to distinguish accurately CTTS and WTTS in the Orion Nebula Cluster, and to identify 15 new ONC members.

2.1 Optical UVRI Photometry

The optical photometry observations of Tr 37 and NGC 7160 were carried out at the 1.2m telescope in the Fred Lawrence Whipple Observatory (FLWO), using the 4Shooter CCD

Table 2.1. Summary of Observations.

Instrument	Date	Filter/Configuration	Fields
4Shooter/1.2m	September 1998	VRI	NGC 7160
″	September 2000	VRI	Tr 37, NGC 7160
″	September 2001	Hα,VRI	Tr 37,NGC 7160
″	September 2002	UVRI	Tr 37, NGC 7160
″	October 2003	UVRI	Tr 37, NGC 7160
Hydra/WIYN	August 1999	316@10.1	NGC 7160
″	January 1999	316@10.1	NGC 7160
″	November 2000	400@4.2	Tr 37
″	November 2002	600@10.1	Tr 37, NGC 7160
FAST/1.5m	July 2000-November 2002	Combo Mode	Tr 37, NGC 7160
Hectospec/MMT	June 2004	270gpm	Tr 37, NGC 7160
″	November 2004	270gpm	Tr 37, NGC 7160
Hectochelle/MMT	December 2003	Hα, Li, He I	ONC
″	March 2003	Hα	ONC
IRAC/Spitzer	December 2003	3.6,4.5,5.8,8.0 μm	Tr 37
″	April 2004	3.6,4.5,5.8,8.0 μm	NGC 7160
MIPS/Spitzer	July 2004	24.0 μm	Tr 37
″	August 2004	24.0 μm	NGC 7160

Note. — Summary of instruments, dates, filters/configurations, and targets during the different observing runs.

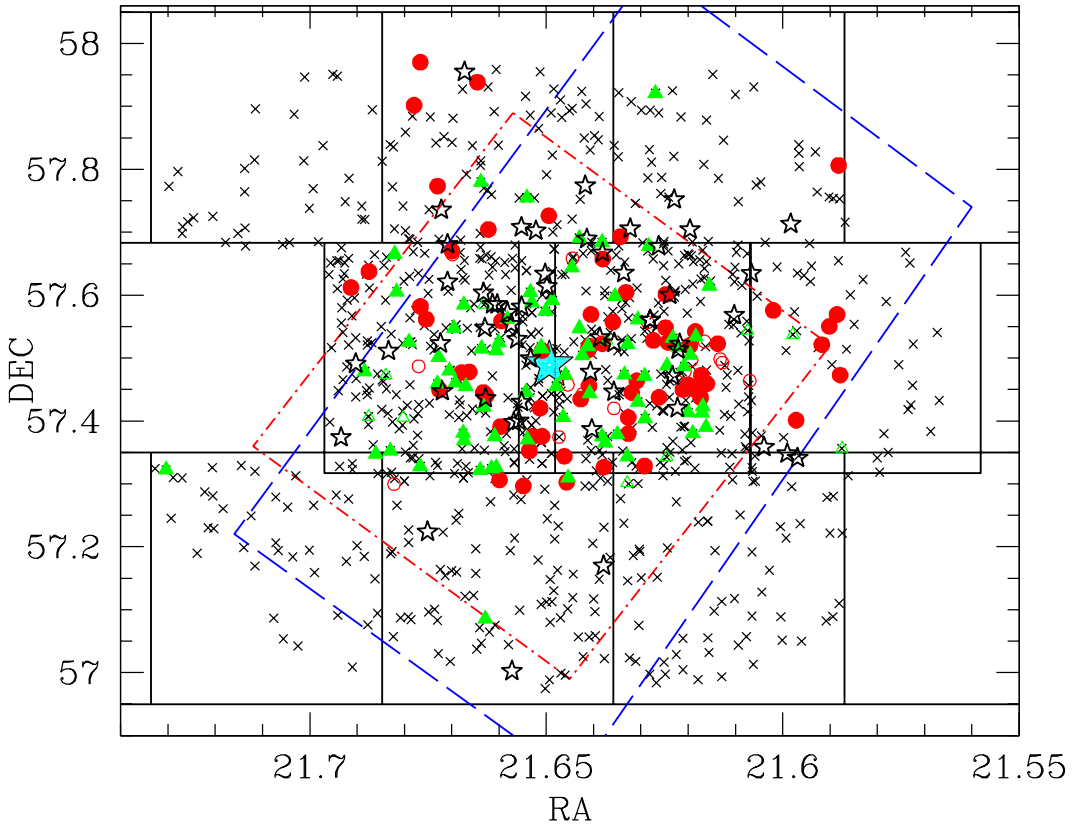

Figure 2.1 Observations in Tr37: Members, 4Shooter, and IRAC and MIPS fields. The O 6 star is denoted by a large, solid star. High- and intermediate-mass members are denoted by small open stars. For the low-mass stars, detections confirmed by Lithium absorption are solid figures, open figures represent cases where Li was not detected due to poor spectra; CTTS are red circles, WTTS are green triangles (see Section 3 for further explanations). 4Shooter optical fields are encircled by solid lines; IRAC field is denoted by a red dotted-dashed line; MIPS field is limited by a blue dashed line. Hectospec targets are represented by small crosses.

array(Caldwell & Falco, 1993)[1], between 1998 and 2002. The 4Shooter is an array of four CCDs, covering a square of ∼25 arcminutes per side, with the four chips of approximately 12 arcminutes per side.The blank space between the CCDs was used to partially cover the bright star HD 206267 and other bright stars in the field, to obtain the least saturation possible and to observe objects closer to the O6 star (see Figure 2.3). A total of 9 fields in Tr 37 (covering an area of about 1 degree radius), and 3 fields in NGC 7160 were taken between September 2000 and October 2003.

During the run in September 2000, several short (30-45 sec) and long (3×300sec) exposures of the clusters where taken using the filters VR_cI_c (from now VRI) in order to cover the whole range from V=14 to V=19, which corresponds to spectral types of K4 to M3 approximately (Kenyon & Hartmann, 1995). The data were reduced using the IRAF[2] reduction package

[1]http://linmax.sao.arizona.edu/help/FLWO/48/4CCD.primer.html
[2]IRAF is distributed by the National Optical Astronomy Observatories, which are operated by the Association

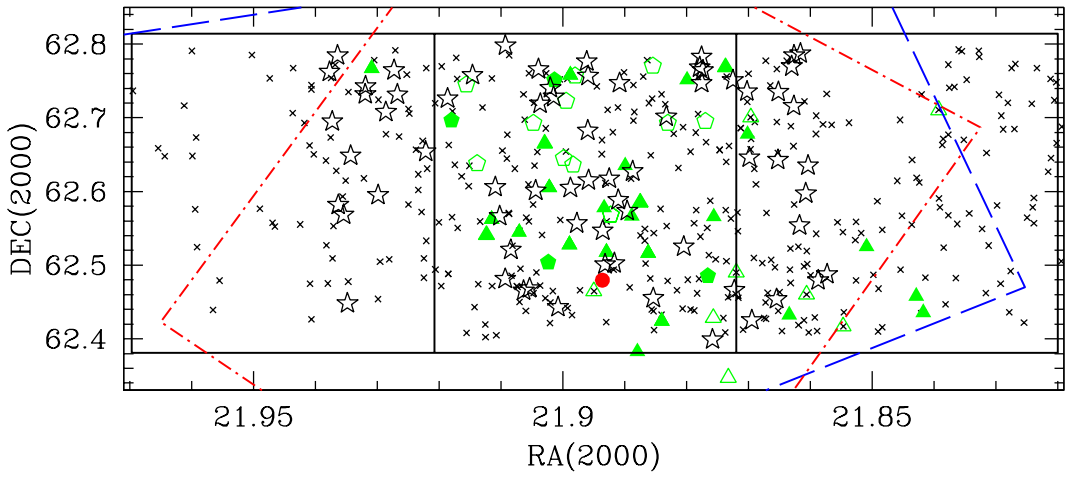

Figure 2.2 Observations in NGC 7160: Members, 4Shooter, and IRAC and MIPS fields. High- and intermediate-mass members are denoted by small open stars. For the low-mass stars, detections confirmed by Lithium absorption are solid figures, open figures represent cases where Li was not detected due to poor spectra; CTTS are red circles, WTTS are green triangles and green pentagons(see Section 4 for further explanations). 4Shooter optical fields are encircled by solid lines; IRAC field is denoted by a red dotted-dashed line; MIPS field is limited by a blue dashed line. Hectospec targets are represented by small crosses.

mscred, which is designed to handle CCD mosaic images. The long exposure images were combined in order to remove cosmic rays. The stars in the fields were identified with the IRAF task *daofind* in the package *daophot*, and aperture photometry was done using task *phot* in the package *apphot*. Several groups of standard stars from Landolt (1992) were observed and used for flux calibration with *photcal*. The dependence of the measured flux with the aperture radius was calculated for the standard stars, in order to be able to use an aperture of 6 pixels for the stars in our fields plus the aperture correction (of about 5-10% of the total flux) to the flux derived from the standards. This way, we avoid both including flux from surrounding stars and underestimating the measured flux. Accurate positions were obtained using tasks in the IRAF package *imcoords*, comparing with USNO positions. More than 20 stars were required for the match, producing a solution for each frame with less than ∼0.3 arcsecs error. The R and I observations were repeated for 5 to 7 nights, both long and short exposures, during consecutive days in September 2000. This repeated data is used to find optical variability, as it will be described in Section 2.2.

For the U filter, 3x1800 sec exposures were obtained, covering all the fields in Tr 37 and the two flanking fields in NGC 7160. Due to the presence of the bright O6 star HD 206267 in Tr 37, as well as some B stars, which can saturate a large surface of the chips during the 1800 sec exposures, we obtained several fields moving the telescope to place the bright stars at the edges and between the chips, so that the saturated stars would cover a small surface. Reduction, photometry and calibration was done in a similar way as for the VRI data. We also obtained coordinates for the U band detections, and we matched them with their optical

of Universities for Research in Astronomy, Inc., under cooperative agreement with the National Science Foundation.

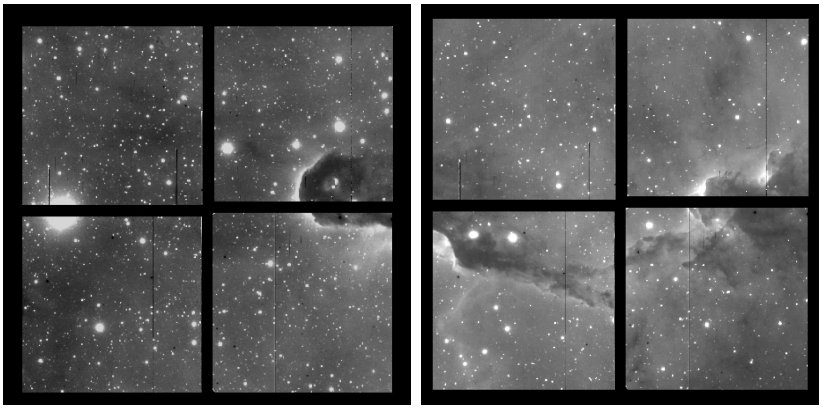

Figure 2.3 Hα Image of the mid-western part of Tr 37 taken with the 4Shooter Camera. 4Shooter produces images of the four chips simultaneously, covering four squares of $\sim$12 arcmin side, or a total surface of a square of 25 arcmin side. The blank spaces between the chips can be used to cover the bright stars that would otherwise saturate a large surface of the chips. The bright star between the two chips in the left is the O6 star HD 206267. The structure in the globule can be seen, although the stars revealed with Spitzer remain invisible at optical wavelengths.

counterparts, creating a UVRI catalog of objects in the fields in Tr 37 and NGC 7160. The optical data for Tr 37 and NGC 7160 are listed in Tables 2.3 and 2.4, respectively.

2.2 Optical Variability

During the 4Shooter/1.2m observing run of September 2000, we were able to take repeated observations using R and I filters for a total of 5 to 7 nights, both with long and short exposures, during consecutive days. All the nights were reduced according to the procedure described in Section 2.1. In the multi-epoch data obtained during the September 2000 4Shooter/1.2m run, the night with the highest indication of being photometric was selected and calibrated; the remaining nights were used to detect photometric variations that could be indicative of the potential youth of the star. Young stars are variable due to several reasons: The accretion processes in accreting stars produce considerable optical variation, and the strong chromospheric activity and extended stellar spots in the non accreting stars cause photometric variations at optical wavelengths as well, with periods that are usually 3-20 days (Herbst et al., 1994), and additional longer time variations (Herbst et al., 1994). The changes in magnitude are some tenths of a magnitude or even larger (Hartmann, 1998; Briceño et al., 2001, 2005; Rhode et al., 2001). Therefore, a selection based on variable stars is an unbiased (sensitive to both CTTS and WTTS) and effective method (i.e. Briceño et al., 2001, found that about 50% of variable stars are indeed young).

In order to detect variations of about 0.10 magnitudes, we compared our fields to the calibrated fields from the photometric night. Each night had a different correction due to different atmospheric conditions, so we used a relative calibration, matching all the stars in each one of the chips taken during the different nights to their counterparts in the photometric night. Since most of the stars in the chip are non-variable field stars, we set the average offset

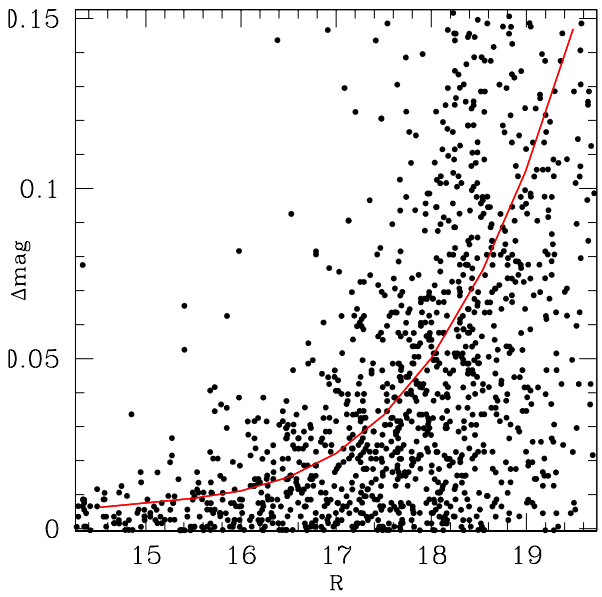

Figure 2.4 Example of the Detection of Variability: The stars detected in R band in the photometric night ("night 1") are matched to their counterparts detected in any other night("night 2"), and the absolute value of difference between the R magnitudes is what we call Δmag. Since photometric errors increase for fainter magnitudes, the average Δmag increases with R. We fit a 4-order polynomial to the average Δmag calculated in 1-magnitude bins, and this polynomial is consider to give the standard deviation σ or error in the photometry as a function of the magnitude R. Values over 3σ are consider as "variable", when 3σ differences are found in 3 or more nights, the χ^2 test indicates that the star has a 99% probability of being a real variable.

as the zero point, and measured the deviations from this zero point as possible variations. The scatter in magnitudes varies, as the error in the photometry increases for fainter magnitudes. We fitted the average value of the deviation for each night and chip, using 4-order polynomia to define the 1σ deviation as a function of the magnitude (see Figure 2.4). Stars showing deviations equal or larger than 3σ for at least 3 nights and/or were out of the 99% probability region for a χ^2 test, were considered as variables. The R and I data were combined to give priority as most probable varying objects those showing parallel variations in R and I. Given that the R band photometry is more accurate than the I band, we also considered, although with lower priority, stars showing only R band variations, and finally, those showing only I variability (although these were only marginal cases).

We used these selection criteria for giving priority to the variable objects in our spectroscopic observations. We found that more than 40% of the cluster members found in the 2000 run were RI variables, which added up to more than 50% stars having any of the R or I variations. Conversely, as we will mention later on, about 50% of the objects that were classified as variables for our 2002 run, turned out to be young cluster members. These numbers are in good agreement with the variability selection of Briceño et al. (2001), considering that our study is based on less number of nights for the variability detection.

2.3 Optical Spectroscopy

2.3.1 Hydra/WIYN

Optical spectra of the most likely cluster members were taken in three Hydra/3.5m WIYN observing runs in January-August 1999, November 2000 and November 2002. Hydra is a multifiber spectrograph, which is mounted on the 3.5m WIYN telescope in Kitt Peak (Barden & Armandroff, 1995)[3]. It has a total of ∼90 fully working fibers than can be arranged within a 1 degree field. Usually, 50 to 60 objects can be assigned to each configuration, plus numerous sky positions, and the position of the telescope is fixed to the targets using a set of ∼10 guide stars, with magnitudes V=10-14. Three different Hydra setups were used: the red fibers and the 316@10.1 grating in 1999 (yielding a wavelength range of 4000-9000 Å), the blue fibers and the 400@4.2 grating in 2000 to obtain spectra in the range 3800-7000 Å, and the red fibers and the 600@10.1 grating, in order to obtain low resolution spectra over a range of 4500-7500 Å, more centered in Hα and Lithium absorption at 6707 Å. The spectral resolution varies in the range of approximately 5-3Å. These Hydra setups were used for observing the fainter candidates (V=16-19), taking sets of 3×1800 sec, 2×1200 sec and 3×1200 sec exposures, depending on the limited observing time with this instrument during each one of the observing runs.

These configurations allowed us to detect the most important features of young (accreting and non accreting) stars: Hα and $H\beta$ from the Hydrogen Balmer series in emission, characteristic of accretion processes and strong chromospheric activity (Hartmann, 1998; Muzerolle et al., 1998a); Lithium absorption at 6707 Å, indicative of the youth of a star (Randich et al., 2001; Hartmann, 2003); and several molecular (mainly TiO) bands and lines that can be used to obtain the spectral types of low to intermediate mass stars (M-G).

The Hydra runs of 1999 and 2000 covered a set of stars with optical colors consistent with pre-Main Sequence stars with ages over the 20 Myr isochrone, assuming the appropriate distance for the cluster and using the V vs. V-I color magnitude diagram, which is the least affected by extinction. We included as well a set of stars in Tr 37 showing near-IR excess, using the data from a special release of the 2MASS survey (J. Carpenter & M. Skrutskie, private communication). The selection, based on near-IR excesses, is biased toward the stars with accretion disks, since the disk is heated by the star producing an excess radiation in the infrared, which adds on to the stellar photosphere (Kenyon et al., 1996; Meyer et al., 1997; Hartmann, 1998; Hillenbrand et al., 1998). For the 2002 Hydra run, the candidates were selected considering those stars consistent with ages over the 100 Myr isochrone, according to the Siess et al. (2000) isochrones, and giving priority to the variable objects. Since the input list for Hydra can include a set of priorities, we gave first priority to the objects showing variability in R and I bands, secondary priority to objects for which variability was detected only in one of the two bands, and finally we added a list of potentially young objects that did not have any variability detection. This second set of observations should be unbiased with respect to disks, since both accreting and non accreting stars show photometric variations (Briceño et al., 2001; Rhode et al., 2001), allowing us to do some disk frequency estimations. A total of 12 fields containing stars from V=16 to V=19 were observed.

The Hydra spectra were reduced using IRAF package *noao.hydra* and the reduction routine *dohydra*, which allowed us to work with all the fibers at a time, to do a flat field correction, and a wavelength calibration (using the CuAr comparison lamp available at the WIYN telescope).

[3] http://www.noao.edu/kpno/manuals/hydraman/hydrawiynmanual.html

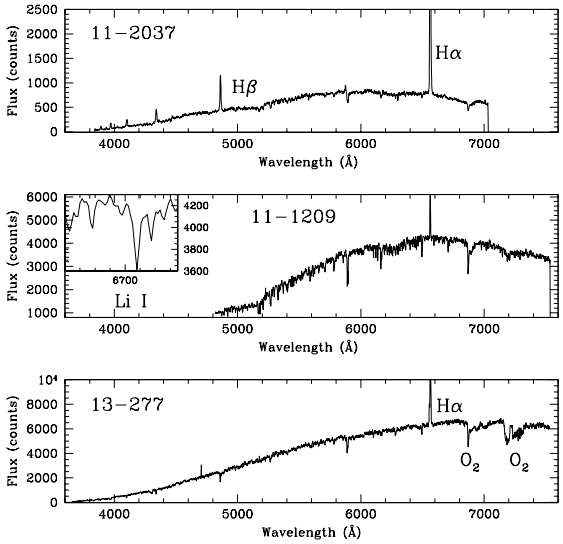

Figure 2.5 Typical Hydra (blue cable, 400@4.2 grating for 11-2037, and red cable, 600@10.1 grating for 11-1209) and FAST spectra (for 13-277, see Section 2.3.2) of young TTS in Tr 37, showing the Balmer series in emission (mainly, Hα) and Li absorption at 6707 Å (detail in the inset figure in the middle panel).

For NGC 7160, the sky subtraction could be done using *dohydra* as well, but for Tr 37, a different method had to be used for sky subtraction, since Tr 37 is embedded in a very inhomogeneous H II region with spatially variable Hα emission. Typical spectra are shown in Figure 2.5.

In the case of Tr 37, given that we use Hα as a marker for young stars (CTTS show strong and broad Hα emission, but WTTS show narrow chromospheric Hα emission that could be misidentified with the background emission), and since the nebular background emission is highly inhomogeneous, the sky subtraction was done in a more precise way than the simple use of an averaged sky. The location of the different sky positions was taken into account in order to define "bright", "intermediate" and "low" brightness locations within the H II region. We defined the brightness of the H II region based on the ratio of H II lines (mainly, Hα) to night sky lines, in order to determine the brightness of the nebula in each position. Three combined sky sets of different brightness were constructed using the brightest, intermediate and faintest sky spectra (according to the brightness of the nebular emission) available for each Hydra configuration, combining 5-10 spectra for each one of them. The three combined sky templates were subtracted separately from each one of the object spectra, and the resulting spectra were examined carefully to determine whether the subtraction of lines like OI 6300 Å and 6368 Å and NII 6583 Å was correct. For each case, the best of these subtractions was selected. In the cases for which none of the three sky templates worked fine, a new sky template was constructed. For undersubtracted stars, only the brightest sky templates were used, and the faintest for the oversubtracted ones, until the background lines were completely subtracted. This procedure reduces the possibilities of confusion of the nebular Hα with the stellar emission. In a few cases (basically, those showing the most noisy spectra) for which

the background lines did not completely disappear with this method, we rely on the other spectral features, and on the spectral types and extinction, in order to determine membership.

2.3.2 FAST/1.2m

In order to complete the sample of stars with magnitudes V=14.5 to V=16 in Tr 37 and NGC 7160 (corresponding to spectral types early K to G), the FAST slit spectrograph (Fabricant, 1994; Fabricant et al., 1998), equipped with the Loral 512 × 2688 CCD, was used. The spectrograph was set up in the standard configuration used for "FAST COMBO" projects, a 300 groove mm^{-1} grating and a 3″ wide slit. This combination offers 3400 Å of spectral coverage centered at 5500 Å, with a resolution of about 6 Å. The candidates were observed during several remote observing runs from July 2001 until July 2003 (observers: P. Berlind & M. Calkins).

The bright stars in NGC 7160 (spectral types BAF) were observed with FAST as well, in order to complete the region of the Main Sequence in the color-magnitude diagram, to check the distance estimate in Contreras et al. (2002), and to produce a sample to study debris disks with Spitzer. Since our 4Shooter/1.2m photometry saturates for magnitudes brighter than V=14, we selected our sample of candidates from the literature. We chose the stars consistent with the Main Sequence in the V vs. B-V diagram, using the colors given in De Graeve (1983) and the Siess et al. (2000) isochrones.

Exposure times ranged from 60 sec to 1200 sec. The spectra were reduced at the CfA (S. Tokarz) using software developed specifically for FAST COMBO observations. With a resolution and wavelength coverage similar to those in the Hydra spectra (see Figure 2.5), and to Hectospec (see below), the same analysis methods and techniques remain valid, according to the magnitude of the stars.

2.3.3 Hectospec/MMT

The spectroscopic followup of most of the candidates was achieved using the Hectospec[4] multifiber spectrograph, mounted on the 6.5m MMT telescope in Mount Hopkins (Fabricant et al., 1994). Hectospec is a low-resolution optical spectrograph, with a total of 300 fibers that can be placed within a 1 degree diameter field. We used the 270 gpm grating, obtaining spectra in the range ∼3700-9000 Å, with a resolution of 6.2 Å. The field position is fixed using 2 to 3 guide stars. Very accurate coordinates (better than 0.3 arcsec) are required for fiber positioning; the fibers subtend a circle of 1.5 arcsec diameter. Since guide stars are drawn from the 2MASS catalog (Cutri et al., 2003), we used 2MASS coordinates for our optical candidates. With Hectospec/MMT, the signal-to-noise ratio of the spectra was largely improved; therefore, Li 6707 Å absorption, an indicator of youth (Randich et al., 2001; Hartmann, 2003), was detectable in about 90% of the low-mass, young stars in the clusters. Moreover, the 300 fibers (compared to the about 90 useful fibers in Hydra, or the one star at a time of FAST) allowed us to observe a very numerous sample, covering most of our candidate list in 1.5 nights observing time, in June and November 2004.

The selection of candidates for spectroscopic followup was based on VRI photometry, RI variability, U band, and 2MASS colors. For the two clusters, all the stars with V=15-19 that appeared over the 100 Myr isochrone in the V vs. V-I color-magnitude diagram, using

[4]Observations reported here were obtained at the MMT Observatory, a joint facility of the Smithsonian Institution and the University of Arizona.

the isochrones from Siess et al. (2000), were selected. An average extinction correction was applied, using A_V=1.5, consistent with the average extinction obtained in Contreras et al. (2002) and the preliminary results from the Hydra/WIYN observations. Individual extinction variations did not affect much the selection, since the extinction vector runs nearly parallel to the isochrones for the low-mass stars. For the run in June 2004, higher priority was given to RI variable stars (see Briceño et al. 2001, 2005; from the Hydra runs it was found that ∼40% of the detected variables are young), to the objects showing near-IR excess in 2MASS colors, and U excess in the V-I vs. U-V diagram. The selection based on 2MASS and U excesses is obviously biased toward accreting stars, so it could affect the disk fraction estimates. Although both accreting and non-accreting stars show variability (Briceño et al., 2001; Rhode et al., 2001), variations in accreting stars show larger amplitudes and this may result in a bias as well. Before the run in November 2004, nearly 95% of the objects with higher priority had been observed. We included the rest of low-priority objects, together with a sample of stars showing IRAC excesses, 2MASS counterparts (for coordinate verification), and no optical counterparts. Most of these stars presented JHK magnitudes consistent with spectral types later than M1 (which at the detection limit of the VRI photometry). The sample of stars drawn from the IRAC catalog is obviously biased toward stars with disks, therefore one must be cautious when estimating accretion disk fractions. Since most of the stars from the IRAC selected sample are below the visual magnitude limit or in between the 4Shooter chips, and they are all stars with disks, we will not consider them for disk fraction estimates, as we will explain later on. The disk fraction estimates (see Section 3) are obtained for stars of spectral types late G to M2 in the central fields (which are nearly complete), and we calculate the errors depending on the number of potential objects that may be missing, and whether they are probably CTTS or WTTS.

In June 2004, a total of 3 configurations were observed in Tr 37, repeating 3×900 sec or 720 sec integrations, plus 2 configurations in NGC 7160, repeating 2 integrations of 900 sec. For the run in November 2004, 1 more field was done in each cluster, obtaining 3×900 sec integrations. The objects and regions covered in both clusters were shown in Figures 2.1 and 2.2. In order to make an unbiased estimation of disk fraction in Tr 37, we gave priority to obtaining spectra of the objects within the two central fields in this cluster, achieving a very complete coverage of the objects above the Main Sequence in this region (see Figure 2.1). In order to avoid the difficulties encountered with Hydra when subtracting background emission lines from the highly variable HII region, we took 600 sec exposures offset by ∼5 arcsecs after each one of the Tr 37 configurations. This way, a sky spectrum was obtained for each star in a location very close to the star, and taken with the same fiber (to account for the likely differences in gain). In case of NGC 7160, due to the lack of strong nebular emission found with Hydra, we simply selected a large number of sky fibers (∼50) and subtracted an averaged sky for each field.

The data reduction was done by S. Tokarz through the CfA Telescope Data Center, using IRAF tasks and other customized reduction scripts. The reduction procedure was the standard for Hectospec data, except for the special individual sky subtraction in Tr 37. The background subtraction for NGC 7160 objects was done using the IRAF program *skysub*. For the Tr 37 fields, the background was subtracted separately using IRAF task *sarith* to remove the wavelength-calibrated and normalized sky spectrum from the corresponding wavelength-calibrated and normalized object spectrum. A sample of spectra in Tr 37 and NGC 7160 is displayed in Figure 2.6.

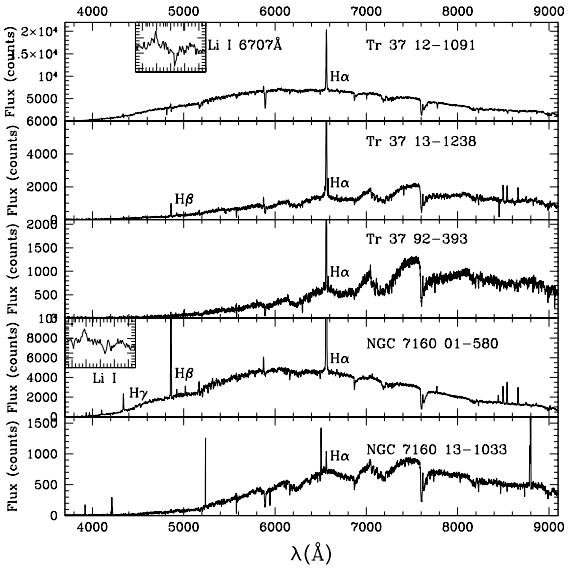

Figure 2.6 Hectospec Spectra: A sample of spectra from stars in Tr 37 and NGC 7160. Hydrogen Balmer Series in emission (Hα, Hβ, Hγ) is labeled. Insets reveal the Li I 6707 Å absorption line.

2.3.4 Hectochelle/MMT

In order to test the information that high-resolution optical spectra could add to the multi-wavelength study of Tr 37 and NGC 7160, a sample of well-known young stars in the Orion Nebula Cluster (ONC) was targeted with Hectochelle during one of the engineering runs of the instrument.

Hectochelle is a fiber-fed multi-object echelle spectrograph, fed by a robotic fiber positioner, and mounted at the Cassegrain focus of the MMT (Szentgyorgyi et al., 1998; Fabricant, 1994; Fabricant et al., 1998). The positioner is shared between a moderate dispersion spectrograph, Hectospec (Fabricant, 1994), and Hectochelle. The optical fibers are 250 microns in diameter, and subtend approximately 1.5 arcsec on the sky at the plate scale of the MMT in its F/5, wide field configuration (170 microns/arcsec). The diametral field of view of the robot positioner is 1 degree.

Hectochelle can take up to 240 simultaneous spectra consisting of single echelle orders; order separation is achieved with interference filters. The spectral orders are approximately 150 Å wide near Hα. The predicted resolution is R$\sim$32,000-40,000 and the efficiency of the spectrograph, due exclusively to losses in the telescope, is estimated to be 6-10%, depending on the location within an order and the order selected. The design resolution has been achieved; however a failure of the reflective coatings on the Hectochelle collimator and camera mirrors reduced the efficiency during the data taking for this paper. The total efficiency, including the losses at all points in the optical train, was approximately 4% in the diffractive order containing Hα. (The mirrors will be recoated in the future).

The first set of observations was taken on the night of 8 Dec 2003. Three exposures of 15, 30, and 30 minutes were taken in the spectral order centered on Hα. Due to time constraints, only 15 minute exposures were taken in spectral orders centered on 6700Å and 5890 Å. For

these observations, we selected a total of 146 stars in the ONC member list from Hillenbrand (1997), plus an additional sample of 40 stars from the 2MASS All Sky Survey (Cutri et al., 2003). The 2MASS objects were selected by the positioner programmer according to their K magnitudes. The Hillenbrand sample was selected from a list ordered in brightness, and was otherwise unbiased with respect to previous attempts to find accretion signatures. Almost all of the Hillenbrand sample stars were within 15 arcmin of the ONC center, corresponding to a radius $\sim$ 2 pc at a distance of $\sim$ 470 pc. The 2MASS candidates were located all around this sample, filling a field of $\sim$ 27 arcmin radius.

The second set of observations consisted of three 15 minute exposures in the Hα order on 10 March 2004. A total of 150 stars from Hillenbrand (1997) were targeted, about 25% of which had been observed in December. An additional 15 minute exposure was taken with an offset of 20 arcsec north in an attempt to make some subtraction of the nebular emission lines (principally Hα and N [II] at 6548 and 6583 Å).

The spectra were reduced with standard IRAF tasks. The initial setup in December 2003 yielded very weak Thorium-Argon comparison lines, not sufficient to produce an accurate wavelength scale. The wavelength calibrations for these data were estimated from nebular emission lines. This procedure does not yield accurate radial velocities but is adequate for analyzing the broad stellar line profiles. For the March 2004 data, the Thorium-Argon lamps were bright enough so that accurate wavelength solutions in the Hα order could be obtained, permitting the measurement of radial and rotational velocities (See Section 6.2.5).

2.4 Infrared Observations

The Spitzer Infra-Red Space Telescope opens a window to study the properties of the disks of these stars. The clusters Tr 37 and NGC 7160 were included in a GTO Spitzer program, and were observed with Spitzer using the IRAC (Fazio et al., 2004) and MIPS (Rieke et al., 2004) instruments. The IRAC photometry covers the wavelength range from 3.6 to 8.0 μm (using broad band filters at 3.6, 4.5, 5.8 and 8.0 μm), and the MIPS photometry provides the flux at 24 μm. Combining these data with the optical and near-IR photometry, it is possible to trace the spectral energy distributions (SEDs) of the known cluster members, determining clearly the presence of a disk at different distances from the star (from tenths to few AU, corresponding to the locations where planets are supposed to form).

2.4.1 IRAC/Spitzer

Tr 37 and NGC 7160 were observed using IRAC on Spitzer on December 2003-March 2004, as a part of an IRAC GTO program to study protoplanetary disks and disk evolution. IRAC is equipped with a four-channel camera, which allows to take images at 3.6, 4.5, 5.8 and 8.0 μm (Fazio et al., 2004). Each one covers a square area of approximately 5.2 arcmin per side. We obtained a total of 5 positions for each field, covering a total area of 9×8 IRAC fields in both Tr 37 and NGC 7160, or a square of about 50 arcmin per side. This area corresponds to a large fraction of the area covered optically (see Figures 2.1 and 2.2), and includes most of the cluster members we identified with optical spectra. The images are taken in pairs (3.6 and 5.8 μm; 4.5 and 8.0 μm), which produces an offset in the final mosaic fields of 5.2 arcmin. Observations were repeated taking long (30 sec) and short (1 sec) exposures, in order to cover a large range of non-saturated magnitudes with good signal-to-noise. This way, we can cover the magnitude range 9.5 to 14.5 (at 3.6 and 4.5 μm), and 8 to 13 (at 5.8 and 8.0 μm). Data is

Table 2.2. IRAC and MIPS Zero Points for Data Calibration

λ (μm)	Zero Flux (JY)	arcsec/pixel	(MJy/sr)/(DN/s)	SIP Zero Point	BCD Zero Point
3.6	277.5	1.2206	0.1144	19.660	17.306
4.5	179.5	1.2129	0.1375	18.965	16.811
5.8	116.6	1.2220	0.5871	16.870	16.292
8.0	63.13	1.2197	0.1989	17.383	15.629
24.0	7.3	—	0.150	—	0.0

Note. — Tr 37 data used the BCD calibration zero-point; NGC 7160 used the SIP calibration zero-point.

calibrated using the standard pipeline procedures for Spitzer, and it is provided in the BCD (Basic Calibrated Data) format.

The image mosaics were created using Mopex mosaicker for Tr 37 and the IDL mosaicking software developed by R. Gutermuth (Gutermuth et al., 2004) for NGC 7160. Both programs produce similar quality mosaics, although the flux units and calibration are different and need to be taken into account differently in each case (see Table 2.2). Photometry was done using the *PhotVis* IDL software created by R. Gutermuth. *PhotVis* was used for object detection in the mosaics (using a daofind-like routine, and a 10 sigma threshold over the sky variance for the detection of sources), and for the photometry. We obtained aperture photometry using 5 pixels apertures and an aperture correction up to 10 pixel radius. Sky annuli covering radii from 10 to 20 pixels were used for measuring sky fluxes. Geometrical corrections have to be applied to account for the different area subtended per pixel (ranging from 1.21 to 1.22 arcsec) in each one of the channels. The BCD data is already calibrated in units of MJy/sr, and the calibrated magnitudes were obtained using the zero-point fluxes for Vega and the appropriate BDC zero-point magnitude. *PhotVis* also estimates the errors in the measured magnitudes according to the number of counts and background noise from the subtracted sky. An additional source of error comes from problems in the flat-fielding of the images, which are not yet resolved. The flat-fielding error introduces an extra 5% error, which is dominating the errors for most of the sources. The parameters and zero points used in the calibration are listed in Table 2.2.

Each channel was measured and calibrated independently, and matched to the rest of channels using their coordinates. The optical counterparts (when available) were matched to the IRAC data using 2MASS coordinates. Tables 2.5, 2.6, 2.7, and 2.8 show the IRAC magnitudes for the members of the clusters. Nearly all the stars in our optically selected sample with V>19 within the IRAC fields show low-error, well-detected fluxes at IRAC wavelengths.

2.4.2 MIPS/Spitzer

We obtained 24 μm photometry for Tr 37 and NGC 7160 using the Multiband Imaging Photometer for Spitzer (MIPS, see Rieke et al. 2004) in July and August 2004. The MIPS 24 μm detector covers a square field of 5 arcmin per side. A total of 100 fields (arranged in a 10×10 mosaic) were observed in Tr 37, and 49 more in NGC 7160 (arranged as a 7×7 square). The area covered by the MIPS fields is displayed in Figures 2.1 and 2.2. Exposure times were 4 sec, and each field was done combining a total of 10 dithers per scan, resulting

in 20 combined images per point since there is a half-array overlap.

The mosaics were created using the MIPS instrument team Data Analysis Tool (DAT), which calibrates the data, applies a distortion correction to each image, and finally combines them (Muzerolle et al., 2004). The object detection and aperture photometry was done using *PhotVis*, considering an aperture of 6 pixels, and correcting up to 12. The magnitudes were calibrated using the flux for a Vega-type star (see Table 2.2). Finally, MIPS detections were matched with the clusters members using their respective coordinates. The magnitudes at 24 μm are listed in Tables 2.5, 2.6, 2.7 and 2.8.

From the observations of diskless B stars (see Sections 3.2 and 4.2), we can confirm the lower limit for the detectability of 24 μm flux to be $\lambda F_\lambda \sim 1{\times}10^{-13}$ erg cm^{-2} s^{-1}, or magnitude $\sim$10, although detectability may vary depending on the brightness of the background, among other factors. We can consider these values as an upper limit to all the stars within the MIPS field and without 24.0 μm data in the tables. This would explain why most of the detections occur for the earlier (B- and A-type) stars, for which hotter disks are expected, and suggests that some disks around late A- and F-type stars might be missing in our study, due to their lower fluxes, so any final conclusion about debris disk frequencies is not possible.

2.5 Data from Other Sources

2.5.1 The 2MASS JHK Survey

The Two Micron All Sky Survey (2MASS) is a joint project of the University of Massachusetts and the Infrared Processing and Analysis Center/California Institute of Technology, funded by the National Aeronautics and Space Administration and the National Science Foundation. It was designed to map more than 99% of the sky in both the northern and southern hemispheres, providing a catalog of point and extended sources in JHK. The complete catalog was released on March 25, 2003 [5].

The 2MASS JHK data was used in this study to connect the optical and IR photometry. Moreover, 2MASS provides very accurate coordinates for the registered sources, so the 2MASS sources and coordinates have become standard for other purposes, like selecting the guide stars for Hectospec and Hectochelle on the MMT (which also requires that the coordinates of the observed objects are in the 2MASS system). Therefore, the optical and IR candidates in Tr 37 and NGC 7160 were matched with their 2MASS counterparts (see Tables 2.3 and 2.4), and the 2MASS photometry is used together with the optical and IR data available for this work.

2.5.2 Photometry for the High- and Intermediate-Mass Stars

As a secondary topic, in addition to the study of the evolution of accretion disks around low-mass stars, the Spitzer photometry is used in order to detect the presence of optically thick and optically thin (debris) disks around the higher-mass members in Tr 37 and NGC 7160. Since the 4Shooter optical photometry saturates for magnitudes V=13.5 or larger, optical colors for the high- and intermediate-mass members (spectral types B,A,F) in Tr 37 and NGC 7160 were obtained from the literature. For Tr 37, the BV photometry was taken from the work by Marschall & van Altena (1987) and by Kun et al. (1987); and NGC 7160 had been studied using UBV filters by De Graeve (1983). This photometry is listed, together with the revised membership, in Tables 3.4 and 4.3.

[5] http://pegasus.phast.umass.edu/2mass.html

The membership of the BAF stars had been studied in the sources from which the optical photometry was obtained and in Contreras et al. (2002), for the younger cluster Tr 37 only. The knowledge of the low-mass members in the clusters provides new information in order to determine the membership of these higher-mass stars, which is usually complicated. Therefore, the cited optical photometry was included as a first step to the revision of the cluster membership of BAF stars in Tr 37 and NGC 7160, in order to obtain samples of stars with well-determined ages (from the low-mass members) to study the presence of accretion and debris disks during the epoch of planet formation.

2.6 Data Tables

Table 2.3. Summary of Optical and Near-IR Observations for Low-Mass Stars in Tr37.

ID1	2MASS	V	V-R	V-I	J	H	K	Variability
73-758	21350835+5736028	17.062	1.217	2.301	13.330±0.028	12.533±0.032	12.163±0.028	—
72-489	21351481+5721232	18.114	1.056	2.049	14.607±0.038	13.837±0.043	13.543±0.044	—
72-1427	21351627+5728222	18.080	1.258	2.500	14.005±0.031	13.067±0.029	12.673±0.028	—
81-541	21351745+5748223	17.519	1.197	2.340	13.399±0.031	12.469±0.033	12.037±0.026	—
73-472	21351861+5734092	16.851	1.096	2.046	13.219±0.024	12.299±0.031	11.829±0.022	—
73-311	21352451+5733011	18.378	1.252	2.491	14.014±0.034	13.115±0.037	12.674±0.030	—
73-71	21353021+5731164	16.989	1.176	2.295	12.979±0.034	12.105±0.037	11.715±0.029	—
72-875	21354975+5724041	18.367	0.985	2.189	14.092±0.031	13.006±0.027	12.500±0.026	—
73-194	21355223+5732145	18.059	1.111	2.115	14.734±0.042	13.957±0.052	13.764±0.050	—
73-537	21360723+5734324	17.300	1.027	2.048	14.047±0.052	13.159±0.039	12.674± ...	—
—	21362507+5727502	—	—	—	14.952±0.044	14.031±0.048	13.518±0.040	—
14-306	21362676+5732374	18.399	1.112	2.276	14.258±0.040	13.294±0.042	12.936±0.034	—
—	21364596+5729339	—	—	—	14.211±0.039	12.416±0.036	11.189±0.025	—
—	21364762+5729540	—	—	—	13.568±—	12.342±0.042	11.655±0.033	—
14-141	21364941+5731220	15.810	1.130	2.291	11.918±0.022	10.914±0.029	10.355±0.021	RI
14-1229	21365579+5736533	17.806	1.068	2.069	14.361±0.029	13.501±0.041	13.351±0.034	—
11-2146	21365767+5727331	16.917	1.229	2.505	12.442±0.031	11.327±0.032	10.640±0.025	RI
11-1209	21365850+5723257	15.414	0.892	1.818	12.200±0.024	11.433±0.033	11.122±0.023	RI
—	21365947+5731349	—	—	—	14.520±0.034	13.403±0.038	12.765±0.028	—
11-1659	21370088+5725224	17.241	1.079	2.124	13.611±0.042	12.844±0.044	12.656±0.039	RI
11-1499	21370140+5724458	17.225	1.043	2.377	13.305±0.040	12.459±0.055	12.206±0.055	—
11-2322	21370191+5728222	16.687	1.096	2.304	12.854±0.029	11.969±0.033	11.560±0.025	RI
11-1871	21370254+5726144	18.154	1.071	2.469	14.074±0.045	13.331±0.044	13.129±0.045	No
14-222	21370607+5732015	15.812	1.074	2.163	12.105±0.021	11.273±0.026	11.077±0.021	RI
14-287	21370649+5732316	17.850	1.339	2.682	13.321±0.023	12.327±0.028	11.909±0.023	RI
11-2037	21370703+5727007	16.033	0.948	1.906	12.649±0.026	11.752±0.027	11.258±0.020	RI
11-1067	21370843+5722484	18.071	1.149	2.366	14.402±0.035	13.614±0.037	13.475±0.048	No
—	21370936+5729483	—	—	—	13.385±0.027	12.325±0.047	11.837±0.034	—
14-11	21371031+5730189	17.528	1.383	2.754	13.057±0.029	12.216±0.034	11.956±0.026	No
14-125	21371054+5731124	16.738	1.005	2.037	13.090±0.026	12.170±0.029	11.732±0.021	RI
11-1513	21371183+5724486	17.171	1.192	2.414	13.162±0.029	12.348±0.029	12.145±0.028	RI
11-2131	21371215+5727262	17.722	1.289	2.474	13.393±0.027	12.214±0.031	11.523±0.025	RI
11-2397	21371450+5728409	18.535	1.060	2.197	14.511±0.038	13.559±0.041	12.954±0.034	—
11-2487	21371498+5729123	17.611	1.134	2.344	13.726±0.032	12.946±0.033	12.734±0.035	No
11-2031	21371591+5726591	15.483	0.901	1.786	12.499±0.025	11.534±0.028	10.856±0.020	RI
14-103	21371976+5731043	17.826	0.902	2.005	14.283±0.027	13.387±0.031	13.193±0.040	RI
14-197	21372368+5731538	17.071	1.060	2.076	13.446±0.025	12.635±0.031	12.473±0.026	RI
—	21372447+5731359	—	—	—	14.543±0.032	13.790±0.046	13.278±0.038	—
14-160	21372732+5731295	16.909	1.066	2.077	13.218±0.037	12.349±0.041	11.954±0.033	RI
11-2503	21372805+5729155	18.070	1.378	2.853	13.440±0.027	12.556±0.033	12.329±0.029	—
11-581	21372828+5720326	16.734	1.096	2.128	13.095±0.044	12.332±0.045	12.104±0.039	RI
14-1017	21372894+5736042	18.661	1.358	2.742	13.994±0.031	13.027±0.029	12.630±0.026	RI
14-335	21372915+5732534	17.144	1.046	2.156	13.236±0.035	12.142±0.031	11.553±0.026	RI
11-1864	21373420+5726154	17.546	1.079	2.113	14.065± ...	13.686±0.070	13.198± ...	No
83-343	21373696+5755149	16.667	1.119	2.242	13.006± ...	12.277±0.045	11.940± ...	—
14-183	21373849+5731408	16.613	1.242	2.396	13.303±0.029	12.229±0.031	11.668±0.045	RI
14-2148	21374184+5740400	18.246	1.317	2.627	13.985±0.030	13.087±0.034	12.832±0.030	No
—	21374275+5733250	—	—	—	12.561±0.023	11.308±0.026	10.388±0.021	—
11-1384	21374486+5724135	17.132	1.099	2.229	13.351±0.030	12.593±0.034	12.387±0.029	RI
11-383	21374514+5719423	17.613	1.124	2.263	13.903±0.025	12.971±0.033	12.582±0.026	No
11-2318	21374521+5728173	18.003	1.136	2.338	14.176±0.035	13.248±0.036	13.005±0.037	I
13-924	21375018+5733404	16.934	1.004	2.013	13.225±0.027	12.360±0.036	12.108±0.024	No
12-1984	21375022+5725487	16.596	0.910	1.798	13.288±0.029	12.451±0.031	12.251±0.022	No
12-2519	21375107+5727502	17.274	1.043	2.064	13.647±0.030	12.816±0.036	12.460±0.022	No
12-1968	21375487+5726424	16.495	0.988	1.949	13.185±0.038	12.344±0.032	12.026±0.027	RI
12-1422	21375756+5724197	18.766	1.289	2.678	14.458±0.045	13.606±0.043	13.337±0.043	RI
12-1091	21375762+5722476	16.587	0.935	1.857	13.182±0.024	12.215±0.029	11.673±0.020	RI

Table 2.3 (continued)

ID1	2MASS	V	V-R	V-I	J	H	K	Variability
13-269	21375812+5731199	16.945	1.152	2.299	12.829±0.027	12.001±0.032	11.724±0.020	RI
12-583	21375827+5720354	17.477	1.216	2.554	13.427±0.040	12.574±0.038	12.306±0.029	I
12-94	21375841+5718046	17.389	1.107	2.081	13.780±0.026	12.899±0.033	12.673±0.026	No
13-1238	21375926+5736162	18.355	1.528	2.985	13.321±0.027	12.400±0.032	11.889±0.018	RI
12-2373	21380058+5728253	17.660	1.180	2.424	13.552±0.032	12.728±0.050	12.477±0.033	RI
82-272	21380350+5741349	17.257	1.087	2.260	12.502±0.026	11.483±0.029	10.847±0.019	—
12-1081	21380593+5722438	18.346	1.201	2.404	14.354±0.035	13.533±0.033	13.271±0.031	RI
13-1161	21380772+5735532	18.050	1.245	2.407	14.111±0.039	13.249±0.038	12.973±0.028	No
12-1613	21380848+5725118	18.422	1.273	2.641	14.062±0.032	13.241±0.040	12.951±0.035	No
13-1426	21380856+5737076	19.669	1.607	3.238	14.306±0.029	13.425±0.033	12.901±0.030	No
13-669	21380928+5733262	15.836	0.979	1.914	12.391±0.029	11.566±0.029	11.195±0.020	No
13-350	21381384+5731414	18.079	1.105	2.270	14.475±0.066	13.621±0.060	13.389±0.043	No
12-1017	21381509+5721554	16.831	1.008	1.986	13.283± . . .	12.654± . . .	12.554±0.028	No
54-1781	21381612+5719357	18.180	1.181	2.526	13.991±0.032	13.092±0.032	12.792±0.030	—
13-1877	21381703+5739265	16.829	1.238	2.384	12.935±0.039	11.954±0.043	11.263±0.024	RI
13-277	21381731+5731220	13.915	0.963	1.774	10.279±0.026	9.329±0.029	8.593±0.020	No
13-2236	21381749+5741019	17.542	1.140	2.191	13.873±0.034	13.004±0.037	12.767±0.035	No
12-1009	21381750+5722308	16.166	0.833	1.782	13.119±0.045	12.361±0.043	12.130±0.036	RI
13-819	21382596+5734093	16.439	1.018	1.991	13.032±0.027	12.234±0.029	11.993±0.020	RI
12-1955	21382692+5726385	17.533	1.073	2.112	14.096±0.043	13.320±0.044	13.122±0.042	No
13-236	21382742+5731081	15.641	0.935	1.785	12.355±0.036	11.363±0.040	10.774±0.024	No
12-2113	21382743+5727207	17.143	1.223	2.474	12.856±0.030	11.986±0.035	11.506±0.024	RI
13-157	21382804+5730464	16.234	0.979	1.907	12.912±0.030	11.979±0.036	11.249±0.052	RI
13-232	21382834+5731072	17.356	1.158	2.247	13.647±0.043	12.804±0.042	12.561±0.040	RI
—	21383216+5726359	—	—	—	14.811±0.045	13.860±0.044	13.175±0.034	—
13-52	21383255+5730161	17.265	1.083	2.117	13.738±0.047	12.842±0.040	12.607±0.031	RI
12-1825	21383382+5726053	19.227	1.373	2.710	14.976±0.063	14.141±0.047	13.877±0.066	No
91-155	21383470+5741274	18.306	1.363	2.791	13.741±0.035	12.875±0.048	12.489±0.036	—
13-566	21383481+5732500	18.049	1.239	2.581	13.899±0.029	13.049±0.035	12.789±0.022	—
13-1891	21384001+5739303	18.163	1.104	2.273	14.509±0.027	13.600±0.042	13.215±0.030	No
13-1709	21384038+5738374	16.700	1.002	1.880	13.563±0.027	12.715±0.032	12.507±0.023	RI
54-1613	21384332+5718359	16.577	0.979	1.848	13.446±0.027	12.688±0.029	12.457±0.025	—
—	21384350+5727270	—	—	—	14.246±0.034	13.447±0.037	13.065±0.034	—
54-1547	21384446+5718091	16.653	0.955	1.840	13.421±0.027	12.647±0.035	12.180±0.026	—
12-2363	21384544+5728230	17.681	1.317	2.629	13.523±0.032	12.733±0.038	12.500±0.033	No
12-595	21384622+5720380	18.507	1.081	2.162	15.375±0.066	14.634±0.082	14.327±0.081	No
12-1423	21384707+5724207	17.043	1.099	2.205	13.250±0.026	12.459±0.031	12.288±0.023	RI
12-1010	21385029+5722283	18.185	1.001	2.238	14.372±0.040	13.507± . . .	13.076± . . .	No
12-2098	21385253+5727184	18.431	1.250	2.699	14.137±0.053	13.365±0.056	13.156±0.050	RI
13-1087	21385542+5735299	16.044	0.930	1.812	12.878±0.024	12.110±0.028	11.943±0.023	RI
—	21385669+5730484	—	—	—	14.919±0.053	14.163±0.055	13.902±0.065	—
91-506	21385807+5743343	16.842	1.076	2.086	13.386±0.031	12.521±0.036	12.040±0.022	—
24-692	21390054+5734280	18.431	1.295	2.550	14.294±0.035	13.402±0.033	13.138±0.039	RI
12-1027	21390319+5722318	18.576	1.066	2.626	14.249±0.041	13.561±0.048	13.308±0.040	No
24-77	21390346+5730527	17.527	0.930	2.088	13.771±0.029	12.987±0.035	12.687±0.028	RI
—	21390321+5730420	—	—	—	14.338±0.045	13.500±0.046	13.146±0.042	—
24-108	21390390+5731037	17.266	1.051	2.152	13.540±0.029	12.739±0.035	12.471±0.028	RI
12-1617	21390468+5725128	17.856	1.330	2.681	13.542±0.026	12.627±0.028	12.129±0.024	RI
21-840	21391012+5722323	18.975	1.440	2.886	14.435±0.051	13.562±0.058	13.233±0.051	—
13-1048	21391088+5735181	18.903	1.324	2.478	13.695±0.024	12.714±0.028	12.165±0.026	—
13-1250	21391213+5736164	16.049	0.959	1.814	12.920±0.024	12.119±0.029	11.799±0.023	RI
12-705	21391288+5721088	17.589	1.223	2.460	13.489±0.026	12.685±0.032	12.425±0.025	RI
12-942	21391424+5722129	17.153	1.166	2.358	13.238±0.029	12.431±0.037	12.196±0.028	RI
91-815	21391465+5745177	18.295	1.270	2.653	14.142±0.052	13.379±0.061	13.091±0.052	—
21-1590	21391554+5726440	18.099	1.311	2.480	14.053±0.030	13.252±0.038	12.941±0.034	RI
54-1488	21391748+5717474	16.478	0.827	1.653	13.774±0.047	13.013±0.046	12.799±0.044	—
24-542	21392957+5733417	15.879	0.912	1.784	12.823±0.024	12.053±0.031	11.867±0.023	RI

Table 2.3 (continued)

ID1	2MASS	V	V-R	V-I	J	H	K	Variability
24-515	21393407+5733316	17.896	1.196	2.320	14.057±0.028	13.125±0.033	12.704±0.028	RI
21-998	21393480+5723277	17.478	1.083	2.177	13.850±0.029	12.972±0.033	12.476±0.028	RI
21-33	21393561+5718220	18.677	1.280	2.536	14.501±0.039	13.581±0.040	13.220±0.044	No
24-170	21393612+5731289	17.399	1.127	2.298	13.444±0.032	12.648±0.035	12.398±0.030	RI
53-1803	21393803+5719332	18.246	1.134	2.093	14.643±0.043	13.744±0.044	13.448±0.048	—
24-48	21393805+5730439	18.109	1.302	2.477	14.129±0.032	13.278±0.027	13.073±0.029	RI
21-833	21393926+5722320	18.088	1.232	2.575	13.836±0.037	13.098±0.044	12.797±0.032	—
21-230	21394169+5719274	18.169	1.231	2.478	14.210±0.037	13.345±0.036	13.174±0.038	No
92-393	21394408+5742159	18.272	1.446	2.918	13.619±0.026	12.765±0.028	12.505±0.023	—
21-1536	21394570+5726242	18.849	1.238	2.691	14.561±0.040	13.756±0.044	13.224±0.042	—
52-1649	21394643+5705072	17.215	0.968	1.837	14.213±0.041	13.557±0.050	13.310±0.042	—
21-2251	21394754+5725210	18.048	1.318	2.735	13.800±0.028	12.995±0.032	12.709±0.030	RI
24-820	21394746+5735059	18.349	1.074	2.033	15.104±0.036	14.363±0.049	14.069±0.060	No
21-1586	21394793+5726427	18.231	1.092	2.389	14.479±0.041	13.615±0.038	13.375±0.038	No
24-78	21394936+5730546	17.909	1.319	2.642	13.561±0.022	12.767±0.030	12.465±0.025	RI
92-1162	21394974+5746468	18.163	1.321	2.697	13.791±0.027	12.897±0.030	12.563±0.028	—
53-1762	21395029+5719177	17.941	1.213	2.320	14.134±0.024	13.293±0.032	12.984±0.030	—
93-361	21395237+5756186	16.735	1.140	2.143	12.847± . . .	11.793±0.038	10.760±0.025	—
21-1974	21395861+5728404	16.769	0.979	1.906	13.446±0.032	12.707±0.044	12.497±0.032	—
21-1692	21400128+5727184	18.578	1.357	2.640	14.305±0.030	13.460±0.040	13.243±0.040	I
21-763	21400259+5722090	17.651	1.154	2.279	13.849± . . .	13.164± . . .	12.968±0.035	RI
24-817	21400273+5735050	17.823	1.204	2.329	13.968±0.026	13.122±0.030	12.916±0.028	RI
21-895	21400321+5722505	16.392	0.956	1.905	13.216±0.026	12.508±0.033	12.306±0.028	No
—	21400451+5728363	—	—	—	13.011±0.032	12.210±0.036	11.810±0.029	—
21-1762	21400924+5727393	16.998	1.044	2.058	13.391±0.024	12.727±0.033	12.413±0.028	RI
24-382	21401023+5732511	17.907	1.096	2.243	14.132±0.030	13.317±0.036	13.091±0.035	RI
24-1736	21401134+5739518	19.068	0.946	2.715	14.309±0.024	13.443±0.036	12.968±0.028	No
24-1796	21401182+5740121	17.395	1.028	2.083	13.876±0.035	13.076±0.039	12.734±0.037	RI
21-2006	21401390+5728481	16.994	0.989	1.974	13.704±0.029	12.920±0.038	12.488±0.030	No
22-2651	21402130+5726579	18.433	1.331	2.422	14.500±0.038	13.405±0.032	12.624±0.028	RI
—	21402192+5730054	—	—	—	13.608±0.039	12.754±0.038	12.538±0.032	—
92-1103	21402274+5746240	16.520	1.132	2.222	12.816±0.032	11.935±0.033	11.553±0.026	—
22-1418	21402287+5727329	17.588	-0.092	2.341	14.134±0.032	13.174±0.030	12.591±0.028	RI
23-405	21403134+5733417	16.455	0.987	1.810	13.389±0.032	12.504±0.033	12.125±0.028	RI
23-570	21403574+5734550	16.847	1.132	1.974	13.477±0.030	12.556±0.030	12.194±0.028	RI
93-540	21403586+5758130	18.471	1.402	2.662	14.176±0.030	13.177±0.037	12.646±0.032	—
53-1843	21403592+5719398	17.648	1.098	2.144	13.945±0.027	13.172±0.041	12.938±0.026	—
—	21403721+5729127	—	—	—	14.640±0.053	13.815±0.053	13.512±0.061	—
23-1161	21405543+5739555	17.806	1.157	2.067	14.407±0.032	13.602±0.038	13.425±0.039	—
93-168	21404061+5754064	16.599	1.043	2.001	13.423±0.024	12.520±0.030	12.092±0.026	—
23-162	21404450+5731314	17.974	1.269	2.285	14.044±0.030	13.144±0.037	12.588±0.029	RI
22-939	21404883+5724186	17.575	1.039	2.089	14.266±0.035	13.507±0.038	13.210±0.039	—
23-753	21405391+5736199	18.083	1.103	2.069	14.664±0.027	13.855±0.043	13.663±0.054	RI
53-1561	21405592+5717591	17.855	1.265	2.412	13.814±0.027	12.830±0.035	12.245±0.024	—
22-445	21405869+5721095	17.902	1.073	2.396	13.906±0.034	13.104±0.042	12.818±0.023	No
22-1526	21410212+5728220	17.759	0.899	2.197	14.383±0.062	13.476±0.059	13.382±0.051	RI
22-404	21410970+5720507	16.020	0.645	1.513	13.479±0.027	12.892±0.035	12.681±0.035	—
23-969	21411497+5738149	16.385	1.104	1.874	13.144±0.026	12.325±0.032	11.919±0.021	RI
22-960	21411523+5724256	18.234	1.126	2.560	14.222±0.050	13.364±0.049	13.107±0.046	RI
22-1569	21411837+5728433	17.578	0.881	2.494	13.607±0.032	12.826±0.033	12.578±0.030	No
23-798	21412864+5736432	18.755	1.332	2.395	14.410±0.022	13.533±0.035	12.820±0.030	RI
43-795	21434932+5719208	17.099	1.055	2.079	13.376±0.026	12.582±0.031	12.331±0.019	—

Note. — Summary of 4Shooter optical and 2MASS near-IR data for Tr37. ID1 correspond to the 4Shooter ID, 2MASS is the 2MASS identification for each star. Errors are given for the 2MASS magnitudes; lack of definite errors in 2MASS is an indication of possible problems in the photometry. Photometric errors in the 4Shooter visual magnitudes are very small, the larger deviations are produced by the intrinsic variability of the stars. Optical variability (see text): RI=observed significant variability (over 3σ) in both R and I bands, I=observed significant variability in I band, No=no significant (over 3σ) variations detected in our variability study.

Table 2.4. Summary of Optical and Near-IR Observations for Low-Mass Stars in NGC 7160.

ID1	2MASS	V	V-R	V-I	J	H	K	Variability
14-655	21502124+6242386	16.745	0.812	1.617	14.058±0.033	13.509±0.037	13.361±0.039	—
11-195	21503036+6226092	16.322	0.788	1.583	13.590±0.029	12.990±0.032	12.725±0.027	—
11-327	21503429+6227286	18.202	1.012	2.012	14.870±0.042	13.988±0.049	13.807±0.054	—
12-825	21510326+6231312	17.646	0.978	2.003	14.259±0.035	13.649±0.037	13.444±0.040	—
12-102	21511680+6225011	16.638	0.769	1.560	13.914±0.024	13.489±0.039	13.308±0.037	—
14-1139	21512919+6235018	20.323	—	2.731	16.117±0.100	15.156±0.095	14.924±0.118	—
12-436	21513816+6227375	18.059	1.155	2.251	14.368±0.033	13.575±0.038	13.454±0.048	—
12-255	21514828+6225571	19.331	1.392	2.611	15.212±0.050	14.380±0.056	14.153±0.068	—
04-575	21521069+6242023	18.739	1.408	2.972	14.272±0.032	13.647±0.033	13.368±0.032	No
13-440	21521255+6240396	16.574	0.989	1.901	13.149±0.027	12.381±0.031	12.141±0.024	—
12-595	21521911+6229247	17.757	1.014	1.923	14.506±0.045	13.849±0.044	13.639±0.048	—
12-515	21522365+6220507	18.416	—	2.432	14.671±0.039	13.891±0.039	13.562±0.051	—
13-1033	21522548+6246075	18.397	1.080	2.053	14.870±0.040	14.161±0.054	13.993±0.053	No
01-2152	21523220+6233574	19.834	1.151	2.531	15.585±0.064	15.095±0.097	14.799±0.108	No
01-201	21523238+6225432	18.629	1.118	2.476	14.889±0.043	14.240±0.051	13.929±0.056	R
04-882	21524777+6245060	16.951	0.912	1.751	14.199±0.040	13.482±0.045	13.264±0.043	No
01-172	21530238+6225275	17.903	1.105	2.102	14.616±0.038	13.810±0.040	13.577±0.044	No
01-554	21530828+6226234	18.080	0.932	1.790	14.965±0.045	14.116±0.053	13.952±0.059	No
01-820	21531029+6230597	17.403	0.950	1.914	14.296±0.035	13.667±0.036	13.415±0.043	RI
01-1275	21531504+6235066	17.438	0.806	1.847	14.203±0.032	13.432±0.036	13.185±0.035	No
12-1055	21531671+6222577	19.460	—	2.538	15.268±0.052	14.429±0.065	14.276±0.078	No
01-1152	21531982+6234004	18.574	1.204	2.388	14.930±0.044	14.078±0.050	13.764±0.043	No
04-396	21532370+6238060	20.644	1.914	3.837	14.949±0.046	14.287±0.052	13.888±0.054	No
01-827	21533467+6231039	18.330	1.196	2.498	14.339±0.037	13.604±0.040	13.382±0.044	I
01-2313	21533601+6234403	19.420	1.298	2.999	14.758±0.039	14.025±0.047	13.742±0.046	RI
01-580	21533707+6228469	16.937	0.979	1.883	13.707±0.029	12.887±0.031	12.301±0.025	R
01-459	21534202+6227526	17.304	1.008	1.948	13.967±0.039	13.218±0.041	12.997±0.033	No
03-879	21535567+6245296	16.615	0.812	1.550	13.987±0.030	13.315±0.033	13.139±0.028	R
02-734	21535629+6231406	17.374	1.106	2.154	13.861±0.032	13.099±0.035	12.848±0.028	R
03-26	21540786+6236189	17.806	1.041	2.007	14.602±0.053	13.764±0.056	13.621±0.049	R
03-331	21541054+6239542	17.712	1.041	2.023	14.403±0.043	13.579±0.044	13.418±0.033	No
02-833	21542552+6232418	16.329	0.829	1.652	13.475±0.033	12.791±0.035	12.639±0.028	R
02-936	21544147+6233446	17.750	1.191	2.346	13.904±0.026	13.130±0.035	12.910±0.026	R
02-812	21544457+6232283	17.427	1.091	2.170	13.832±0.030	12.995±0.033	12.707±0.028	R
54-867	21555124+6246022	16.398	0.838	1.668	13.696±0.027	12.986±0.033	12.828±0.032	—

Note. — Summary of 4Shooter optical and 2MASS near-IR data for NGC 7160. ID1 correspond to the 4Shooter ID, 2MASS is the 2MASS identification for each star. Errors are given for the 2MASS magnitudes; lack of definite errors in 2MASS is an indication of possible problems in the photometry. Photometric errors in the 4Shooter visual magnitudes are very small, the larger deviations are produced by the intrinsic variability of the stars. Optical variability (see text): RI=observed significant variability (over 3σ) in both R and I bands, I=observed significant variability in I band, No=no significant (over 3σ) variations detected in our variability study.

Table 2.5. Summary of IRAC and MIPS Observations for Low-Mass Stars in Tr37.

ID1	3.6 μm	4.5 μm	5.8 μm	8.0 μm	24.0 μm	Comment
73-758	—	11.95±0.052	—	10.347±0.042	6.723±0.016	CTTS
72-489	—	—	—	—	—	NoMIPS
72-1427	—	—	—	—	6.701±0.020	NoIRAC
81-541	—	—	—	—	6.798±0.018	NoIRAC
73-472	—	11.257±0.038	—	10.924±0.055	6.149±0.010	
73-311	—	11.891±0.051	—	10.809±0.055	8.151±0.052	
73-71	13.221±0.078	11.116±0.036	12.395±20.756	11.196±0.065	7.938±0.061	
72-875	—	—	—	—	5.872±0.037	NoIRAC
73-194	13.89±0.101	13.985±0.133	13.22±0.130	12.307±0.148	—	e8
73-537	12.557±0.055	12.645±0.072	11.601±19.962	10.849±0.080	—	
21362507+5727502	12.723±0.116	12.251±0.117	11.834±0.119	10.621±0.094	7.236±0.033	
14-306	12.408±0.053	12.496±0.068	10.39±0.039	8.73±0.030	—	
21364596+5729339	9.956±0.033	9.326±0.030	8.278±0.024	7.573±0.027	1.783±0.002	cI
21364762+5729540	10.061±0.034	9.625±0.035	9.22±0.039	8.772±0.059	—	
14-141	9.939±0.033	9.45±0.032	9.198±0.066	8.694±0.176	6.014±0.434	CTTS,Gl
14-1229	13.385±0.159	13.393±0.201	13.515±0.263	13.368±0.344	—	
11-2146	10.365±0.020	9.885±0.020	9.588±0.022	8.72±0.020	4.951±0.007	
11-1209	10.962±0.051	10.655±0.056	10.334±0.060	9.907±0.066	7.814±0.035	CTTS
21365947+5731349	11.819±0.077	11.51±0.084	10.705±0.086	9.204±0.076	5.641±0.113	
11-1659	12.558±0.055	12.494±0.067	12.445±0.083	12.312±0.108	—	
11-1499	11.726±0.073	11.838±0.097	11.625±0.109	11.602±0.148	—	
11-2322	11.245±0.030	10.958±0.033	10.576±0.034	9.955±0.035	6.887±0.037	Gl
11-1871	13.019±0.068	12.999±0.084	12.976±0.106	12.423±0.217	—	WTTS,e8
14-222	92.604±9.999	11.107±0.071	10.853±0.077	10.019±0.072	—	e8
14-287	11.18±0.029	10.764±0.030	10.381±0.032	9.723±0.033	6.144±0.054	Gl
11-2037	11.061±0.027	10.784±0.030	10.597±0.035	9.706±0.033	5.777±0.010	
11-1067	13.644±0.090	13.649±0.114	14.032±0.184	15.387±1.211	—	
21370936+5729483	11.335±0.061	10.952±0.064	10.457±0.064	9.613±0.062	5.731±0.034	
14-11	11.763±0.038	11.627±0.045	11.214±0.049	10.621±0.063	6.015±0.075	TO,Gl
14-125	11.349±0.031	11.041±0.034	10.551±0.035	9.857±0.036	5.768±0.047	Gl
11-1513	12.225±0.047	12.257±0.060	12.278±0.076	12.467±0.121	—	
11-2131	11.022±0.027	10.649±0.029	10.373±0.031	9.814±0.035	6.290±0.013	
11-2397	12.006±0.083	11.535±0.085	11.333±0.095	10.654±0.099	6.998±0.025	
11-2487	12.75±0.060	12.786±0.077	12.816±0.098	13.11±0.287	—	
11-2031	10.657±0.044	10.287±0.047	9.935±0.050	8.834±0.041	5.195±0.012	
14-103	13.233±0.075	13.318±0.099	13.69±0.158	15.499±1.001	—	
14-197	12.538±0.054	12.556±0.069	12.554±0.087	12.427±0.122	—	
21372447+5731359	12.785±0.121	12.512±0.135	12.135±0.141	11.143±0.122	7.135±0.027	
14-160	11.055±0.027	10.766±0.030	10.396±0.032	9.618±0.031	6.073±0.012	
11-2503	12.344±0.097	—	12.358±0.153	12.405±0.213	—	
11-581	11.794±0.075	11.923±0.101	11.797±0.118	11.736±0.156	—	
14-1017	12.197±0.091	11.851±0.097	11.537±0.104	10.885±0.106	7.818±0.042	
14-335	10.738±0.024	10.372±0.025	10.027±0.027	9.269±0.025	5.730±0.013	
11-1864	12.923±0.127	12.897±0.159	12.848±0.192	12.484±0.123	—	WTTS
83-343	—	—	—	—	—	NoIRAC
14-183	10.896±0.025	10.791±0.031	10.655±0.036	10.265±0.041	6.382±0.015	P
14-2148	12.953±0.065	12.997±0.084	12.746±0.095	12.266±0.106	—	e8
21374275+5733250	9.818±0.030	—	8.765±0.029	7.836±0.026	4.196±0.013	
11-1384	12.346±0.049	12.36±0.063	12.244±0.074	12.428±0.112	—	
11-383	11.76±0.074	11.306±0.076	10.898±0.078	9.985±0.069	6.685±0.015	
11-2318	12.465±0.103	12.615±0.140	12.425±0.160	12.311±0.204	—	
13-924	12.362±0.050	12.378±0.063	12.401±0.083	12.294±0.105	—	
12-1984	12.098±0.044	12.134±0.057	12.112±0.071	12.237±0.109	—	
12-2519	12.05±0.043	11.835±0.049	11.536±0.054	10.859±0.054	7.098±0.031	
12-1968	10.416±0.020	10.369±0.025	10.224±0.029	10.397±0.043	7.636±0.025	
12-1422	13.013±0.133	13.005±0.167	12.969±0.205	13.08±0.298	—	WTTS
12-1091	11.237±0.030	10.952±0.033	10.616±0.035	9.78±0.032	6.410±0.013	

Table 2.5 (continued)

ID1	3.6 μm	4.5 μm	5.8 μm	8.0 μm	24.0 μm	Comment
13-269	11.875±0.040	11.853±0.050	11.828±0.061	11.87±0.086	—	
12-583	11.972±0.082	92.098±9.999	11.839±0.120	11.67±0.151	—	
12-94	12.809±0.061	12.901±0.081	12.697±0.092	12.541±0.127	—	e8
13-1238	11.489±0.033	11.164±0.036	10.795±0.038	9.959±0.035	6.525±0.014	
12-2373	12.393±0.051	12.361±0.063	12.138±0.071	12.121±0.100	—	
82-272	10.271±0.019	9.925±0.020	9.629±17.989	8.834±0.021	4.936±0.006	
12-1081	13.439±0.082	13.49±0.106	13.515±0.139	13.167±0.188	—	
13-1161	13.11±0.071	13.128±0.090	13.083±0.113	12.861±0.141	—	
12-1613	12.919±0.127	12.895±0.159	12.892±0.197	12.817±0.258	—	WTTS
13-1426	11.78±0.075	11.418±0.080	11.152±0.087	10.595±0.091	7.523±0.022	
13-669	10.969±0.051	10.603±0.055	10.273±0.058	9.367±0.052	6.599±0.016	
13-350	13.076±0.070	13.048±0.087	12.721±0.094	12.263±0.105	—	CTTS
12-1017	12.666±0.057	12.654±0.072	12.672±0.092	12.51±0.128	—	
54-1781	12.468±0.104	12.238±0.119	11.961±0.129	11.473±0.139	8.293±0.035	
13-1877	10.869±0.025	10.529±0.027	10.105±0.028	9.302±0.026	5.764±0.009	
13-277	7.684±0.011	7.286±0.012	6.643±0.011	5.872±0.010	2.412±0.002	
13-2236	12.89±0.064	12.994±0.084	13.01±0.108	13.346±0.178	—	
12-1009	10.463±0.021	10.494±0.027	10.426±0.032	11.525±0.075	—	
13-819	12.144±0.045	12.135±0.057	12.145±0.071	12.313±0.111	—	WTTS
12-1955	13.108±0.070	13.149±0.091	13.099±0.113	13.033±0.153	—	
13-236	10.471±0.041	10.037±0.042	9.702±0.045	9.166±0.047	6.849±0.016	
12-2113	10.725±0.023	10.308±0.024	9.83±0.024	8.907±0.022	5.804±0.009	
13-157	10.324±0.019	10.035±0.022	9.814±0.024	9.218±0.025	6.237±0.011	
13-232	10.475±0.021	10.044±0.022	9.706±0.023	9.173±0.024	—	P
21383216+5726359	12.476±0.103	12.121±0.111	11.965±0.129	11.462±0.138	—	
13-52	12.493±0.053	12.451±0.066	12.272±0.076	11.551±0.075	8.142±0.032	TO
12-1825	13.674±0.184	13.637±0.230	12.664±0.195	13.209±0.317	—	WTTS
91-155	11.137±0.028	10.849±0.031	10.714±19.075	9.855±0.033	6.145±0.010	CTTS,P
13-566	12.784±0.120	12.816±0.153	12.687±0.183	12.03±0.182	—	e8
13-1891	12.546±0.108	12.28±0.121	11.947±0.128	11.61±0.148	—	
13-1709	12.753±0.060	12.793±0.077	12.762±0.095	12.727±0.130	—	
54-1613	12.653±0.057	12.676±0.073	12.579±0.088	12.028±0.099	—	
21384350+5727270	12.750±0.118	12.453±0.130	12.000±0.132	11.585±0.146	8.536±0.050	
54-1547	11.674±0.036	11.431±0.041	11.219±0.046	10.379±0.043	6.502±0.016	
12-2363	12.519±0.054	12.477±0.067	12.055±0.071	12.248±0.133	—	
12-595	14.022±0.215	13.968±0.266	13.962±0.181	13.184±0.165	—	
12-1423	12.394±0.051	12.414±0.064	12.378±0.080	12.311±0.110	—	
12-1010	12.603±0.056	12.366±0.063	12.247±0.076	11.628±0.081	—	
12-2098	7.755±0.006	7.485±0.007	9.433±0.021	5.246±0.004	—	
13-1087	12.061±0.043	12.114±0.056	12.039±0.068	11.917±0.091	—	
21385669+5730484	12.702±0.117	12.501±0.135	12.068±0.140	11.523±0.146	—	CTTS
91-506	11.704±0.037	11.441±0.041	11.134±19.495	10.472±0.046	6.819±0.015	
24-692	13.211±0.074	13.303±0.097	13.435±0.131	13.658±0.213	—	
12-1027	13.083±0.138	13.073±0.172	13.103±0.219	12.909±0.269	—	WTTS
21390321+5730420	12.492±0.105	12.249±0.118	11.922±0.126	11.417±0.137	8.269±0.055	
24-77	12.811±0.062	12.788±0.078	12.898±0.106	13.206±0.207	—	
24-108	12.61±0.056	12.595±0.070	12.59±0.089	12.504±0.127	—	
12-1617	11.86±0.040	11.646±0.045	11.381±0.050	10.868±0.054	7.146±0.017	
21-840	12.474±0.103	12.302±0.120	12.002±0.129	11.365±0.131	—	
13-1048	11.721±0.073	11.479±0.082	11.318±0.094	10.795±0.100	6.770±0.014	
13-1250	11.424±0.032	11.258±0.038	10.988±0.041	9.836±0.033	5.917±0.009	TO
12-705	12.483±0.053	12.467±0.066	12.378±0.080	12.062±0.096	—	
12-942	12.218±0.047	12.162±0.057	12.149±0.071	12.123±0.097	—	
91-815	12.744±0.060	12.732±0.075	12.907± . . .	12.443±0.129	—	e8
21-1590	13.093±0.070	13.116±0.089	13.397±0.132	13.64±0.206	—	
54-1488	12.491±0.104	12.311±0.120	11.601±0.108	11.244±0.123	8.463±0.049	
24-542	12.044±0.084	12.068±0.108	11.969±0.127	11.908±0.171	—	

Table 2.5 (continued)

ID1	3.6 μm	4.5 μm	5.8 μm	8.0 μm	24.0 μm	Comment
24-515	12.826±0.062	12.644±0.072	12.463±0.085	11.651±0.087	7.876±0.027	
21-998	11.706±0.037	11.369±0.040	11.031±0.042	10.5±0.045	6.827±0.020	
21-33	12.842±0.123	12.532±0.134	12.265±0.146	11.551±0.142	8.575±0.043	
24-170	12.48±0.053	12.467±0.066	12.442±0.081	12.416±0.111	—	TO
53-1803	13.509±0.085	13.963±0.135	12.204±0.075	14.126±0.273	—	
24-48	13.095±0.070	13.099±0.089	13.028±0.110	13.13±0.162	—	
21-833	12.624±0.111	12.633±0.140	12.631±0.174	12.877±0.266	—	
21-230	13.255±0.077	13.257±0.099	13.471±21.832	14.038±0.278	—	
92-393	12.408±0.051	12.237±0.059	12.064±20.425	11.504±0.072	—	WTTS
21-1536	12.577±0.109	12.366±0.124	12.114±0.137	11.158±0.120	7.499±0.025	
52-1649	13.29±0.152	—	—	—	—	
21-2251	12.847±0.062	12.878±0.080	12.775±0.096	12.944±0.145	—	
24-820	—	—	—	—	—	NoMIPS
21-1586	13.326±0.155	13.337±0.197	13.452±0.261	13.35±0.349	—	WTTS
24-78	12.578±0.055	12.622±0.071	12.127±0.071	12.358±0.108	—	
92-1162	12.582±0.055	12.521±0.068	12.351±20.711	11.974±0.091	—	NoMIPS,e8
53-1762	12.682±0.058	12.425±0.065	12.08±0.070	11.687±0.079	—	CTTS
93-361	—	—	—	—	—	NoMIPS
21-1974	11.956±0.081	—	11.544±0.104	10.996±0.110	—	
21-1692	13.283±0.152	13.279±0.191	13.237±0.234	13.389±0.340	—	
21-763	12.998±0.067	13.064±0.087	12.302±0.077	13.488±0.187	—	
24-817	13.001±0.067	13.000±0.084	12.994±0.107	13.011±0.160	—	
21-895	12.423±0.051	12.47±0.066	12.296±0.077	12.106±0.098	—	
21400451+5728363	11.165±0.056	10.873±0.062	10.363±0.060	9.477±0.054	6.521±0.013	
21-1762	12.554±0.055	12.521±0.068	12.519±0.086	12.517±0.122	—	
24-382	13.173±0.073	13.184±0.092	13.229±0.119	13.209±0.167	—	
24-1736	12.369±0.098	12.062±0.107	11.898±0.124	11.414±0.136	—	
24-1796	12.466±0.052	12.33±0.062	12.191±0.074	11.64±0.082	—	e8
21-2006	11.687±0.037	11.38±0.040	11.098±0.044	10.287±0.041	7.472±0.021	CTTS
22-2651	11.812±0.039	11.442±0.041	11.221±0.046	10.777±0.051	7.686±0.025	
21402192+5730054	12.422±0.101	12.272±0.119	11.932±0.126	11.257±0.124	8.556±0.042	CTTS
92-1103	—	—	—	—	—	NoMIPS
22-1418	12.28±0.048	12.117±0.056	11.751±0.059	11.328±0.066	—	CTTS
23-405	11.407±0.032	11.118±0.036	10.862±0.039	10.72±0.051	7.540±0.027	
23-570	11.754±0.038	11.444±0.041	11.054±0.043	10.433±0.044	—	
93-540	—	—	—	—	—	NoMIPS
53-1843	12.926±0.065	12.981±0.084	12.99±0.105	13.158±0.160	—	
21403721+5729127	12.877±0.126	12.515±0.134	12.094±0.137	11.238±0.124	8.290±0.034	
93-168	—	—	—	—	—	NoMIPS
23-162	11.841±0.039	11.489±0.042	11.158±0.045	10.353±0.042	7.284±0.021	CTTS
22-939	13.336±0.153	13.383±0.198	13.293±0.235	13.323±0.327	—	
23-753	13.68±0.093	13.531±0.112	13.825±0.193	14.057±0.317	—	NoMIPS
23-1161	—	—	—	—	—	NoMIPS
53-1561	11.52±0.066	—	11.044±0.083	—	7.065±0.016	
22-445	12.951±0.066	12.884±0.081	12.884±0.107	11.285±0.219	—	
22-1526	13.156±0.072	13.253±0.095	13.312±0.125	14.077±0.274	—	
22-404	12.802±0.120	—	12.573±0.170	—	—	
23-969	—	—	—	—	—	NoMIPS
22-960	11.531±0.034	11.657±0.045	11.604±0.055	11.466±0.070	—	
22-1569	12.658±0.057	12.65±0.072	12.621±0.090	12.269±0.111	—	
23-798	—	—	—	—	—	NoMIPS
43-795	—	—	—	—	—	NoMIPS

Note. — Summary of IRAC and MIPS data for Tr37. A comment was added when the star is not contained in the MIPS field (NoMIPS) or in the IRAC field (NoIRAC). Note that all the stars not contained in the MIPS field are out of the IRAC field as well, with the exception of 23-753 and 92-1162, and that stars near the edges of the IRAC field lack in many cases of either 3.6 and 5.8 μm or 4.5 and 8.0 μm observations. Further comments were included according to: Gl=star related to the globule; cI=class I star; TO= transition object, or WTTS with disk; CTTS=star has been re-classified as CTTS; WTTS=star has been re-classified as WTTS; e8=small excess at 8.0 μm but no other wavelengths; P=IRAC and optical/JHK magnitudes do not match, possible problems or strong variations.

Table 2.6. Summary of IRAC and MIPS Observations for Low-Mass Stars in NGC 7160 .

ID1	3.6 μm	4.5 μm	5.8 μm	8.0 μm	24.0 μm	Comment
14-655	—	—	—	—	—	NoIRAC
11-195	—	—	—	—	—	NoIRAC
11-327	—	—	—	—	—	NoIRAC
12-825	13.538±0.011	13.612±0.016	13.596±0.048	13.424±0.057	—	
12-102	—	—	—	—	—	NoIRAC
14-1139	—	—	—	—	—	NoIRAC
12-436	13.605±0.011	13.636±0.016	13.526±0.046	13.58±0.053	—	
12-255	14.273±0.016	14.367±0.023	14.185±0.070	13.932±0.073	—	
04-575	13.445±0.013	13.496±0.016	13.448±0.048	13.51±0.058	—	
13-440	12.375±0.006	12.411±0.009	12.354±0.024	12.343±0.025	—	
12-595	13.937±0.013	13.985±0.019	13.934±0.060	13.985±0.079	—	
12-515	—	—	—	—	—	NoMIPS
13-1033	13.945±0.016	14.023±0.023	13.785±0.064	13.825±0.090	—	
01-2152	—	—	—	—	—	NoIRAC
01-201	13.951±0.015	13.979±0.019	14.014±0.068	13.762±0.086	—	
04-882	13.329±0.011	13.322±0.014	13.182±0.037	12.945±0.048	—	
01-615	11.825±0.005	11.79±0.007	11.767±0.018	11.745±0.017	—	
04-537	12.135±0.006	12.241±0.009	12.166±0.027	12.203±0.024	—	
04-521	12.274±0.006	12.336±0.009	12.272±0.023	12.256±0.022	—	
01-172	13.776±0.013	13.789±0.017	13.882±0.059	14.01±0.080	—	
04-1027	12.134±0.006	12.192±0.008	12.17±0.022	12.192±0.022	—	
01-554	14.076±0.008	14.157±0.012	14.066±0.049	13.632±0.049	—	e8
01-820	13.58±0.012	13.591±0.016	13.548±0.048	13.613±0.058	—	
01-1275	13.2±0.011	13.236±0.014	13.171±0.044	13.12±0.039	—	
12-1055	—	—	—	—	—	
01-1152	13.587±0.025	13.325±0.020	12.749±0.049	11.914±0.027	9.582±0.084	TO
04-396	13.959±0.015	13.859±0.018	13.863±0.059	14.21±0.095	—	
01-1164	12.285±0.006	12.374±0.009	12.29±0.024	12.326±0.024	—	
01-827	13.455±0.011	13.487±0.015	13.44±0.045	13.415±0.049	—	
01-2313	13.729±0.013	13.726±0.018	13.779±0.053	13.87±0.068	—	
01-580	11.672±0.005	11.387±0.006	11.237±0.014	10.674±0.009	8.565±0.036	
01-459	—	—	—	—	—	NoIRAC
03-180	12.098±0.006	12.092±0.008	12.092±0.021	12.032±0.020	—	
03-879	13.356±0.011	13.445±0.015	13.386±0.044	13.698±0.073	—	
02-734	13.022±0.009	13.067±0.012	12.973±0.034	12.934±0.034	—	
03-654	11.18±0.004	11.242±0.005	11.222±0.014	11.204±0.012	—	
03-228	12.07±0.006	12.116±0.008	12.14±0.022	12.085±0.020	—	
03-835	11.198±0.004	11.263±0.005	11.237±0.014	11.241±0.012	—	
03-26	13.667±0.007	13.72±0.009	13.793±0.038	14.155±0.091	—	
03-331	13.539±0.011	13.623±0.016	13.533±0.046	13.997±0.071	—	
03-479	11.968±0.005	12.046±0.007	11.987±0.020	11.99±0.019	—	
02-833	12.773±0.008	12.89±0.011	12.814±0.030	12.706±0.029	—	
02-936	13.083±0.010	13.115±0.013	13.077±0.036	13.033±0.038	—	
02-812	12.979±0.009	13.01±0.012	12.908±0.033	12.956±0.036	—	
03-193	10.807±0.003	10.844±0.004	10.804±0.011	10.794±0.010	—	
03-791	11.951±0.006	12.014±0.008	11.732±0.019	11.8±0.020	—	
03-500	11.481±0.004	11.527±0.006	11.479±0.015	11.464±0.014	—	
54-867	13.016±0.009	13.064±0.012	13.042±0.036	12.989±0.035	—	

Note. — Summary of IRAC and MIPS data for NGC 7160. A comment was added when the star is not contained in the MIPS field (NoMIPS) or in the IRAC field (NoIRAC). Further comments were included according to: Gl=star related to the globule; TO= transition object, or WTTS with disk; e8=small excess at 8.0 μm but no other wavelengths.

Table 2.7. Summary of IRAC and MIPS Observations for High- and Intermediate-Mass Stars in Tr37.

ID1	3.6 μm	4.5 μm	5.8 μm	8.0 μm	24.0 μm	Comment
KUN-56	—	—	—	—	—	NoIRAC
KUN-58	—	—	—	—	—	NoIRAC
MVA-1312	—	—	—	—	6.482±0.063	D
KUN-314S	—	—	—	—	6.369±0.013	NoIRAC,Ae:,cH:
MVA-81	—	10.595±0.055	10.367±0.071	10.577±0.093	—	
MVA-63	—	—	—	—	—	
MVA-232	11.64±0.070	11.646±0.089	11.678±0.111	11.566±0.143	—	
SBZ-2-46	—	—	—	—	—	NoIRAC
MVA-182	—	—	—	—	—	NoIRAC
MVA-164	—	—	—	—	—	NoIRAC
MVA-252	—	—	—	—	—	NoIRAC
MVA-169	—	—	—	—	—	NoIRAC
MVA-234	—	—	—	—	—	NoIRAC
MVA-258	—	—	—	—	—	NoIRAC
KUN-318	11.5±0.065	11.542±0.084	11.572±0.106	11.538±0.145	—	
CCDM+5734Ae	7.964±0.013	8.018±0.017	7.927±0.020	7.745±0.025	4.660±0.025	D,(1)
CCDM+5734Aw	7.964±0.013	8.018±0.017	7.927±0.020	7.745±0.025	4.660±0.025	D,(1)
MVA-257	92.604±9.999	12.621±0.140	12.071±0.165	12.364±0.215	—	
MVA-224e	11.764±0.074	11.774±0.094	11.774±0.117	11.837±0.164	—	
MVA-468	10.195±0.036	10.01±0.041	9.879±0.048	9.733±0.061	7.876±0.026	D
MVA-426	—	—	—	—	2.916±0.002	cH
AG+561491	10.381±0.039	10.318±0.048	10.296±0.059	—	—	
MVA-545	—	—	—	—	—	NoIRAC
MVA-472	—	—	—	—	—	NoIRAC
KUN-191	12.165±0.089	12.201±0.115	12.236±0.145	12.143±0.189	—	
MVA-447	—	—	—	—	8.184±0.038	D
BD+572355	10.022±0.033	9.852±0.039	9.838±0.047	9.856±0.065	—	
MVA-276	—	—	—	—	—	NoIRAC
BD+572356	8.431±0.016	8.393±0.020	8.327±0.024	8.329±0.032	7.714±0.025	
MVA-523	—	—	—	—	—	NoIRAC
MVA-535	10.619±0.043	10.583±0.054	10.597±0.067	10.569±0.090	—	
MVA-564	—	—	—	—	—	NoIRAC
MVA-463	—	—	—	—	—	NoIRAC
MVA-437	10.464±0.041	10.422±0.050	10.402±0.062	10.397±0.083	—	
KUN-83	12.086±0.086	12.112±0.110	12.019±0.134	12.246±0.200	—	
MVA-566	—	—	—	—	—	NoIRAC
KUN-84	—	—	—	—	—	NoIRAC
MVA-497	—	—	—	—	—	NoIRAC
KUN-85	—	—	—	—	—	NoIRAC
KUN-327	—	—	—	—	—	NoIRAC
KUN-86	12.517±0.106	12.497±0.132	12.433±0.161	11.903±0.174	—	e8
KUN-87	—	—	—	—	—	NoIRAC
MVA-657	—	—	—	—	—	NoIRAC
MVA-660	—	—	—	—	—	NoIRAC
KUN-89	12.199±0.091	12.257±0.118	12.268±0.147	12.03±0.183	—	
MVA-640	—	—	—	—	—	NoIRAC
MVA-662	10.191±0.036	10.047±0.042	9.981±0.051	9.963±0.068	—	
MVA-641	—	—	—	—	—	NoIRAC
BD+572362	—	—	—	—	—	NoMIPS
KUN-196	11.429±0.063	11.277±0.075	10.993±0.081	10.565±0.090	—	Be
KUN-197	11.856±0.077	11.9±0.099	11.913±0.124	11.917±0.169	—	
KUN-198	11.518±0.066	11.517±0.083	11.306±0.106	11.276±0.127	—	
KUN-92	—	—	—	—	—	NoIRAC
KUN-93	11.781±0.075	11.787±0.094	11.82±0.119	11.717±0.154	—	
tr37-185	10.172±0.036	—	9.979±0.051	—	—	
KUN-97	—	—	—	—	—	NoIRAC
KUN-100	12.47±0.103	12.425±0.128	12.498±0.164	—	—	

Table 2.7 (continued)

ID1	3.6 μm	4.5 μm	5.8 μm	8.0 μm	24.0 μm	Comment
MVA-805	10.359±0.039	—	10.374±0.061	—	—	

Note. — IRAC and MIPS magnitudes for high- and intermediate-mass stars in Tr 37. A comment was added when a star is not contained in the MIPS (NoMIPS) or IRAC (NoIRAC) fields. Other comments: Ae/Be= A/B-type emission line star; cH= classical Herbig star; D= debris disk; e8= excess emission at 8 μm; :=uncertain value; (1)= for these close companions, it is unclear whether the Spitzer magnitudes measured belong to one, the other or both stars together.

Table 2.8. Summary of IRAC and MIPS Observations for High- and Intermediate-Mass Stars in NGC 7160 .

ID1	3.6 μm	4.5 μm	5.8 μm	8.0 μm	24.0 μm	Comment
DG-349	12.186±0.006	12.313±0.009	12.192±0.022	12.256±0.020	—	
DG-371	11.48±0.004	11.536±0.006	11.522±0.017	11.498±0.015	—	
DG-382	11.661±0.005	11.669±0.006	11.642±0.017	11.665±0.015	—	
DG-392	11.703±0.005	11.7±0.006	11.694±0.017	11.67±0.015	—	
DG-394	12.205±0.006	12.21±0.008	12.208±0.022	12.306±0.024	—	
DG-399	12.136±0.006	12.117±0.008	12.109±0.021	12.17±0.020	—	
DG-398	11.885±0.005	11.892±0.007	11.894±0.019	11.937±0.018	—	
DG-408	12.455±0.007	12.446±0.009	12.481±0.026	12.532±0.026	—	
DG-409	11.617±0.005	11.674±0.006	11.625±0.020	11.733±0.017	—	
DG-414	11.865±0.005	11.965±0.007	11.885±0.019	11.908±0.018	—	
DG-423	11.603±0.004	11.602±0.006	11.526±0.016	11.578±0.015	—	
DG-422	11.546±0.004	11.568±0.006	11.611±0.017	11.529±0.015	—	
DG-424	11.337±0.004	11.39±0.006	11.394±0.015	11.428±0.013	—	
DG-455	11.631±0.004	11.727±0.006	11.692±0.017	11.714±0.015	—	
DG-460	11.19±0.004	11.243±0.005	11.249±0.014	11.277±0.012	—	
DG-462	10.704±0.003	10.706±0.004	10.708±0.011	10.69±0.009	—	
DG-472	10.299±0.003	10.196±0.003	10.183±0.008	10.167±0.007	—	
DG-481	11.529±0.004	11.334±0.005	11.027±0.013	10.568±0.008	9.017±0.068	D
DG-513	9.437±0.002	9.284±0.002	9.057±0.005	9.054±0.004	8.555±0.037	
DG-526	11.736±0.005	11.701±0.006	11.697±0.017	11.825±0.021	—	
DG-529	11.058±0.004	11.085±0.005	11.035±0.014	11.104±0.017	—	
DG-531	9.806±0.002	9.583±0.002	9.473±0.006	9.497±0.005	10.344±0.157	
DG-533	11.911±0.006	11.933±0.007	11.952±0.020	11.971±0.020	—	
DG-40	10.976±0.003	11.007±0.005	10.986±0.012	11.019±0.011	—	
DG-67	12.393±0.006	12.376±0.009	12.34±0.024	12.308±0.023	—	
DG-603	11.952±0.005	11.984±0.007	11.976±0.020	11.96±0.018	—	
DG-41	11.039±0.003	11.044±0.005	11.036±0.013	11.072±0.011	—	
DG-64	12.186±0.006	12.219±0.008	12.131±0.027	12.109±0.024	—	
DG-644	11.89±0.005	11.949±0.007	11.929±0.019	11.984±0.019	—	
DG-39	11.699±0.006	11.674±0.007	11.631±0.018	11.545±0.016	8.642±0.041	D
DG-61	12.173±0.006	12.247±0.008	12.212±0.023	12.264±0.024	—	
DG-55	11.647±0.005	11.67±0.006	11.646±0.017	11.716±0.018	—	
DG-50	11.17±0.004	11.202±0.005	11.198±0.013	11.185±0.011	—	
DG-42	11.828±0.005	11.876±0.007	11.886±0.019	11.94±0.018	—	
DG-682	11.623±0.005	11.608±0.007	11.359±0.022	11.373±0.022	7.892±0.025	D
DG-685	12.58±0.007	12.689±0.010	12.604±0.030	12.732±0.031	—	
DG-45	11.606±0.004	11.64±0.006	11.617±0.017	11.711±0.016	—	
DG-687	12.034±0.005	12.104±0.008	12.072±0.021	12.07±0.024	—	
DG-49	11.941±0.005	12.004±0.007	11.972±0.020	11.997±0.017	—	
DG-47	11.875±0.005	11.904±0.007	11.809±0.020	11.842±0.019	—	
DG-720	11.43±0.004	11.433±0.006	11.444±0.016	11.434±0.015	—	
DG-725	12.608±0.007	12.611±0.010	12.575±0.027	12.688±0.034	—	
DG-56	11.701±0.005	11.718±0.006	11.724±0.017	11.755±0.016	—	
DG-48	11.927±0.005	11.97±0.007	11.943±0.019	11.925±0.020	—	
DG-36	11.045±0.004	11.116±0.005	11.065±0.013	11.156±0.012	—	
DG-58	11.612±0.004	11.626±0.006	11.617±0.017	11.682±0.017	—	
DG-37	10.79±0.003	10.795±0.004	10.785±0.011	10.836±0.010	—	
DG-32	10.363±0.003	10.325±0.003	10.274±0.009	10.308±0.007	—	
DG-62	11.324±0.004	11.246±0.005	11.159±0.013	11.12±0.011	—	e8
DG-60	11.966±0.005	11.983±0.007	11.979±0.020	11.989±0.019	—	
DG-794	12.512±0.007	12.499±0.009	12.421±0.025	12.485±0.027	—	
DG-65	12.413±0.007	12.446±0.009	12.384±0.024	12.418±0.023	—	
DG-59	11.839±0.005	11.894±0.007	11.863±0.019	11.939±0.019	—	
DG-57	12.091±0.006	12.096±0.008	12.091±0.021	12.111±0.021	—	
DG-825	10.839±0.003	10.875±0.004	10.832±0.011	10.847±0.011	—	
DG-853	12.368±0.007	12.329±0.009	12.294±0.025	12.19±0.022	—	
DG-52	11.503±0.004	11.493±0.006	11.513±0.016	11.564±0.014	—	

Table 2.8 (continued)

ID1	3.6 μm	4.5 μm	5.8 μm	8.0 μm	24.0 μm	Comment
DG-895	11.698±0.005	11.762±0.007	11.732±0.017	11.696±0.016	—	
DG-899	11.293±0.004	11.276±0.005	11.289±0.014	11.286±0.012	—	
DG-907	11.864±0.005	11.907±0.007	11.901±0.019	11.927±0.018	—	
DG-912	9.859±0.005	9.6±0.004	9.064±0.011	9.284±0.008	—	
DG-920	12.111±0.006	12.142±0.008	12.137±0.021	12.116±0.020	—	
DG-921	11.053±0.003	11.108±0.005	11.101±0.013	11.067±0.011	—	
DG-934	11.021±0.003	11.074±0.005	11.068±0.013	11.099±0.012	—	
DG-936	11.546±0.004	11.53±0.006	11.519±0.016	11.55±0.015	—	
DG-940	9.572±0.002	9.443±0.002	9.276±0.005	9.281±0.004	9.428±0.065	
DG-946	9.605±0.002	9.402±0.002	9.226±0.005	9.238±0.004	9.829±0.100	
DG-949	—	—	—	—	10.113±0.132	NoIRAC
DG-952	12.183±0.006	12.263±0.008	12.185±0.023	12.24±0.023	—	
DG-954	—	—	—	—	—	NoIRAC

Note. — IRAC and MIPS magnitudes for the high- and intermediate-mass stars in NGC 7160. A comment was added when a star is not contained in the MIPS (NoMIPS) or IRAC (NoIRAC) fields. Other comments: D= debris disk; e8= excess emission at 8 μm; :=uncertain value;

Table 2.9. Stars in the Tr 37 Globule.

ID	J	H	K	3.6 μm	4.5 μm	5.8 μm	8.0 μm	24.0 μm	Comment
21355793+5729099	15.910±0.089	15.182±0.107	14.354±0.092	13.420±0.180	12.794±0.158	12.469±0.224	11.433±0.355	8.412±0.688	ξ,II
21355905+5730233	14.499±0.047	13.864±0.057	13.402±0.046	12.827±0.125	12.582±0.140	12.298±0.151	11.583±0.157	11.833±5.008	II,Er
21360798+5726371	18.366± ...	17.484± ...	14.507±0.088	10.793±0.049	9.498±0.034	8.051±0.024	7.040±0.024	1.974±0.007	γ,I
21361420+5727379	10.088±0.022	9.226±0.028	8.960±0.020	9.736±0.030	9.486±0.034	9.270±0.038	9.193±0.052	—	P,II
—	—	—	—	12.706±0.121	11.030±0.067	9.551±0.044	8.645±0.051	3.312±0.014	ϵ,I
—	—	—	—	12.848±0.128	11.274±0.077	9.985±0.053	8.886±0.051	3.282±0.011	δ,I
21360389+5727121	14.700±0.042	13.077±0.037	12.297±0.024	11.909±0.082	12.031±0.106	11.161±0.122	10.060±0.177	5.744±0.105	II
21361664+5728404	17.017±0.198	14.958±0.086	14.026±0.056	12.694±0.120	12.014±0.107	11.308±0.112	10.528±0.168	5.085±0.030	I
21362368+5732452	14.685±0.045	13.650±0.045	13.105±0.035	12.710±0.119	12.508±0.135	12.309±0.175	11.775±0.323	7.922±0.342	II
21362507+5727502	14.952±0.044	14.031±0.048	13.518±0.040	12.765±0.123	12.292±0.123	11.833±0.122	10.727±0.105	7.236±0.033	II,(1)
21363300+5728493	15.816±0.076	14.827±0.070	14.220±0.064	13.761±0.197	13.369±0.204	13.120±0.382	—	—	P,II
21363531+5729311	14.059±0.044	12.825± ...	12.223± ...	11.688±0.077	11.399±0.083	10.994±0.165	10.418±0.435	4.031±0.034	II,Er
21363691+5731326	13.754±0.031	12.631±0.037	12.021±0.026	11.438±0.066	11.087±0.070	10.631±0.075	9.703±0.089	4.947±0.048	ι,II
21363841+5729174	14.265±0.027	13.013±0.031	12.303±0.025	11.670±0.074	11.274±0.077	11.071±0.102	10.617±0.225	—	II
21364146+5730278	15.921±0.081	14.293±0.058	13.542±0.040	12.707±0.129	12.360±0.131	11.393±0.173	9.966±0.214	5.174±0.059	II
21364165+5732175	16.147±0.102	14.901±0.085	13.796±0.046	13.008±0.139	12.627±0.143	11.890±0.144	10.693±0.156	5.868±0.141	II
21364398+5729287	14.232±0.027	13.012±0.031	12.364±0.024	11.875±0.081	11.455±0.083	11.095±0.095	10.506±0.136	4.868±0.038	II,Er
21364596+5729339	14.211±0.039	12.416±0.036	11.189±0.025	10.187±0.037	9.676±0.037	9.147±0.036	8.527±0.042	1.783±0.002	I,(1)
21364660+5729384	16.458± ...	15.194±0.187	12.673±0.038	9.897±0.032	8.863±0.025	7.302±0.015	6.696±0.017	1.674±0.002	α,I
21364941+5731220	11.918±0.022	10.914±0.029	10.355±0.021	10.099±0.036	9.528±0.034	9.018±0.034	8.329±0.039	6.014±0.435	LkHα349a,II,14-141
21365281+5729438	15.666±0.068	13.956±0.043	13.286±0.034	12.859±0.127	12.589±0.140	12.165±0.151	11.421±0.188	—	II
21365450+5730051	13.948±0.027	12.045±0.031	10.926±0.023	10.517±0.043	10.297±0.049	10.112±0.057	9.966±0.106	—	P,II:
21365520+5730301	14.714±0.078	12.665±0.063	11.382±0.034	10.175±0.037	9.643±0.036	9.049±0.035	8.280±0.041	4.853±0.076	β,II
21365543+5731391	14.199±0.032	12.456±0.029	11.723±0.021	11.429±0.068	11.534±0.086	10.887±0.145	9.658±0.208	—	II
21365698+5729227	16.991±0.187	14.564±0.057	13.195±0.030	11.612±0.072	11.216±0.073	10.717±0.093	9.516±0.118	4.980±0.068	II
21365783+5730561	17.425± ...	15.365±0.135	14.000±0.072	12.562±0.116	11.580±0.089	10.644±0.096	9.434±0.125	4.132±0.037	η ,I
21365793+5729107	13.621±0.028	12.025±0.032	11.215±0.023	10.652±0.046	—	9.726±0.047	8.944±0.048	5.193±0.129	ν,II
21365890+5730292	17.551± ...	16.181±0.218	14.615±0.093	12.606±0.122	12.345±0.127	10.507±0.097	9.219±0.126	5.069±0.101	I
21365947+5731349	14.520±0.034	13.403±0.038	12.765±0.028	12.116±0.093	11.713±0.095	11.429±0.127	10.227±0.130	5.641±0.113	II,(1)
21370191+5728222	12.854±0.029	11.969±0.033	11.560±0.025	11.173±0.058	10.949±0.064	10.572±0.067	9.949±0.068	6.887±0.037	II,11-2322
21370200+5731553	15.871±0.087	13.808±0.044	12.881±0.030	12.228±0.100	12.157±0.115	10.673±0.119	—	6.857±0.465	II
21370232+5731152	16.946± ...	15.588± ...	13.254±0.045	11.055±0.056	10.151±0.046	9.422±0.041	8.583±0.040	4.643±0.070	ζ,I
21370649+5732316	13.321±0.023	12.327±0.028	11.909±0.023	11.168±0.058	10.789±0.061	10.453±0.065	9.821±0.069	6.144±0.054	II,14-287
21370771+5732110	14.606±0.035	13.785±0.039	13.522±0.047	12.896±0.134	12.672±0.149	12.415±0.170	11.439±0.161	—	P,II
21370936+5729483	13.385±0.027	12.325±0.047	11.837±0.034	11.276±0.061	10.950±0.064	10.458±0.064	9.614±0.062	5.731±0.034	II,(1)
21370944+5730367	13.884±0.030	13.036±0.034	12.648±0.033	12.401±0.104	12.166±0.115	11.854±0.125	11.110±0.130	5.127±0.018	II,Er
21371013+5731266	14.972±0.045	14.241±0.055	13.806±0.059	13.391±0.167	13.133±0.183	12.859±0.203	—	—	II
21371031+5730189	13.057±0.029	12.216±0.034	11.956±0.026	11.683±0.074	11.604±0.087	11.082±0.091	10.610±0.122	6.015±0.075	II,14-11

Table 2.9 (continued)

ID	J	H	K	3.6 μm	4.5 μm	5.8 μm	8.0 μm	24.0 μm	Comment
21371054+5731124	13.090±0.026	12.170±0.029	11.732±0.021	11.363±0.064	11.085±0.070	10.670±0.072	10.053±0.078	5.768±0.047	II,14-125

Note. — Stars with excesses found in the Tr 37 globule. ID and JHK magnitudes from 2MASS (Cutri et al., 2003); IRAC and MIPS magnitudes; Comment contains the ID from Reach et al. (2004), the type (II=class II, or classical T Tauri Star; I= class I protostar, := uncertain class) based on the IRAC colors and SEDs, and the ID of the optical counterpart, if there were any. P denotes the uncertain cluster members. (1)= Observed with Hectospec, confirmed member, no optical counterparts; Er=note that the errors at 24 μm may be larger than indicated because of the strong emission from the globule.

3 Tr 37

Published in "Low Mass Stars and Accretion at the Ages of Planet Formation in the Cep OB2 Region" by Sicilia-Aguilar, A., Hartmann, L., Briceño, C., Muzerolle, J., & Calvet, N., 2004, AJ128, 805; "Cep OB2: Disk Evolution and Accretion at 3-10 Myr", by Sicilia-Aguilar, A., Hartmann, L., Hernández, J., Briceño, C., & Calvet, N., 2005, AJ in press; and "Disk Evolution in Cep OB2: Results from Spitzer Space Telescope", by Sicilia-Aguilar, A., Hartmann, L., Calvet,N., Megeath, S.T., Muzerolle, J., Allen, L., D'Alessio, P., Merín B., and Stauffer, J., 2005, in preparation.

Tr 37 is the younger of the two known clusters in Cep OB2. Located at the rim of the Cep OB2 bubble, as if it had been triggered by the expansion and winds of NGC 7160, it contains the O6 star HD 206267 near its center, which produces the highly inhomogeneous H II region IC 1396. IR images reveal an important concentration of dust distributed mostly to the West of the O6 star. About 4 parsecs to the West of HD 206267, a bright dust globule is being blown away by the stellar winds of the high-mass star, which illuminates the structure (see Figure 3.1). With a dynamical age of ∼3 Myr (Patel et al., 1995, 1998), the existence of younger populations associated to the dust globule is suggested by the presence of several embedded protostars (Reach et al., 2004), maybe indicating a further episode of triggered star formation, or the continuation of the star formation processes that gave birth to HD 206267 and the rest of the cluster members.

3.1 Low-Mass Stars in Tr 37

3.1.1 Identification of Low-Mass Cluster Members

The membership of young, low-mass (G-M) stars can be established using low resolution, optical spectra. Two main features at optical wavelengths are used for the identification of the spectra of young stars: Hα emission at 6562 Å, and Lithium absorption at 6707 Å. Of all the lines that are produced in the magnetospheric accretion flows, Hα is the strongest one, and the best indicator of accretion processes (Calvet & Hartmann, 1992; Hartmann, 1998; Muzerolle et al., 1998a).

Hα emission (and, in general, all the Hydrogen Balmer series emission lines, which are not always detectable), is produced in the accreting columns of accreting, classical T Tauri stars (CTTS, see Calvet & Hartmann 1992, Hartmann et al. 1994, Hartmann 1998, Muzerolle et al. 1998). Weaker Hα emission is produced in the chromosphere of non-accreting, weak-lined T Tauri stars (WTTS). In the case of Hα emission from accretion processes, the large velocities

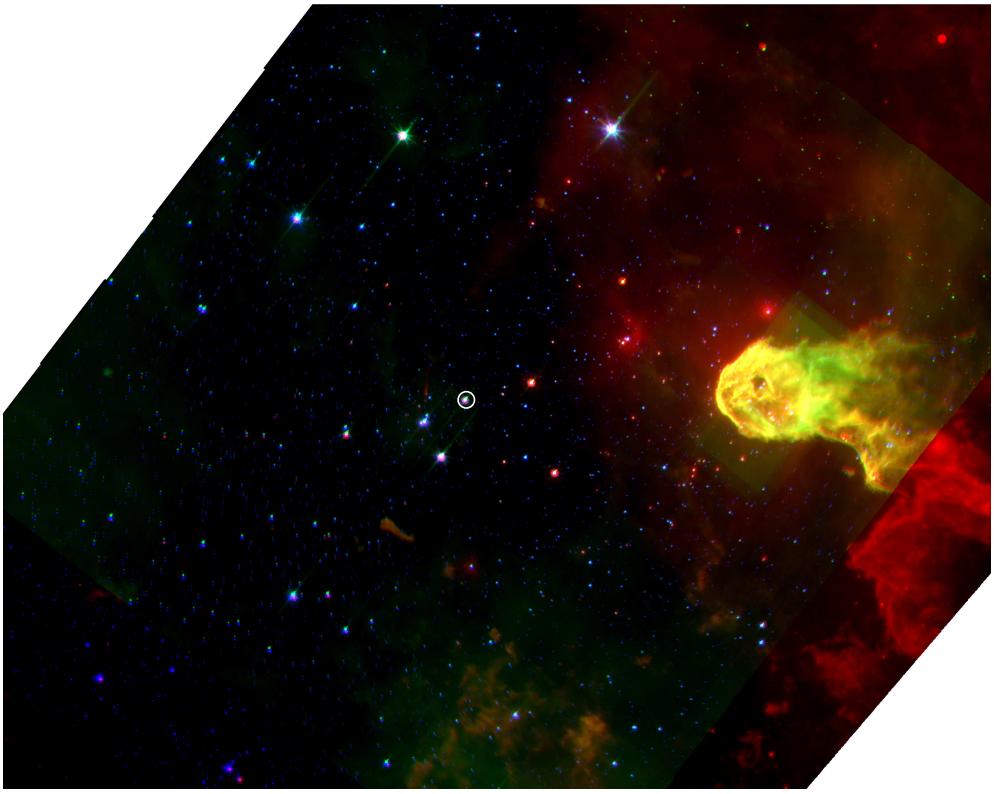

Figure 3.1 Composite image of Tr 37. Red =24 μm; Green=8.0 μm; Blue=3.6 μm. The white circle indicates the position of the O6 star HD 206267.

of the accreting material (that can be up to $\sim$200 $\mathrm{km\,s^{-1}}$) produce significant velocity wings and, in general, the equivalent width (EW) of the line is larger than what is observed in WTTS (Herbig & Bell, 1988; Hartmann, 1998; Muzerolle et al., 2001). Several criteria have been established to distinguish accreting and non-accreting stars based on their Hα EW (Herbig & Bell 1988; Hartmann 1998; Muzerolle et al. 2001). Here we use the criteria by White & Basri (2003), considering accreting CTTS those with Hα emission EW>20 for stars later than M2, EW>10 for spectral types M2-K5, and EW>3 for spectral types K5-G.

The main problem in the detection of Hα is that, very frequently, young stellar clusters are embedded in inhomogeneous H II regions, which produce highly variable emission in Hα over-imposed to the emission of the stars. A very careful background subtraction is required to avoid over- and under-subtraction of nebular Hα, since otherwise this could lead to confusion, affecting primarily the WTTSs. The background subtraction is an important problem in Tr 37, where the nebular emission is very strong and inhomogeneous; in contrast, there is no significant nebular emission in NGC7160, where we used a standard average sky spectra.

Using Hectospec spectra and their corresponding sky offset of $\sim$5 arcsec (producing sky spectra from a location very close to the star and with the same fiber), a very clean background subtraction is achieved, improving the identification of WTTSs in the cluster. Since it was observed that the multiple background and night sky lines are properly subtracted using this method, the error in the subtraction of nebular Hα is minimal, enabling to detect clearly EW

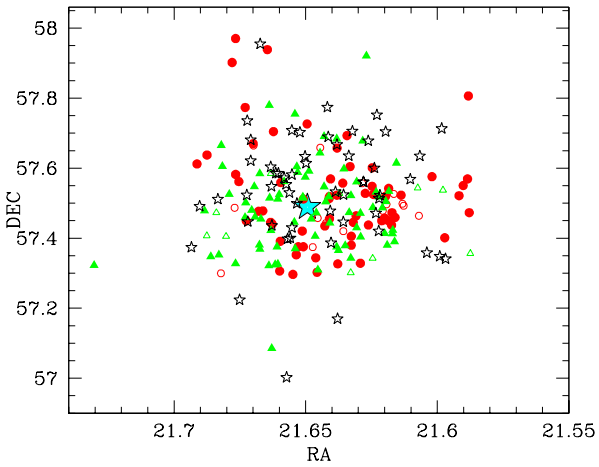

Figure 3.2 Tr 37 Members: CTTS are represented by red circles; WTTS are represented by green triangles; filled symbols denote confirmed members or those where Li absorption is detected in the Hectospec/Hydra/FAST spectra, open figures denote likely members where Li is not detectable due to poor signal-to-noise. The O6 star HD 206267 is depicted in blue. The rest of high- and intermediate-mass stars in the cluster are represented by open stars.

as low as ∼0.5 Å, and confirming the youth of the candidates with very low Hα EW via the presence of Li absorption.

The second indicator of the youth of low-mass stars is the Li absorption line at 6707Å, since Li is depleted from low-mass, partially convective stars in timescales ∼30 Myr (Strom et al., 1989; Briceño et al., 1997, 1998; Randich et al., 2001; Hartmann, 2003). Although Li EWs are usually $\sim 0.3 - 0.8$ Å in absorption, requiring good signal to noise in the 6707Å region, Li absorption is a very good criterion for determining the youth of the star, since it does not depend on the quality of the background subtraction as Hα does. It is also very efficient to distinguish contaminating dMe stars, of which we found a couple of dozens among the Hectospec spectra. These stars are foreground and background M type (sometimes late K) stars with weak Hα emission due to their chromospheric activity, but they are older and they do not show Li absorption. Unfortunately, the Li indicator cannot be used for stars with spectral types of early K or earlier, since it is not depleted with time in case of these earlier stars, and moreover the EW are at or under our detection levels (∼0.1Å).

Due to the poorer signal-to-noise, in some cases it was not possible to detect the Li absorption using the Hydra spectra. On the other hand, the stars targeted with FAST were brighter and did not show problems for Li detection (although most of the FAST targets were early K and G stars where no Li could be detected). The higher quality of the Hectospec spectra allowed to detect the Li line (or to determine the absence of it) in more than 90% of the stars, so both the contamination of our final member list and the rejection of members among the observed stars are very small, since we also re-observed with Hectospec most of the low signal-to-noise objects that had been observed with Hydra. In the few cases where some doubts arose, we additionally used the extinction values as an extra criterion for membership. We preferred to be conservative in the identification of members rather than to include low-probability members in the study.

The EW for the Hα and Li lines was measured using the task *splot* in the IRAF spectra

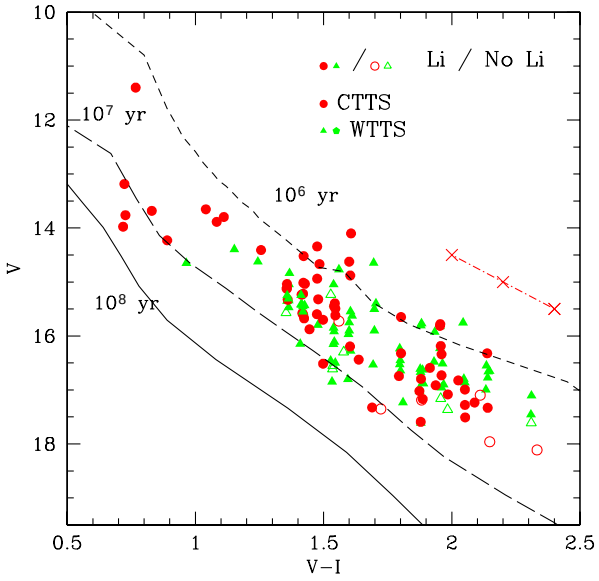

Figure 3.3 Low-Mass Stars: V vs. V-I diagram for all the low-mass members in Tr 37. Photometry from the 4Shooter/1.2m in FLWO. A reddening correction (Bessell & Brett, 1988) has been applied for each star using the individual reddenings; a reddening vector with X for A_V=0.5 intervals is represented as a dotted-dashed line. Isochrones from Siess et al. (2000) for 1, 10 and 100 Myr are shown. Red circles: CTTS; green triangles: WTTS. Filled symbols: Li was detected (for late-type stars), or confirmed membership based on extinction (see text, for G-type stars). Open symbols: Li was not detected due to poor signal-to-noise (in low-mass stars), or most likely membership (based on extinction, see text).

reduction package *noao.hydra*. All the low-mass stars identifications for which Li was detected are considered to be safe. Using Li, the authenticity of some of the weakest Hα measurements could be probed, concluding that Hα EWs as low as 0.5-1 Å are true detections and not background contamination.

The values of Hα and Li EWs for the low-mass members in Tr 37 are listed in Table 3.3, including the derived membership based on these detections. The 4Shooter V vs. V-I colors of the cluster members, compared to the isochrones by Siess et al. (2000), is shown in Figure 3.3. The J-H vs. H-K diagram constructed using the 2MASS colors (Cutri et al., 2003) is displayed in Figure 3.4.

Attending to the number of CTTS and WTTS in the central two fields (which reached a nearly complete coverage, see Section 3.3), we can estimate the disk fraction in Tr 37. Considering only the stars coming from the unbiased survey (excluding the 14 IRAC-selected objects), about 40-45% of the stars have disks. These numbers will be revised more carefully in Section 3.3.

3.1.2 Spectral Types

The spectral type classification of the stars was obtained via two different classification schemes, which are roughly equivalent for the later spectral types (K4 to M5). The two classification methods use similar schemes, although the second classification was generated

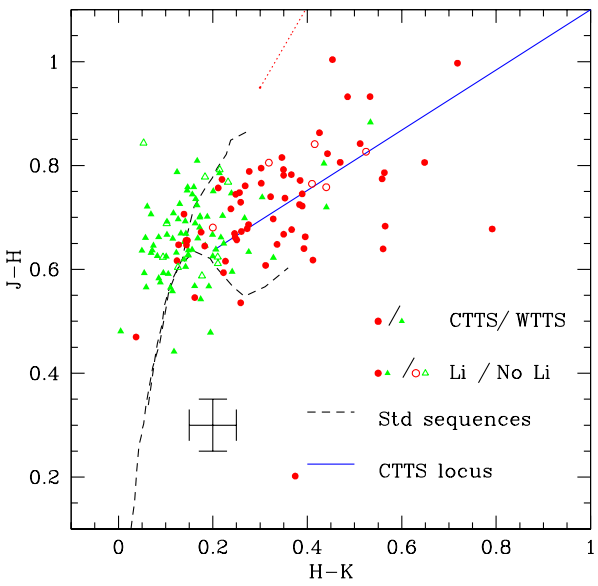

Figure 3.4 Low-Mass Stars: J-H vs. H-K diagram for all the low-mass members in Tr 37. JHK colors from the 2MASS survey (Cutri et al., 2003). Stars are dereddened using their individual A_V (Bessell & Brett, 1988). The Main Sequence and Giant Branch are represented as dashed lines; the CTTS locus starting for a K7 star (Meyer et al., 1997) is represented as a solid line stars with disks would deviate parallel to this line from their Main Sequence position. Symbols as in Figure 3.3.

as an extension of the first by Hernández et al. (2004), including more indices and a set of indicators in order to be able to classify early spectral types.

Classification of the Hydra Spectra for Low-Mass Stars

The first method for the spectral type classification was especially developed for the Hydra and FAST spectra obtained during the first years of this study. A set of strong features for the spectral classification was selected, together with the temperature range in which they are valid. These features are listed in Table 3.1.

The *splot* task in IRAF *onedspec* package allowed to define band and line widths, as well as the best places to measure the continuum. Indices were calculated as either flux ratios for band-like (broad) features ($I = F_c/F_f$), or line-flux to continuum ratios for line-like (narrow) features ($I = (F_f - F_c)/F_c$), where 'c' refers to continuum flux, and 'f' to feature flux. We measured the fluxes with the IRAF task *sband* in the *onedspec* package. The bands are broad enough to allow small wavelength variations of 2-3Å without losing a substantial part of the flux, and narrow enough to avoid contamination by other features. The continuum flux was obtained as average continuum on both sides of the feature, when it was possible.

The errors in the band measurements and indices were estimated assuming that the read noise of both Hydra and FAST instruments is negligible compared to the quantum noise, therefore the total error could be computed converting the instrumental flux into number of photons using the instrument gain, ϵ. The error in the number of photons is given by the number of photons divided by the signal-to-noise, which is proportional to the square root of

Table 3.1. Optical Features for Spectral Typing (Method 1).

Feature	Center (Å)	Width(Å)	C_{left} (Å)	C_{right} (Å)	Temperature Range (K)
Mg I	5170	20	5015	5235	4800-6000
G band	4304	28	4190	4360	5600-6000
Ca I	6165	20	6010	6310	3000-3600 and 3600-5100
TiO4775	4775	50	4655	4965	3000-4800
TiO4975	4975	50	4860	5300	3000-3600 and 3600-5000
TiO6185	6185	50	6125	—	3000-3900
TiO7140	7140	30	7035	—	3000-3700
Band-1	4650	200	4450	4950	4200-6000
Band-2	5150	200	4950	5350	4300-6000

Note. — C stands for central wavelength for continuum. Continuum and feature have the same width. Double temperature ranges are given for lines that were fitted with two different straight lines.

the number of photons, according to photon counting statistics. Then, the error in the flux, for both the flux in the band and the flux in the continuum region, is determined as the error in the number of photons, divided by the instrument gain, or the total flux divided by the signal-to-noise, $\sigma_f = F(S/N)^{-1} = N_\gamma \epsilon^{-1}(S/N)^{-1} = N_\gamma \epsilon^{-1} N_\gamma^{-1/2} = N_\gamma^{1/2}\epsilon^{-1}$. Considering that the band and continuum measurements are independent, the error in the indices can be propagated in the usual way (Bevington, 1969).

The same index measurements were obtained for a set of spectral type standards chosen among Gliese stars and stars in Praesepe (Allen & Strom, 1995; Kirpatrick et al., 1991; Kirpatrick & McCarthy, 1994), and their spectral types were converted to effective temperatures with the calibration in Kenyon & Hartmann (1995). Indices were plotted against the temperatures (see Figure 3.5) and one or two straight lines were fit to the data. In order to improve the fit and the error estimation, we shifted the coordinates for our linear fit to define the zero point as the value for average index and average temperature of each data set. This produces a linear dependence for the temperature as a function of the spectral index, $T(I) = \langle T \rangle + a + b(I - \langle I \rangle)$ where T and I are the effective temperature and index, respectively, $\langle T \rangle$ and $\langle I \rangle$, their average values, and a and b are the coefficients of the fit. Given our selection of zero point, a is always essentially zero, and b can be taken as an independent index. This procedure removes the possible correlation of a and b, allowing to derive the errors by error propagation (Bevington, 1969).

As it can be seen, not all the features are useful in all the temperature ranges (Figure 3.5), so the routine to determine the spectral types was designed to avoid confusion with the bivalued indices. Three ranges of effective temperatures/spectral types were defined: "later" (∼3000-4000K, M6-K7), "medium" (∼3800-5000K, M0-K1) and "earlier" (∼4800-6000K, K3-G0). These correspond approximately to the three ranges where a different set of indices is applicable. Since the limits are sometimes unclear, some overlap between these

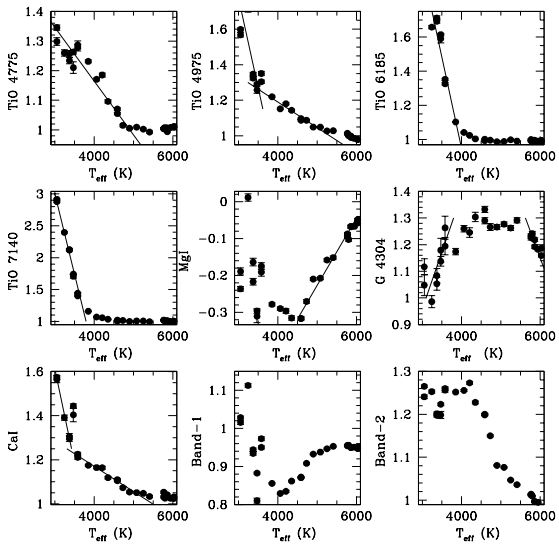

Figure 3.5 Fits to the different spectral lines and features used for spectral type classification.

three preliminary classes is allowed. A value of the TiO bands index for 4775 and 4975 Å higher than 1.2 and 1.26 respectively, is indicative of the "later" spectral type. A value of the 4775 and 4975 Å TiO bands lower than 1.02 and 1.04, together with a value over 0.92 for Band-1 and lower than 1.13 for Band-2, is typical for the "earlier" stars. A value of the two bluer TiO bands in between the limits within "later" and "earlier" spectral types, together with a value of Band-1 band lower than 0.92, and a value higher than 1.13 for Band-2 will reveal a "medium" type star.

This preliminary classification allows us to avoid the degeneracy of the indices, so we can continue computing the final effective temperature and spectral type for each case:

- For the "later" type, we use the four TiO bands (4775, 4975, 6185 and 7140 Å) and CaI (6165 Å). A preliminary effective temperature is calculated, and the result is improved giving more weight to the best indices in this range (TiO bands at 6185 and 7140 Å).
- For the "medium" spectral types, the bluer TiO bands and CaI are applicable, being TiO-4775 Å the most accurate for temperatures under 4200K.
- For the "earlier" stars, Mg I is usually applicable for the whole range, and the G band will be used in case Mg I gives a temperature higher than 5600K.

The final effective temperature is obtained as a weighted average. The errors are a combination of the fit errors and the experimental error in the flux measurement, as described before. The range of spectral types covers M6-G0. Stars earlier than G0 are detected and rejected, and no spectral type is obtained for them with this calibration. Spectral type errors are obtained directly taking into account the effective temperature errors.

This procedure works well for the spectra obtained with FAST and with the 316@7.0 and 400@4.2 grating Hydra configurations, with wavelength ranging from 3700-7500 Å, 4000-9000

Å and 3800-7000Å respectively. For the last Hydra configuration, which used the 600@10.1 grating, the wavelength range is only 4500-7500 Å, so some bands were missing. Therefore, this method was applied to obtain approximate spectral types. A refinement was then obtained by visual inspection of the spectra divided by standard ones. All the remaining spectral types were re-checked dividing by the standard corresponding to the spectral type given by the algorithm, to remove any possible errors, mainly in the cases of low signal-to-noise spectra. The bright end of our sample, where the lack of lines tends to produce a larger ($\sim$2 subtypes) variation (as we will describe later), was visually revised as well to ensure the quality of the classification.

To check the accuracy of our spectral typing algorithm and the error estimates, a collection of spectra from members of the Taurus-Auriga molecular cloud (Kenyon & Hartmann, 1995) was used. Although this complex is younger than the two Cep OB2 clusters, and it is located at the closer distance of 140 pc (Kenyon & Hartmann, 1995), the Taurus stars are similar in spectral type to the stars observed with Hydra.

The FAST spectra of Taurus TTS were taken with the same configuration as used for Cep OB2. A total of 116 spectra for 43 different stars were available. In general, 1-6 spectra were available for each star with different signal-to-noise ratios, which were also used to estimate the errors and the efficiency of the method in case of poor signal-to-noise. The spectral types were calculated with the algorithm, and compared with the spectral types given in Kenyon & Hartmann (1995). Comparison of the 64 spectra in the range M6-M0, 38 spectra for K7-K5, and 13 spectra in the K4-G0 range shows that the results are fairly consistent with our estimates. We obtained consistent results even for most of the fainter and noisier spectra. Moreover, the errors inferred by comparison with the Kenyon & Hartmann (1995) spectral types are consistent with our calculations: about 1 subtype or less for M stars, 1-2 subtypes for K7-K5 stars, and up to 2 subtypes for K4-G0 stars, although the effect of very low signal-to-noise and/or a poor background subtraction must be taken into account, as they introduce larger errors. We also checked that the scheme was able to discard spectral types earlier than G0, as we need for removing background reddened distant objects.

Classification of the Hectospec Spectra and the High-Mass Members

The rest of the objects were classified following the scheme of Hernández et al. (2004). This scheme is optimized for the FAST wavelength range and resolution, which are similar to those of Hectospec, takes into account more features than the method described in the preceding section, and covers a much wider range of spectral types. The organization of the scheme, and the error estimates, are nevertheless similar to the ones described in the first method. The scheme uses two different sets of indices, the first one for stars with spectral types in the range from O to early G stars, and the second for stars later than G5. The sets of indices were calibrated as a function of spectral type, using a collection of FAST spectra from O8 to M6 Main Sequence standard stars (García, 1989; Gray et al., 2001; Keenan & Barnbaum, 1999; Jaschek, 1978; Buscombe, 2001). For each index, the width and center of the blue continuum band (BCB), red continuum band (RCB), and central band (FB) were optimized.

The scheme for early stars (O8-early G) is based on 33 spectral indices, which are sensitive to changes in T_{eff} but insensitive to reddening, stellar rotation, luminosity class, and signal-to-noise ratio. This scheme is designed to largely avoid problems caused by non-photospheric contributions (mostly originated from material surrounding the star). We require that the various spectral types calculated from each index agree with the others; wildly discrepant

Table 3.2. Spectral classification indices for late type stars (Method 2)

Index	Center(Å)	Width(Å)	BCB(Å)	W_{BCB}(Å)	RCB(Å)	W_{RCB}(Å)
L1	7150	50	7045	10	7385	15
L2	7100	50	7045	10	7385	15
L3	6800	50	6530	10	7030	10
L4	6255	50	6080	10	6530	10
L5	5950	75	5810	15	6080	10
L6	5600	50	5415	10	5810	15
L7	5475	75	5385	15	5810	15
L8	5225	75	4940	15	5415	20
L9	4975	50	4940	15	5385	15
L10	4775	30	4745	15	4925	15

Note. — List of the spectral indices used for the classification of late-type stars, as well as the widths and positions of bands and continuum regions (see text).

values are rejected, and a weighted mean spectral type is obtained. The errors in our estimated spectral types have two contributions, the error from the fit of each index to the standard Main Sequence, and the error in the measurement of each index (Hernández et al. 2004).

In order to classify stars with spectral type later than $\sim$ G5, the scheme was extended to incorporate and optimize spectral indices in the spectral type range G0-K5 and K5-M6 (see Hernández et al. 2004, Briceño et al. 2005, and Table 3.2). Following Hillenbrand (1995), the EW for each spectral feature is obtained by measuring the decrease in flux in FB due to line absorption, considering the continuum expected when interpolating between the two adjacent bands, BCB and RCB.

Using the V-I color predicted by Kenyon & Hartmann (1995) for stars with different spectral types, the VI photometry, and the relation between A_V and E(V-I) from Bessell & Brett (1988), A_V=2.5E(V-I), the individual extinction of each star was calculated. These values are listed in Table 3.3 . We used the confirmed members (named "Y" in Table 3.3) to calculate the average extinction in each cluster, as well as the standard deviation of the extinction within the cluster, obtaining $A_V = 1.56 \pm 0.55$ for Tr37 (calculated with only the 135 confirmed members), where 0.55 represents the standard deviation over the cluster, and not the individual errors in extinction (these depend on the spectral type and photometry, and are typically 0.1-0.3 in magnitudes). The values of the extinction of the probable members ("P" in the tables) are consistent with those of the confirmed members ("Y" in the tables).

Except for stars very close to the globules to the West and North in Tr 37, no evident spatial variation of the extinction within the clusters was found. Therefore, we assume that extinction is mostly foreground, and that the standard deviation of A_V is produced by both individual extinction variations and the error derived from spectral typing, colors, and photometry. An analysis of the statistical distribution of A_V for the confirmed members in both clusters shows that it can be considered as pseudo-gaussian (as for the probabilities, notice

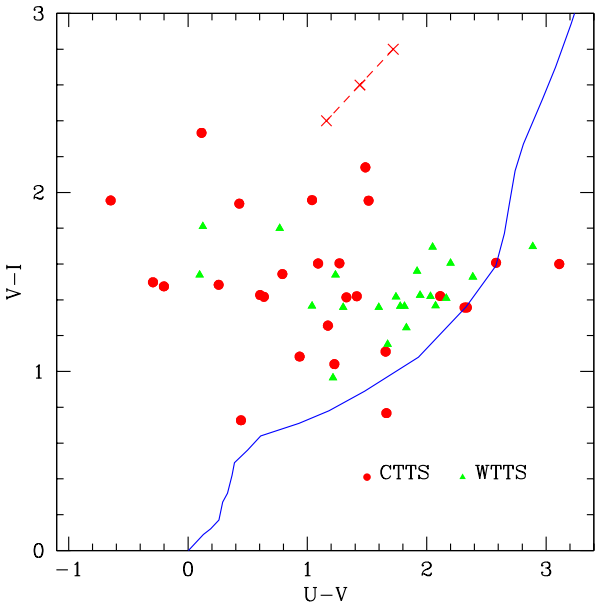

Figure 3.6 U-V vs. V-I color-color diagram for Tr 37: Excesses in U band color are correlated to Hα excesses. Strong Hα stars are denoted by red dots, weak Hα stars are represented by green triangles. The blue line represents the Main Sequence; the reddening vector is denoted by the dotted red line (crosses mark A_V=0.5 intervals). It is important to take into account the extinction and the spectral types in order to determine the excess luminosity in U band (see text).

the absence of negative A_V values), with ∼76% of the stars in Tr 37 in the $\pm1\sigma$ region, ∼96% of stars in the $\pm2\sigma$ region, and ∼98% of them in the $\pm3\sigma$ region (only 3 stars, related to the globules, have higher extinctions beyond 3σ). We consider these nearly-gaussian probabilities in order to define membership for the high- and intermediate-mass stars, as it will be described below.

3.1.3 Accretion Processes and Accretion Rates

One of the main characteristics of Tr 37 is that the optical spectra of its members show strong Hα emission in about 40% of the stars in our sample, indicative of accretion processes (Hartmann, 1998; Muzerolle et al., 2000). The strong and wide Hα emission is originated in the magnetospheric accretion columns. The accretion shock onto the surface of the star produces a hot continuum, which can be identified as a blue and ultraviolet excess flux above the photospheric level (Edwards et al., 1994; Hartmann, 1998; Calvet & Gullbring, 1998). Therefore, if we compare U-V vs. V-I color with the normal values for the given spectral types, we find that there is an excess in the U band, as it would correspond to a hot continuum added to the photospheric emission from the star. Moreover, this excess is correlated to the presence of broad Hα emission (Figure 3.6).

Calvet & Gullbring (1998) and Gullbring et al. (1998) found that the U band excess emission is directly correlated to the accretion luminosity. Therefore, we can derive accretion luminosities, L_{acc}, using the calibration by Gullbring et al. (1998) as a function of the excess

luminosity in U band, L_U, i.e.:

$$\log(L_{acc}/L_\odot) = 1.09\log(L_U/L_\odot) + 0.98 \tag{3.1}$$

$$L_{acc} \approx \frac{GM_*\dot{M}}{R_*}(1 - R_*/R_{in}) \tag{3.2}$$

Masses and radii of the stars (M_*, R_*) can be deduced by placing the stars on the HR diagram and comparing them with theoretical evolutionary tracks (Siess et al., 2000). For this purpose, we calculated the luminosity from the I magnitude, with the appropriate bolometric correction provided in Kenyon & Hartmann (1995), given that I is less affected by extinction than V and R; and the effective temperatures derived from the spectral types, also according to Kenyon & Hartmann (1995). The infall radius, R_{in}, is usually a few (i.e. 5) times the stellar radius (Hartmann et al., 1998). Using our U band photometry, and correcting for the average extinction, we find accretion rates of $\sim 10^{-8} M_\odot yr^{-1}$ in Tr 37 (Table 3.5).

There is a good agreement between the measurements of stars with multiple observations, although differences of the order of a factor of 2-3 can be observed between the two epochs in some cases (these are the typical variations found in measurements of the accretion rates). This may be related to variations in the accretion rate from epoch to epoch, or to large errors in the photometry, likely to occur in the U band. We can estimate the error in the accretion rates, and the lower limit for detecting accretion (due to average errors in the U band photometry) from the errors in U magnitudes (which can be up to 0.1-0.2 magnitudes) with respect to the Main Sequence in the V-I vs. U-V diagram. We obtain a lower limit for accretion detection via U band of a few times $10^{-10} M_\odot yr^{-1}$, and errors that can be up to 1-2 times $\sim 10^{-9} M_\odot yr^{-1}$. Errors in the extinction correction and spectral type could affect the mass accretion rates determined via U band as well. Therefore, we must be cautious when reading the lowest mass accretion rates. The average accretion rate, $2\times10^{-8} M_\odot yr^{-1}$ is in good agreement with the average rates obtained in other clusters (Taurus, Chameleon, Ophiuchus) and with the models of viscous disk evolution (Hartmann et al., 1998; Muzerolle et al., 2000).

3.1.4 Protoplanetary Disks at the Age of 4 Myr

In order to visualize the disks and the colors of the cluster members, we can use the color-color diagrams for the clusters and the SEDs for each one of the stars. Figure 3.7 shows different IR colors for the low-mass stars in Tr 37, together with a comparison with the colors of the young, low-mass stars in other (younger) regions (Taurus, from Hartmann et al. 2005; NGC 7129, from Muzerolle et al. 2004), and with the models by D'Alessio et al. 2004 for late-K stars with accreting disks (see Section 5.4 for more details). A first-order comparison shows a good agreement for the low-mass stars in all the mentioned regions and models, but there are significant trends or deviations from the standard that require further explanation and a close look at each one of the stars in the sample.

The most remarkable differences affect some of the stars classified as WTTS, or non-accreting stars, since several of them, even though they do not exhibit an excess at 3.6 and 4.5 μm, have considerable excesses at longer wavelengths. The other interesting difference is that magnitudes at 24 μm are smaller than expected according to the shorter wavelengths for many of the stars, producing H-[24] and [8]-[24] colors to be redder than the predictions of

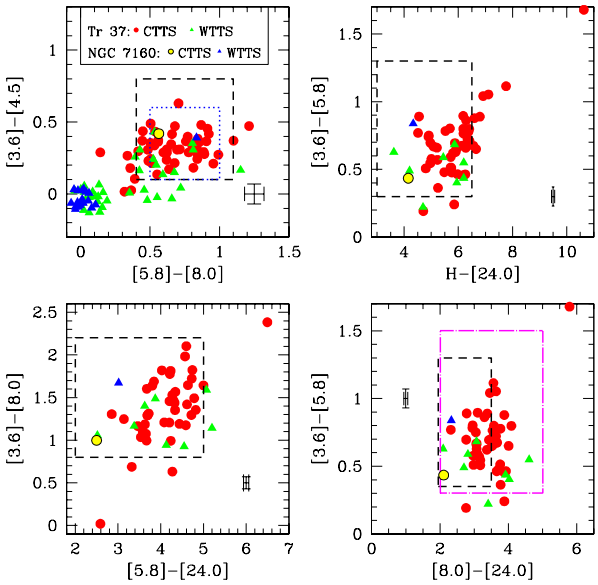

Figure 3.7 Spitzer and 2MASS color-color diagrams for the Tr 37 and NGC 7160 members: According to the Hα classification by White & Basri (2003), CTTS are represented by red circles, WTTS are represented by green triangles (in Tr 37), and by yellow circles and blue triangles (in NGC 7160), respectively. Since extinction effects at these bands are expected to be very small for the average A_V, no dereddening has been applied. For comparison, the regions defined by the IRAC colors observed for Taurus stars (blue dotted line in the first diagram, see Hartmann et al. 2005), and the MIPS colors observed for stars in NGC 7129 (purple dotted-dashed line in the last diagram, see Muzerolle et al. 2004) are displayed, as well as the regions defined by the accretion disk models by D'Alessio et al. 2004 (dashed black lines in all the diagrams, see Section 5). Note the large excess for the protostar 213645+572933 in the [3.6]-[5.8] vs. [8.0]-[24.0] diagram. The comparison with Taurus reveals as well a lower excess at shorter wavelengths, related to dust settling/grain growth as well (see Section 5).

the models, and a very well defined tendency to redder colors even within the model boxes. Both observations suggest a further degree in the evolution of the disk that had not been observed in younger systems, and that needs to be explored and considered case by case in more detail (see below).

The presence of the infrared excess produced by a disk can be easily inferred by examining the SED of each star. Moreover, putting together all the available information, we can check whether the presence of a disk is related to the signatures of accretion, strong Hα emission, and accretion rates derived from U band photometry. Figures 3.8 to 3.12 contain the SEDs for the Tr 37 low-mass members.

The Hα emission equivalent width (EW) was used for the diagnosis of accretion among low-mass (spectral types late G-M) members in Cep OB2, according to the criteria defined by White & Basri (2003), together with the accretion rates, derived from U band excess emission Gullbring et al. (1998). Even though the classification is consistent for most of the stars, in some cases the Hα classification by White & Basri (2003) reports some CTTS as WTTS and vice-versa. This problem could be caused in some cases by the difficulties subtracting

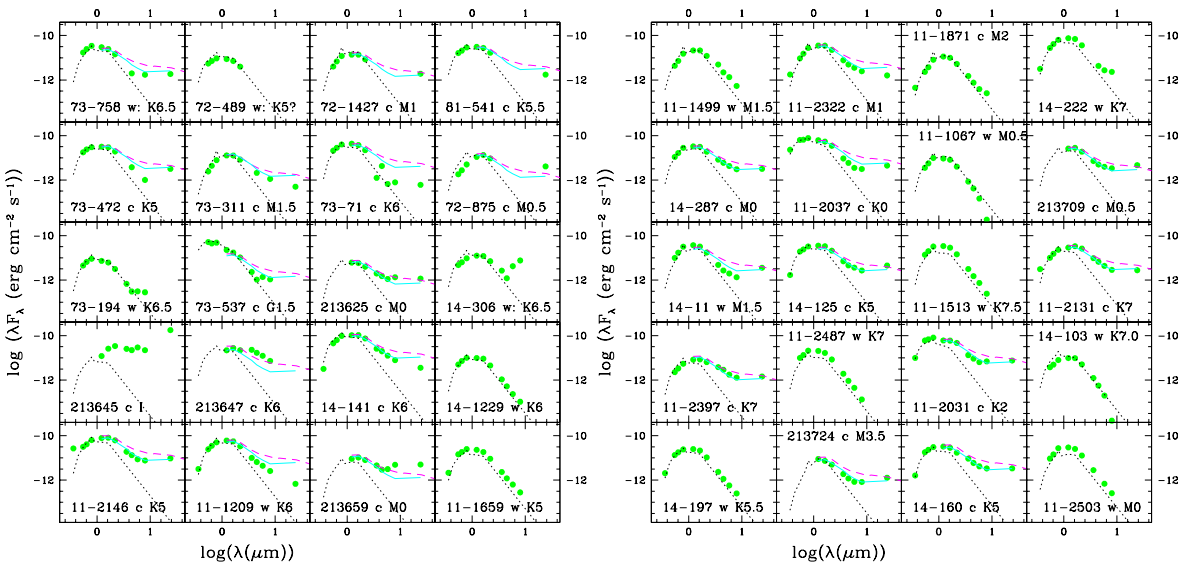

Figure 3.8 Spectral Energy Distributions for low-mass stars in Tr 37. The fluxes are calculated from the UVRI photometry (4Shooter/1.2m), JHK 2MASS photometry (Cutri et al., 2003), and IRAC/MIPS magnitudes. The individual reddening correction has been applied in each case. For comparison, we display: the photospheric emission of a similar spectral type (derived from Kenyon & Hartmann 1995) as a black dotted line; the median disk emission in Taurus (Hartmann et al., 2005) as a magenta dashed line; the median disk emission in Tr 37 as a light blue line.

the nebular background, since it affected mostly stars with Hα EW near the limits between CTTS and WTTS, but definitely requires a more detailed study with the Spitzer data.

Using the near-IR colors JHK from 2MASS (Cutri et al., 2003) to detect accretion is not a good choice, since only about half of the accreting stars in Tr 37 present a significant JHK excess. The IRAC and MIPS data from Spitzer, covering longer wavelengths, is a much stronger way to determine the presence of a disk at distances of tenths to few AU, even if accretion rates are very small or zero, and cannot be easily detected through low-resolution spectra of the Hα region, nor U band excess. Since the presence of non-accreting stars with disks produces one of the deviations of the diagrams in Figure 3.7, here we examine case by case all the stars in our sample, in order to find an explanation of these phenomena.

The Spitzer observations confirm the result previously found, that about 40-45% of the members in Tr 37 have accreting, circumstellar disks (see Figures 3.8 through 3.12). The Spitzer data can also clarify most of the confusing cases, for which Hα emission would correspond to a WTTS according to White & Basri (2003), but for which an excess in U band was detected. Spitzer also helps to explore the rest of cases, in which no obvious contradiction had been found, but the Hα indicator was very close to the limit separating CTTS and WTTS.

Some objects that would be classified as CTTS according to Hα (see Table 3.3), present no signs of a disk: 11-1871 (M2, Hα=-13.4), 11-1864 (G-K, Hα=-5.0), 12-1422 (M0, observed with Hydra, Hα=-17.0), 12-1613 (M1, Hα=-13.0), 13-819 (K5.5, Hα=-10.2), 12-1825 (M0, observed with Hydra, Hα=-10.0), 12-1027 (M0, observed with Hydra, Hα=-11.0),92-393 (M2, Hα=-33.8), and 21-1586 (K7, observed with Hydra, Hα=-16.0). All of them but 92-393

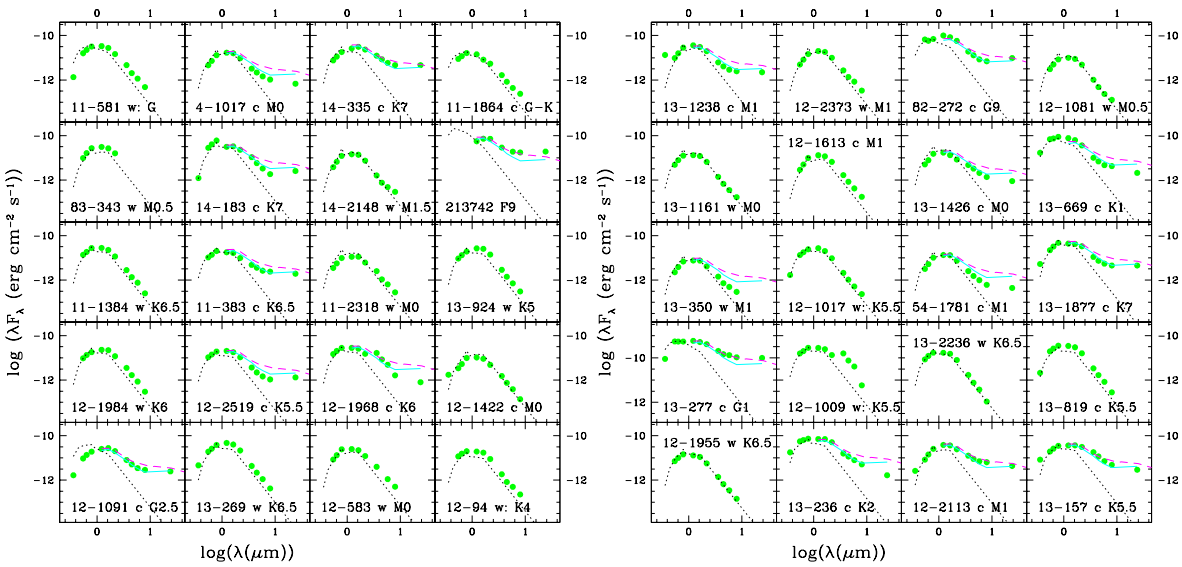

Figure 3.9 Spectral Energy Distributions for low-mass stars in Tr 37 (continued). The fluxes are calculated from the UVRI photometry (4Shooter/1.2m), JHK 2MASS photometry (Cutri et al., 2003), and IRAC/MIPS magnitudes. The individual reddening correction has been applied in each case. For comparison, we display: the photospheric emission of a similar spectral type (derived from Kenyon & Hartmann 1995) as a black dotted line; the median disk emission in Taurus (Hartmann et al., 2005) as a magenta dashed line; the median disk emission in Tr 37 as a light blue line.

represent limiting cases of Hα EW, taking into account that the Hydra spectra have larger errors due to background subtraction. This idea is supported by the fact that most of them are located to the West of the cluster, where the emission from the HII region is stronger, making the background subtraction more complicated. In case of 92-893, errors could be due to the difficulties measuring Hα in a low signal-to-noise spectrum of a faint star, taking additionally into account, that EW of late spectral types may be much larger (20 Å in absorption, White & Basri 2003). Another point of consideration is that 92-393 and 11-1864 present a small excess at 8.0 μm, as it has been observed in stars with inner gaps (CoKu Tau/4, Hartmann et al. 2005). None of the two stars were found to have a detectable counterpart at 24 μm, so we cannot confirm this detection, but it would require further study, since the expected emission would be close to the detection limit at 24 μm.

A similar presence of a small excess at 8.0 μm, sometimes accompanied by an even smaller excess at 5.8 μm, can be observed in other 9 stars classified as WTTS (73-194, 11-1871, 14-222, 14-2148, 12-94, 13-566, 91-815, 92-1162, 24-1796), and could be indicative, at least in some of them, of the presence of a remaining, non-accreting disk at longer distances from the star.

On the other hand, the stars 73-758 (K6.5, Hα=-8.7), 11-1209 (K6, Hα=-4.0), 14-141 (K6, Hα=-5.0), 13-350(M1, Hα=-9.0), 91-155 (M2.5, Hα=-7.8), 21385669+5730484 (K5, Hα=-4.1), 53-1762(M0, Hα=-1.7), 21-2006 (K5, Hα=-1.8), 21402192+7730054 (K6, Hα=-8.5), 22-1418 (M1.5, Hα=-2.2), 23-162 (K7, Hα=-6.4), which had been classified as WTTS according to their Hα, have excesses at all the IRAC and MIPS wavelengths comparable to the normal

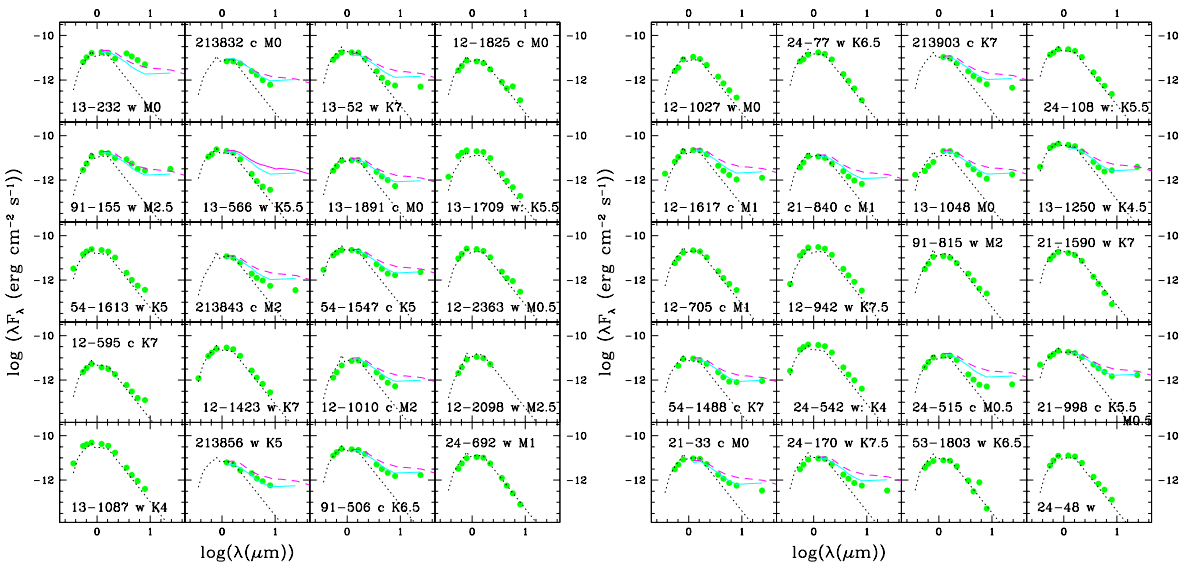

Figure 3.10 Spectral Energy Distributions for low-mass stars in Tr 37 (continued). The fluxes are calculated from the UVRI photometry (4Shooter/1.2m), JHK 2MASS photometry (Cutri et al., 2003), and IRAC/MIPS magnitudes. The individual reddening correction has been applied in each case. For comparison, we display: the photospheric emission of a similar spectral type (derived from Kenyon & Hartmann 1995) as a black dotted line; the median disk emission in Taurus (Hartmann et al., 2005) as a magenta dashed line; the median disk emission in Tr 37 as a light blue line.

CTTS. This is consistent with the detection of accretion via U band excesses in the two first and the last ones (see Table 3.5). Problems in the sky subtraction could have affected the EW of 11-1209, 14-141, and/or 13-350, which were observed with the Hydra spectrograph. 73-758, 21385669+5730484, and 21402192+7730054 are near the limits established by (White & Basri, 2003) for CTTS and WTTS. For the others, given that errors in the measurement of Hα from Hectospec and FAST spectra are small, and errors in the spectral type beyond 2 subtypes are very improbable, we find a disagreement with the (White & Basri, 2003) Hα criteria. Nevertheless, the existence of accreting WTTS has been reported previously (Littlefair et al., 2004), and in some cases, the weak lines may be caused because of optically thick accretion shocks, high variability, and several other factors. This matter would require further study and observations of the Hα line at high-resolution in order to detect the presence of high velocity wings, related to accretion (See Section 6).

In case of the stars 14-183, 13-232, and 91-155, we observe a "jump" in the SEDs, as the optical fluxes do not match accurately the IR data. We have revised the observations, errors are reasonably small, optical and IR observations match well within themselves, and confusion with the photometry of nearby sources does not seem likely. Since the optical and IR data was taken in different epochs, and accreting stars are highly variable, these differences may be caused by luminosity and/or accretion rate variations. In fact, the variability information available for the two first stars showed important variations in R and I bands, although more variability and accretion studies would be required in order to answer this question definitely.

Finally, the last case of unusual colors comprises some other weak-lined objects, which

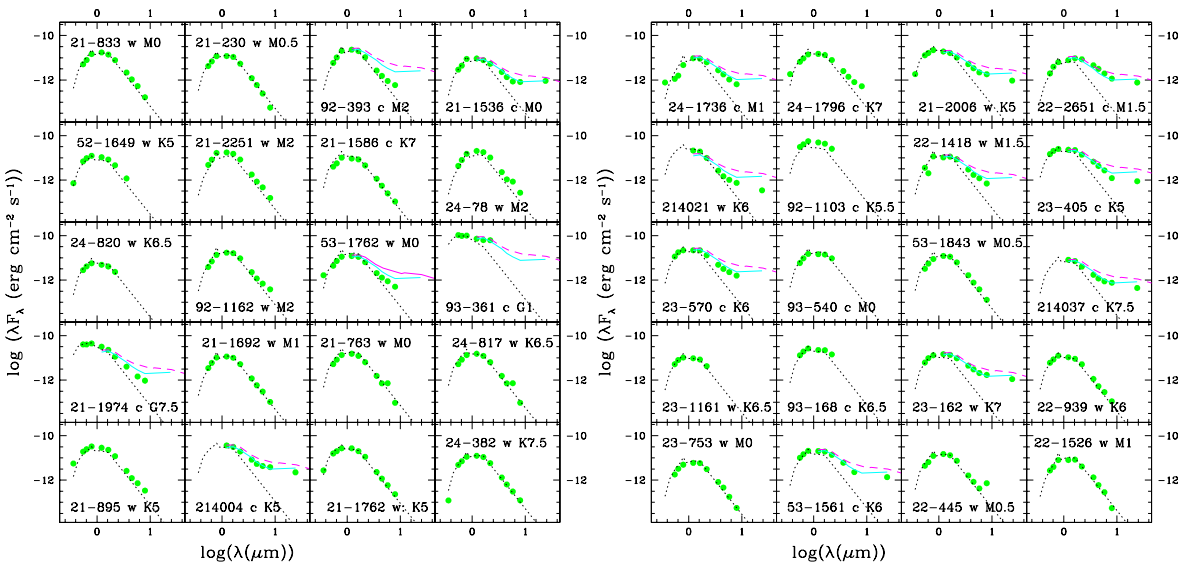

Figure 3.11 Spectral Energy Distributions for low-mass stars in Tr 37 (continued). The fluxes are calculated from the UVRI photometry (4Shooter/1.2m), JHK 2MASS photometry (Cutri et al., 2003), and IRAC/MIPS magnitudes. The individual reddening correction has been applied in each case. For comparison, we display: the photospheric emission of a similar spectral type (derived from Kenyon & Hartmann 1995) as a black dotted line; the median disk emission in Taurus (Hartmann et al., 2005) as a magenta dashed line; the median disk emission in Tr 37 as a light blue line.

have significant differences with the precedent ones. The stars 14-11 (M1.5, Hα=-5.3), 13-52 (K7, Hα=-0.8), 13-1250 (K4.5, Hα=-2.5), and 24-170 (K7.5, Hα=-4.4) have disks which are only detectable at wavelengths of 5.8 μm and longer. Their excesses at 5.8, 8.0 and 24.0 μm suggest the presence of an outer disk, but any excess from an inner disk (JHK, 3.6, 4.5 μm) is undetectable. Moreover, the U band magnitudes available for 13-1250 (taken during two epochs, see Table 3.5) are consistent with extremely weak or zero accretion. The fact that no U magnitudes could be obtained for the rest of them, even though they are located in the region with U observations, suggests as well very small or zero accretion (the available U photometry enabled us to detect U from photospheric emission down to ∼K6-K7, in cases of zero accretion). The lack of emission at shorter wavelengths in these objects, together with the lack of any signs of accretion, seem to indicate that the inner part of the disk has been cleared out, maybe because of the formation of planets. These objects would be, then, in an intermediate stage between CTTS and WTTS, so we can call them "transition objects". A more detailed analysis of the "transition objects" will be given in Section 5.3. Further study, including the determination of whether there is any gas in the inner disk, and the detection of any very slow accretion rates, would be the next step on the characterization of these objects.

3.1.5 Spatial Distribution in Tr 37: Photoevaporation?

The spatial distribution of members in Tr 37 can be seen in Figure 3.2. Examining the central fields (Figure 3.13), we find ∼60% of the cluster members to be concentrated to the West

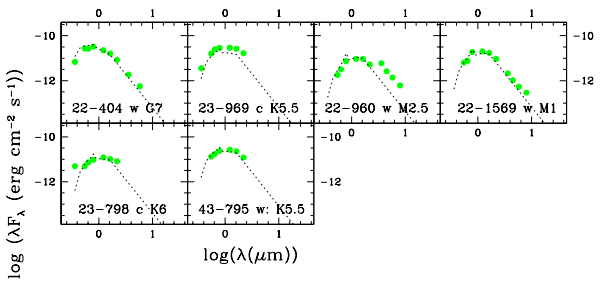

Figure 3.12

of HD 206267. About ∼95% of the estimated extra members (that will be, 9 out of 10, see Section 3.3) would be located on this side as well, so there are about twice as many stars in the West as there are to the East.

The disk fraction for the low-mass stars is slightly higher in the western side of the O6 HD 206267 star (∼50% in contrast to ∼35%), as well as in the southern part. We have done a KS test to compare the distribution of CTTS and WTTS in RA and DEC. We find a probability of 24% and 29% that the two samples have the same distributions in RA and DEC, respectively, so even if there is some degree of asymmetry, it is not statistically significant. Nevertheless, a similar asymmetry is found among the lower-mass IRAC candidates (see Section 3.3), since 102 of the 152 candidates are located to the West of HD 206267.

It seems plausible to suggest that disk evaporation is more effective in the eastern side because stars to the West of HD 206267 were protected by dust structures (part of which we can still see), although this would require further study beyond the scope of this thesis work. Disk photoevaporation has been observed in the Orion Nebula Cluster (Johnstone et al., 1998; Bally et al., 1998, 2000). Although it does not seem to be able to remove effectively many disks in 1 Myr (Hillenbrand, 1997), it may have a greater influence on disk dissipation after 3-5 Myr. Nevertheless, given the disk fraction that we find, the disk removal cannot be complete, or the strong photoevaporation effects must be restricted to a small region in the cluster, in the surroundings of the O6 star.

In order to test whether any photoevaporative effects have altered the distribution of CTTS versus WTTS, the number of stars versus the projected radius to HD 206267 was studied for the two groups, since the distance to the O6 star should be the most important parameter to determine the chances of photoevaporating a disk. Figure 3.14 shows the results of this comparison. Since the presence of younger populations may affect the distribution for radii larger than 0.4 degrees (see Section 3.1.6), only the central part of the cluster was taken into account. A KS test gives a 48% probability for the two distributions to be drawn from the same samples, which is consistent with CTTS and WTTS being equally distributed in distance to the O6 star. The larger differences in the cumulative distribution come from regions other than the surroundings of the O6 star. Nevertheless, the lack of CTTS in the innermost part of the cluster can neither confirm nor rule out the hypothesis of photoevaporation since, due to the low density of stars in the cluster, the number of stars in the center is too small to do any statistics. We only find 2 CTTS, compared to 7 WTTS, inside a 0.07 degrees radius (corresponding to ∼1pc for a cluster located at 900 pc, which is of the order of the radius predicted by Störzer et al. 1999 to have effective photoevaporation). IRAC colors reveal that no other objects with disks are found inside this radius, whereas there could be some more

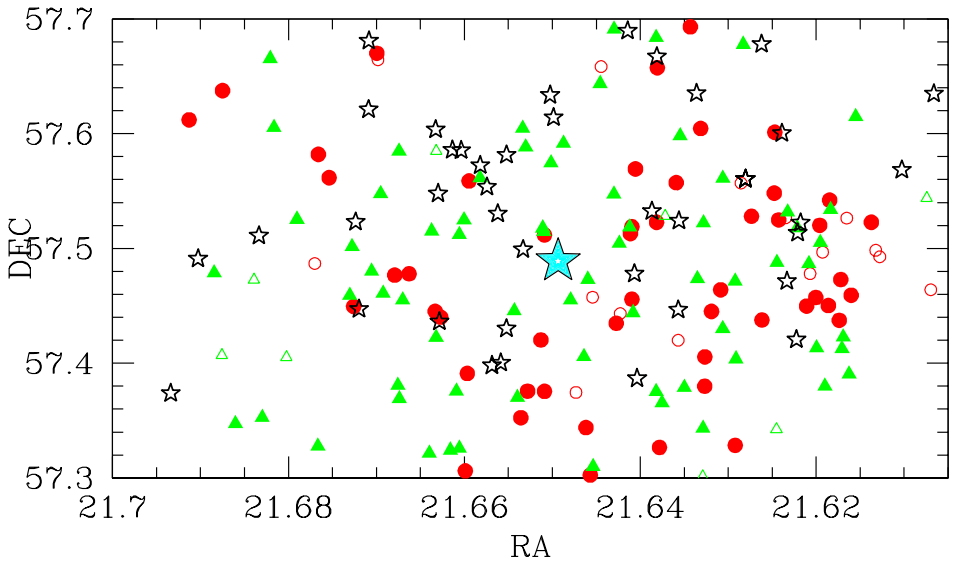

Figure 3.13 Zoom in the central part of the cluster Tr 37. The two 4Shooter central fields (see Figure 3.2 are displayed. The O6 star HD 206267 is represented by a large star; BFA-type stars are denoted by small open stars. For the low-mass stars: CTTS are represented by circles; WTTS are represented by triangles; confirmed members (where Li absorption was detected) are filled symbols; probable members (no Li detected due to poor signal-to-noise) are open symbols.

diskless stars. Considering that the possible projection effects, we would have in average about 2 stars in the line of sight that would be projected into the central region (assuming an uniformly distributed spherical cluster). The probability (assuming also a spherical cluster) of having at least one of the two accreting stars inside the 0.07 degrees sphere surrounding HD 206267 is around 20%, so no final conclusion can be drawn. Some other observations (imaging in forbidden lines, for instance) would be very interesting in the future to detect the presence of photoevaporating disks in this region. Finally, it must be also considered that in the ONC, photoevaporating structures have been detected around both CTTS and WTTS (see 6.3.4).

3.1.6 Triggered or Ongoing Star Formation? The Stars in the Tr 37 Globule

The additional, probably younger population associated to the dust globules on the West (see Figure 3.16) can add up to explain the asymmetric appearance described before. The location of all the 15 objects appearing over the 1 Myr isochrone in the V vs. V-I diagram depicts a very clear shell-shape region to the West of the cluster (Figure 3.15). It is improbable that these large deviations toward higher luminosities are due to variations in the photometry, and are too large to be caused by an equal-mass binary sequence. This suggests that they are in fact younger objects. Besides the location of the 1 Myr-old objects, no other significant age gradient has been observed throughout the cluster.

The Spitzer observations reveal a population consistent with embedded protostars, which

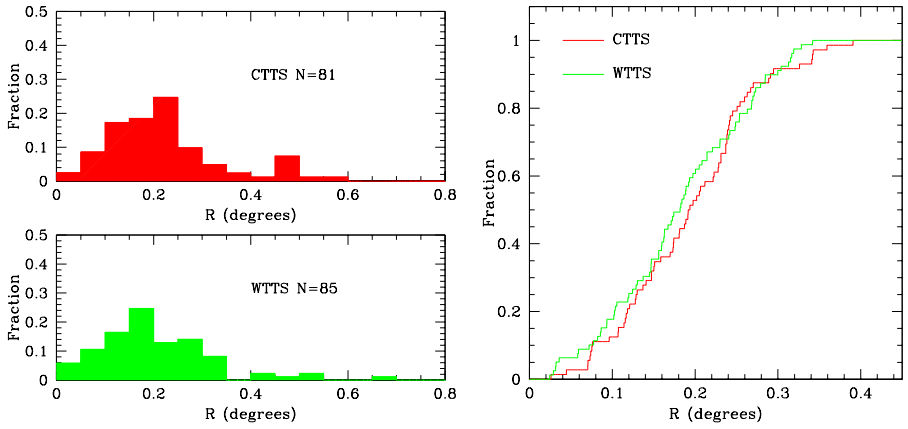

Figure 3.14 Left: Histogram of the distribution of CTTS and WTTS in Tr 37 versus the projected distance to the O6 star HD 206267. We can observe a lack of CTTS in the central region, which could indicate effective disk removal by photoevaporation (see text). We can also observe an accumulation of CTTS at ∼0.45 degrees that correspond with the younger population associated to the gas and dust structures in the cluster. Right: Cumulative distribution of CTTS and WTTS in the central 0.4 degrees of the cluster. The absence of CTTS in the inner 0.07 degrees radius could be caused by complete photoevaporation of disks closer than 0.8 parsecs from HD 206267.

would be a further indication of younger members in this region. This younger population may as well be responsible for the higher disk fraction on the western part of the cluster. Since most of the globule is opaque to optical wavelengths, but the extinction at Spitzer wavelengths is much lower, the presence of sources in the globule, visible at 3.6 to 24 μm, was investigated.

The photometry in the globule was done selecting by hand the point-like objects visible at each one of the wavelengths, and using *PhotVis* (see Section 2.4)for measuring fluxes and magnitudes. Smaller apertures of 3 pixels with their corresponding aperture corrections were used in the photometry, in order to avoid contamination from the emission from the globule as much as possible. The total number of sources detected was around 200, although only ∼140 of them could be clearly identified at all wavelengths. We also required the detected objects to have JHK colors from the 2MASS survey consistent with young stars, in order to reduce the contamination from other objects and errors in the IRAC photometry, likely to occur in the bright IR emission of the globule. We removed the stars in the Main Sequence from the J-H vs. H-K color-color diagram, and the J vs. J-H diagram. About 120 of the stars in the globule had JHK colors consistent with low-mass stars with disks, although some could still correspond to giants and/or heavily reddened background objects. The IRAC detections were matched with our 24 μm MIPS photometry, although the use of the MIPS data for candidate selection is very hard due to the strong dust emission at 24 μm from the globule (this is the reason of the "strange" 24 μm colors of some of the stars listed). Finally, the potential CTTS and protostars in the globule were selected as objects showing IRAC excesses similar to those observed for CTTS and those predicted by the D'Alessio et al.(2005) models for protostars. In general, 2MASS and IRAC magnitudes for all the objects are well over the dust emission from the globule. A total of 32 potential stars were identified (see Figure 3.17

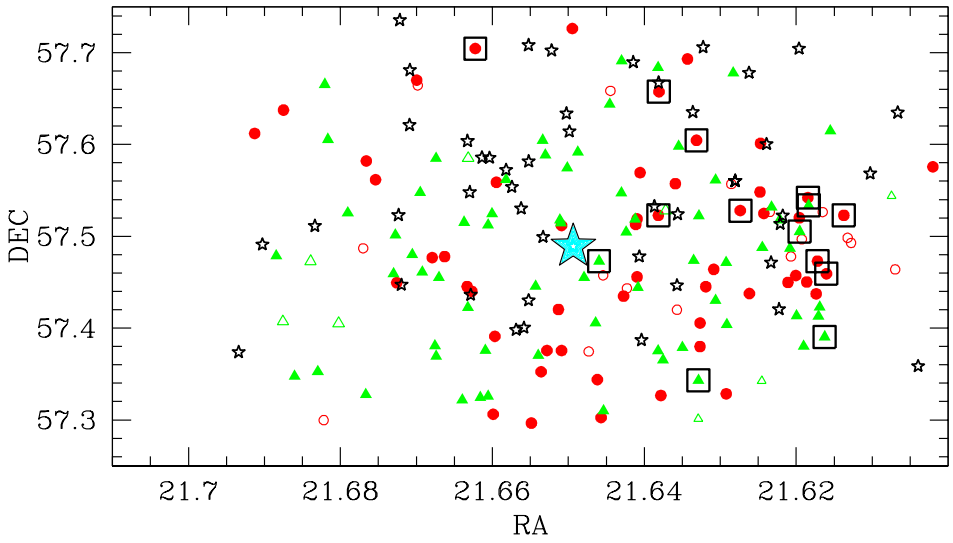

Figure 3.15 Zoom in the central part of the cluster Tr 37, with the younger stars (over or at the 1 Myr isochrone) marked with open boxes. The young 1 Myr stars appear very clearly in a shell to the West of the cluster, which includes the dust globule as well. The characteristic spatial distribution suggest them to belong to a new, triggered population. The young embedded protostars (some of them already studied in Reach et al. 2004) in the dust globule may be part of this young population as well.

and Table 2.9), of which 4 are regarded as "probable members" (denoted by "P" in Table 2.9), since the color excesses are not so strong at one or more of the wavelengths. We also included the photometry of two stars detected by Reach et al. 2004, ϵ and δ, even though they did not show good 2MASS counterparts.

A total of 9 of the selected objects had been studied with Hectospec (see Table 2.9), although only 5 of them had optical VRI counterparts. All of them but one are class II objects or CTTS, and the other one is a class I protostar. Some other $\sim$15 objects with IRAC excesses had been observed with Hectospec as well, although their emission at optical wavelengths was so faint that no reasonable spectra could be obtained (they may correspond to heavily reddened objects). There were another 4 objects detected optically that were not found through this selection; 3 of them are WTTS and one more is CTTS. We did not expect to find the WTTS because they do not show excesses; the missing CTTS did not have very strong excesses at shorter wavelengths, so it was rejected because of this selection procedure. Although these numbers are small for doing statistics, we can estimate that about 10% of the CTTS in the globule may be missing with our selection criteria, and maybe more, if objects with large gaps are present. We may be missing as well some of the most embedded objects with large extinctions.

The 5 members with optical counterparts in the globule (14-141, 11-2322, 14-287, 14-11, 14-125) can be used to estimate the age of the globule population. The individual ages of these members are 0.6, 0.9, 1.0, 0.7 and 2.9 Myr, respectively, giving an average age of 1.2 Myr with a dispersion of 1 Myr (mostly due to the "old" age of 14-125). Therefore, we can estimate an average age of 1 Myr for the population in the globule, significantly lower than the average age of the rest of Tr 37 members, and comparable to the age of the younger

Figure 3.16 IRAC Image of the Globule in Tr 37: blue (3.6 μm), green (4.5 μm) and red (8.0 μm) false colors reveal the structure of the globule, as well as the presence of many embedded objects.

population in a rim described previously.

According to their colors (Figure 3.18) and the shape of their SEDs (Figure 3.19), the objects were classified as CTTS or class II objects, and protostars or class I objects. We also compared them to the protostars found by Reach et al. (2004), finding 10 objects in common. The classes we find for the common stars are similar to the ones described by Reach et al. (2004), differing only in the stars γ, δ, and ϵ, which we classify as class I (and not I/0), and ζ, which looks clearly like a class II object with a disk and not like an intermediate stage between I and II. Attending to the colors and shape of the SEDs, most of the objects in the globule are class II objects or CTTS. A total of 8 are clearly protostars, and the rest are class II objects (see Table 2.9 and Figure 3.19).

The small-excess probable members may be WTTS with excesses only at the longer wavelengths ("transition objects"), although some contamination from the globule could affect some of their colors. It is worth to mention that a total of 15 more objects were identified as having excesses only at 5.8 and 8.0 μm. These have colors similar to the "transition objects" as well, but their large number and their location in parts of the globule with strong background at 5.8 and 8.0 μm indicates that they are most likely contaminated, so at this point we rejected them and they were not included in the member/potential member list.

Some of these objects were observed with Hectospec in order to obtain optical spectra but, due to the high extinction at optical wavelengths and/or the faint optical emission of the candidates, we only obtained a spectrum with good signal-to-noise for 21364596+5729339. This object is clearly accreting, has a class I SED, and no clear spectral type could be assigned to it.

Inspecting by eye the image (Figure 3.17), some other sources can be identified, specially some highly embedded objects located within some of the fiber-like structures in the globule, and in the bright rim of the dusty structure. These objects are very likely to be young cluster members. Unfortunately, we were not able to obtain low error photometry for them, due to the very strong contamination by the emission from the globule, but a followup of these objects would be of great interest. As it was already mentioned before, with this detection method, class III or diskless WTTS stars in the globule would not be detected, due to the

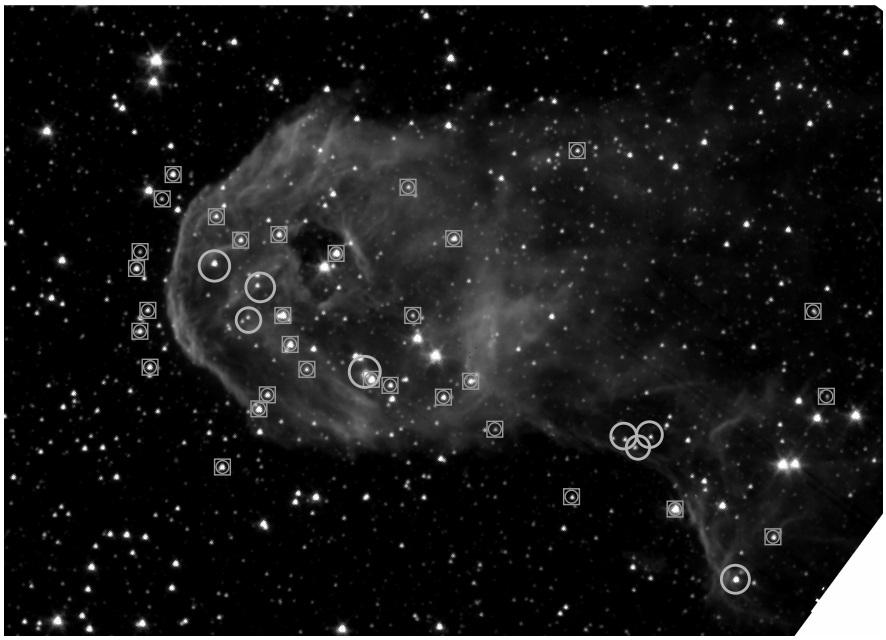

Figure 3.17 Stars in the Tr 37 globule: Detected cluster members as seen at 3.6 μm. Class I sources (protostars) are denoted by circles; class II sources (CTTS) are denoted by squares. Note the presence of embedded sources within the filaments in the globule. These sources are very likely to be cluster members, but measuring their measured fluxes have strong contamination from the globule emission, and cannot be classified.

lack of excess emission from the disk. These stars are likely to be among the ∼120 objects consistent with low-mass stars according to their JHK colors, but we cannot determine their membership with the data available at this point. The high extinction over some parts of the globule would ensure low or zero contamination from background stars, so the removal of the main-sequence, foreground objects would leave the cluster members, but the globule is partially thin in some areas, so the contamination by non-members can be certainly high.

The presence of this important population of protostars and CTTS in the globule points to the existence of a second population of stars toward the western region of the cluster, consistent with the lower ages of many of the stars in this region. It could also suggest that the star formation process giving birth to HD 206267 and the 4 Myr old stars in Tr 37 still continues to the present.

3.2 High- and Intermediate-Mass Stars in Tr 37

The high- and intermediate-mass stars are more difficult to identify, because Li depletion timescales for young stars of spectral types of early K, G or earlier are comparable to the Main Sequence ages, and the Li EW is very small (∼0.1Å) and mostly undetectable in low-resolution spectra (Briceño et al., 1997, 1998; Hartmann, 2003). Moreover, the Hα absorption, characteristic of the spectra of the earlier types (F,A,B), constitutes a problem to detect the Hα emission from accretion and/or chromospheric accretion using low resolution spectra, but

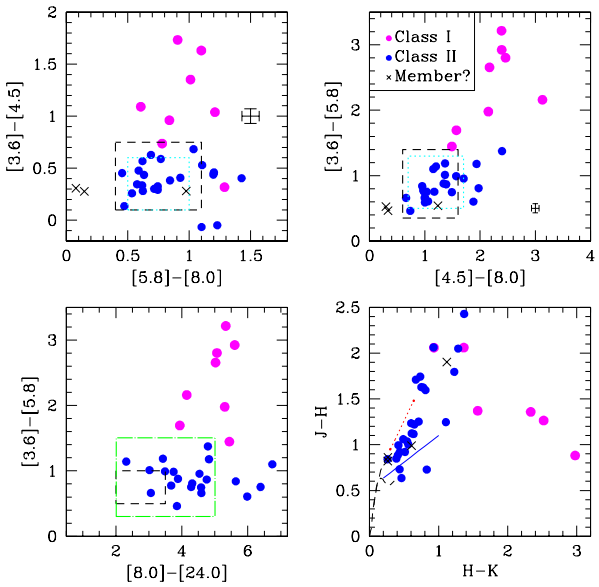

Figure 3.18 IRAC and 2MASS color-color diagram for the stars and protostars detected in the Tr 37 globule. Class I sources are open circles; class II sources are solid circles; uncertain members are represented by crosses. Models by D'Alessio et al. 2005 are represented as dashed lines in the first three panels. Taurus data (Hartmann et al. 2005) is depicted as a dotted line in the two upper panels, and NGC 7129 (Muzerolle et al. 2004) data is represented by the dotted-dashed line in the third panel. The standard sequences are represented by dashed lines, and the CTTS locus is depicted as a solid line in the fourth diagram; reddening vector for A_V=5 is represented as a dotted line.

in the cases of very strong accretion. Therefore, we use the extinction in order to determine the membership.

For Tr 37, we revised the work by Contreras et al. (2002). Since the 4Shooter/1.2m observations are saturated for magnitudes brighter than V∼14, we used the BV photometry (see Figure 3.20) and coordinates from Marschall & van Altena (1987) and Kun et al. (1987). We also obtained their JHK counterparts in the 2MASS survey (see Figure 3.21). This information is shown in Table 3.4. Using the B-V colors in Kenyon & Hartmann (1995) and the relation $A_V = 3.23E(B-V)$ (Bessell & Brett, 1988), we calculated individual extinctions (Table 3.4). We consider as confirmed members (labeled "Y" in the table) those stars with A_V values in the $\pm 1\sigma$ region around the cluster average, as probable members ("P" in the table) if their A_V is located out of the $\pm 1\sigma$ and within $\pm 2\sigma$ of the cluster average, as probable non-members ("PN") if they belong to the region from $\pm 2\sigma$ to $\pm 3\sigma$, and as non-members ("N") if their extinction places them beyond $\pm 3\sigma$ from the average extinction.

3.2.1 Disks around High- and Intermediate-Mass Stars in Tr 37

Thanks to the Spitzer photometry, the presence of disks around high- and intermediate-mass stars in Tr 37 could be studied. The MIPS 24 μm photometry contributes to detect optically-thin debris disks around the BAF-type stars, in addition to any optically-thick disks detectable at shorter wavelengths. Given that the ages for these stars are well established by

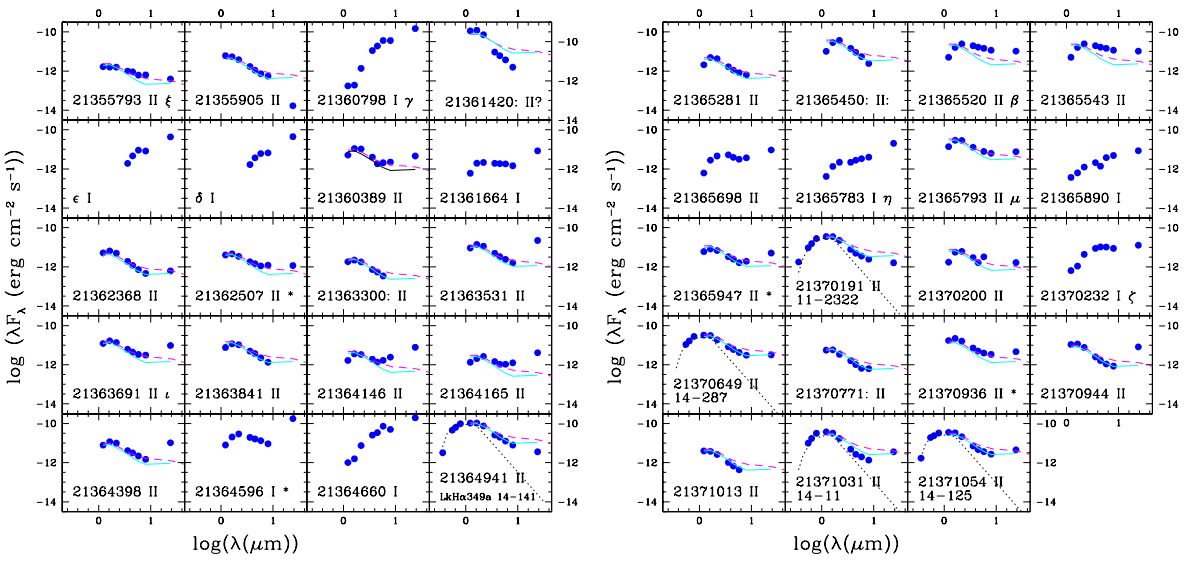

Figure 3.19 SEDs for the stars and protostars detected in the Tr 37 globule. Fluxes correspond to JHK (from 2MASS, Cutri et al. 2003), 3.6, 4.5, 5.8, 8.0 and 24.0 μm. An asterisk or the optical ID was added when the star had been observed with Hectospec; VRI colors are included in such cases if the VRI photometry was available as well. For comparison, we display: the photospheric emission of a similar spectral type (derived from Kenyon & Hartmann 1995) as a black dotted line (when the spectral type is known); the median disk emission in Taurus (Hartmann et al., 2005) as a magenta dashed line; the median disk emission in Tr 37 as a light blue line.

means of the lower mass cluster members, we can determine the age of the disks and debris disks around the BAF-type stars, which is usually hard to do for stars in the Main Sequence. In order to explore the presence of disks, the spectral energy distributions (SEDs) for the high- and intermediate-mass stars are traced in Figures 3.22 and 3.23. A comparison with the expected SED for a similar spectral type star (obtained from the colors given in Kenyon & Hartmann 1995), and with the emission from the debris disk around the young star HR 4796A (Jayawardhana et al., 1998) is displayed in the Figures, as well as the BV, JHK, IRAC and MIPS colors.

In Tr 37, the presence of three potential optically thick disks and/or classical Herbig Ae/Be stars had been suggested by Contreras et al. (2002) and Hernández et al. (2005), who found three stars in Tr 37 with emission line spectra (KUN-314S, MVA-426 and MVA-437). MVA-426 shows an excess in JHK colors from the 2MASS survey (Cutri et al., 2003), suggesting an optically thick disk, but no other significant JHK excess was detected for the rest of cluster members. Examining Figure 3.22, we find 3 stars with these characteristics: KUN-314S, MVA-426, and probably KUN-196. KUN-314S (spectral type undetermined by Contreras et al. 2002, SED consistent with A type) is located out of our IRAC field, but a small K excess, together with a large 24 μ excess (comparable to HR 4796), seems to indicate the presence of an optically thick disk, rather than just a debris disk. MVA-426 (spectral type B7) is out of the IRAC field, too, but the large JHK excess and its high flux at 24 μm (an order of magnitude larger than HR 4796) suggest the presence of an optically thick disk as

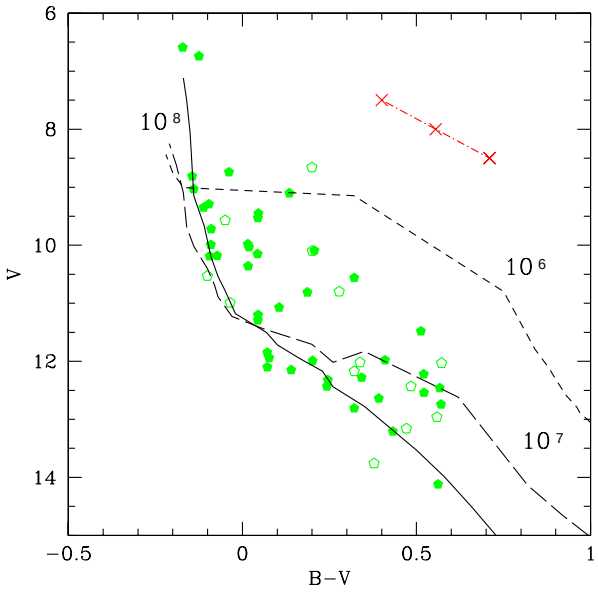

Figure 3.20 High- and Intermediate-Mass Members: B vs. B-V diagram for all the high- and intermediate-mass members in Tr 37. Photometry from Marschall & van Altena (1987); Kun et al. (1987), dereddened with the individual A_V. 1, 10 and 100 Myr isochrones from Siess et al. (2000). Filled symbols: confirmed members (according to A_V, see text). Open symbols: probable members (according to extinction). The reddening vector for intervals of A_V=0.5 is represented as a dotted-dashed line.

well. Finally, KUN-196 (spectral type B9) shows a moderate excess at the IRAC wavelengths, which could be produced by free-free emission in a gaseous disk. Given that this star is out of the MIPS field, we cannot confirm any excess at 24 μm. Some small IRAC excess at 8.0 μm seems to appear for KUN-86 (spectral type F9), although the lack of MIPS observations does not allow us to confirm the detection. We do not detect any IRAC excess for the third emission line star, MVA-437, and no MIPS observations are available for it, so we do not have any information about the presence of a disk.

In addition, the MIPS 24 μm observations reveal a total of 4-5 debris disks around other stars in Tr 37: MVA-1312 (spectral type B4), CCDM+5734Ae (spectral type B3) and/or CCDM+5734Aw (spectral type B5), MVA-468 (spectral type B7), and MVA-447 (spectral type F0). For the binary star CCDM+5734Ae/w (spectral types B3 and B5), we find only one IR counterpart, which could correspond to either of them or both. According to the Hyparcos survey of double and multiple stars (Perryman et al., 1997), both stars form part of a multiple system, so the presence of a debris disks around one or both of the stars is remarkable, since it could indicate that either long survival of the disks and/or formation of planetesimals has taken place in the system. The F9 accreting star 21374275+5733250 is close to the system, as well, although we do not have any information about whether it forms part of the multiple system. These 3 stars are also located to the West of the cluster, and associated to a brighter small clump, detectable in IR, which may suggest that they belong to the younger, ∼1 Myr population.

Therefore, the total number of disks detected in Tr 37 is 7-8. It is also remarkable that

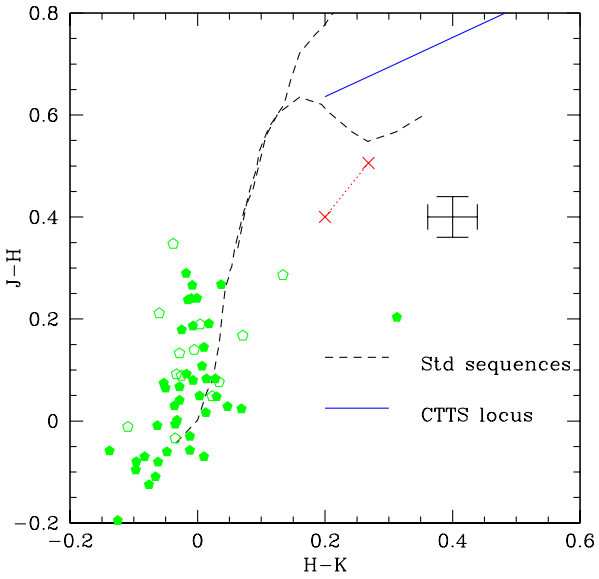

Figure 3.21 High- and Intermediate-Mass Members: J-H vs. H-K diagram for all the high- and intermediate-mass members in Tr 37. Photometry from the 2MASS survey (Cutri et al., 2003), dereddened with the individual extinctions (Bessell & Brett, 1988). Main Sequence and Giant Branch are represented by a dashed line; CTTS locus for a K7 star(Meyer et al., 1997) is represented as a solid line; stars with disks would deviate parallel to this line from their Main Sequence position. Symbols as in Figure 3.20. The star in Tr 37 which shows a large JHK excess is MVA-426, identified as an emission line star by Contreras et al. (2002). The other two emission line stars detected by Contreras et al. (2002) and studied by Hernández et al. (2005), KUN-314S and MVA-437, do not show any noticeable near-IR excess.

most of the high- and intermediate-mass stars with excesses (and the two stars with optically thick disks and emission lines) are located to the West of the cluster, like the younger ∼1Myr population, and like the nebular structures visible at IR wavelengths.

3.3 Completeness and Statistical Significance

In order to give accurate statistical information about the clusters, we need to estimate the completeness of the member list. For the high- and intermediate-mass members (spectral types O,B,A), for which the photometric information was drawn from several sources, the survey is fairly complete for spectral types earlier than A. Since F and early G stars are at the lower end of the magnitudes in these studies (V∼14), and near the saturation limit for our 4Shooter photometry (V∼13.5), we cannot ensure completeness for spectral types F-G. This incompleteness of F and G members may be more important in Tr 37, where there were fewer FAST spectra for V∼14 stars, due to observing time limitations. The 4Shooter photometry is reasonably complete for V=13.5-18.5, corresponding approximately to spectral types mid-G to M2.

We can use the stellar mass function to check completeness comparing our results of the number of stars in each spectral type or mass range in Tr 37, where the member sample is

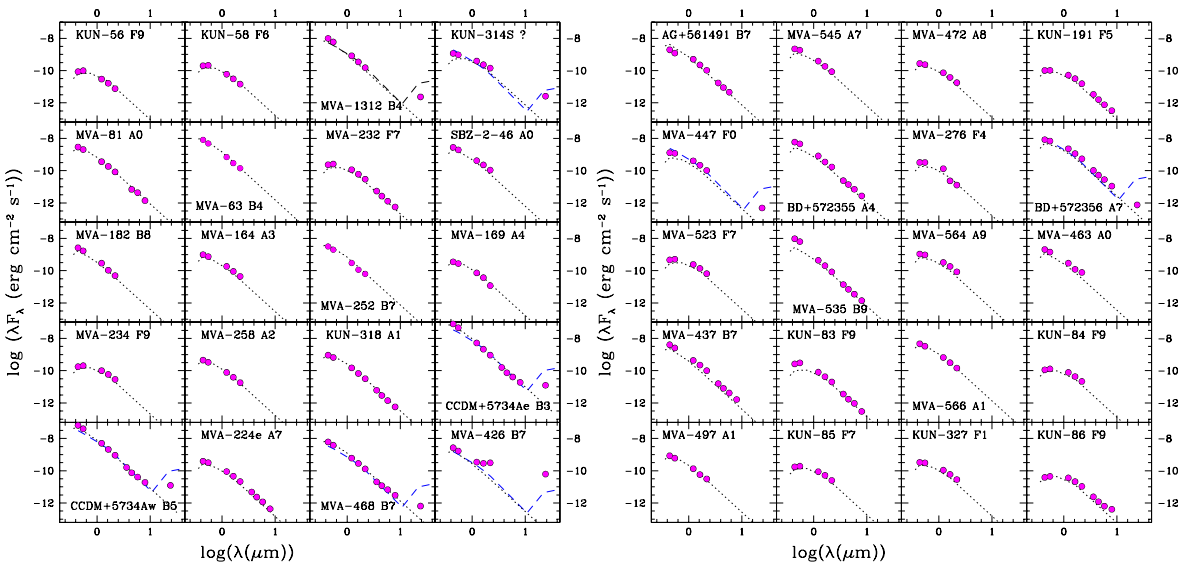

Figure 3.22 Spectral Energy Distributions for high- and intermediate-mass stars in Tr 37. The fluxes correspond to the BV photometry for Tr 37 (Marschall & van Altena, 1987; Kun et al., 1987), UBV photometry for NGC 7160 (De Graeve, 1983), and 2MASS JHK magnitudes, and IRAC and MIPS observations for both clusters. For comparison, the photosphere for a similar spectral type (derived from the colors in Kenyon & Hartmann 1995) is displayed as a dotted line. We also display the emission of the debris disk HR 4796 (Jayawardhana et al., 1998).

large enough for good statistics. If we consider that our survey is complete for the early type (O,B,A) members, we can predict the number of members expected in each one of the other spectral type bins. Figure 3.24 shows the comparison with a Miller-Scalo mass distribution (Kroupa et al., 1999), calibrated with the number of B stars in the cluster. The agreement of the results with the Miller-Scalo predictions are very good for B,A,F, and K stars, suggesting fairly good completeness for these types. The incompleteness for the G-type stars described above appears when comparing with the theoretical mass function. Moreover, the range M0-M2, which would be in principle covered by our 4Shooter photometry, appears to be relatively incomplete, probably because of non-uniform sampling of the faintest members due to the difficulties in finding strong evidence of variability and U excesses for stars of magnitude V∼18.

With the Spitzer photometry, it is possible to make a prediction of the number of lowest mass members which are missing in this study, taking the stars with excesses in the IRAC bands. This way, we are able to search for CTTS that may have been missing in the optical study, since objects showing IRAC excesses are likely to be stars with disks. Moreover, the saturation near the bright stars that appeared in our optical survey will not be so important at IR wavelengths, so that we can also explore the distribution of CTTS in the surroundings of the O6 star HD 206267. This is important to determine if photoevaporation by the UV flux of the massive star played a major role dissipating the disks of the nearby low-mass stars (see Section 3.1.5).

Since we did not use IRAC excesses for the selection of the candidates for spectroscopic

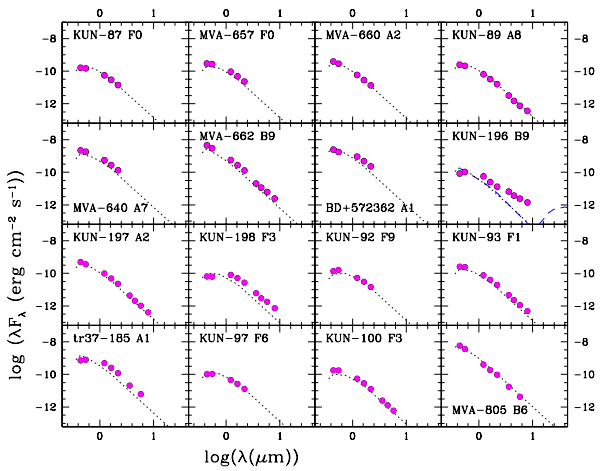

Figure 3.23 Spectral Energy Distributions for high- and intermediate-mass stars in Tr 37. The fluxes correspond to the BV photometry for Tr 37 (Marschall & van Altena, 1987; Kun et al., 1987), UBV photometry for NGC 7160 (De Graeve, 1983), and 2MASS JHK magnitudes, and IRAC and MIPS observations for both clusters. For comparison, the photosphere for a similar spectral type (derived from the colors in Kenyon & Hartmann 1995) is displayed as a dotted line. We also display the emission of the debris disk HR 4796 (Jayawardhana et al., 1998).

followup, we checked how many of the stars, for which we obtained optical spectra (see Section 2.3.3) were found to have IRAC excess, and how many of them were found to be non-members despite of having IRAC excesses consistent with the normal CTTS location. Since we found significant confusion of IRAC sources with poor photometry in objects that had no 2MASS counterparts, and moreover extinction is low enough throughout most of the clusters to allow good JHK photometry for members down to ∼M5, we preferred to include only objects detected by 2MASS for safety. Moreover, 2MASS colors allow us to roughly estimate the spectral type and age of the candidates, even though accreting objects show an excess in JHK in something less than 50% of the cases. Counting these with small errors in their IRAC colors and having 2MASS counterparts, only a few percent of the studied objects had strong IRAC excess (similar to the excesses observed for confirmed CTTS) and were found to be non-members. Therefore, most of the objects selected as having IRAC excess and 2MASS counterparts are safe.

The total number of objects of these characteristics within the IRAC field in Tr 37 is 152, of which approximately half have errors smaller than 0.05 mags in all the IRAC channels, and the other half presents errors of 0.05-0.10 mags in one or more of the IRAC channels. All objects with errors larger than 0.1 mags were rejected, as they can lead easily to spurious color excesses. We also rejected a few objects with 2MASS colors inconsistent with the low-mass stars region in the J-H vs. H-K and J vs. J-H diagrams. We found that, in the range and for the spectral types late G to M2, contamination by non-members would suppose less than 5% of the total number of candidates (even though this contamination may increase in the case of fainter objects). The J color from 2MASS (Cutri et al., 2003) is the least affected by the presence of a disk, and can be used to roughly determine the magnitude and spectral type range of the candidates. About 20 of them have J<14, which would correspond to the average

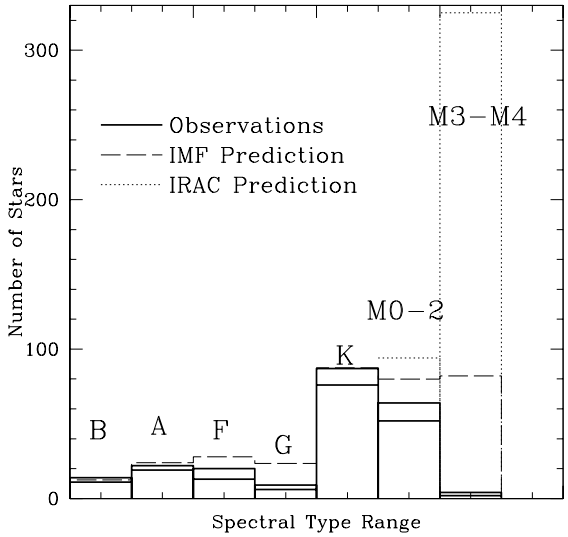

Figure 3.24 Stellar Mass Function for Stars in Tr 37. We display the number of stars in each spectral type range, compared to a Miller-Scalo distribution. Our observational result is shown as a thick continuous line (the lower line contains only the confirmed members, upper line contains additionally the most likely members); the Miller-Scalo distribution is represented by a dashed line; the total number including the extra members predicted based on IRAC excesses is shown as a dotted line. Note the likely contamination of the lower IRAC bin by objects later than M4. The bin M3-M4 is beyond the limit of our 4Shooter photometry. The incompleteness in G and M2 discussed in the text is visible here.

objects of spectral types K6-M2 that we detected in our optical study. The rest corresponds mostly to stars with J=14-16.5. For a cluster at 900pc, this would correspond to spectral types M2-M4, approximately, although some of them could be later than M5, taking into account that these stars may have a near-IR excess caused by their disks.

If we assume that disk fractions will be the same for the later M stars, we would expect a total of about 40-50 more stars in the range M1-M2, and up to 300-350 in the range M3-M4 (according to their J colors). The number of new M0-M2 stars would be in good agreement with the mass function (see Figure 3.24), but the number of M3-M4 seems to be too high in more than 100 stars. This is most likely due to the contamination by later spectral type star (M5, M6, maybe even brown dwarfs) with disks, which could have large IR excesses. We cannot rule out contamination by other objects (galaxies?) and/or larger errors in the photometry of these fainter stars, that would need to be studied in more detail. The Hectospec observations of objects with IRAC excesses produced about 60 optical spectra of objects detected with IRAC, of which only 50% could be classified as cluster members, showing most of the others extremely poor signal-to-noise in optical, and, in a few cases, non-stellar spectra. Part of the excess objects corresponds to embedded protostars within the globule (see Reach et al. 2004 and Section 3.1.6), which are likely to be a second population, maybe triggered by the older one.

Therefore, we will consider from now on that our survey is fairly complete in the range

mid-G to M1, and ∼50% complete for M2; the following analysis is valid only within this range.

The spatial distribution of all the Tr 37 cluster members is displayed in Figure 3.2. The area covered by our 4Shooter photometry (and by our Hectospec fields) is approximately 1 square degree. The spatial distribution of Tr 37 members suggests that we have surveyed the main area subtended by the cluster. The total number of stars above the Main Sequence (from the V vs. V-I diagram and the Siess et al. 2000 isochrones) in the 4Shooter fields is ∼4100 in Tr 37 (of which ∼970 are concentrated in the two central fields). Our spectroscopic survey covered a total of ∼25% of all stars over the Main Sequence in the Tr 37 fields (∼85% of coverage for the stars in the two central fields). Therefore, the statistics obtained in the two central fields, where most of the possible candidates were observed, will be significant, whereas the results coming from the peripheral fields in Tr 37 are tentative and will require more observations for reaching completeness.

We have estimated the total number of members that could be missing among the candidates in the two central fields in Tr 37, for which we do not have Hectospec spectra. They are ∼170 stars located above the Main Sequence. We have examined the properties of these non-observed stars: variability, JHK excess colors, and U excess (from the UVI diagram), in the same way we did for the candidate selection and for giving priorities in the Hectospec observations. From the stars with optical spectra (members and non-members), we can calculate the percentage of stars showing none, one, two or three of the listed properties, that were found to be members, defining a "membership probability". The probability range from more than 80% for objects showing 2 or more of these properties, to ∼25% probability for objects showing only 1 property, and to ∼6% for any objects above the Main Sequence without any excess nor variability detected. These probabilities give us approximately 10 more objects among the rest of candidates over the Main Sequence. Therefore, we can estimate our survey in the two central fields to be ∼95% complete in the range mid-G to M1, with about ∼10 members estimated to be missing (or 165 members known out of the 175 members expected). Since those missing objects do not show strong variability nor excesses, they are most likely WTTS. A similar estimate in the peripheral fields in Tr 37 predict around ∼120 extra members, which would complete the total stellar content of the cluster in the spectral type range mid-G to M1, although these estimates are less accurate out of the two central fields due to the much lower spectroscopic coverage in these regions and due to the fact that some of these regions seem to be out of the cluster boundaries.

Taking into account these results, we can estimate the accretion disk fraction in Tr 37, from the nearly-complete two central fields. Excluding the objects from the biased IRAC selection, we find a total of 46 CTTS and 60 WTTS in this region, giving a ∼43% disk fraction. Including the 14 IRAC-selected objects and the ∼10 new members expected from the non-observed stars (which are most likely WTTS due to their lack of excesses), accretion disk fraction could come up to a maximum of ∼45% and a minimun of ∼40%, so our final accretion disk fraction would be 45±5% at an age of ∼4 Myr. It must be mentioned that setting an upper limit to the number of accreting stars is easier than setting the lower limit, thanks to the efficiency detecting stars with excesses, but the large coverage of the central fields for spectral types mid G to M1 guarantees a good estimate within few percent. Small spatial variations of the disk fraction are found throughout the cluster, so that the disk fraction is ∼35% in the eastern part, and ∼50% to the West of HD 206267, and probably larger in the globule. This can be related to the presence of the younger population in the globule. Note that we do not include the fainter objects detected with IRAC (spectral type M2-M4) since

they are not confirmed and since we have no information about the diskless stars with M2-M4 spectral types. A fraction of ∼40-45% of accreting stars is consistent with the expected result comparing younger and older regions (see, for instance, Lada et al. 2000). Nevertheless, it is important to mention that this fraction correspond to the number of actively accreting stars. As mentioned, Spitzer reveals non-accreting stars with disks ("transition objects"), which are a few percent of the cluster members.

3.4 Data Tables

Table 3.3. Summary of Spectroscopy, Extinction and Membership for Low-Mass Stars in Tr37.

ID1	Instrument	Spec. Type	Hα EW(Å)	Li EW(Å)	TTS Type	A_V	Age(Myr)	Member	Comments
73-758	Hecto	K6.5 ± 0.5	-8.7	0.4	w:	1.9	1.8	Y	IR,c
72-489	Hecto	K5.0? ± 3.0	-5.5	—	w:	1.7	22	P	
72-1427	Hecto	M1.0 ± 1.0	-76.7	—	c	1.4	2.2	Y	IR
81-541	Hecto	K5.5 ± 1.0	-60.2	0.4	c	2.3	2.8	Y	IR
73-472	Hecto	K5.0 ± 1.0	-10.3	0.7	c	1.7	3.3	Y	L,IR
73-311	Hecto	M1.5 ± 0.5	-29.4	—	c	1.1	2.8	Y	L,IR
73-71	Hecto	K6.0 ± 1.0	-11.9	0.4	c	2.1	1.8	Y	IR,acc
72-875	Hecto	M0.5 ± 1.0	-20.7	0.1	c	0.8	8.4	Y	IR
73-194	Hecto	K6.5 ± 1.0	-4.1	—	w	1.5	1.8	P	
73-537	Hecto	G1.5 ± 3.5	-5.3	0.3	c	3.3	27	Y	IR
21362507+5727502	Hecto	M0.0±1.0	-85.6	—	c	—	—	P	
14-306	Hecto	K6.5 ± 2.0	-8.4	—	w:	1.9	13	P	
21364596+5729339	Hecto	—	-46.9	—	c	—	—	P	
21364762+5729540	Hecto	K6.0±2.5	-75.8	0.5	c	—	—	P	
14-141	Hydra	K6.0 ± 0.5	-5.0	0.6	c	1.7	0.6	Y	Yg,L,IR,c
14-1229	Hecto	K6.0±1.0	-4.6	0.4	w	1.3	11	Y	
11-2146	Hecto	K6.0 ± 0.5	-32.9	0.5	c	2.6	0.9	Y	Yg,L,IR,acc
”	Hydra	— ± —	-33.0	0.5	—	—	—	—	
11-1209	Hydra	K6.0 ± 1.0	-4.0	0.7	w	0.7	1.0	Y	Yg,L,IR,c,acc
21365947+5731349	Hecto	M0.0±2.5	-109.0	—	c	—	—	P	
11-1659	Hecto	K5.0 ± 0.5	-1.8	0.5	w	1.9	5.0	Y	acc:
11-1499	Hecto	M1.5±1.0	-7.3	0.3	w	0.6	1.4	Y	
11-2322	Hecto	M1.0 ± 0.5	-23.2	0.4	c	0.9	0.9	Y	Yg,L,IR,acc
”	Hydra	— ± —	-22.0	—	—	—	—	—	
11-1871	Hecto	M2.0 ± 1.5	-13.4	1.0	c:	0.8	2.6	Y	w:,acc:
14-222	FAST	K7 ± 0.5	-5.0	0.6	w	1.2	0.7	Y	Yg,IR,c,acc
14-287	Hecto	M0.0 ± 0.5	-35.3	0.5	c	2.2	1.0	Y	Yg,IR
11-2037	Hecto	K4.5 ± 0.5	-50.0	0.5	c	1.6	2.5	Y	L,IR,acc
”	Hydra	— ± —	-63.0	0.3	—	—	—	—	
11-1067	Hecto	M0.5 ± 0.5	-6.8	—	w	1.2	2.9	Y	
21370936+5729483	Hecto	M0.5±1.5	-21.3	0.2	c	—	—	P	
14-11	Hecto	M1.5 ± 0.5	-5.3	0.3	w	1.8	0.7	Y	Yg,IR,TO
14-125	Hecto	K5.0 ± 1.0	-13.1	0.6	c	1.7	2.9	Y	IR
”	Hydra	— ± —	-16.0	0.4	—	—	—	—	
11-1513	Hecto	K7.5 ± 1.0	-4.8	0.5	w	1.8	1.2	Y	
11-2131	Hecto	K6.5 ± 0.5	-9.6	0.5	c	2.3	2.3	Y	IR,acc
”	Hydra	— ± —	-4.0	0.7	—	—	—	—	
11-2397	Hecto	K7.0±1.5	-80.8	—	c	1.2	15	P	

Table 3.3 (continued)

ID1	Instrument	Spec. Type	Hα EW(Å)	Li EW(Å)	TTS Type	A_V	Age(Myr)	Member	Comments
11-2487	Hecto	K7.0 ± 2.0	-3.9	0.4	w	1.9	2.8	Y	
11-2031	Hydra	K2.0 ± 0.5	-5.0	0.4	c	1.7	2.5	Y	IR
14-103	Hecto	K7.0 ± 1.0	-1.5	0.3	w	1.0	14	Y	
14-197	Hecto	K5.5 ± 1.0	-2.3	0.5	w	1.7	4.2	Y	acc:
21372447+5731359	Hecto	M3.5±1.0	-41.0	—	c	—	—	P	
14-160	Hecto	K5.0 ± 1.0	-22.5	0.6	c	1.8	3.1	Y	IR
”	FAST	— ± —	-8.0	—	—	—	—	—	
11-2503	Hecto	M0.0±1.5	-7.2	0.3	w	2.3	0.9	Y	
11-581	FAST	G ± 0.0	-9.0	—	w:	1.5	2.1	P	
14-1017	Hydra	M0.0 ± 0.5	-55.0	0.5	c	2.1	2.2	Y	IR
14-335	Hecto	K6.5 ± 1.0	-19.7	0.6	c	1.5	2.8	Y	L,IR
”	Hydra	— ± —	-18.0	0.6	—	—	—	—	
11-1864	Hydra	G-K ± 0.0	-5.0	0.3	c	1.7	7.4	Y	w
83-343	Hecto	M0.5 ± 0.5	-3.0	0.5	w	0.9	0.9	Y	Yg
14-183	Hecto	K7.0 ± 1.0	-65.3	1.2	c	2.0	0.9	Y	Yg,IR
”	Hydra	— ± —	-18.0	0.5	—	—	—	—	
14-2148	Hecto	M1.5 ± 0.5	-2.0	0.4	w	1.5	2.0	Y	
21374275+5733250	Hecto	F9.0±1.5	-53.5	0.1	c	—	—	P	
11-1384	Hecto	K6.5 ± 1.0	-4.7	0.6	w	1.7	2.4	Y	
11-383	Hecto	K6.5 ± 1.0	-22.6	0.4	c	0.8	4.4	Y	IR
”	Hydra	— ± —	-23.0	1.3	—	—	—	—	
11-2318	Hydra	M0.0 ± 0.5	-8.0	0.5	w	1.1	2.9	Y	
13-924	Hecto	K5.0 ± 0.5	-4.3	0.6	w:	1.6	4.7	Y	
”	Hydra	— ± —	-7.0	0.8	—	—	—	—	
12-1984	Hecto	K6.0 ± 1.0	-4.8	0.7	w	0.8	5.8	Y	
12-2519	Hecto	K5.5 ± 1.0	-7.5	0.5	c	1.6	2.6	Y	IR
12-1968	Hecto	K6.0 ± 1.0	-11.3	0.4	c	1.2	2.6	Y	IR
12-1422	Hydra	M0.0 ± 0.5	-17.0	0.7	c	1.9	2.7	Y	w,acc:
12-1091	Hecto	G2.5 ± 1.5	-17.4	0.5	c	2.8	23	Y	IR,acc
”	Hydra	— ± —	-10.0	0.6	—	—	—	—	
13-269	Hecto	K6.5 ± 0.5	-6.7	0.4	w	1.9	1.6	Y	acc:
12-583	Hydra	M0.0 ± 0.5	-7.0	—	w	1.6	1.0	Y	Yg
12-94	Hydra	K4.0 ± 1.0	-4.0	—	w:	1.8	7.2	P	
13-1238	Hecto	M1.0 ± 0.5	-63.8	0.7	c	2.6	0.8	Y	Yg,IR,acc
”	Hydra	— ± —	-107.0	—	—	—	—	—	
12-2373	Hecto	M1.0 ± 0.5	-6.5	0.4	w	1.2	1.8	Y	
82-272	Hecto	G9.0 ± 1.0	-12.7	0.4	c	3.6	11	Y	IR,acc
12-1081	Hecto	M0.5 ± 0.5	-3.5	0.7	w	1.3	4.0	Y	

Table 3.3 (continued)

ID1	Instrument	Spec. Type	Hα EW(Å)	Li EW(Å)	TTS Type	A_V	Age(Myr)	Member	Comments
”	Hydra	— ± —	-8.0	—	—	—	—	—	
13-1161	Hecto	M0.0 ± 1.0	-1.1	0.5	w	1.5	2.8	Y	
”	Hydra	— ± —	-7.0	—	—	—	—	—	
12-1613	Hydra	M1.0 ± 0.5	-13.0	—	c	1.3	2.3	P	w
13-1426	Hydra	M0.0 ± 0.5	-109.0	—	c	3.2	1.8	P	IR
13-669	Hydra	K1.0 ± 1.0	-22.0	0.6	c	2.2	2.8	Y	IR,acc
13-350	Hydra	M1.0 ± 1.0	-9.0	—	w	0.7	4.2	P	c
12-1017	Hecto	K5.5 ± 0.5	-3.8	0.6	w:	1.4	4.1	Y	IR,acc:
54-1781	Hecto	M1.0±2.0	-12.8	0.3	c	1.2	2.3	Y	
13-1877	Hecto	K7.0 ± 1.0	-68.5	0.4	c	2.0	1.0	Y	Yg,L,IR,acc
13-277	Hydra	G1.0 ± 2.0	-10.0	—	c	2.5	2.6	Y	Yg,L,IR,acc
12-1009	Hecto	K5.5 ± 0.5	-4.5	0.6	w:	0.9	2.9	Y	
13-2236	Hecto	K6.5 ± 1.0	-0.5	0.6	w	1.6	5.2	Y	
13-819	Hecto	K5.5 ± 1.5	-10.3	0.5	c	1.4	2.4	Y	w,acc:
12-1955	Hecto	K6.5 ± 0.5	-1.6	0.4	w	1.4	6.9	Y	
”	Hydra	— ± —	-7.0	0.4	—	—	—	—	
13-236	Hydra	K2.0 ± 1.0	-47.0	—	c	1.8	2.8	Y	L,IR,acc
12-2113	Hecto	M1.0 ± 1.0	-28.0	0.4	c	1.2	1.1	Y	L,IR,acc
”	FAST	— ± —	-15.0	0.4	—	—	—	—	
13-157	Hecto	K5.5 ± 1.0	-14.0	0.5	c	1.2	2.4	Y	L,IR,acc
13-232	Hecto	M0.0 ± 0.5	-3.3	0.3	w	1.1	2.2	Y	
21383216+5726359	Hecto	M0.0±3.0	-129.0	0.3	c	—	—	P	
13-52	Hecto	K7.0 ± 0.5	-0.8	0.7	w	1.3	4.1	Y	IR,TO
12-1825	Hydra	M0.0 ± 0.5	-10.0	0.6	c	2.1	4.8	Y	w
91-155	Hecto	M2.5 ± 0.5	-7.8	0.4	w	1.2	1.7	Y	IR,c
13-566	Hecto	K5.5±1.5	-5.2	0.4	w	2.4	2.5	Y	
13-1891	Hydra	M0.0 ± 0.5	-11.0	—	c	1.0	5.1	P	IR
13-1709	Hecto	K5.5 ± 0.5	-3.2	0.4	w:	1.2	5.2	Y	acc:
54-1613	Hecto	K5.0 ± 0.5	-0.7	0.5	w	1.2	5.2	Y	acc:
21384350+5727270	Hecto	M2.0±2.0	-22.6	0.4	c	—	—	P	
54-1547	Hecto	K5.0 ± 1.0	-33.8	0.4	c	1.2	5.7	Y	L,IR,acc
”	Hecto	— ± —	-41.2	0.5	—	—	—	—	
”	Hydra	— ± —	-37.0	0.6	—	—	—	—	
12-2363	Hecto	M0.5 ± 0.5	-3.0	0.6	w	1.9	1.0	Y	Yg
12-595	Hydra	K7.0 ± 0.5	-17.0	1.6	c	1.2	19	Y	IR
12-1423	Hecto	K7.0 ± 1.0	-1.5	0.5	w	1.5	2.3	Y	acc:
12-1010	Hecto	M2.0 ± 0.5	-20.3	0.2	c	0.3	5.3	P	L,IR
12-2098	Hecto	M2.5 ± 0.5	-5.9	0.4	w	1.0	2.3	Y	

Table 3.3 (continued)

ID1	Instrument	Spec. Type	Hα EW(Å)	Li EW(Å)	TTS Type	A_V	Age(Myr)	Member	Comments
”	Hecto	— ± —	-7.1	0.7	—	—	—	—	
13-1087	Hecto	K4.0 ± 0.5	-1.6	0.6	w	1.7	4.2	Y	acc
21385669+5730484	Hecto	K5.0±1.5	-4.1	—	w	—	—	P	c
91-506	Hecto	K6.5 ± 0.5	-47.1	0.6	c	1.4	2.6	Y	L,IR,acc:
24-692	Hecto	M1.0 ± 0.5	-1.5	0.5	w	1.5	2.7	Y	
12-1027	Hydra	M0.0 ± 0.5	-11.0	0.8	c	1.3	2.6	Y	w
24-77	Hecto	K6.5 ± 1.0	-3.0	0.5	w	1.4	7.4	Y	
21390321+5730420	Hecto	K7.0±1.5	-41.5	0.3	c	—	—	Y	
24-108	Hecto	K5.5 ± 0.5	-3.3	0.4	w:	1.9	4.3	Y	
12-1617	Hecto	M1.0 ± 0.5	-29.9	0.6	c	1.6	1.2	Y	L,IR,acc
”	Hecto	— ± —	-25.1	0.3	—	—	—	—	
”	Hydra	— ± —	-19.0	0.9	—	—	—	—	
21-840	Hecto	M1.0±1.5	-14.2	0.5	c	2.2	2.1	Y	
13-1048	Hecto	M0.0±2.0	-7.0	0.4	w	1.7	7.4	Y	
13-1250	Hecto	K4.5 ± 1.0	-2.5	0.4	w	1.4	3.3	Y	IR,TO
”	Hydra	— ± —	-3.0	0.9	—	—	—	—	
12-705	Hecto	M1.0 ± 0.5	-2.0	0.3	c	1.3	1.5	Y	
12-942	Hecto	K7.5 ± 1.0	-4.1	0.7	w	1.7	1.5	Y	
”	Hydra	— ± —	-3.3	0.5	—	—	—	—	
91-815	Hecto	M2.0 ± 0.5	-4.3	0.2	w	1.3	2.0	Y	
21-1590	Hecto	K7.0 ± 1.0	-4.1	0.6	w	2.2	3.4	Y	
”	Hydra	— ± —	-4.3	0.4	—	—	—	—	
54-1488	Hecto	K7.0±2.0	-13.1	0.4	c	0.1	7.2	Y	
24-542	Hydra	K4.0 ± 1.0	-4.0	1.3	w:	1.0	2.3	Y	
24-515	Hecto	M0.5 ± 0.5	-10.9	—	c	1.1	2.8	Y	IR
21-998	Hecto	K5.5 ± 1.0	-15.9	0.3	c	1.9	5.6	Y	L,IR,acc
21-33	Hydra	M0.0 ± 0.5	-107.0	—	c	1.7	4.0	Y	IR
24-170	Hecto	K7.5 ± 0.5	-4.4	0.4	w	1.5	2.4	Y	IR,TO
53-1803	Hecto	K6.5 ± 1.0	-1.2	0.4	w	1.4	20	Y	
24-48	Hecto	M0.5 ± 1.0	-0.9	0.5	w	1.5	2.4	Y	
21-833	Hecto	M0.0±1.5	-7.4	0.3	w	1.6	1.9	Y	
21-230	Hecto	M0.5 ± 0.5	-3.2	0.5	w	1.5	2.5	Y	
92-393	Hecto	M2.0 ± 1.0	-33.8	—	c	2.0	0.9	Y	Yg,w
21-1536	Hecto	M0.0±2.0	-26.3	0.2	c	1.8	2.8	Y	
52-1649	Hecto	K5.0±1.0	-3.3	0.4	w	1.1	12	Y	
21-2251	Hecto	M2.0 ± 0.5	-4.3	0.4	w	1.5	1.3	Y	
21-1586	Hydra	K7.0 ± 1.0	-16.0	0.9	c	1.5	3.9	Y	w
24-78	Hecto	M2.0 ± 0.5	-6.1	0.3	w	1.3	1.4	Y	

Table 3.3 (continued)

ID1	Instrument	Spec. Type	Hα EW(Å)	Li EW(Å)	TTS Type	A_V	Age(Myr)	Member	Comments
24-820	Hecto	K6.5 ± 1.0	-1.7	—	w	1.2	27	PN	
92-1162	Hecto	M2.0 ± 1.0	-6.7	0.5	w	1.4	1.6	Y	
53-1762	Hecto	M0.0 ± 1.0	-1.7	0.4	w	1.3	3.0	Y	c,acc
93-361	Hecto	G1.0 ± 2.5	-78.0	0.4	c	3.6	16	Y	L,IR
21-1974	Hecto	G7.5±1.5	-7.6	0.4	c	2.5	13	Y	
21-1692	Hydra	M1.0 ± 0.5	-5.0	0.5	w	1.7	2.5	Y	
21-763	Hecto	M0.0 ± 0.5	-2.8	0.4	w	1.2	2.6	Y	
24-817	Hecto	K6.5 ± 1.0	-3.8	0.6	w	2.0	4.6	Y	acc
”	Hydra	— ± —	-14.0	—	—	—	—	—	
21-895	Hecto	K5.0 ± 0.5	-0.6	0.5	w	1.4	2.8	Y	acc
21400451+5728363	Hecto	K5.0±1.5	-31.8	0.4	c	—	—	Y	
21-1762	Hecto	K5.0 ± 0.5	-3.1	0.5	w:	1.8	4.3	Y	acc
24-382	Hecto	K7.5 ± 1.0	-5.4	0.4	w	1.4	6.0	Y	
24-1736	Hydra	M1.0 ± 1.0	-61.0	—	c	1.0	3.9	P	L,IR,acc:
24-1796	Hecto	K7.0 ± 1.0	-124.5	0.3	c	1.2	6.0	Y	IR,acc
21-2006	Hecto	K5.0 ± 0.5	-1.8	0.4	w	1.5	6.1	Y	IR,c,acc
22-2651	Hecto	M1.5 ± 0.5	-33.6	—	c	0.9	3.9	Y	L,IR
21402192+5730054	Hecto	K6.0±1.0	-8.5	0.5	w	—	—	Y	c
92-1103	Hecto	K5.5 ± 1.0	-7.2	0.9	c	2.0	1.2	Y	IR
22-1418	Hecto	M1.5 ± 0.5	-2.2	0.5	w	0.7	2.1	Y	L,IR,c
23-405	Hecto	K5.0 ± 0.5	-13.9	0.4	c	1.1	5.0	Y	IR
23-570	Hecto	K6.0 ± 0.5	-47.1	0.4	c	1.3	4.2	Y	IR,acc
93-540	Hecto	M0.0 ± 0.5	-18.0	0.3	c	2.2	2.3	Y	IR
53-1843	Hecto	M0.5 ± 0.5	-4.2	0.6	w	0.7	3.6	Y	
21403721+5729127	Hecto	K7.5±2.0	-41.3	—	c	—	—	P	
23-1161	Hecto	K6.5±1.0	-6.7	0.7	w	1.4	11	Y	
93-168	Hecto	K6.5 ± 1.0	-21.8	0.5	c	1.2	2.5	Y	L,acc:
23-162	Hecto	K7.0 ± 1.0	-6.4	0.4	w	1.7	6.6	Y	L,IR,c
22-939	Hecto	K6.0±1.5	-1.3	—	w	1.3	7.6	P	
23-753	Hecto	M0.5-M0 ± 0.5	-2.4	0.5	w	0.5	8.5	Y	
53-1561	Hecto	K6.0±2.0	-28.1	0.1	c	2.1	3.0	P	
22-445	Hecto	M0.5 ± 0.5	-3.6	0.4	w	1.3	2.4	Y	
22-1526	Hecto	M1.0 ± 0.5	-1.0	0.5	w	0.6	3.2	P	
22-404	Hecto	G7.0±1.5	-1.3	0.4	w	1.4	14	Y	
23-969	Hecto	K5.5 ± 0.5	-36.4	0.5	c	1.2	2.9	Y	acc
22-960	Hecto	M2.5 ± 0.5	-2.6	0.4	w	0.6	2.5	P	
22-1569	Hecto	M1.0 ± 0.5	-2.7	0.6	w	1.4	1.3	Y	
23-798	FAST	K6.0 ± 1.0	-150.0	0.5	c	2.2	15	Y	L,acc

Table 3.3 (continued)

ID1	Instrument	Spec. Type	Hα EW(Å)	Li EW(Å)	TTS Type	A_V	Age(Myr)	Member	Comments
43-795	Hecto	K5.5 ± 0.5	-4.3	0.5	w:	1.7	4.4	Y	

Note. — Summary of spectroscopic data extinction and membership for Tr37. Given the better quality of Hectospec spectra, they were given preference for obtaining spectral types. Errors in the spectral types are given in number of subtypes. Colon denotes uncertain values. Referred to the type of TTS, they denote the objects with Hα in the limit between CTTS and WTTS according to White & Basri (2003). Ages are derived using the (Siess et al., 2000) isochrones in the V vs. V-I diagram. Membership: Y=confirmed member; P=probable member; PN= probable non-member. Comment: Yg="maybe younger", meaning it is over the 1 Myr isochrone in the V vs. V-I diagram; L=JHK colors consistent with the CTTS locus; IR=IRAC/MIPS excess consistent with a disk; w=WTTS according to the absence of an accreting disk down to 24 μm (even if Hα was over the limit for CTTS); c=CTTS according to the presence of an accreting disk (even if Hα was weak); TO= "transition object" or non-accreting WTTS with disk (see text); acc= accretion detected via U band.

Table 3.4. Summary of Optical, Near-IR and Spectroscopic Data for High- and Intermediate-Mass Stars in Tr37 .

ID1	2MASS	B	V	J	H	K	Spec.Type	A_V	Member
KUN-56	21354864+5720283	16.32	15.16	13.341±0.024	12.953±0.032	12.831±0.029	F9	1.9	Y
KUN-58	21355394+5742474	15.77	14.61	12.664±0.024	12.300±0.029	12.180±0.021	F6	2.2	P
MVA-1312	21355654+5720529	10.67	10.34	9.718±0.031	9.636±0.037	9.594±0.025	B4	1.5	Y
KUN-314S	21361422+5721309	12.87	12.24	10.388±0.032	10.033±0.037	9.623±0.026	—	1.6	Y
MVA-81	21362383+5738053	12.00	11.51	10.427±0.024	10.325±0.031	10.269±0.023	A0	1.5	Y
MVA-63	21363690+5734060	11.51	11.03	9.887±0.022	9.745±0.026	9.692±0.020	B4	2.0	Y
MVA-232	21371062+5742155	15.40	14.25	11.946±0.023	11.493±0.028	11.370±0.021	F7	2.0	Y
SBZ-2-46	21371840+5731206	12.42	11.84	10.385±0.023	10.119±0.027	10.049±0.023	A0	1.8	Y
MVA-182	21371956+5730489	12.40	11.93	10.892±0.023	10.786±0.027	10.763±0.020	B8	1.8	Y
MVA-164	21372008+5725140	12.97	12.44	11.169±0.026	10.983±0.029	10.918±0.023	A3	1.4	Y
MVA-252	21372258+5745072	12.48	11.96	10.766±0.025	10.653±0.026	10.616±0.020	B7	2.0	Y
MVA-169	21372394+5728169	14.74	14.02	12.296±0.023	12.033±0.027	11.956±0.024	A4	1.9	Y
MVA-234	21373432+5740408	15.28	14.18	11.896±0.025	11.424±0.031	11.325±0.025	F9	1.7	Y
MVA-258	21375610+5742208	14.27	13.66	12.240±0.029	11.975±0.031	11.844±0.021	A2	1.7	Y
KUN-318	21372600+5736015	13.21	12.70	11.395±0.021	11.266±0.026	11.176±0.020	A1	1.5	Y
CCDM+5734Ae	21374093+5733372	8.58	8.24	7.697±0.019	7.647±0.031	7.611±0.021	B3	1.7	Y
CCDM+5734Aw	21374093+5733372	8.58	8.24	7.697±0.019	7.647±0.031	7.611±0.021	B5	1.5	Y
MVA-257	21375658+5742526	14.99	14.28	12.872±0.035	12.685±0.041	12.561±0.033	B2	2.9	PN
MVA-224e	21380095+5738069	13.58	13.05	11.856±0.027	11.696±0.032	11.594±0.021	A7	1.1	Y
MVA-468	21380816+5731267	10.91	10.60	9.868±0.027	9.738±0.032	9.712±0.018	B7	1.3	Y
MVA-426	21380845+5726476	11.93	11.59	10.510±0.026	9.724±0.029	8.767±0.020	B7	1.4	Y
AG+561491	21381636+5710115	11.70	11.50	9.988±0.024	9.919±0.029	9.888±0.018	B7	1.0	P
MVA-545	21381720+5740020	12.17	11.52	10.434±0.027	10.215±0.032	10.146±0.021	A7	1.4	Y
MVA-472	21381921+5731567	14.36	13.69	12.188±0.030	11.960±0.038	11.839±0.028	A8	1.4	Y
KUN-191	21382530+5723124	15.07	14.30	12.469±0.027	12.086±0.029	11.975±0.022	F5	1.1	Y
MVA-447	21382638+5728406	12.44	11.75	10.310±0.027	10.005±0.029	9.949±0.020	F0	1.2	Y
BD+572355	21382918+5741227	11.20	10.60	9.700±0.029	9.547±0.032	9.480±0.018	A4	1.5	Y
MVA-276	—	14.80	13.82	—	—	—	F4	1.8	Y
BD+572356	21383028+5746265	9.96	9.50	8.310±0.025	8.132±0.051	8.100±0.022	A7	0.8	P
MVA-523	21385949+5736506	13.63	12.73	10.893±0.024	10.520±0.028	10.445±0.022	F7	1.3	Y
MVA-535	21390090+5738009	11.40	10.80	10.409±0.024	10.249±0.024	10.247±0.022	B9	2.1	Y
MVA-564	21390788+5742085	12.10	11.58	10.400±0.022	10.241±0.028	10.154±0.020	A9	0.8	P
MVA-463	21391198+5729572	12.42	11.92	10.750±0.025	10.642±0.026	10.548±0.021	A0	1.6	Y
MVA-437	21391876+5725487	12.08	11.59	10.423±0.023	10.195±0.028	10.104±0.021	B7	1.9	Y
KUN-83	21391873+5734534	15.34	14.12	12.333±0.024	11.900±0.028	11.818±0.026	F9	2.1	P
MVA-566	21391887+5742291	11.33	10.85	9.837±0.021	9.687±0.029	9.624±0.022	A1	1.4	Y
KUN-84	21392104+5724013	14.75	13.90	11.984±0.023	11.717±0.031	11.582±0.023	F9	0.9	P
MVA-497	21392231+5731488	13.26	12.76	11.577±0.025	11.372±0.033	11.269±0.024	A1	1.5	Y

Table 3.4 (continued)

ID1	2MASS	B	V	J	H	K	Spec.Type	A_V	Member
KUN-85	21392469+5723530	15.59	14.47	12.152±0.023	11.681±0.031	11.558±0.025	F7	1.9	Y
KUN-327	21392614+5700092	13.34	12.77	11.602±0.021	11.333±0.028	11.278±0.018	F1	0.8	P
KUN-86	21392674+5733132	16.28	15.34	12.909±0.027	12.539±0.032	12.457±0.030	F9	1.2	Y
KUN-87	21392950+5734203	14.69	14.00	12.439±0.021	12.205±0.027	12.117±0.025	F0	1.2	Y
MVA-657	21393729+5735075	13.67	13.07	11.843±0.027	11.608±0.030	11.552±0.021	F0	0.9	P
MVA-660	21394087+5735089	13.77	13.32	12.415±0.026	12.269±0.031	12.173±0.028	A2	1.2	Y
KUN-89	21394621+5726103	14.31	13.68	12.291±0.021	12.130±0.031	11.998±0.025	A8	1.3	Y
MVA-640	21394674+5732525	11.44	10.97	9.879±0.022	9.738±0.032	9.656±0.022	A7	0.9	P
MVA-662	21394774+5736131	10.87	10.60	9.931±0.026	9.730±0.030	9.693±0.021	B9	1.0	P
MVA-641	21395385+5733086	14.86	14.20	12.796±0.024	12.729±0.033	12.573±0.030	B1	2.9	PN
BD+572362	21400219+5757182	11.70	11.30	9.363±0.022	9.217±0.027	9.070±0.022	A1	1.2	Y
KUN-196	21401508+5740513	13.85	13.20	12.145±0.035	11.922±0.046	11.881±0.051	B9	2.2	P
KUN-197	21401520+5737163	13.31	12.91	11.810±0.026	11.618±0.028	11.553±0.021	A2	1.1	Y
KUN-198	21401908+5726495	15.16	14.54	11.937±0.026	11.568±0.031	11.381±0.023	F3	0.8	P
KUN-92	21401987+5744074	15.97	14.77	12.746±0.024	12.340±0.029	12.184±0.023	F9	2.0	Y
KUN-93	21402050+5731233	14.26	13.53	12.151±0.038	11.874±0.044	11.779±0.039	F1	1.3	Y
tr37-185	21403033+5713262	11.50	11.00	9.821±0.024	9.735±0.031	9.625±0.023	A1	1.5	Y
KUN-97	21410008+5730401	14.81	14.06	12.708±0.042	12.265±0.038	12.242±0.035	F6	0.9	P
KUN-100	21412500+5729278	15.56	14.57	12.714±0.024	12.417±0.032	12.303±0.026	F3	1.9	Y
MVA-805	21413621+5722257	11.40	11.00	10.470±-100.000	10.346±-100.000	10.475±0.052	B6	1.7	Y

Note. — Summary of optical and near-IR data for the high- and intermediate-mass stars in Tr37. ID1, Photometry from Contreras et al. (2002); Marschall & van Altena (1987); Kun et al. (1987). 2MASS from the 2MASS survey (Cutri et al., 2003). Non-defined error in 2MASS photometry is an indication of probable problems. Spectral type for KUN-314S is not well defined; its extinction is considered to be the mean of the cluster; membership is proved by the emission lines in the spectrum. No 2MASS counterpart was found within 2 arcsec of MVA-276. All spectra were taken with the FAST slit spectrograph on the 1.5m telescope. Spectral types from Contreras et al. (2002). Membership based on average extinction for the cluster and its standard deviation (see text; confirmed members=Y if extinction is within 1σ of the average, most likely members=P if extinction is within 1-2σ of the average, most likely non members=PN if extinction is within 2-3σ of the average).

Table 3.5. U Photometry and Mass Accretion Rates in Tr 37.

ID1	U	$L_U(\mathrm{L}_\odot)$	$L_{acc}(\mathrm{L}_\odot)$	dM/dt ($10^{-8} M_\odot yr^{-1}$)	Epoch
73-71	18.92	0.030	0.210	2.112	2003
14-141	19.35	0	—	—	2002
11-2146	18.16	0.152	1.225	16.216	2002
”	18.34	0.126	0.999	13.218	2003
11-1209	17.70	0.006	0.035	0.404	2002
11-1659	20.08	0.004	0.020	0.127:	2002
11-2322	18.69	0.006	0.036	0.800	2002
11-1871	20.10	0.001	0.008	0.124:	2002
14-222	18.52	0.007	0.040	0.614	2002
”	18.36	0.009	0.057	0.860	2003
11-2037	18.11	0.023	0.159	0.974	2002
”	17.51	0.056	0.411	2.508	2003
14-125	20.03	0	—	—	2002
11-2131	19.82	0.020	0.132	1.090	2002
11-2031	18.08	0	—	—	2002
”	17.40	0.037	0.260	1.582	2003
14-197	19.74	0.004	0.021	0.129:	2002
14-160	20.23	0	—	—	2002
11-581	19.96	0	—	—	2002
14-183	20.84	0	—	—	2002
12-1422	20.23	0.008	0.046	0.457	2002
12-1091	18.61	0.026	0.181	0.807	2002
”	18.22	0.095	0.737	3.291	2003
13-269	19.25	0.015	0.101	0.995	2002
13-1238	19.15	0.064	0.477	10.682	2002
82-272	18.32	0.514	4.624	23.934	2003
13-669	18.29	0.015	0.097	0.589	2002
”	17.90	0.050	0.367	2.238	2003
12-1017	19.56	0.002	0.010	0.063:	2002
13-1877	19.19	0.019	0.125	1.890	2002
”	18.91	0.026	0.181	2.742	2003
13-277	16.99	0	—	—	2002
”	16.25	0	—	—	2003
13-819	19.35	0.001	0.005	0.035:	2002
”	19.01	0.005	0.029	0.205	2003
13-236	17.56	0.036	0.258	1.549	2002
”	17.08	0.085	0.652	3.912	2003
12-2113	18.79	0.011	0.067	1.407	2002
13-157	17.51	0.032	0.226	1.615	2002
13-1709	19.38	0.001	0.006	0.034:	2002
54-1613	18.56	0.009	0.059	0.367	2002
54-1547	18.66	0.006	0.037	0.212	2002
12-1423	20.08	0.002	0.011	0.111:	2002
13-1087	18.64	0.007	0.046	0.281	2002
”	18.56	0.010	0.060	0.368	2003
91-506	19.50	0.003	0.018	0.141:	2003
12-1617	19.73	0.010	0.066	1.315	2002
”	19.72	0.008	0.047	0.876	2002
13-1250	18.68	0.003	0.017	0.101:	2002
”	19.01	0	—	—	2003
12-942	20.96	0	—	—	2002
24-542	18.54	0	—	—	2002
”	18.63	0	—	—	2003
21-998	19.18	0.019	0.126	0.731	2002
53-1762	19.44	0.007	0.041	0.437	2002
24-817	19.03	0.028	0.193	1.276	2002
21-895	18.19	0.018	0.122	0.848	2002

Table 3.5 (continued)

ID1	U	$L_U(L_\odot)$	$L_{acc}(L_\odot)$	dM/dt ($10^{-8} M_\odot yr^{-1}$)	Epoch
21-1762	19.58	0.006	0.036	0.231	2002
24-382	22.37	0	—	—	2002
24-1736	19.72	0.004	0.020	0.185:	2002
24-1796	19.16	0.007	0.042	0.312	2002
”	18.70	0.012	0.075	0.554	2003
”	17.84	0.028	0.197	1.449	2003
21-2006	19.66	0.003	0.016	0.094	2002
23-570	18.51	0.013	0.085	0.617	2003
93-168	19.46	0.001	0.006	0.047:	2003
23-969	18.36	0.010	0.063	0.414	2002
23-798	19.72	0.022	0.151	0.791	2002

Note. — U band observations for the low-mass stars in Tr 37: U band magnitudes, U band excess luminosity (L_U) in solar luminosities, accretion luminosity (L_{acc}) in solar luminosities, and mass accretion rate (dM/dt) in 10^{-8} solar masses per year. Excess U luminosity measures only the excess luminosity in U over what would be expected for each spectral type. The total luminosity, calculated from I photometry and the bolometric correction corresponding to each spectral type (Kenyon & Hartmann, 1995). See text and Gullbring et al. (1998). Epoch correspond to the observing run of the observations. Some stars were observed in the two epochs, or included in two overlapping fields during the same observing run, and have therefore multiple U measurements. Colons in the mass accretion rate denote measured values of U band excess at the detection limit, which must be considered cautiously.

4 NGC 7160

Published in "Low Mass Stars and Accretion at the Ages of Planet Formation in the Cep OB2 Region" by Sicilia-Aguilar, A., Hartmann, L., Briceño, C., Muzerolle, J., & Calvet, N., 2004, AJ128, 805; "Cep OB2: Disk Evolution and Accretion at 3-10 Myr", by Sicilia-Aguilar, A., Hartmann, L., Hernández, J., Briceño, C., & Calvet, N., 2005, AJ in press; and "Disk Evolution in Cep OB2: Results from Spitzer Space Telescope", by Sicilia-Aguilar, A., Hartmann, L., Calvet,N., Megeath, S.T., Muzerolle, J., Allen, L., D'Alessio, P., Merín B., and Stauffer, J., 2005, in preparation.

NGC 7160 is the older cluster in the Cep OB2 bubble, and its population of high-mass stars (including, maybe, O-type members that would have exploded as supernova some ∼7 Myr ago, Patel et al. 1998) is thought to have triggered the expanding gas and dust bubble that gave birth to Tr 37. Any significant amounts of gas and dust have already been removed from this ∼10 Myr cluster, and no H II regions nor substantial inhomogeneities are to be seen at IR wavelengths (see Figure 4.1). Among the low-mass stars, only 1 object is found to have an actively accreting disk (out of ∼55 members), and only a one more has a non-accreting disk, suggesting disk fractions of few percent. Among the high-mass stars, 3 objects present optically think debris disks, which also suggests differences in the disks of more massive stars compared to the younger Tr 37.

4.1 Low-Mass Stars in NGC 7160: The End of Accretion

The low-mass stars in NGC 7160 were identified according to the same procedures followed for Tr 37 (see Section 3.1.1). The Hα emission line, together with the Li I 6707 Å absorption, were used to pick the cluster members with spectral types from early K to M3. The main difference in the spectra reduction was that no special techniques for sky subtraction were required for this older cluster, since there is no remaining gas nor extra emission from an H II region, so the sky spectra are very uniform across the cluster, and subtracting an average sky produces good results. The spectral types for the stars in NGC 7160 were obtained with the same classification schemes which are described in Section 3.1.2. Table 4.1 displays the measurements of Hα and Li for the low-mass members in NGC 7160, together with the spectral types and extinctions. The average extinction over the cluster was obtained as it was done in Tr 37, using only the sure members (labeled 'Y' in Table 4.1), the mean value is $A_V = 1.17$, with a standard deviation of 0.45 magnitudes. As in Tr 37, no spatial trends of higher and lower extinction could be found, and typical individual errors in the extinction range 0.1 to

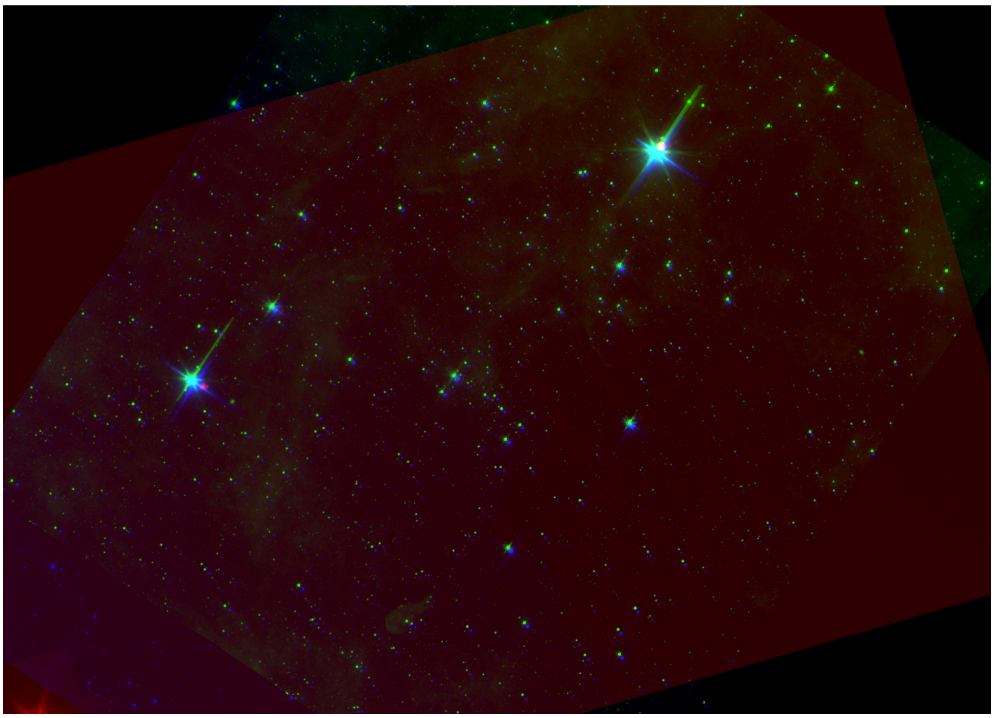

Figure 4.1 NGC 7160: Combined image using the observations from Spitzer at 24 μm (red), 8 μm (green), and 5.8 μm (blue).

0.3 magnitudes in A_V, depending on the spectral type and the photometry. Examining the percentages of stars with deviations from the average extinction in the 1,2, and 3σ regions, we obtain 79%, 97% and 97%, respectively, since only one star shows extinction over the 3σ limit. These values are used to define the probability of the membership for the high- and intermediate-mass stars: members ("Y") are stars within less than 1σ deviation; probable members ("P") are stars within less than 2σ deviation; probable non-members ("PN") show deviations up to 3σ; and non-members ("N") are beyond the 3σ limit.

The most striking result examining the cluster members in NGC 7160, compared to Tr 37, is that only one star shows Hα emission consistent with accretion (the star 01-580). All the rest cluster members show very small Hα emission lines, suggesting that accretion processes are nearly terminated by the age of 10 Myr.

Displaying the V vs. V-I colors for the stars in NGC 7160, we notice that the diagram is much cleaner than the one for Tr 37 (Figure 4.2). The stars are aligned with very little dispersion along the 10 Myr isochrone (Siess et al., 2000), with an average age of $\sim$11 Myr, and it is possible to clearly distinguish the binary sequence of more luminous stars. These facts are due to the lower apparent age dispersion in this older cluster, and will be discussed in detail in Section 5.1.

Examining the 2MASS counterparts of the NGC 7160 members, the difference with Tr 37 is evident once more. Only the accreting star 01-580 shows a reasonable JHK excess, slightly over the 3-σ error (see Figure 4.3). No other significant excess is found for the rest of the

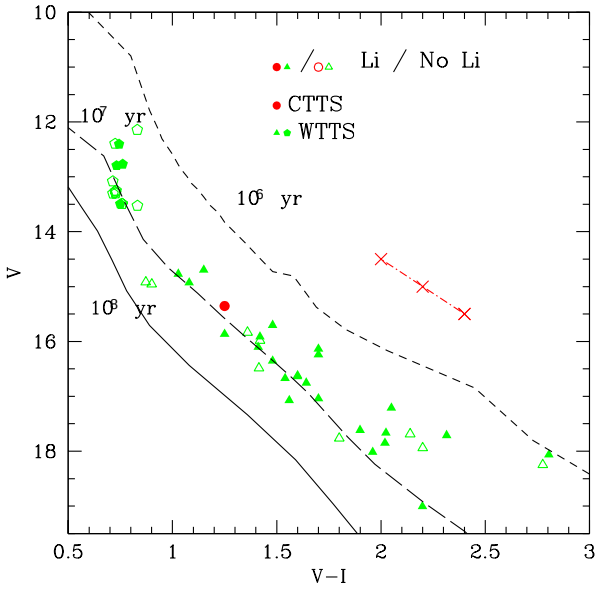

Figure 4.2 Low-Mass Stars: V vs. V-I diagram for all the low-mass members in NGC 7160. Photometry from the 4Shooter/1.2m in FLWO. A reddening correction (Bessell & Brett, 1988) has been applied for each star using the individual reddenings; a reddening vector with X for A_V=0.5 intervals is represented as a dotted-dashed line. Isochrones from Siess et al. (2000) for 1, 10 and 100 Myr are shown. Red circles: CTTS; green triangles: WTTS; green pentagons: G-type WTTS. Filled symbols: Li was detected (for late-type stars), or confirmed membership based on extinction (see text, for G-type stars). Open symbols: Li was not detected due to poor signal-to-noise (in low-mass stars), or most likely membership (based on extinction, see text).

cluster members, not even among the rest of objects over the Main Sequence in the region. Therefore, further evidence of an important evolution of the accretion processes and the disks is found to occur during the period from ∼4 to ∼ 10 Myr.

The spatial distribution and coverage of NGC 7160 members was shown in Figure 2.2. The area covered is approximately a third of a square degree. Figure 2.2 does not clearly indicate that we have covered the main area in NGC 7160, especially considering that the low-mass members of an older cluster are likely to be more dispersed. Therefore, final numbers regarding the total disk fraction or the number of transition objects are not as well determined as in Tr 37, even though the generalized absence of objects with an IR excess throughout all the IRAC fields (except the two ones described here) suggests that both fractions are of the order of very few percent.

The number of stars in this field appearing above the Main Sequence in the V vs. V-I diagram is ∼730, of which we have covered about 75%. We can estimate ∼10-15 new mid-G to M2 members among the rest of the candidates in NGC 7160 using the probabilities described in Section 3.3, but estimates of the total number of members are not possible since the limits of the cluster are not well determined, and it is very likely to extend beyond our 4Shooter fields.

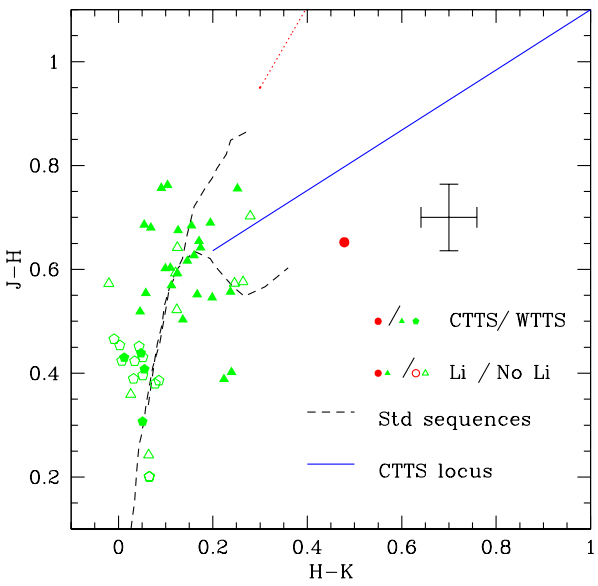

Figure 4.3 Low-Mass Stars: J-H vs. H-K diagram for all the low-mass members in NGC 7160. JHK colors from the 2MASS survey (Cutri et al., 2003). Stars are dereddened using their individual A_V (Bessell & Brett, 1988). The Main Sequence and Giant Branch are represented as dashed lines; the CTTS locus starting for a K7 star (Meyer et al., 1997) is represented as a solid line stars with disks would deviate parallel to this line from their Main Sequence position. Red circles: CTTS; green triangles: WTTS; green pentagons: G-type WTTS.

4.1.1 Protoplanetary Disks at the Age of 10 Myr

The Spitzer colors for NGC 7160 were displayed in Figure 3.7, together with the colors for Tr 37, for comparison. The IRAC and MIPS observations confirm the results from Hα emission about NGC 7160 as well as they did for Tr 37 (see Figures 4.4 and 4.5). There is clearly a disk around the only one star with strong Hα, 01-580, which had Hα=-90, consistent with rapid accretion, and spectral type K4.5. The Spitzer colors reveal another disk around the star 01-1152, which has spectral type M1.5 and Hα=-5.5. For this spectral type, the value of Hα indicates no accretion, and furthermore, no significant excess is measured at wavelengths shorter than 4.5 μm. Given that no misleading background emission is found in NGC 7160, and that the errors in Hα measurements with Hectospec are very small for these two high signal-to-noise spectra, 01-1152 must be either a very slow accretor, or has an inner gap which prevents it from accreting like those weak-lined stars with disks in Tr 37. Both options will be tested via high-resolution spectroscopy in the Hα region (as it is done for the stars in the ONC in Section 6), and/or near IR spectroscopy in the future.

Regarding the presence of disks with a small excess at 8.0 μm and no excesses at other wavelengths, only 01-554 shows such an excess. As in the case of Tr 37, a more detailed study is required to determine whether a disk is present around this stars. In any case, this observation would be consistent with the lower number of disks at the ages of 10 Myr, since the number of WTTS is nearly the same in both clusters, and suggests that maybe some of the 8 μm-excess objects are real and not caused by errors in the 8 μm photometry, so they deserve further study.

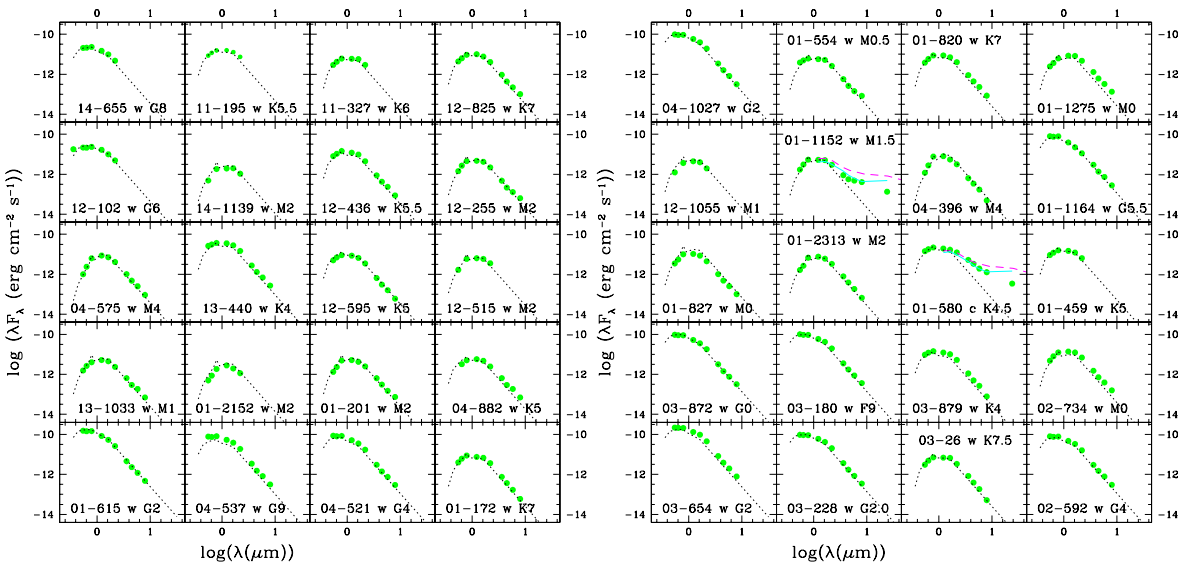

Figure 4.4 Spectral Energy Distributions for low-mass stars in NGC 7160. The fluxes are calculated from the UVRI photometry (4Shooter/1.2m), JHK 2MASS photometry (Cutri et al., 2003), and IRAC/MIPS magnitudes. The individual reddening correction has been applied in each case. For comparison, we display: the photospheric emission of a similar spectral type (derived from Kenyon & Hartmann 1995) as a black dotted line; the median disk emission in Taurus (Hartmann et al., 2005) as a magenta dashed line; the median disk emission in Tr 37 as a light blue line.

Examining the IRAC colors of the rest of the objects within the IRAC fields, only two more objects (besides the two found to have disks) have excesses that could be typical from disks. Both objects had been observed with Hectospec, although they were not classified as cluster members due to extremely poor signal-to-noise, being most likely heavily reddened background objects. The lack of objects with IR excess over the larger area subtended by the IRAC fields provides an additional and stronger constraint to the disk frequency, even if the limits of the cluster were not clearly reached by the optical survey. This suggests that disk fractions as low as a few percent are to be found by the age of 10 Myr; therefore strong disk dissipation and probably planet (or planetesimal) formation must have occurred by this time.

4.2 High- and Intermediate-Mass Stars in NGC 7160

In the case of NGC 7160, stars could be divided in two groups. We had a set of intermediate-mass stars, for which the 4Shooter photometry was under the saturation limit (see pentagons in Figure 4.2), which were observed with FAST/1.5m. For the brightest stars, we used the UBV photometry (see Figure 4.6) and coordinates from De Graeve (1983), obtained FAST spectra for them, and found their 2MASS JHK counterparts (Figure 4.6).

The photometric information is listed in Table 4.2 . We computed individual extinctions using the V-I color for stars with 4Shooter photometry, and the B-V color for stars with UBV photometry from De Graeve (1983), as described for Tr 37. We also used the same membership criterion, with the average value and standard deviation for NGC 7160 (A_V=1.17, standard

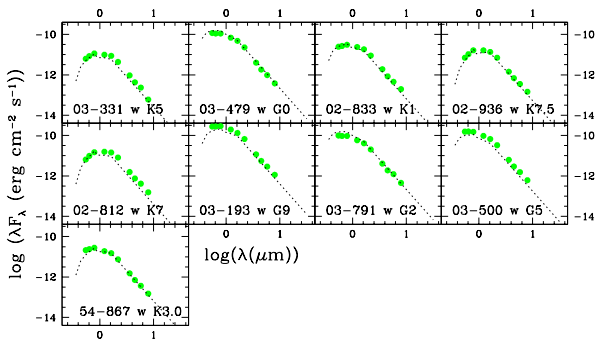

Figure 4.5 Spectral Energy Distributions for low-mass stars in NGC 7160 (continued). The fluxes are calculated from the UVRI photometry (4Shooter/1.2m), JHK 2MASS photometry (Cutri et al., 2003), and IRAC/MIPS magnitudes. The individual reddening correction has been applied in each case. For comparison, we display: the photospheric emission of a similar spectral type (derived from Kenyon & Hartmann 1995) as a black dotted line; the median disk emission in Taurus (Hartmann et al., 2005) as a magenta dashed line; the median disk emission in Tr 37 as a light blue line.

deviation σ=0.45). Spectroscopic and membership information appears in Tables 4.2 and 4.3.

The V vs. B-V diagram for the high- and intermediate-mass stars in NGC 7160 (Figure 4.6), together with the Siess et al. (2000) isochrones, shows that the stars on the Main Sequence (MS) are in good agreement with the tracks, confirming the distance estimate of 900 pc found by Contreras et al. (2002) by fitting the MS, consistent with the two clusters being at approximately the same distance and in the same region.

4.2.1 "Debris" Disks at 10 Myr

The SEDs for the high-mass members in NGC 7160 are displayed in Figures 4.7 and 4.8. As a difference with Tr 37, no emission stars had been identified in NGC 7160, and no object showed strong JHK excess from the 2MASS survey, suggesting that no optically thick disks are present around 10 Myr old high- and intermediate-mass stars.

Nevertheless, from Figures 4.7 and 4.8 we can infer the presence of optically-thin debris disks, similar to the 4 debris disks found in Tr 37, and to the debris disk around the young A star HR 4796A (Jayawardhana et al., 1998). A total of 3 debris disks with excess at 24 μm can be detected: DG-481 (spectral type A7), DG-39 (spectral type A0) and DG-682 (spectral type A2). DG-481 could have a small excess at 8.0 μm. DG-62 has also a very small excess at 5.8 and 8.0 μm, although the lack of MIPS observations in this area does not allow us to confirm it as another detection. Therefore, we detect 3 plus another potential disk in NGC 7160. We do not find any thick disk with strong emission as we see in Tr 37.

As in Tr 37, the presence of debris disks around very young stars suggests either rapid formation of planetesimals and breaking-up of them to create debris disks, or the long survival of accretion disk remnants after the inner part of the disk has been dissipated and/or agglomerated. Both aspects will be revised in more detail in Section 5.

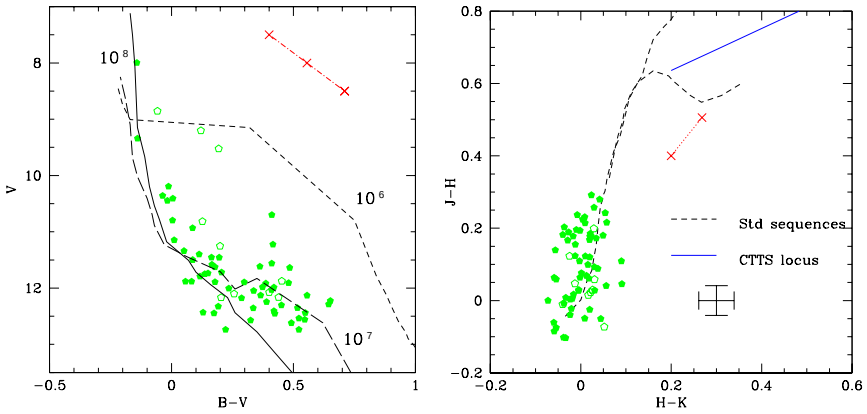

Figure 4.6 Left: High- and Intermediate-Mass Members: B vs. B-V diagram for all the high- and intermediate-mass members in NGC 7160. Photometry from De Graeve (1983), dereddened using the individual A_V. 1, 10 and 100 Myr isochrones from Siess et al. (2000). Filled symbols: confirmed members (according to A_V, see text). Open symbols: probable members (according to extinction). The reddening vector for intervals of A_V=0.5 is represented as a dotted-dashed line. Right: High- and Intermediate-Mass Members: J-H vs. H-K diagram for all the high- and intermediate-mass members in NGC 7160. Photometry from the 2MASS survey (Cutri et al., 2003), dereddened using the individual extinctions (Bessell & Brett, 1988). Main Sequence and Giant Branch are represented by a dashed line; CTTS locus for a K7 star(Meyer et al., 1997) is represented as a solid line; stars with disks would deviate parallel to this line from their Main Sequence position.

4.3 Data Tables

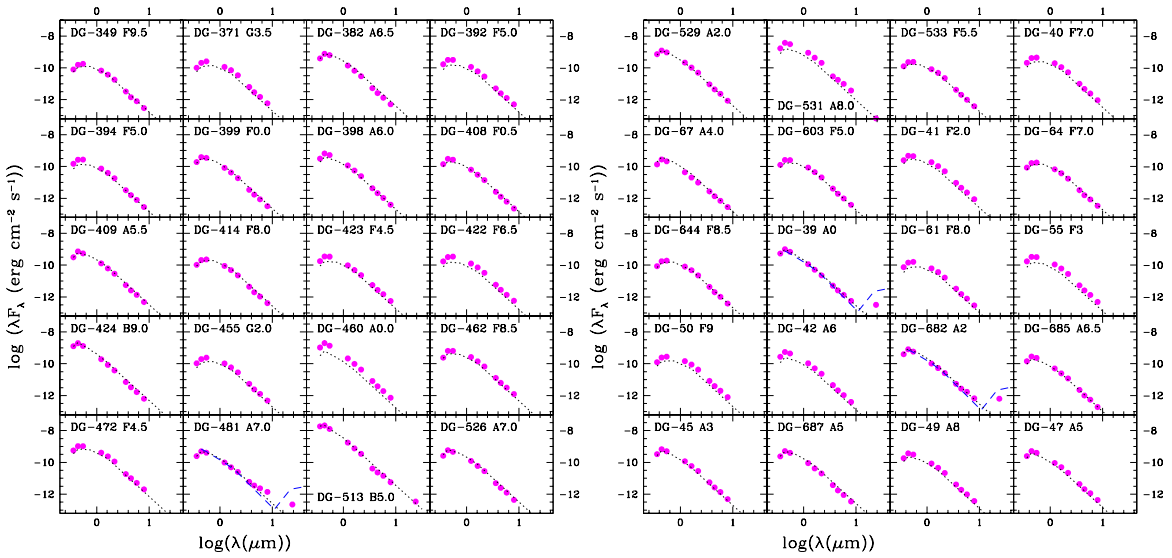

Figure 4.7 Spectral Energy Distributions for high- and intermediate-mass stars in NGC 7160. The fluxes correspond to the BV photometry for Tr 37 (Marschall & van Altena, 1987; Kun et al., 1987), UBV photometry for NGC 7160 (De Graeve, 1983), and 2MASS JHK magnitudes, and IRAC and MIPS observations for both clusters. For comparison, the photosphere for a similar spectral type (derived from the colors in Kenyon & Hartmann 1995) is displayed as a dotted line. We also display the emission of the debris disk HR 4796 (Jayawardhana et al., 1998).

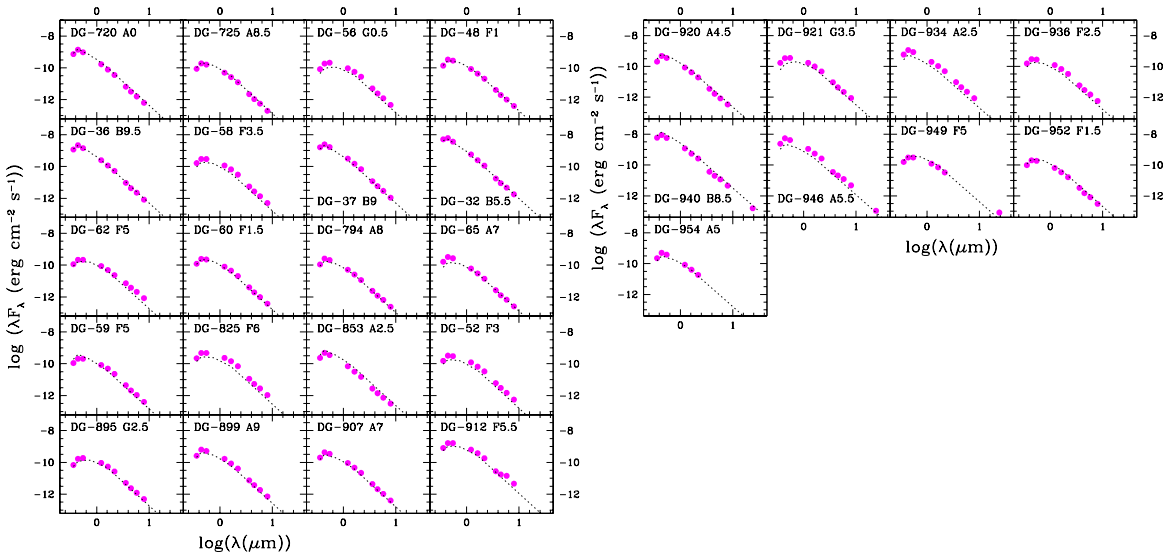

Figure 4.8 Spectral Energy Distributions for high- and intermediate-mass stars in NGC 7160 (continued). The fluxes correspond to the BV photometry for Tr 37 (Marschall & van Altena, 1987; Kun et al., 1987), UBV photometry for NGC 7160 (De Graeve, 1983), and 2MASS JHK magnitudes, and IRAC and MIPS observations for both clusters. For comparison, the photosphere for a similar spectral type (derived from the colors in Kenyon & Hartmann 1995) is displayed as a dotted line. We also display the emission of the debris disk HR 4796 (Jayawardhana et al., 1998).

Table 4.1. Summary of Spectroscopy, Extinction and Membership for Low-Mass Stars in NGC7160.

ID1	Instrument	Spec. Type	Hα EW(Å)	Li EW(Å)	TTS Type	A_V	Age(Myr)	Membership	Comment
14-655	Hecto	G8.0±1.5	1.8	0.2	w	1.8	26	P	
11-195	Hecto	K5.5±1.0	-0.3	0.2	w	0.4	8.4	Y	
11-327	Hecto	K6.0±2.5	-1.1	0.3	w	1.1	24	Y	
12-825	Hecto	K7.0±0.5	-0.8	0.3	w	1.0	10	Y	
12-102	Hecto	G6.0±1.5	1.5	0.1	w	1.7	28	P	
14-1139	Hydra	M2.0±0.5	-5.0	—	w	1.5	15	Y	
12-436	Hecto	K5.5±1.0	-1.2	0.2	w	2.1	9.0	P	
12-255	Hydra	M2.0±0.5	-5.0	—	w	1.5	7.0	Y	
04-575	Hecto	M4.0±1.0	-10.0	-100.0	w	0.5	2.2	P	BS
13-440	Hecto	K4.0±1.0	-0.7	—	w	1.9	6.5	Y	
12-595	Hecto	K5.0±1.5	-0.7	-100.0	w	1.3	20	P	
12-515	Hydra	M2.0±0.5	-4.0	—	w	0.7	3.6	P	BS
13-1033	Hecto	M1.0±1.0	-5.1	0.5	w	1.0	8.0	Y	
”	Hecto	—	-2.5	—	w	—	—	—	
01-2152	Hydra	M2.0±0.5	-9.0	—	w	0.8	16	Y	
01-201	Hydra	M2.0±1.0	-3.0	—	w	0.7	4.4	P	BS:
04-882	Hecto	K5.0±1.5	1.2	0.7	w	0.9	11	Y	
01-172	Hecto	K5.5±1.0	-0.7	0.3	w	1.7	9.8	Y	
”	Hecto	—	-1.4	0.4	w	—	—	—	
”	Hydra	—	-2.0	0.4	—	—	—	—	
01-554	Hecto	M0.5±1.0	-1.7	0.3	w	0.0	68	PN	
01-820	Hecto	K7.0±1.0	-1.5	0.6	w	0.8	9.8	Y	
”	Hecto	—	-2.2	0.5	w	—	—	—	
”	Hydra	—	-2.0	0.4	—	—	—	—	
01-1275	Hecto	K6.5±1.5	-5.0	0.3	w	0.8	16	Y	
”	Hydra	—	-4.0	0.5	—	—	—	—	
12-1055	Hydra	M1.0±1.0	-3.0	—	w	1.5	9.6	Y	
01-1152	Hecto	M1.5±1.0	-5.5	0.5	w	0.9	5.6	Y	IR,TO
04-396	Hydra	M4.0±1.0	-9.0	1.0	w	2.6	1.9	Y	BS
01-827	Hecto	M1.5±0.5	-4.5	0.3	w	1.1	2.7	Y	BS
”	Hydra	—	-4.0	—	w	—	—	—	
01-2313	Hydra	M2.0±0.5	-9.0	—	w	1.7	2.6	Y	BS
01-580	Hecto	K4.5±0.5	-96.0	0.5	c	1.6	8.7	Y	L,IR
01-459	Hecto	K5.0±1.0	0.0	1.0	w	1.5	9.3	P	
03-879	Hecto	K4.5±1.5	-0.3	0.4	w	0.8	18	Y	
”	Hydra	—	-1.0	0.4	—	—	—	—	
02-734	Hecto	K7.5±1.0	-2.5	0.5	w	1.1	2.6	Y	BS
”	Hecto	—	-2.3	0.4	w	—	—	—	

Table 4.1 (continued)

ID1	Instrument	Spec. Type	Hα EW(Å)	Li EW(Å)	TTS Type	A_V	Age(Myr)	Membership	Comment
”	Hydra	—	-2.0	0.5	—	—	—	—	
03-26	Hecto	K7.5±1.0	-1.6	0.4	w	0.8	13	Y	
”	Hecto	—	-1.7	0.3	w	—	—	—	
”	Hydra	—	-2.0	0.8	—	—	—	—	
03-331	Hecto	K6.0±1.0	-1.5	0.3	w	1.4	12	Y	
”	Hecto	—	-1.8	0.8	w	—	—	—	
”	Hydra	—	-2.0	0.6	—	—	—	—	
02-833	Hecto	K1.0±1.5	-0.4	0.5	w	1.6	10	Y	
”	Hydra	—	-1.0	0.4	w	—	—	—	
02-936	Hecto	K7.5±1.0	-2.0	0.5	w	1.6	2.9	Y	BS
”	Hydra	—	-2.0	0.7	—	—	—	—	
02-812	Hecto	K6.0±.0	-1.5	0.4	—	—	4.9	P	BS
”	Hydra	—	-2.0	—	w	1.2	—	—	
54-867	Hecto	K3.0 ± 0.5	-0.3	0.5	w	1.5	9.9	Y	
”	Hecto	—	1.0	0.4	w	—	—	—	

Note. — Summary of spectroscopic data extinction and membership for NGC 7160. Given the better quality of Hectospec spectra, they were given preference for obtaining spectral types. Errors in the spectral types are given in number of subtypes. Colon denotes uncertain values. Referred to the type of TTS, they denote the objects with Hα in the limit between CTTS and WTTS according to White & Basri (2003). Ages are derived using the (Siess et al., 2000) isochrones in the V vs. V-I diagram. Membership: Y=confirmed member; P=probable member; PN= probable non-member. Comment: L=JHK colors consistent with the CTTS locus; IR=IRAC/MIPS excess consistent with a disk; TO= “transition object” or non-accreting WTTS with disk (see text); BS=star belongs to the binary sequence.

Table 4.2. Summary of Optical, Near-IR, and Spectroscopic Observations for G-Type Intermediate-Mass Stars in NGC 7160.

ID1	2MASS	V	V-R	V-I	J	H	K	Spec.Type	A_V	Member
01-978	21521066+6232308	15.440	0.820	1.630	12.670±0.026	12.036±0.032	11.882±0.023	G2±1.5	2.2	PN
04-432	21522531+6240338	15.370	0.770	1.540	12.780±0.026	12.232±0.029	12.045±0.023	G0±2.0	2.1	PN
04-801	21522915+6244120	15.040	0.850	1.660	12.200±0.026	11.536±0.033	11.312±0.023	G8±1.5	2.1	PN
01-615	21523560+6229082	14.190	0.630	1.290	12.067±0.026	11.612±0.030	11.466±0.022	G2±2.0	1.4	Y
04-537	21523712+6241437	15.470	0.790	1.610	12.714±0.026	12.056±0.032	11.880±0.024	G9±1.5	2.0	P
04-521	21525891+6241347	15.230	0.730	1.480	12.726±0.024	12.138±0.029	11.963±0.025	G4±1.5	1.8	P
04-1027	21530762+6246144	15.260	0.770	1.520	12.633±0.022	12.033±0.029	11.866±0.025	G2±1.5	2.0	P
01-1164	21533207+6234053	15.370	0.750	1.510	13.032±0.038	12.632±0.058	12.439±0.050	G5.5±1.5	1.9	P
04-218	21533253+6238231	15.220	0.840	1.670	12.427±0.031	11.743±0.036	11.567±0.029	G3±2.0	2.3	PN
01-1067	21533646+6233139	14.100	0.810	1.610	11.453±0.027	10.854±0.031	10.680±0.025	G3±1.5	2.2	PN
03-872	21535296+6245248	15.190	0.760	1.470	12.717±0.027	12.131±0.033	11.917±0.021	G0±2.5	1.9	P
03-180	21535411+6238102	15.260	0.770	1.500	12.643±0.025	11.974±0.031	11.833±0.026	F9±2.0	2.0	P
03-654	21535811+6243213	14.060	0.730	1.390	11.650±0.025	11.008±0.031	10.904±0.021	G2±1.0	1.7	P
03-228	21535959+6238433	15.280	0.810	1.520	12.608±0.027	11.975±0.029	11.806±0.021	G2±2.0	2.0	P
02-512	21540319+6229198	15.250	0.870	1.710	12.322±0.027	11.578±0.029	11.398±0.022	G9±1.5	2.2	PN
03-835	21540498+6245048	14.070	0.740	1.410	11.676±0.027	11.061±0.029	10.900±0.021	G3.5±1.5	1.7	Y
02-592	21540860+6230140	15.020	0.670	1.360	12.728±0.025	12.136±0.032	12.020±0.021	G4±1.5	1.5	Y
03-479	21541722+6241338	15.120	0.790	1.530	12.470±0.025	11.830±0.029	11.684±0.021	G0±2.0	2.0	P
03-388	21542685+6240320	15.450	0.840	1.590	12.698±0.027	12.054±0.032	11.893±0.023	G1±1.5	2.2	PN
03-193	21544992+6238168	14.190	0.870	1.650	11.324±0.024	10.727±0.031	10.510±0.018	G9±2.0	2.1	P
02-803	21545240+6232233	15.140	0.820	1.610	12.434±0.027	11.839±0.033	11.640±0.025	G2±1.5	2.2	PN
03-791	21545624+6244422	15.150	0.770	1.490	12.604±0.024	11.972±0.032	11.791±0.020	G2±1.5	1.9	P
03-500	21550486+6241479	14.090	0.690	1.290	11.895±0.021	11.347±0.028	11.202±0.020	G5±3.0	1.3	Y
02-40	21551191+6224146	15.420	0.980	1.890	12.180±0.027	11.418±0.031	11.178±0.020	K1±1.5	2.4	PN
03-938	21551809+6245556	15.050	0.890	1.740	12.043±0.022	11.245±0.028	11.057±0.022	G2±1.5	2.5	PN
03-457	21552116+6241160	15.370	0.810	1.580	12.823±0.037	12.154±0.038	11.977±0.030	G1±2.0	2.2	PN

Note. — Summary of 4Shooter optical and 2MASS near-IR data. Spectroscopic data from FAST. All the stars listed here are found to be WTTS (no strong Hα emission). Membership: Y=confirmed member; P=probable member; PN= probable non-member.

Table 4.3. Summary of Optical, Near-IR, and Spectroscopic Data for High- and Intermediate-Mass Stars (Spectral Types BAF) in NGC7160.

ID1	2MASS	V	U-B	B-V	J	H	K	Spec.Type	A_V	Member
DG-349	21511753+6243411	13.80	0.31	0.94	12.247±0.029	11.949±0.031	11.834±0.026	F9.5±2.0	1.2	Y
DG-371	21512625+6229161	13.19	0.30	0.95	11.606±0.022	11.212±0.028	11.123±0.022	G3.5±1.0	1.0	Y
DG-382	21513143+6228462	13.03	0.46	0.75	11.622±0.022	11.444±0.028	11.363±0.022	A6.5±2.5	1.8	P
DG-392	21513731+6238065	13.60	0.38	0.92	11.779±0.027	11.499±0.029	11.392±0.021	F5.0±1.5	1.6	Y
DG-394	21513859+6235506	13.91	0.36	0.98	12.302±0.032	11.994±0.037	11.900±0.024	F5.0±2.0	1.8	P
DG-399	21514182+6247138	13.29	0.41	0.73	12.080±0.027	11.869±0.033	11.833±0.024	F0.0±2.5	1.4	Y
DG-398	21514228+6233145	12.99	0.47	0.64	11.748±0.021	11.585±0.030	11.553±0.022	A6.0±2.5	1.5	Y
DG-408	21514544+6247053	13.54	0.46	0.71	12.363±0.022	12.213±0.029	12.139±0.023	F0.5±2.0	1.4	Y
DG-409	21514566+6242582	13.00	0.60	0.61	11.660±0.026	11.473±0.035	11.380±0.023	A5.5±2.5	1.6	Y
DG-414	21514681+6246116	13.72	0.37	0.94	11.996±0.027	11.696±0.037	11.615±0.024	F8.0±1.0	1.4	Y
DG-423	21515464+6244067	13.54	0.43	0.89	11.978±0.067	11.737±0.071	11.614±0.059	F4.5±2.5	1.6	Y
DG-422	21515487+6238346	13.36	0.34	0.93	11.641±0.026	11.298±0.029	11.226±0.019	F6.5±2.0	1.5	Y
DG-424	21515566+6227138	11.50	0.03	0.31	11.061±0.027	11.034±0.031	11.021±0.022	B9.0±1.0	1.1	Y
DG-455	21520998+6225312	13.37	0.22	0.98	11.740±0.027	11.445±0.030	11.322±0.023	G2.0±1.0	1.1	Y
DG-460	21521146+6238456	11.84	0.34	0.45	11.048±0.027	10.957±0.031	10.919±0.023	A0.0±2.0	1.4	Y
DG-462	21521289+6244086	12.11	0.57	0.69	10.676±0.026	10.462±0.032	10.382±0.023	F8.5±1.0	0.9	Y
DG-472	21522024+6227588	11.63	0.19	0.70	10.207±0.026	9.894±0.030	9.821±0.022	F4.5±2.0	0.9	Y
DG-481	21522113+6245034	13.22	0.42	0.67	11.918±0.027	11.713±0.031	11.520±0.021	A7.0±2.0	1.5	Y
DG-513	21523289+6223569	8.94	-0.34	0.15	8.638±0.021	8.640±0.031	8.614±0.022	B5.0±1.5	0.9	Y
DG-526	21523857+6245523	13.08	0.53	0.63	11.677±0.026	11.491±0.032	11.394±0.023	A7.0±2.5	1.5	Y
DG-529	21523925+6244495	11.57	0.04	0.36	10.864±0.026	10.769±0.032	10.701±0.021	A2.0±1.5	0.8	P
DG-531	21523931+6246581	10.32	0.37	0.44	9.330±0.021	9.223±0.031	9.147±0.021	A8.0±2.5	0.8	P
DG-533	21524042+6246066	13.43	0.23	0.80	12.010±0.027	11.666±0.032	11.585±0.021	F5.5±2.5	1.1	Y
DG-40	21524971+6231309	12.59	0.27	0.78	11.021±0.023	10.735±0.024	10.649±0.021	F7.0±2.0	1.0	Y
DG-67	21525985+6242064	13.95	0.43	0.60	12.814±0.024	12.678±0.028	12.555±0.026	A4.0±2.5	1.5	Y
DG-603	21530741+6227196	13.31	0.33	0.72	11.944±0.023	11.755±0.028	11.681±0.023	F5.0±1.5	1.1	Y
DG-41	21531942+6237387	12.64	0.24	0.68	11.086±0.022	10.800±0.026	10.710±0.022	F2.0±2.5	1.0	Y
DG-64	21532252+6234249	13.97	0.35	0.91	12.306±0.024	11.985±0.029	11.910±0.026	F7.0±1.5	1.4	Y
DG-644	21532703+6244504	13.82	0.37	0.92	12.073±0.022	11.706±0.029	11.610±0.023	F8.5±2.0	1.3	Y
DG-39	21532780+6235187	12.40	0.28	0.40	11.687±0.025	11.629±0.032	11.598±0.028	A0.0±1.0	1.3	Y
DG-61	21533014+6230097	13.73	0.26	0.83	12.265±0.030	11.957±0.028	11.926±0.024	F8.0±1.0	1.0	Y
DG-55	21533308+6237031	13.39	0.35	0.81	11.772±0.022	11.456±0.026	11.389±0.022	F3.0±2.5	1.4	Y
DG-50	21533548+6230032	13.08	0.26	0.85	11.334±0.023	10.976±0.028	10.882±0.021	F9.0±2.0	1.0	Y
DG-42	21533684+6232485	12.60	0.29	0.48	11.680±0.023	11.569±0.028	11.536±0.023	A6.0±2.5	1.0	Y
DG-682	21534512+6236548	12.69	0.40	0.47	11.824±0.039	11.588±0.037	11.466±0.026	A2.0±2.5	1.4	Y
DG-685	21534542+6245250	13.58	0.35	0.58	12.568±0.027	12.407±0.033	12.291±0.021	A6.5±2.5	1.3	Y
DG-45	21534551+6240574	12.67	0.36	0.45	11.632±0.027	11.467±0.032	11.331±0.019	A3.0±2.5	1.2	Y
DG-687	21534615+6246354	12.76	0.36	0.45	11.866±0.024	11.809±0.029	11.696±0.023	A5.0±2.5	1.0	Y

Table 4.3 (continued)

ID1	2MASS	V	U-B	B-V	J	H	K	Spec.Type	A_V	Member
DG-49	21535191+6233245	12.99	0.30	0.54	11.926±0.027	11.699±0.031	11.622±0.023	A8.0±2.5	1.0	Y
DG-47	21535561+6236180	12.77	0.33	0.47	11.867±0.025	11.618±0.029	11.604±0.023	A5.0±2.5	1.0	Y
DG-720	21540285+6226348	12.01	0.29	0.38	11.251±0.027	11.162±0.029	11.103±0.022	A0.0±2.5	1.2	Y
DG-725	21540540+6243427	13.99	0.45	0.61	12.587±0.027	12.355±0.029	12.254±0.019	A8.5±2.5	1.3	Y
DG-56	21540728+6244260	13.38	0.40	0.84	11.808±0.027	11.466±0.032	11.348±0.021	G0.5±0.5	0.9	Y
DG-48	21541327+6243092	12.76	0.40	0.46	11.840±0.029	11.712±0.032	11.637±0.023	F1.0±2.0	0.7	P
DG-36	21541424+6245577	11.25	0.18	0.24	10.748±0.027	10.676±0.029	10.636±0.021	B9.5±1.5	0.9	Y
DG-58	21541589+6236045	13.72	0.35	0.91	11.786±0.027	11.416±0.032	11.314±0.019	F3.5±2.5	1.6	P
DG-37	21541940+6228067	11.62	0.11	0.43	10.641±0.027	10.498±0.029	10.438±0.022	B9.0±1.0	1.4	Y
DG-32	21542286+6227553	10.92	-0.13	0.35	10.032±0.027	9.968±0.031	9.894±0.020	B5.5±1.5	1.6	Y
DG-62	21543034+6231157	13.86	0.34	0.87	12.034±0.038	11.702±0.044	11.580±0.029	F5.0±2.5	1.5	Y
DG-60	21543359+6228529	13.63	0.35	0.73	12.077±0.029	11.760±0.029	11.713±0.025	F1.5±2.5	1.3	Y
DG-794	21543351+6247531	13.95	0.60	0.64	12.634±0.026	12.416±0.035	12.368±0.026	A8.0±2.5	1.5	Y
DG-65	21543679+6233595	13.93	0.49	0.75	12.522±0.029	12.288±0.031	12.181±0.029	A7.0±2.5	1.8	P
DG-59	21543940+6236219	13.70	0.28	0.81	12.026±0.022	11.657±0.028	11.580±0.022	F5.0±2.0	1.3	Y
DG-57	21544464+6229379	13.38	0.53	0.61	12.086±0.027	11.897±0.031	11.790±0.020	B8.0±1.5	2.5	PN
DG-825	21545261+6245282	12.46	0.34	0.69	10.814±0.022	10.439±0.028	10.336±0.022	F6.0±2.0	0.9	Y
DG-853	21550713+6243337	13.15	0.41	0.45	12.231±0.021	12.146±0.030	12.051±0.022	A2.5±2.5	1.3	Y
DG-52	21551988+6239150	12.96	0.33	0.62	11.506±0.022	11.300±0.031	11.148±0.022	F3.0±2.5	0.9	Y
DG-895	21553636+6243538	13.70	0.54	0.90	11.878±0.026	11.541±0.033	11.406±0.021	G2.5±1.0	1.1	Y
DG-899	21553835+6245530	12.47	0.51	0.51	11.194±0.024	11.025±0.031	10.938±0.021	A9.0±2.5	1.0	Y
DG-907	21554305+6242289	13.09	0.42	0.55	11.905±0.030	11.714±0.036	11.634±0.028	A7.0±2.5	1.2	Y
DG-912	21554760+6235432	10.99	0.25	0.65	9.679±0.024	9.376±0.031	9.288±0.019	F5.5±2.0	0.8	P
DG-920	21555491+6244334	13.52	0.63	0.59	12.132±0.026	11.929±0.031	11.822±0.019	A4.5±2.5	1.6	Y
DG-921	21555507+6243555	12.61	0.24	0.68	11.108±0.026	10.831±0.029	10.752±0.021	F6.5±1.5	0.7	P
DG-934	21560359+6238548	12.04	0.29	0.43	11.065±0.027	10.824±0.031	10.761±0.023	A2.5±2.5	1.1	Y
DG-936	21560545+6226535	13.40	0.31	0.76	11.630±0.027	11.327±0.032	11.221±0.024	F2.5±1.0	1.3	Y
DG-940	21560766+6234069	9.59	-0.09	0.17	8.985±0.024	8.980±0.031	8.878±0.021	B8.5±1.5	0.7	P
DG-946	21561081+6234549	10.04	0.39	0.38	9.098±0.027	8.980±0.029	8.897±0.019	A5.5±2.5	0.8	P
DG-949	21561116+6247046	13.29	0.32	0.80	11.611±0.029	11.284±0.032	11.200±0.024	F5.0±2.0	1.3	Y
DG-952	21561429+6241417	13.56	0.31	0.63	12.229±0.027	12.036±0.035	11.931±0.019	F1.5±2.5	1.0	Y
DG-954	21561584+6245441	13.22	0.52	0.56	12.067±0.026	11.912±0.031	11.838±0.021	A5.0±2.5	1.4	Y

Note. — Summary of optical data for the high- and intermediate-mass stars in NGC7160. ID1, Photometry from De Graeve (1983). 2MASS identification and JHK magnitudes from 2MASS (Cutri et al., 2003). No 2MASS error is an indication of probable large error in the 2MASS photometry. All spectra were taken with FAST,and spectral types were derived using the scheme described in the text.Membership based on average extinction for the cluster and its standard deviation (see text; confirmed members=Y if extinction is within 1σ of the average, most likely members=P if extinction is within 1-2σ of the average, most likely non members=PN if extinction is within 2-3σ of the average).

5 The Evolution of Protoplanetary Disks: Dust Setting, Grain Growth, and Inner-Disk Evolution

Published in "Cep OB2: Disk Evolution and Accretion at 3-10 Myr", by Sicilia-Aguilar, A., Hartmann, L., Hernández, J., Briceño, C., & Calvet, N., 2005, AJ in press; and "Disk Evolution in Cep OB2: Results from Spitzer Space Telescope", by Sicilia-Aguilar, A., Hartmann, L., Calvet,N., Megeath, S.T., Muzerolle, J., Allen, L., D'Alessio, P., Merín B., and Stauffer, J., 2005, in preparation.

Here, the characteristics of disks and accretion are examined in the context of the different ages of Tr 37 and NGC 7160, in order to put together a picture of disk evolution from 1 to 10 Myr. The differences observed between Cep OB2 and other younger regions suggest that the evolution starts in the inner part of the disk, and propagates outward with time. The comparison with disk models suggests that important dust settling and/or grain growth has occurred in the innermost part of the disk (fractions of AU to few AU) by the age of 4 Myr, and further settling and coagulation extends to distances of ∼10-20 AU in the few disks surviving at the age of 10 Myr.

The presence of "transition objects", or non-accreting stars with outer disks (with "gaps" of few AU) supports the inside-out evolution, assuming that dust in the inner disk must have coagulated in order not to produce any emission at wavelengths shorter than ∼5.8 μm. Moreover, the lack of accretion in these "transition objects" may indicate that the grain growth may have progressed to reach the size of planets, in order to stop accretion. In any case, it seems that large grains and depletion of small grains can occur by the age of 4 Myr, and fast enough so the outer disk still remains optically thick. Timescales for the outer disk to disappear, once the inner disk is coagulated, seem to be of the order of 10^5 yr.

Finally, the presence of debris disks or optically thin disks around BAF-type stars of 4-10 Myr age points as well to the formation of large bodies by the age of 4-10 Myr in high- and intermediate-mass stars.

5.1 Ages and the Color Magnitude Diagrams

The ages of the two clusters Tr 37 and NGC 7160 were estimated via the V vs. V-I color-magnitude diagrams for the low-mass stars, corrected using the individual extinctions, to-

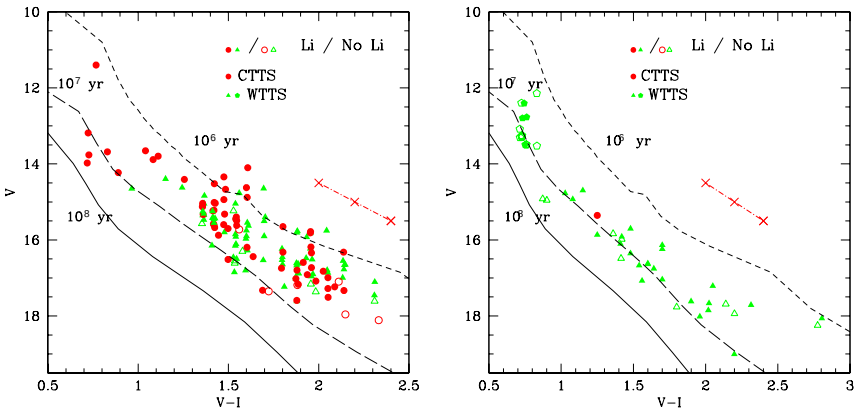

Figure 5.1 Low-Mass Stars: V vs. V-I diagram for all the low-mass members in Tr 37 (left) and NGC 7160 (right). Photometry from the 4Shooter/1.2m in FLWO. A reddening correction (Bessell & Brett, 1988) has been applied for each star using the individual reddenings; a reddening vector with X for A_V=0.5 intervals is represented as a dotted-dashed line. Isochrones from Siess et al. (2000) for 1, 10 and 100 Myr are shown. Red circles: CTTS; green triangles: WTTS; green pentagons: G-type WTTS in NGC 7160. Filled symbols: Li was detected (for late-type stars), or confirmed membership based on extinction (see text, for G-type stars). Open symbols: Li was not detected due to poor signal-to-noise (in low-mass stars), or most likely membership (for the G-type stars, based on extinction, see text).

gether with theoretical isochrones from Siess et al. (2000). Figure 5.1 shows the diagrams for both clusters, and the estimated ages of each star are listed in Tables 3.3 and 4.1. The average ages are consistent with 4 Myr for Tr 37, and 11 Myr for NGC 7160; and consistent with the estimates based on kinematics by Patel et al. (1998). Nevertheless, the standard deviation due to the age in the clusters is high, being about 3.8 Myr in Tr 37, and 4.6 Myr in NGC 7160.

There is a significant difference in the apparent age scatter of the Tr 37 and NGC 7160 members, or Δage/age. We find little dispersion among the NGC 7160 low-mass members, which are mostly located along the 10 Myr isochrone (see Figure 5.1), with some deviations due to more luminous members, which are consistent with a binary sequence. On the contrary, we find a very important dispersion in the V vs. V-I diagram for Tr 37. Tracing the binary sequence in Tr 37 is not possible, due to the scatter of the members, the absence of a clear "separation" between both sequences, and the expected errors in the age, which are usually a factor of 2 (Hartmann, 2001). The lack of significant dispersion in NGC 7160 suggests that photometric errors are minimal. Therefore, the dispersion in Tr 37 must be due to other causes, such as the photometric variability of the stars, age spread, the presence of a younger population, and the obscuration of some stars by their disks. The effect of errors in the extinction correction cannot play a major role for the age determination from the low-mass stars, since the reddening vector is nearly parallel to the isochrones.

The study of the variability in the RI bands revealed that stars in Tr 37 presented noticeably larger variations (up to several tenths of a magnitude) than stars in NGC 7160. These strong variations are more dramatic in accreting stars, and could be responsible for some of the scatter in the V vs. V-I diagram in Tr 37. In order to test this hypothesis, a detailed

study of the variability in V needs to be done; the use of averaged V and I photometry might improve the quality of the V vs. V-I diagram. Another possible cause of the age dispersion toward lower (∼1 Myr) ages could be, as it was suggested before, the presence of a younger population in Tr 37. There is evidence of embedded protostars associated to the dust and gas structures in IC 1396 (Section 3.1.6). Several of the stars found over the 1 Myr isochrone are located close to, or surrounded by, these gas structures, and this could be indicative of later formation (Section 4.2). This younger population, together with the binary stars, could explain most of the stars seen near to or over the 1 Myr isochrone in Figure 5.1.

Four of the stars on or below the 10 Myr isochrone have lower probability of being cluster members (open triangles, denoting WTTS where Li absorption was not detected due to poor signal-to-noise), but the remaining four are *bona fide* cluster members (all of them show Li absorption, and two show strong Hα emission in addition). It is possible that these are disk systems seen edge on, which appear under-luminous for their colors due to scattering. The reason why the other two diskless WTTS appear older than 10 Myr is uncertain. These stars are located at the edge of Tr 37; some older stars could have been formed in NGC 7160, being expelled out of the cluster by their large velocities, but due to the lack of knowledge of the limits of NGC 7160, the total number of members, and the velocities of the stars, it is not possible to reach a final conclusion.

Finally, another fact that could cause part of the larger apparent age dispersion in Tr 37 could be that age differences of 3 Myr among members in a 3 Myr cluster are very noticeable, whereas a similar difference in a 10 Myr cluster would be less striking when plotted against the isochrones in a color-magnitude diagram. This way, a similar dispersion of ∼4 Myr age is present in NGC 7160, considering the small dispersion in the V vs. V-I diagram, even though it is harder to estimate it accurately in this more evolved cluster, for which errors are much larger than for Tr 37. In fact, taking into account the standard deviation, the values for both clusters are similar, so part of this age spread could be real.

Another point that needs to be clarified is the apparent "older" age of the G-type stars in the V vs. V-I diagrams. This effect has been observed in other regions (i.e., ONC, see Hillenbrand et al. 1997; Taurus, see Briceño et al. 2001), and seems to be related to problems defining the birthline of intermediate-mass stars or a faster evolution of these stars that is not well reproduced by the available models (Hartmann, 2003). In Figure 5.1, we observe that the apparent age of the early K and G stars is around 10 Myr for both Tr 37 and NGC 7160, according to the isochrones by Siess et al. (2000), despite the age difference of the later type stars between both clusters (for these reasons, the G stars have been excluded in the calculation of the average age in both clusters).

5.2 Evolution of Accretion?

The evolution of accretion disks is always related to the evolution of the accretion rate (Hartmann et al., 1998; Muzerolle et al., 2000). According to the models of viscous disk evolution, the accretion rate would decrease with time (Hartmann et al., 1998). Unfortunately, due to observing time limitation, no U band observations were obtained for the central region in NGC 7160, which contains the only two low-mass stars with disks in the older cluster (with individual ages around 8 Myr from the V vs V-I diagram).

Nevertheless, since some age spread is observed in Tr 37, a possible evolution of the mass accretion rates with age can be explored. Figure 5.2 shows the mass accretion rates of the stars

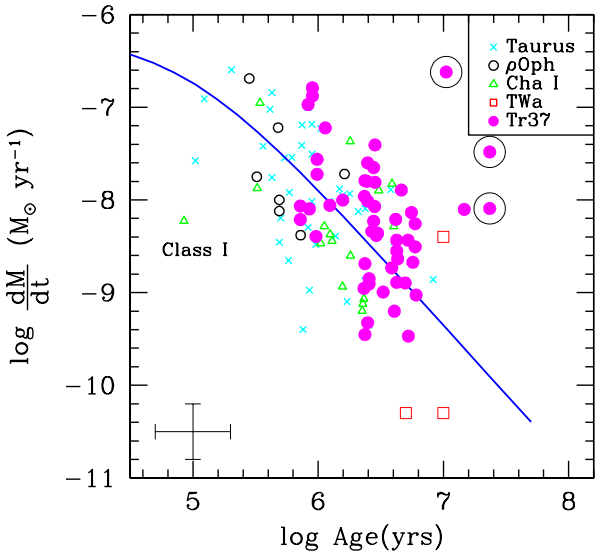

Figure 5.2 Mass Accretion Rates versus Age: We compare the results of dM/dt versus age for Tr 37 (pink dots) with the observations in other clusters (Muzerolle et al., 2000) and the viscous disk evolutionary models (Hartmann et al., 1998). Even though large variations in individual ages are expected from the intrinsic variability of the young stars, binaries, etc, and even though errors up to factors of 2-3 are common in the measurement of accretion rates, the evolution of accretion in Tr 37 is consistent with the viscous disk evolution. Note the higher accretion rates among the younger (∼1Myr) stars associated to the globule. Note as well the presence of several G-type (pink dots encircled by a large circle), accreting stars which show systematically older ages, and systematically higher accretion rates.

in Tr 37 versus their apparent ages from the V vs, V-I diagram, compared to the observations in other regions and to the model of viscous disk evolution (Hartmann et al., 1998). Even though accretion rates are expected to vary with the mass of the star, being higher for higher-mass stars (Muzerolle et al., 2003b), and individual ages must be considered carefully, as it was mentioned in Section 5.1, there is a reasonable agreement with the models of viscous disk evolution. Nevertheless, the values of dM/dt below $\sim 10^{-9} M_{\odot} yr^{-1}$ are uncertain, and can be affected by errors computing the U luminosity.

Individual ages may be affected by the problems described in Section 5.1, but considering only the different populations (i.e., the globule versus the bulk of the cluster), there is some evidence of mass accretion rate evolution from the age of ∼1 to 4 Myr. This evolution would be consistent with the higher disk fraction observed for the younger population near the globule as well. The comparison with other younger regions (Taurus, ρ Ophiuchus, Chameleon, see Figure 5.2 and Muzerolle et al. 2000) suggests that the mass accretion rates evolve with time, becoming smaller for the bulk of 4Myr stars in Tr 37.

5.3 Transition Disks Around Low-Mass Stars

Even though the accretion rates reported in Tr 37 are comparable in average to those detected in other clusters, like Taurus, it is remarkable that the IR emission from disks in Tr 37 is

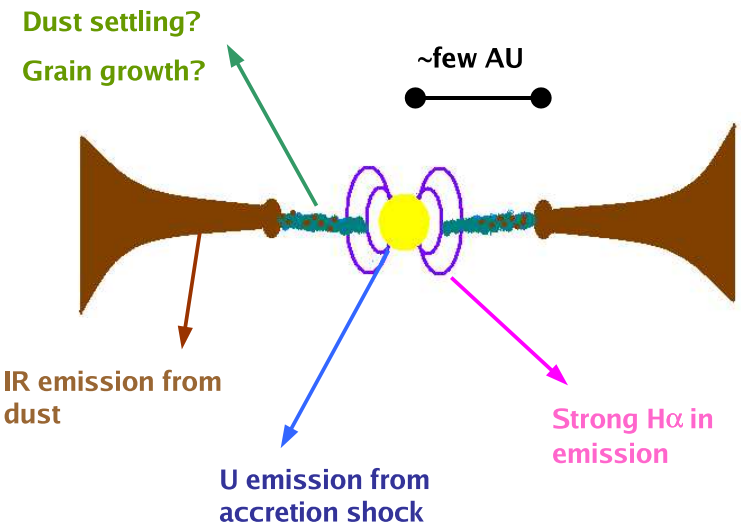

Figure 5.3 Scheme of an Evolved CTTS: If the inner disk has suffered further grain growth and dust settling, the emission at the shorter IR wavelengths would be reduced, whereas the accretion may still continue, and the emission from the outer disk would resemble the one of a "normal" CTTS with a well-mixed gas and dust disk.

systematically lower than the emission in Taurus (Hartmann et al., 2005). This difference is more striking at shorter wavelengths (JHK, 3.6, 4.5 and sometimes 5.8 μm), where the disk emission is, in many cases, one or more orders of magnitude lower than the average disk in Taurus. At longer wavelengths, 24 μm, even though the emission is still lower than in Taurus, the difference is much smaller, being in most cases comparable to the emission at 24 μm in Taurus.This phenomenon had been observed in other younger regions, like the Orion OB1 Association, although it did not affect such a large sample of stars (Uchida et al., 2004; Calvet et al., 2005). Given than most stars are accreting at usual rates, and given than in most cases there is a detectable excess emission at all wavelengths, the lower emission is probably related to dust settling and/or grain growth (Przygodda et al., 2003; Calvet et al., 2005; Uchida et al., 2004; D'Alessio et al., 2005), and is a sign of disk evolution (see Figure 5.3).

Also remarkable is the presence of weak-lined stars with disks. In the case of the WTTS with CTTS-like disks, a similar behaviour of accreting WTTS had been reported previously (see, for instance, Littlefair et al. 2004), and it was suggested that it could be produced by the strong variability of CTTS affecting Hα, eclipses produced by the disk, and/or the presence of optically thick accretion flows (in very rapid accretors). High-resolution spectra in the Hα region could be used in the future as a better way of detecting accretion, since the large velocities of accretion flows (200 km/s or more) can be easily detected with them, independently of the value of the Hα EW (see Section 6). In the case of non-accreting WTTS with disks, these objects could be regarded as "transition objects" in an intermediate state between CTTS and WTTS, where accretion is terminated, the inner part of the disk has been dissipated or agglomerated, but the outer part of the disk still remains (Duvert et al., 2000; Dutrey et al., 2003). The presence of larger bodies could block the accretion onto the star,

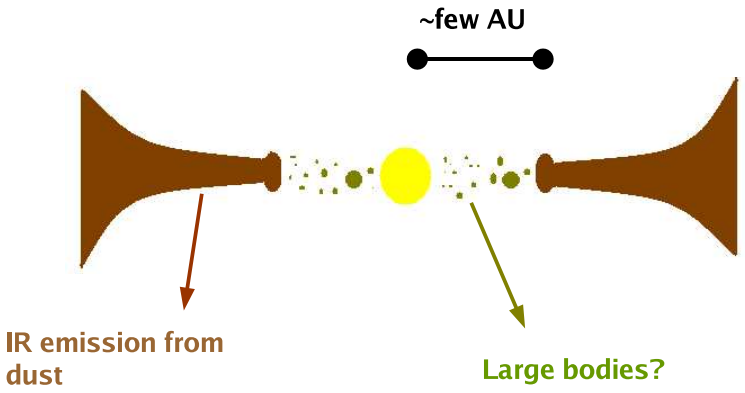

Figure 5.4 Scheme of a "Transition Object": If the grain growth in the inner disk produces large bodies (maybe comparable to planetary sizes), they may stop the flux of gas from the outer disk, so the accretion would terminate once the inner disk is depleted of gas. The outer disk may still remain, although observations suggest that it would disappear in timescales of the order of 10^5 years.

once the left over gas in the inner disk has been accreted (onto the star or onto planets), and could explain why we do not observe accretion even though the outer disk is still optically thick (see Figure 5.4). These objects would be somehow analogous to the "debris disks" that we observe at 24 μm around intermediate-mass stars. Nevertheless, in the case of low-mass stars, the lower temperature of the central star results in a colder disk and a much weaker emission at shorter wavelengths, so that disks cannot be detected unless they are much closer to the star, producing emission detectable at shorter wavelengths. The fact that zero accretion would suggest the presence of planetary-size bodies explains the interest in determining in the future whether these "transition objects" are accreting or not (using high-resolution optical spectra in the Hα region).

Another point to consider is the apparent short life of the "transition objects" (Duvert et al., 2000). Taking into account that there are only 4 (maybe 5) "transition objects" among the ~60 non-accreting stars for which we have bona fide IRAC and/or MIPS photometry, they represent a fraction of less than 10% of the total WTTS, and about 5% of the total content of the cluster, consistent with the picture where the outer disk disappears completely soon after the inner disk is removed/coagulated and accretion is terminated. If ~80% of the stars have disks at the ages of 1 Myr (see Lada et al. 2000, and Section 6), and only ~40% after 4 Myr, about half of these WTTS should have lost their disks after 1 Myr and before the actual age of the cluster. If only less than 10% conserve an outer disk at this age, the timescale for complete disk dissipation after the end of accretion must be of the order of 0.5 Myr or even less.

Moreover, the only "transition object" in NGC 7160, 01-1152, points in the direction of rapid outer disk dissipation once accretion is terminated and the inner disk is removed or agglomerated, as well. Following the same line of reasoning and comparing to Tr 37 (even though we must be cautious when dealing with this small-number statistics), about 35% of the stars in NGC 7160 (~20) should have lost their disks during the period from 4 to 10 Myr.

Assuming that the disks disappear at a constant rate, a few percent of them should have been removed in the past 1 Myr, and therefore, we would expect to see 1 or 2 "transition objects" if their outer disks are dissipated in less than 0.5 Myr, which is consistent with the observations.

5.4 Evolution of the SEDs

The striking differences in disk fraction between Tr 37 and NGC 7160 are a clear example of important disk evolution between the ages of 4 and 10 Myr. Moreover, the differences at shorter wavelengths with the average disks in Taurus (Hartmann et al., 2005) suggest an important degree of dust settling and/or grain growth in the inner disk (Forrest et al., 2004; D'Alessio et al., 2005). The presence of outer disks around ∼10% of the 4 Myr WTTS, and only around ∼2% of the WTTS aged 10 Myr, is another indication of rapid disk evolution during this period.

We can visualize the evolution of the disk emission with time by putting together the median SED for each one of the different aged regions. Figure 5.5 shows a comparison of the median SEDs for disks in Tr 37 and Taurus (Hartmann et al. 2005), the average of the two disks in NGC 7160, and the disk in TW Hya (Hartmann et al. 2005) for comparison. We have separated the data from the "young" population of CTTS in the Tr 37 globule, which may have an age of around 1 Myr, according to the ages of the optical stars around the globule; and the rest of the Tr 37 members, with an average age of 4 Myr.

The sequence of evolution from 1 to 10 Myr is evident. Comparing the 1-2 Myr disks in Taurus with the ones in Tr 37, we observe first a decrease in the emission at shorter wavelengths, originated in the inner disk (Weidenschilling, 1997; Weidenschilling & Davis, 2001; Calvet et al., 2002; Uchida et al., 2004). Differences with Taurus are found at all wavelengths, but they become less striking at 24 μm, for which we find that both regions have similar range of fluxes. This evolution of the inner disk at shorter wavelengths is what causes the trend toward redder colors observed in Figure 3.7.

The comparison of the stars in the globule with the rest of stars in Tr 37 reveals also a difference at the longer wavelengths (from 5.8 μm on), whereas both the globule and the bulk of the stars in Tr 37 show similar colors at wavelengths shorter than 4.5 μm. Compared to the disks in Taurus, and also to the disks in Tr 37, it is remarkable that the disks around 01-580 and 01-1152 in NGC 7160 present systematically lower emission at all the wavelengths, including 24 μm.

These observations support the idea of dust settling and/or grain growth being responsible for the decrease in emission, since these processes would be more important in older objects. Disks would be expected to become nearly flat with time, if they are not dissipated before. The evolution seems to start in the inner part of the disk and to propagate outward with time. If these processes are due to grain growth and/or dust settling, this would be consistent with the observed "transition disks" in which the emission from the inner disk is absent, maybe because of further grain growth to planetesimal sizes, and even by the formation of planets in the inner few AU of the disk. In any case, the dust settling and/or grain growth would favor the formation of larger bodies in the middle plane of the disk. It is interesting to note that the 24 μm emission of the "transition objects" in Tr 37 is stronger than in 01-580, which could be an indication of the inner part of the disk dissipating even when dust settling and/or grain growth is not complete. Nevertheless, a few disks in Tr 37, like 11-1209, show IR emission

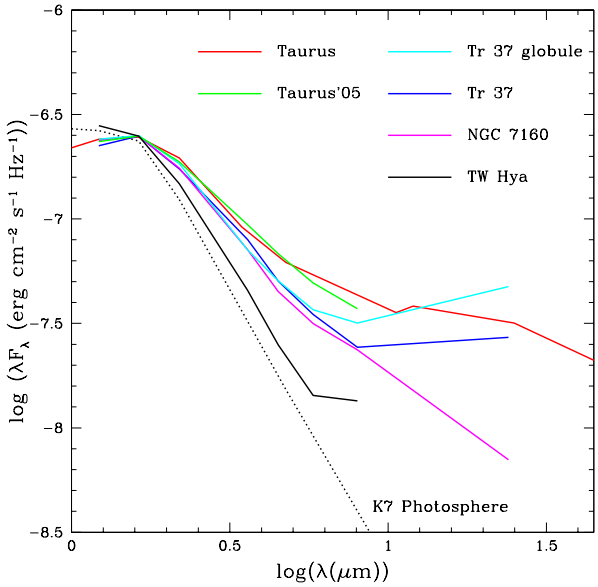

Figure 5.5 Evolution of the low-mass SED from the ages 1-10 Myr. We display the median fluxes for each IR band (JHK, 3.6, 4.5, 5.8, 8.0, 24.0 μm) available for CTTS in regions with different ages: Taurus (1-2 Myr), using both the data in Kenyon & Hartmann (1995) and Hartmann et al. (2005); the globule in Tr 37 (with ages around 1 Myr, according to the V vs. V-I diagram); the rest of Tr 37 (with ages about 4 Myr, and average age 4.5 Myr). We also display the average emission from the two stars with disks in NGC 7160, and the disk in TW Hya (Hartmann et al., 2005). All of them are scaled at H, and fluxes are derived from the absolute magnitudes (10 pc distance). The flattening of the SED starts occurring at shorter wavelengths (up to 5.8 μm) during the first $\sim$ 5Myr, and affects to all wavelengths by the age of 10 Myr (see text).

nearly consistent with a flat disk and similar to 01-580, which is another indication of how diverse protoplanetary disks may be since their formation.

In order to roughly estimate the disk parameters, the colors of the disks can be compared to the colors predicted for the accretion disks models by D'Alessio et al. (2005). These disk models cover a large parameter area, with ages ranging 1-10 Myr, T_{eff}=4000K, different accretion rates (from 10^{-7} to $10^{-9} M_{\odot} yr^{-1}$), inclinations, viscosity parameters (α=0.01-0.001), maximum disk radii (from 100 to 300 AU), and maximum grain sizes (from 1 μm to 10cm). Dust of all sizes and gas are well mixed, and disk flattening is not included. Due to the large number of variable parameters, the attempt to fit or describe individual SEDs would have a very high degree of uncertainty and would produce multiple solutions, since variations of different parameters in the models would produce similar SEDs. This way, distinguishing grain growth from dust settling and disk flattening becomes impossible using our available data: all these processes would result in a decrease of the emission as we observe. Therefore, the only attempt is to describe statistically the properties of our sample, comparing them to a grid of models with reasonable parameters. The colors derived from the models define a region in the color-color diagram, which has been depicted in Figure 5.6.

In order to check the presence of dust settling, grain growth and/or inner holes, other

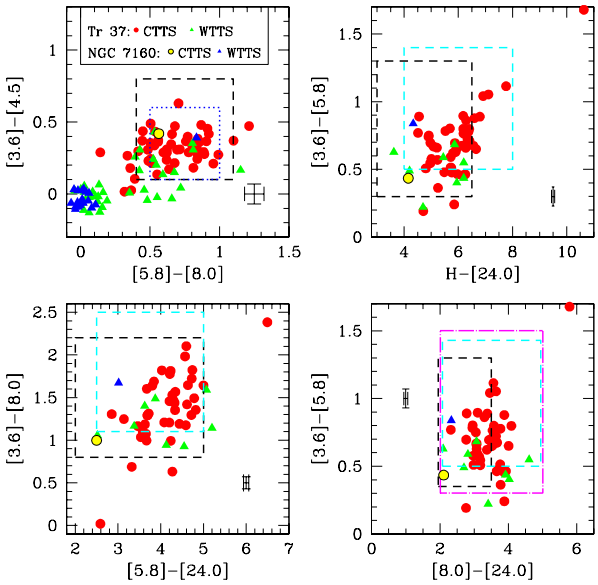

Figure 5.6 Spitzer and 2MASS color-color diagrams for the Tr 37 and NGC 7160 members: According to the Hα classification by White & Basri (2003), CTTS are represented by red circles, WTTS are represented by green triangles (in Tr 37), and by yellow circles and blue triangles (in NGC 7160), respectively. Since extinction effects at these bands are expected to be very small for the average A_V, no dereddening has been applied. For comparison, the colors predicted for CTTS of different accretion rates by the standard models of D'Alessio et al. 2005 (black dashed line) and the preliminary models including dust settling/grain growth (light blue dashed line) are displayed. The regions defined by the IRAC colors observed for Taurus stars (dotted line in the first diagram, see Hartmann et al. 2005), and the MIPS colors observed for stars in NGC 7129 (dotted-dashed line in the last diagram, see Muzerolle et al. 2004) are depicted as well. Note the large excess for the protostar 213645+572933, the highest dot in all the diagrams. The comparison with Taurus reveals as well a lower excess at shorter wavelengths, related to dust settling/grain growth as well (see text).

sets of preliminary models including these particularities (D'Alessio et al. in preparation) have been explored (see light blue boxes in Figure 5.6). According to these tentative models, the introduction of disk flattening via depletion of small grains from the outer layers of the disk (which affects the irradiation of the disk by the star), together with the reduction of the emitting area of the "wall" located at the dust destruction radius, would be a good starting point to account for the color trends of the disks in Cep OB2. Nevertheless, more work on modeling disks with differential settling or grain size (changing both with the distance to the star) would be required and, definitely, the large sample of disks in Tr 37 should be taken into account for the disk modeling.

5.5 Debris Disks at 3-10 Myr

The nature of debris disks around Vega-like stars is still matter of discussion. Debris disks found around Main Sequence stars are supposed to be formed by the reprocessed dust pro-

duced by the collision of planetesimals, after the formation of a planetary system (Backman & Paresce, 1993). According to this picture, disks should appear after timescales similar to those of planet formation, ∼10 Myr (Wyatt & Dent, 2002). On the other hand, the extreme youth of some of the known stars with debris disks (HR 4796A, A0 star, ∼8 Myr old, see Stauffer et al. 1995; Jayawardhana et al. 1998), together with the comparison with Herbig Ae/Be stars, suggests that at least some of these Vega-like disks could belong to the intermediate stage between classical pre-Main Sequence stars with dusty disks and stars well established in the Main Sequence (Dunkin et al., 1997). Finding data to support any of the two pictures encounters difficulties in both determining the age of intermediate-mass stars on the Main Sequence, and detecting the faint IR emission from debris disks.

Even though our debris disk detection at 24 μm is obviously limited by the sensitivity, a comparison of the results for Tr 37 and NGC 7160, for which we know a similar number of high- and intermediate-mass members (58 for Tr 37, 68 for NGC 7160) of similar spectral types, reveals two significant differences. First, there are no optically thick disks in the older cluster NGC 7160, indicating that these have been dissipated or have evolved forming planets by this age. Second, the total number of disks in Tr 37 doubles that of NGC 7160, even though the Tr 37 sample is about 15% smaller. This indication could be related to the fact that accretion disks around low-mass stars are also significantly different for Tr 37 and NGC 7160 as a consequence of disk evolution and dissipation.

Therefore, it could be possible that the disks that we detect in Tr 37 and NGC 7160 are in fact the remaining of protoplanetary disks, instead of the consequence of collisions of protoplanets giving birth to debris disks. It can be expected that similar optically thin disks should exist around low-mass stars, once the inner disk has been accreted/dissipated/agglomerated into planets. In this way, these objects would be similar to the "transition objects" identified among the low-mass stars, although the detection of debris disks around low-mass stars would be very difficult, since they would be orders of magnitude fainter. But, on the other hand, the short lifetimes of disks evacuated in the center deduced from the observations of low-mass stars would suggest that these disks are most likely reprocessed "debris disks", indicating that planetesimals and/or planetary systems are already formed at the early ages of 4 and 10 Myr.

In order to reveal the characteristics of the dust in these disks, and whether it may be similar to the reprocessed dust in debris disks or the dust in protoplanetary, accretion disks, obtaining IR spectra (i.e., using IRS on Spitzer) would be required. Longer wavelengths observations for the detection of larger grains and the outermost disk, as well as UV spectra to detect the emission of H_2 gas in the disk, would be the logical continuation of this work.

6 Accretion, Kinematics, and Rotation in the Orion Nebula Cluster

Published in "Accretion, Kinematics and Rotation in the Orion Nebula Cluster: Initial Results from Hectochelle", by Sicilia-Aguilar, A., Hartmann, L., Szentgyorgyi, A., Fabricant, D., Furezs, G., Roll, J., Conroy, M., Tokarz, S., Hernández, J., 2005, AJ, 129, 363.

We present results from high-resolution spectra of 237 stars in the Orion Nebula Cluster (ONC) obtained during two engineering runs with the Hectochelle multifiber echelle spectrograph on the 6.5m MMT. The ONC is the nearest populous young (ages $\sim$ 1 Myr) cluster, and is therefore an important object for studies of the evolution of protoplanetary disks. Using the high spectral resolution of Hectochelle, we are able to distinguish stellar accretion and wind emission line profiles from nebular emission lines, and identify accreting members of the cluster from Hα profiles with greater accuracy than previously possible. We find 15 new members, based on Li 6707 Å absorption and Hα emission. Line profiles of Hα of some objects that are not too contaminated by nebular emission show features characteristic of mass inflow and ejection. We also present rotational velocities as part of an initial investigation into angular momentum evolution of very young stars, confirming a difference between CTTS and WTTS that had been found in period analysis. Finally, we present an initial study of the radial velocity dispersion of the brighter stars in the central cluster. The very small dispersion derived, $\leq 1.8 km/s$, is in good agreement with estimates from proper motions.

From this study, the use of high-resolution Hα spectroscopy is confirmed as a very efficient method to distinguish accreting and non-accreting stars, even if accretion rates are small, and it could be applied in the future to the study of "transition objects" and very slow accretors in older clusters like Tr 37 and NGC 7160.

6.1 Introduction and Motivation

The Orion Nebula Cluster (ONC) is the youngest nearby populous cluster, (Hillenbrand, 1997; Hillenbrand et al., 1998), and the nearest HII region as well (Bally et al., 1998). Therefore, the ONC is a crucial object for the study of the evolution of protoplanetary accretion disks at early ages (Hillenbrand, 1997). It has been difficult to study protoplanetary disk accretion in the ONC, due to the very bright nebular background, which makes it hard to detect the accretion-powered ultraviolet continuum and optical line emission. The recent study of Robberto et al. (2004), which uses the high spatial resolution of the *Hubble Space Telescope*

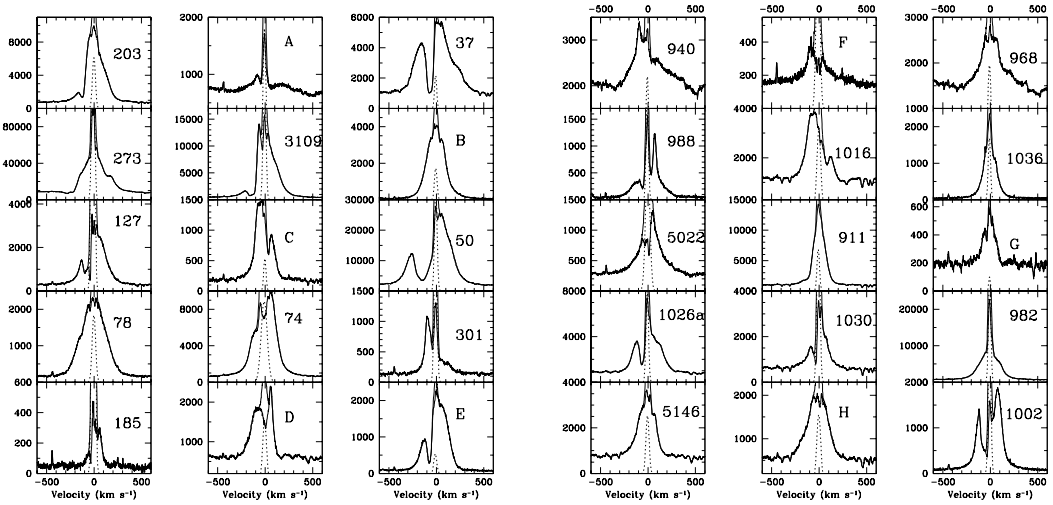

Figure 6.1 Sky-subtracted spectra of broad-lined CTTS from December 2003. All spectra for which a correct sky subtraction could be done, plus some of the typical WTTS spectra, are displayed here. The thin line is the unsubtracted spectrum, the dotted line is the Gaussian fit to the narrow nebular component, and the thick line is the resultant spectrum after the subtraction of the fitted nebular component. Numbers indicate the star JW ID in Hillenbrand et al. (1998). New stars from the 2MASS survey are designed with letters: A = 05343856-0547350, B = 05334668-0523256, C = 05334167-0524042, D = 05350333-0456430, E = 05350945-0457117, F = 05354885-0500285, G = 05364005-0512231, H = 05364760-0536312.

to detect ultraviolet continuum excesses, and thus infer mass accretion rates in 40 stars, is an important first step toward characterizing accretion properties in the ONC. This sample, however, constitutes only a small fraction of the stars in the cluster. It is desirable to identify many more accreting members, as well as non-accreting stars, to help to interpret studies of disk infrared excess emission (Lada et al., 2000), and to understand the origin of stellar angular momenta distribution (Herbst et al., 2000; Stassun et al., 1999; Rhode et al., 2001).

The ONC is also a prime target for studying the kinematics of a very young cluster, with a view toward constraining mechanisms of cluster formation. In addition, this populous young cluster has been used as an important benchmark for understanding the evolution of stellar angular momentum (Herbst et al., 2000, 2002; Stassun et al., 1999; Rhode et al., 2001). High spectral resolution is necessary to measure the small radial velocity shifts about the cluster mean and modest rotational line broadening of most young, late-type stars in this cluster.

Here we report preliminary observations of ONC stars using the Hectochelle multifiber spectrograph (Szentgyorgyi et al., 1998) on the 6.5m MMT on Mt. Hopkins, Arizona. In limited engineering observing time, we obtained spectra to study the kinematics and rotation in the cluster, and to measure emission line profiles indicative of accretion, achieving reasonable to good signal-to-noise values for 237 objects. We were able to identify approximately 93 certain CTTS, 62 WTTS (objects with narrow Hα), 43 possible CTTS (Hα broader than typical WTTS and nearby nebular emission, but not clearly as broad as in typical CTTS),

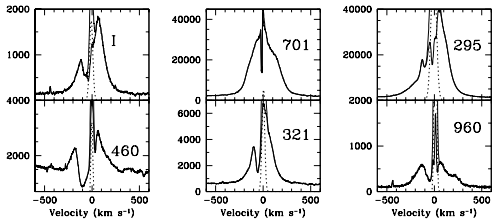

Figure 6.2 Sky-subtracted spectra of broad-lined CTTS from December 2003 (continued). All spectra for which a correct sky subtraction could be done, plus some of the typical WTTS spectra, are displayed here. The thin line is the unsubtracted spectrum, the dotted line is the Gaussian fit to the narrow nebular component, and the thick line is the resultant spectrum after the subtraction of the fitted nebular component. Numbers indicate the star JW ID in Hillenbrand et al. (1998). New stars from the 2MASS survey are designed with letters: I = 05355690-0545191 .

and 39 possible WTTS. With this better system for the identification of accreting stars, we re-examine the different criteria that have been used in the literature in order to distinguish CTTS and WTTS, trying to find the strongest method. The utility of Ca II infrared triplet emission and K-band excesses for detecting accreting disks in the ONC are compared to the efficiency of Hα high-resolution profiles. We also present Hα profiles for 70 CTTS, for which the nebular emission could be corrected or ignored. We also present initial radial velocities for 79 stars, suggesting that the radial velocity dispersion in the central region is of order $1.8\,\mathrm{km\,s^{-1}}$ or smaller, at least for the relatively bright population studied here. Finally, we present rotational velocities for approximately 130 stars, 40 of which were initially studied by Rhode et al. (2001), and with whom we find good agreement. These results could be applied in the future to the investigation of stellar properties, kinematics, and accretion in Tr 37, NGC 7160, and other regions, in addition to the ONC.

6.2 Accretion and Membership in the ONC

Table 6.2 lists the objects observed in December 2003, along with the 2MASS identifications and the spectral types from Hillenbrand (1997), CTTS/WTTS classification, Hα and Li I equivalent widths, and other comments. Table 6.3 lists results for the March 2004 observations, for which we had good Thorium-Argon wavelength solutions. Identifications and spectral types are as in Table 6.2, including the 2MASS identifications, photometry from Hillenbrand (1997), and the measured velocities.

6.2.1 Hα signatures of accretion

Magnetospheric accretion yields emission lines with very large velocity widths, usually greater than $\pm$ 100 $\mathrm{km\,s^{-1}}$ (Hartmann, 1998). White & Basri (2003) showed that Hα full widths at 10% $> 270\,\mathrm{km\,s^{-1}}$ are good indicators of accretion independent of spectral type (see also Bonnell et al. 1998). Nebular emission in the ONC is generally much narrower than this, making it possible to infer accretion with high-resolution spectra. It is much more difficult to

detect the chromospheric emission of WTTS, which can only be done if the nebular emission is relatively weak near the star. Given that the data in the two runs had different sets of sky spectra, the analysis is slightly different in the two cases. In the case of strong nebular emission with very weak spectra, we cannot distinguish weak broad stellar Hα from wings of the nebular lines, so we have tried to be conservative in citing detections of accretion. We therefore distinguish between certain detections of broad Hα as identifying secure CTTS. In other cases we are not certain whether the broad line is stellar or merely wings of the nebular emission, and we call these possible CTTS. Conversely, in some objects, the nebular emission is relatively weak and the stellar photospheric continuum strong, and it is obvious that there is no broad stellar Hα. We refer to these objects as certain WTTS. This leaves objects that we identify as possible WTTS, and "noisy" systems with low signal that are impossible to classify.

In the initial December 2003 observations, we did not attempt to take independent "sky" exposures, and had only the randomly placed "sky" fibers for analysis. The spatial variability of the nebular emission precludes a direct subtraction of the sky emission using these fibers. We found that the maximum FWHM of the Hα emission at any of the sky positions was $\sim 0.7 - 0.8$Å. We therefore conclude that the profiles with emission at much larger velocities are stellar and are signatures of accretion. In some cases, the nebular line widths are much smaller, < 0.6Å, and we can detect smaller line widths. There are as well some regions in the field where the nebular emission exhibits a double peak, making the identification of weak objects even more difficult. Therefore, each star is classified after comparing its Hα emission with that of all the closest sky templates, to detect if the emission could have been produced by a similar background.

In cases of very broad Hα emission with good signal-to-noise spectra, it is possible to distinguish the narrow nebular component added to the very wide stellar component. For the December data, we fit a model composed of several Gaussians to each spectrum, in order to subtract then the Gaussian fit of the narrow nebular component. A similar method has been used before for deblending spectral lines composed of narrow and wide components by Muzerolle et al. (1998a). Although none of the components is exactly Gaussian, this procedure works moderately well for many of the broad CTTS detected (see Figures 6.1 and 6.2).

We used IRAF task *fitprofs* in the IRAF package *noao.imred.specred* to fit two or three Gaussians to each spectra, providing a starting model with the centers, flux at the peak and equivalent width (EW) of each one of the visible components of the spectrum. All these values were previously measured using task *splot* in the same package. The program provides a fairly accurate model fitting the whole spectrum in the Hα region to a set of Gaussians plus a continuum level. We only use the Gaussian component associated to the narrow emission, which is identified with the background nebular emission, and subtracted it from the real spectrum (Figure 6.1).

Out of a sample of 156 spectra in the December 2003 data with good signal-to-noise, we identify 63 CTTS and 33 WTTS with reasonable confidence. Additionally, we classify another 37 stars as "possible CTTS" and another 23 as "possible WTTS". These identifications are given in Table 6.2, and the profiles for which we could subtract most of the sky emission are displayed in Figure 6.1 as thick lines, with the original spectra and their estimated sky Gaussian profiles shown by the thin and dotted lines, respectively.

For the March 2004 run, we took a "sky" spectrum, offsetting the telescope 20 arcsec north with the fibers in the same position. Given the spatial variability of the nebular emission and its strength, subtracting this "sky" spectrum does not yield good results in many cases.

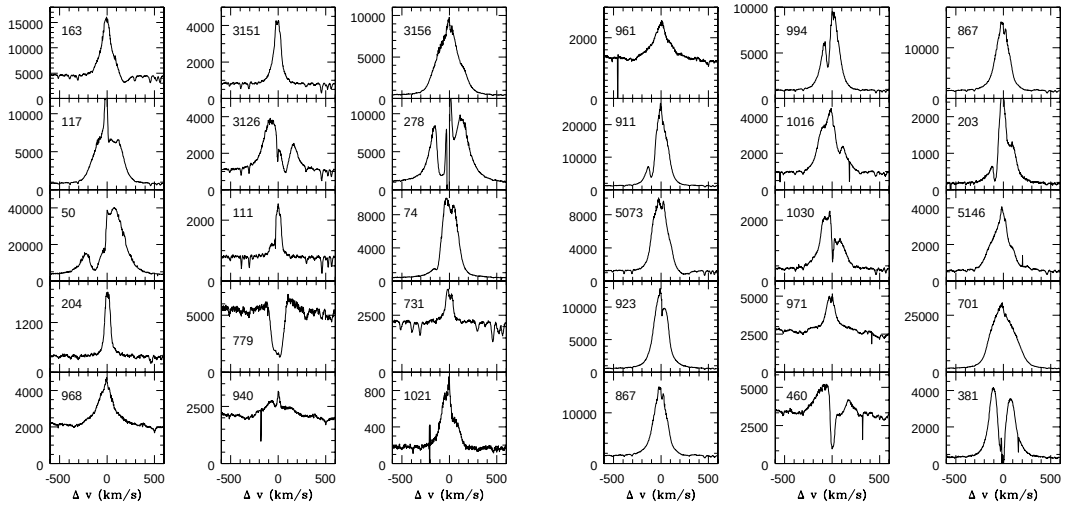

Figure 6.3 Sky-subtracted spectra of ONC stars from March 2004. Spectra with properly subtracted sky are displayed here.

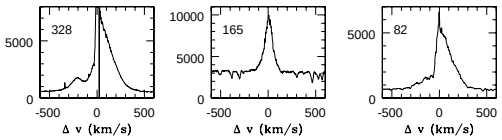

Figure 6.4 Sky-subtracted spectra of ONC stars from March 2004 (continued). Spectra with properly subtracted sky are displayed here.

However, we were still able to identify 30 CTTS and 29 WTTS, with another 7 possible CTTS and 15 possible WTTS, in addition to the stars previously identified in the December 2003 run. Of the 40 stars in common between the two runs, only two had disagreements in the classification. JW 63 was identified as a WTTS in December 2003 and as a CTTS in March 2004; JW 940, identified as a CTTS in December, was classified as a WTTS in March. We were unable to confirm the December 2003 classification for another star (JW 981) in March 2004. Thus, our classifications appear to be secure in most cases. Table 6.3 shows the results for the 2004 run, and the profiles that had reasonable sky subtraction are shown in Figures 6.3 and 6.4.

Combining the results from the two runs, we classify 93 stars as certain CTTS and 62 stars as certain WTTS; adding in the possibles, we arrive at ~ 136 CTTS and ~ 101 WTTS. Thus, approximately 60% of the stars in our ONC sample show the Hα signature of disk accretion. Our results are reasonably consistent with the estimated inner disk frequency of about 70% found by Hillenbrand et al. (1998) based on near-IR excesses, and with the results of Muench et al. (2001), who estimate a frequency of disks larger than 50%. This frequency of accretion disks is also similar to that in Taurus (Kenyon & Hartmann, 1995).

Once the nebular emission was subtracted, we obtained the Equivalent width (EW) of

the lines. We measured the line flux using IRAF task *splot*, and the continuum flux from the *fitprofs* model (for the 2003 data) or measured directly from the spectrum with *splot* (for the 2004 data). The resultant equivalent widths are given in Å (Tables 6.2 & 6.3).

As might be expected, the agreement of equivalent widths measured in December and in March is much poorer than that of simple classification as CTTS or WTTS. In particular, the comparisons between December/March equivalent widths (in Å) were particularly poor for: JW 91, -31/-11; JW 50, -152/-60; JW 940, -4.6/-1; JW 911, -33/-62; JW 980, -75/-24. Although these objects are variable, much of the discrepancy could be due to difficulties of measurement. Our Hα equivalent widths should therefore be regarded with caution, with a preference for adopting the sky-subtracted values of the March 2004 observations.

The Hα profiles of CTTS are often asymmetric, showing in many cases blue-shifted emission and red-shifted absorption that can be explained with the magnetospheric accretion models (Calvet & Hartmann, 1992; Edwards et al., 1994; Muzerolle et al., 1998b, 2001; Hartmann, 1998). The red-shifted absorption due to infall is not always detected; models show that this feature is highly dependent on geometry of the flow and on the inclination at which the system is observed (Hartmann, Hewett, & Calvet, 1994; Muzerolle et al., 2001). Blue-shifted Hα absorption, produced in winds, is strongly correlated with high accretion rates (Edwards et al., 1994; Hartmann, 1998). We have detected these signatures for some stars in our sample spectra, which are listed as PC (P Cygni profiles, wind-dominated) or IPC (Inverse P Cygni profiles, infall) in Tables 6.2 & 6.3. In total, we detected 26 stars showing IPC, and 18 with a PC profile. Some variability in the profiles is detected. For example, JW 74 and JW 911 showed much clearer high-velocity blue-shifted absorption in March than in December, and JW 460 showed blue-shifted absorption in December but clear red-shifted absorption in March.

6.2.2 Herbig-Haro Emission in JW 868

The spectrum of JW 868 deserves special comment. As shown in Figure 6.5, the Hα and [NII] emission lines are extremely strong; most remarkably, they exhibit emission blue-shifted to very high velocities.

The [N II] λ6583 profile suggests that this emission extends out to at least $-650\,\mathrm{km\,s^{-1}}$; the H$\alpha$ profile is consistent with this estimate, though it clearly runs into the [N II] 6548 Å line. The profile shapes are difficult to interpret near central velocities because of the strong nebular emission in the region, which also renders it difficult to estimate true equivalent widths; however, we can state that the [N II] λ6583 line has an emission equivalent width larger than 16 Å, which is extremely unusual for a T Tauri star. Thus, we conclude that we are basically detecting a Herbig-Haro object (HH), for which such large [N II] emission is likely, although the velocity widths are also quite large for an HH object (see, e.g., Hartigan, Raymond, & Hartmann 1987).

It is difficult to be certain that this HH object is associated with JW 868 in such a crowded region as the ONC. An association might be more likely if it could be shown that JW 868 is a rapid accretor. In principle, one can infer something about the stellar accretion rate by measuring the continuum "veiling" of photospheric absorption lines (Hartigan et al., 1991). Inspection of the stellar absorption lines suggests that the veiling in JW 868 might be appreciable, with around half of the continuum flux near Hα coming from accretion, not the stellar photosphere. However, we are reluctant to make certain estimates of veiling from our data, because of instrumental problems that yielded a significant amount of stray light on the

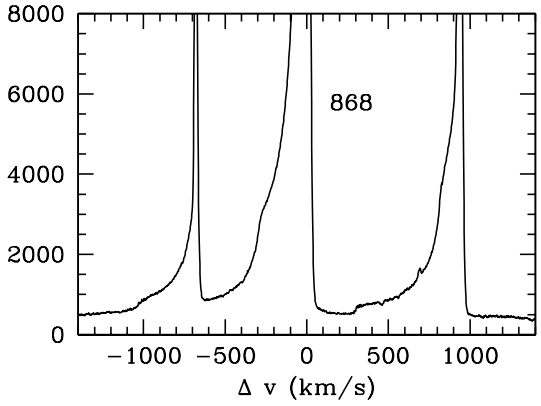

Figure 6.5 Spectrum of JW 868, showing broad Hα and the 6548 Å and 6583 Å [N II] lines (see text).

CCDs, with a resultant uncertain subtraction of this extra emission. It is clear, however, that in the future we will be able to use Hectochelle to measure veiling and thus provide at least additional rough estimates of accretion rates for ONC stars (especially in the red, where the nebular continuum is much weaker).

Another possibility would be that we are detecting the extended emission from a nearby HH object. We have inspected the 2MASS catalog (Cutri et al., 2003) to identify possible candidates. There are two other objects within 20 arcsec of JW 868. One of them, at RA(2000)=5:35:31.0, DEC(2000)=-5:23:22.30, shows JHK colors consistent with an early K star in the Main Sequence (J-H=0.42, H-K=0.11). The other object is located at about ∼15 arcsec distance from JW 868, coordinates RA(2000)=5:35:31.89, DEC(2000)=-5:23:54.6, and shows JHK colors of J-H=0.30, H-K=0.62. These colors are consistent with these of typical HAeBe stars in young clusters (Hernández et al., 2005), which have disks. This object could be responsible for the HH emission lines that we observe over the JW 868 spectrum, although this explanation needs to be confirmed with further observations.

6.2.3 Li 6707 Å Absorption and New ONC Members

Lithium absorption at 6707 Å is an indicator of the youth of stars with later spectral types (Randich et al., 2001). Lithium is depleted in low and intermediate (K-M) mass stars by the ages of 30-50 Myr (Randich et al., 2001; Hartmann, 2003), so in general it can be used to distinguish the young cluster members from background and foreground stars.

Due to the time limitations during these engineering runs, we could only take spectra in the Lithium region during the 2003 observations. The exposure time was only 900 sec, which did not yield enough signal-to-noise to measure Li absorption in many spectra. Nevertheless, for most of the stars in our sample, Li was detected and its EW was estimated using *splot* task in IRAF, although in some cases the signal-to-noise ratio was not high enough for very accurate measurements. The EW are shown in Table 6.2. Since most of our 2003 sample was taken from Hillenbrand (1997) and consists of confirmed cluster members with 95 or 99% certainty from proper motions, the use of Lithium as a discriminant of non-members is

not strongly required. Nevertheless, no obvious contradiction with the membership stated in Hillenbrand (1997) was found, although Li could not be detected in all the cases due to poor signal to noise.

For the other 40 stars that were selected from 2MASS survey in the December observations, no membership probabilities are available, so here Lithium absorption plays a more important role. Since the stars from 2MASS were systematically fainter than those taken from Hillenbrand (1997), nearly half of the spectra taken with this reduced exposure time did not have enough signal-to-noise for further study. Of the 22 spectra from the 2MASS selection with enough signal-to-noise in the Hα region, 8 of them (3 WTTS, and 5 CTTS) show clear Lithium absorption, so they can be classified as young stars. In addition, 7 objects show strong Hα, and are thus young stars as well. These 2MASS-selected young stars lie to the East, at a distance up to ~ 27 arcmin from the center of the ONC, and about ~ 12 arcmin or less from the Hillenbrand members. This suggests that they are ONC members (Mandel & Herbst, 1991). Membership of the remaining objects from 2MASS is more problematic, since the narrow Hα line might be of nebular and not stellar origin, so we cannot comment about their membership at this point. As a final comment, there are 5 of the low signal-to-noise objects that show significant 2MASS excess (see Table 6.2, where excesses are denoted as a "nIR" comment). Although no information about their Hα nor other lines is available from the Hectochelle spectra, the excess could be indicative of ongoing accretion (Meyer et al., 1997), so they are interesting candidates for further studies.

6.2.4 He 5876 Å and Na I profiles

The He I emission line at 5876 Å is another feature that has been used to characterize accretion processes (Muzerolle et al., 1998a). This line shows a narrow and a broad component, and the broad emission is indicative of accretion (Muzerolle et al., 1998a). We checked the presence of broad He 5876 Å emission in our targets. In most of the cases, the reduced exposure time did not allow us to obtain enough signal-to-noise to measure equivalent widths, but the line was detected in some of the brightest objects. It was noticeable that very broad lines were strongly correlated with the presence of very broad Hα, as expected (see Table 6.2). This line could be used to distinguish between the probably CTTS and probably WTTS in case of uncertain sky subtraction, although in this study, due to the short exposure times and low signal-to-noise, this feature can not be fully used in most of the cases. As in the case of observing Li 6707 Å, this is an important point to consider for further observations. Typical broad He 5876 Å profiles are displayed in Figure 6.6. This figure shows the Na I lines as well, which are also produced in the magnetospheric infall zone (Muzerolle et al., 1998a) and show evidence of accretion.

6.2.5 Radial and Rotational Velocity Distributions

In Table 6.3 we present the results for the radial and rotational velocities of the stars observed in March 2004. These measurements were made using the cross-correlation routine *xcsao* in the IRAF *saotdc* package. The position of the cross-correlation peak yields the radial velocity (see, e.g., Tonry & Davis 1979), while the width of the cross-correlation peak can be related to the rotational velocity using the techniques described in Hartmann et al. (1986). We used a non-member, slowly-rotating K star in the field as the template, which yielded good correlations for our target stars. Hα and NII regions were excised before correlation. Error

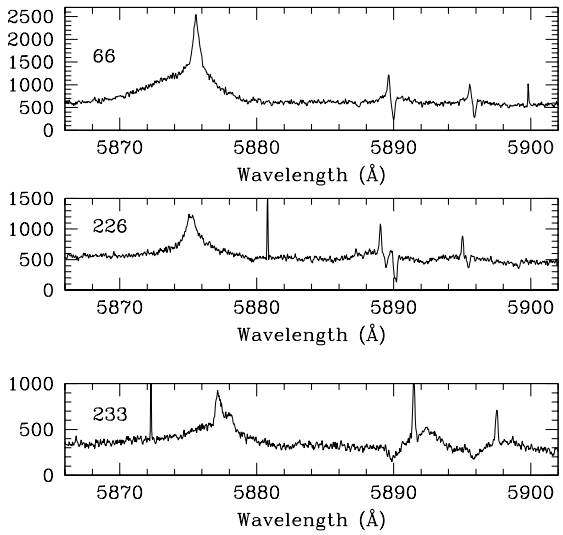

Figure 6.6 Examples of broad He 5876 Å profiles, characteristic of strongly accreting CTTS, for some of the most active accretors. Evidences of excess blue emission are present in the first and third panels, which can be indicative of winds. Na I lines is also displayed (see text) showing evidences of blueshifted absorption in the third panel.

estimates are based on the signal-to-noise values of the cross-correlation peak and its intrinsic width (see Hartmann et al. 1986 for details).

Of the 150 targets in the March data, 79 objects yielded a cross-correlation with a signal-to-noise of $R \geq 10$; 133 yielded $R \geq 4.0$. For most of these objects, which are slow rotators, the estimated velocity error is roughly $\sim 1\,\mathrm{km\,s^{-1}}$ at $R \sim 10$ and $\sim 2\,\mathrm{km\,s^{-1}}$ at $R \sim 4$ (the rapid rotators have bigger errors, but generally have poor R-values).

Figure 6.7 shows the central region of the resulting velocity histogram. Gaussian fits were made at $\pm 7\,\mathrm{km\,s^{-1}}$ from the mean cluster velocity for both $R \geq 10$ and $R \geq 4$ samples (i.e., between relative velocity bins of $-14\,\mathrm{km\,s^{-1}}$ and $0\,\mathrm{km\,s^{-1}}$). The mean velocities for the two samples differ only by about $0.3\,\mathrm{km\,s^{-1}}$, which is consistent with the observed dispersion and number statistics. The velocity dispersions of the two samples estimated in this way are $\sim 1.78\,\mathrm{km\,s^{-1}}$ and $\sim 2.27\,\mathrm{km\,s^{-1}}$, with the lower-$R$ sample having the larger dispersion. The Gaussian "fits" suggest that the observations may have a slightly sharper "core"; the velocity distribution is not Gaussian at larger velocities, where widely-offset objects are found. There may be a zero point shift in radial velocity of the standard of up to 2 $\mathrm{km\,s^{-1}}$, which could introduce a similar constant offset in the absolute radial velocities of the ONC stars but would not affect any conclusions about velocity dispersions. We will refine the zero point from future observations.

To put these results in context, the estimated dispersion in *proper motion* for the Orion Nebula cluster from the Jones & Walker (1988) study is $\sigma \sim 2.5\,\mathrm{km\,s^{-1}}$. Both the JW study and the study by Van Altena et al. (1988) indicate that the brighter stars ($I \leq 11$, $R \leq 12$) (which constitute the majority of the current sample) have a smaller velocity dispersion, $\sigma \sim 1.6\,\mathrm{km\,s^{-1}}$; our results are in good agreement.

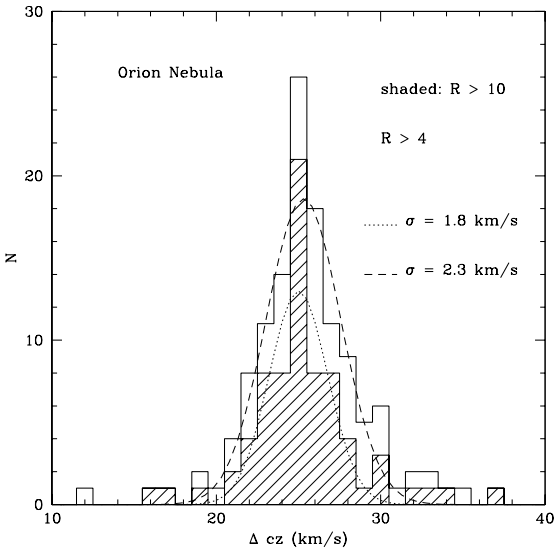

Figure 6.7 Radial velocity distribution for ONC stars, selected according to signal-to-noise values R of the cross-correlation peak (see text).

Six objects have either large velocity offsets (LV) suggesting that they are single-lined spectroscopic binaries (SB1s) or non-members. The cross-correlation results indicate that three systems – JW 239, JW 80 (a proper motion non-member) and JW 1049 are new double-lined binaries (SB2s) (see Table 6.3). Within our sample, Rhode et al. (2001) previously found that JW 50, and JW 961 were SB2s.

Figure 6.8 shows a comparison of the rotational velocities measured here and those of Rhode et al. (2001) for stars in common. The agreement is good, within error limits, except for a few objects which may be unrecognized SB2s. Rhode et al. (2001) estimated that their lower limit for detecting rotational velocities was $v \sin i \sim 11\,\mathrm{km\,s^{-1}}$. As we have higher spectral resolution (a resolving power of $\sim$ 34,000 vs. 21,500 for Rhode, Herbst & Mathieu 2001), we estimate that we can detect rotation down to $v \sin i \sim 6-7\,\mathrm{km\,s^{-1}}$ for spectra with high signal-to-noise. Our result (Table 6.3) seems to indicate that a significant number of ONC stars have such low rotational velocities, suggesting further studies of a broader ONC sample would be useful.

6.3 Characteristics of CTTS and WTTS in the ONC

6.3.1 Near-IR Excesses and Accretion

In some cases, the presence of accretion disks can be inferred from near-IR color excesses (Meyer, Calvet & Hillenbrand 1997, and references therein). The near-infrared excesses of most T Tauri stars are the result of heating by the radiation from the central star (Muzerolle et al., 2003a). The K-band excess (i.e., calculated as H-K color) in particular is sensitive to inclination and to the size of the hole in the inner disk (see Muzerolle et al. 2003a for additional discussion), although in clusters like Tr 37, we find that only about 50% of the

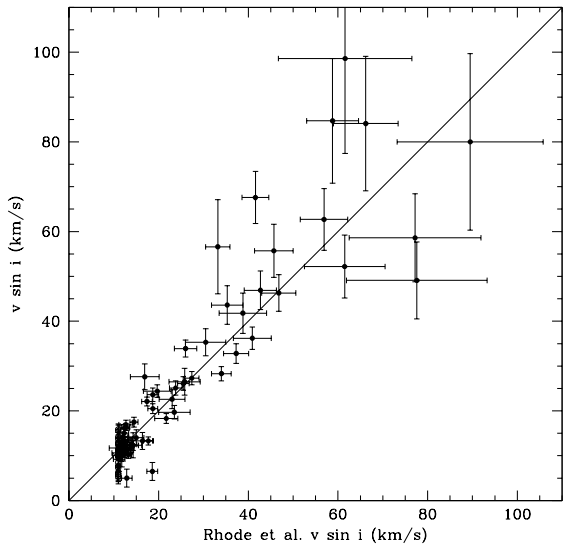

Figure 6.8 Measured rotational velocities compared with results from Rhode et al. (2001) for stars in common (see text).

accreting stars present an excess in K band.

All but 11 of the 146 stars selected from Hillenbrand (1997) in 2003, and the whole sample observed in 2004, could be matched within 1 arcsec to their 2MASS counterparts (see 2MASS ID numbers in Tables 6.2 and 6.3). The J-H vs. H-K diagrams for the objects are shown in Figure 6.9, for the objects from Hillenbrand (1997) observed in 2003 and 2004, and in Figure 6.10, for the 2MASS objects from the 2003 run. We also display the standard sequences for Main Sequence stars and for the giant branch, and the CTTS locus for a star of spectral type K7, as well as the reddening vectors (Bessell & Brett, 1988; Meyer et al., 1997). Stars without disks and those stars with holes or substantial dust settling in the inner disk should lay along the Main Sequence tracks; stars with disks should deviate along the CTTS locus.

As shown in Figures 6.9 and 6.10, the correlation between near-IR colors and the selection based on Hα emission is very consistent, within the 2MASS errors, taking into account that some CTTS may not show near-IR excess due to the geometry and properties of their disks and/or orientation (Muzerolle et al., 2003a). About five objects among the Hillenbrand (1997) sample show anomalous colors out of the Main Sequence and CTTS locus (see Figure 6.9). We examined these objects closely, finding that their 2MASS colors have large errors (sometimes bigger than 0.1 mags in each color). In Tables 6.2 and 6.3, we attach the label "nIR" to objects consistent with large excesses and the CTTS locus (selected empirically from the Figure, using the criteria $J-H > 0.7$ and $J-H < 0.38+1.53(H-K)$, which basically selects the objects above the Main Sequence and with colors consistent with reddening from the CTTS locus. This selection, although rough, gives results consistent with the CTTS/WTTS classification.

We next comment on the effectiveness of the $\Delta(I-K)$ index as an indicator of accretion. As discussed above, the K band excess can be used to determine the presence of circumstellar disks (Hillenbrand, 1997; Hillenbrand et al., 1998). For low mass stars, the I optical color is the less affected by both reddening and circumstellar disks, and K magnitudes are readily

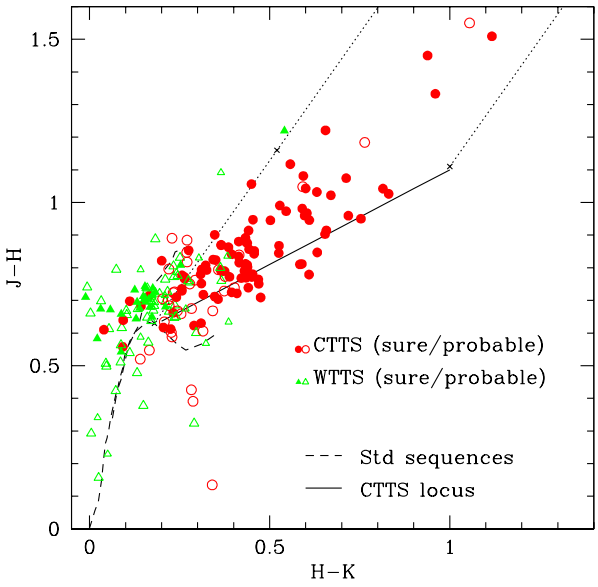

Figure 6.9 2MASS (Cutri et al., 2003) near-IR color-color diagram for the sample of stars in Hillenbrand (1997) that were observed in 2003 and 2004. Black symbols denote CTTS, open symbols denote WTTS. Circles are used for certain CTTS (black) and WTTS (open); triangles denote uncertain CTTS (black) or WTTS (open). Standard sequences and CTTS locus from Meyer et al. (1997). Stars are de-reddened using their individual A_V given in the Hillenbrand (1997) tables. Reddening vector (calculated with the standard reddening law) is displayed at the ends of the CTTS locus, with an X to denote an extinction of A_V=5 magnitudes. It is remarkable the agreement between our spectral selection of CTTS and the near-IR excess that defines the CTTS locus for the accreting objects.

available, so Hillenbrand et al. (1998) defined a $\Delta(I-K)$ index, corrected for reddening and spectral type, in order to quantify this excess. A complication is that T Tauri stars are highly variable with periods of days (Hillenbrand et al., 1998; Rhode et al., 2001), so the use of non-simultaneous photometry in I and K can add more uncertainty. The $\Delta(I-K)$ index is also variable depending on the accretion rate and the size of the inner hole, and becomes less sensitive for the later spectral types (Hillenbrand et al., 1998).

Comparing the classification based on Hα broad emission with the $\Delta(I-K)$ index given in Rhode et al. (2001) (Figures 6.11 and 6.12), we find that, although this index is fairly efficient in the case of strongly accreting CTTS, there is a significant overlap mainly for weak accretors. This could be suggestive of the high dependence of the near-IR excesses on the presence of inner holes, or dust settling in the disk, effects that have been pointed out by Hillenbrand et al. (1998). Even though imposing $\Delta(I-K) > 0.5$ to detect CTTS is mostly safe (all the objects over this limit, except one, are CTTS), there is a significant fraction of CTTS with a value of $0 < \Delta(I-K) < 0.5$ which would be missed by this criterion, since more than 1/3 of the stars in this region are CTTS. We find that measurements of Hα can resolve this near-IR overlap between the less-extreme CTTS and WTTS. This is similar to what was found in Tr 37, were only $\sim$50% of the CTTS show strong near-IR excess, being most of the CTTS without excess rather slow accretors.

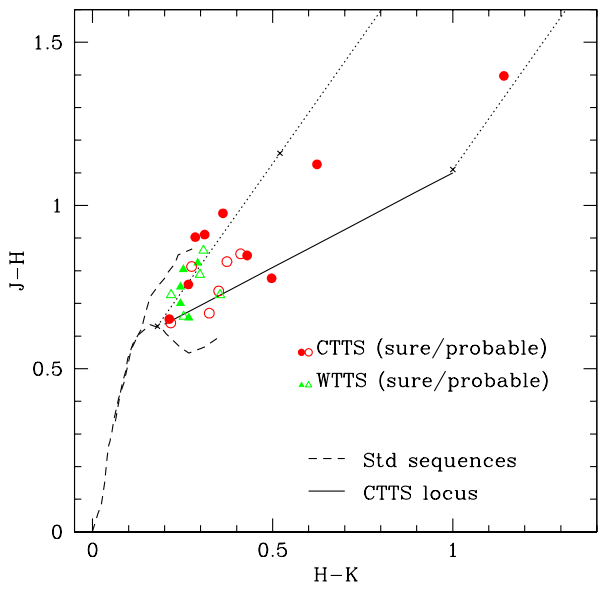

Figure 6.10 2MASS near-IR color color diagram for the sample of stars taken from 2MASS survey (Cutri et al., 2003). Symbols as in Figure 6.9. Although many of the stars in this sample were substantially fainter than the Hillenbrand (1997) ones, not allowing a clear Hα selection, we find again a strong correlation between our spectroscopic selection and the presence of an accretion disk. Note that for these stars no A_V were available, so the effect of reddening has to be taken into account when studying this diagram. Standard sequences and reddening vectors are displayed as in the previous figure.

6.3.2 The CaII Infrared Triplet

The CaII IR triplet (8498 Å, 8542 Å and 8662 Å) has been used to determine the presence of accretion disks in low and intermediate mass stars (Hillenbrand et al., 1998; Muzerolle et al., 1998a; Rhode et al., 2001). These lines show broad and narrow components; and the broad components, produced in the magnetosphere of the stars (Muzerolle et al., 1998a), are found in highly veiled (and thus, accreting) stars (Muzerolle et al., 1998a; Hillenbrand et al., 1998). The CaII triplet lines are good indicators of accretion except in case of weakly accreting CTTS (Muzerolle et al., 1998a). They have been used in combination with $\Delta(I-K)$ in order to clarify the limiting region where there is an overlap between CTTS and WTTS (see below), although it was found that even this combination is unable to detect all the accretion disks (Hillenbrand et al., 1998).

Comparing the values from Hillenbrand et al. (1998) used in Rhode et al. (2001) for classifying CTTS and WTTS with our measurements of Hα equivalent widths, we see that, although there is a common trend, there is considerably overlap, even for some of the strongest Hα values (Figure 6.13). Although the result of combining CaII measurements and $\Delta(I-K)$ leads to a fairly efficient accretion disk detection, it leaves some of the CTTS (mainly, the not so strong accretors) undetected, which the study of Hα can reveal.

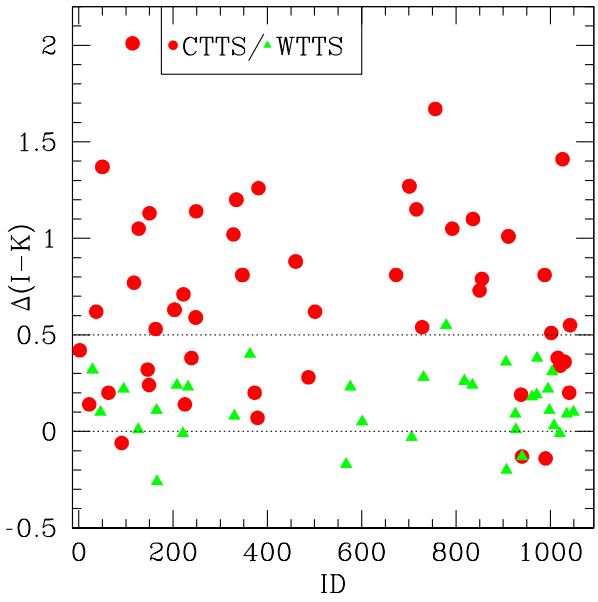

Figure 6.11 Values of the $\Delta(I-K)$ index for CTTS and WTTS. CTTS are denoted by black circles, WTTS are represented by open circles. We explore the accuracy of $\Delta(I-K)$ index as studied in Rhode et al. (2001). Dotted lines represent the limits they discuss (most of the CTTS have $\Delta(I-K)>0$; they define $\Delta(I-K)>0.5$ as a secure limit over which all objects are CTTS). Here we see that the intermediate zone of $0<\Delta(I-K)<0.5$ contains about 2/3 of WTTS and 1/3 of CTTS, which are not differentiated in Rhode et al. (2001). Although this index seems to be accurate for the detection of CTTS over the limit of $\Delta(I-K)=0.5$, it becomes quite unclear under this limit.

6.3.3 Rotational Velocities of CTTS and WTTS: Disk Locking and Angular Momentum Evolution?

Another long standing question about young stars is related to the evolution of their angular momentum. Young stars are rapid rotators (Hartmann, 1998), and usually they show rotational periods of days (Mandel & Herbst, 1991; Attridge & Herbst, 1992; Choi & Herbst, 1996; Stassun et al., 1999; Herbst et al., 2000). Several models postulate that accreting stars may be locked to their disks via their strong magnetic fields channeling the accretion (Shu et al., 1994; Hartmann, 2002). This would result in slower rotation velocities for CTTS, compared to WTTS, which have no inner disks, and some observations suggested that differences up to a factor of two could be found in rotational velocities of CTTS versus WTTS in Taurus (Edwards et al., 1993). But the final answer remains unclear, since several other studies have so far found no significant variations between rotational velocities of CTTS and WTTS in the ONC (Stassun et al., 1999; Rhode et al., 2001). Since the classification of stars as CTTS or WTTS can be a problem, here we use our classification.

We examined only those stars classified as certain CTTS and certain WTTS, to study the distribution of rotational velocities in each class. We use both the rotational velocities provided in the literature (Rhode et al., 2001) and the rotational velocities that we obtained using the Hectochelle spectra. Our CTTS versus WTTS classification is different from that of Rhode et al. (2001), so our analysis using the rotational velocities given in Rhode et al. (2001)

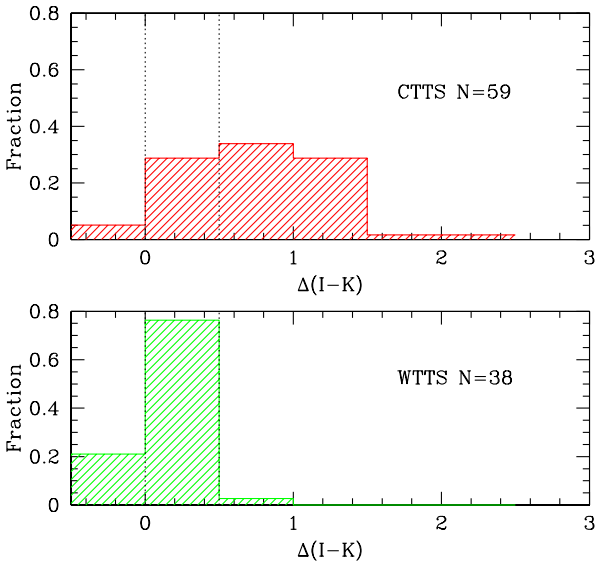

Figure 6.12 $\Delta(I-K)$ histograms for CTTS and WTTS. Only the stars classified as CTTS or WTTS for sure are used in the plot. This histogram shows as well that $\Delta(I-K)$ becomes ambiguous when used to distinguish WTTS from CTTS.

suggests a different result (Figure 6.14). We performed a 2-sided KS test, finding significant difference between the two distributions (confidence level 0.004).

This seems to be due to the fact that in Rhode et al. (2001) some of the stars claimed to be WTTS were in fact CTTS, since using near-IR indices for classification can lead to a very important (up to 30%) contamination of CTTS in the assumed WTTS region (see overlap in Figure 6.11). We repeated the test using the velocities available for the 2004 sample (see Figure 6.15) finding a similar result to that of 2003 (KS test gives a 0.03 probability that the two distributions come from the same sample).

The classical accreting stars have rotational velocities that are in general lower than the WTTS velocities, since the WTTS show a long tail in the region toward higher velocities that is only scarcely populated by the CTTS. Although many WTTS do show small rotational velocities similar to these of the CTTS, our results suggest some differences in the evolution of the angular momentum in CTTS and WTTS. These results are in agreement with the studies by Choi & Herbst (1996) and Herbst et al. (2002), in which significant differences in the rotational periods of CTTS and WTTS suggest the importance of disk locking. Nevertheless, further analysis is necessary to confirm this result.

6.3.4 High Resolution Spectra of Proplyds in ONC: Photoevaporating Accreting Objects

The presence of photoevaporating objects visible in the bright HII region in the ONC had been established clearly, based on HST observations (Bally et al., 1998, 2000; O'Dell & Wen, 1994; O'Dell & Wong, 1996; Johnstone et al., 1998) and Keck high resolution spectroscopy (Henney & O'Dell, 1999). The disks of young stars close to very massive O-type stars (as the ONC Trapezium central stars) can be photoevaporated due to the far and extreme UV

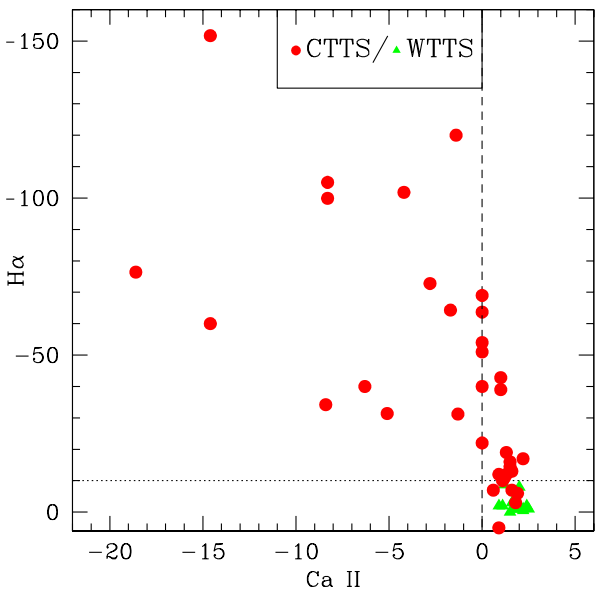

Figure 6.13 Comparison of the EW of Hα against the CaII index Rhode et al. (2001). Symbols are as in Figure 6.11. Both Hα EW and the CaII index are used to distinguish accreting from non accreting stars, but Hα avoids the uncertainty in the limiting cases. CaII is taken from Rhode et al. (2001). Note that positive values of Hα EW and the CaII index correspond to earlier stars, which usually show these lines in absorption and, in the case of young pre-Main Sequence stars, the absorption is partially filled by the chromospheric and/or accretion emission (Hartmann, 1998).

radiation from the massive star. The evaporation of the disk produces an irregular extended shape, usually defined as a cometary shape, with the tail pointing away from the O star (Bally et al., 1998; O'Dell & Wong, 1996). We have identified 7 proplyds among the objects of the run in 2003, and 8 in the run of 2004. These are:

064-705: Classified by O'Dell & Wong (1996) as a circular semistellar object, referred as well by Hillenbrand (1997) as a K6 type proplyd. It is a CTTS with a blue-shifted wind, and with clear Li 6707 Å. The wind is indicative of very active accretion (Edwards et al., 1994), and we can corroborate the presence of a very remarkable accretion disk from its 2MASS colors, since this star shows a very important near-IR excess consistent with the CTTS locus (Meyer et al., 1997).

4596-400: Classified by O'Dell & Wong (1996) as an object with a round head plus a tail, referred as well by Hillenbrand (1997) as a M4 type proplyd. Our Hα classification labels it as a possible WTTS. Li is not well detected due to low signal-to-noise. The weak Hα could be due to a poor signal-to-noise because the object is very faint for the exposure time of the spectra, low mass accretion rate, or it could also suggest that the evaporating disk shows an inner hole and has already ceased accretion processes. Hillenbrand et al. (1998) noticed that some of the objects classified as proplyds by O'Dell & Wong (1996) did not show near-IR excess, which could be as well indicative of the presence of an inner hole; the 2MASS colors are consistent as well with the lack of an at least detectable disk.

106-156: Classified by O'Dell & Wong (1996) as a circular object, present in Hillenbrand

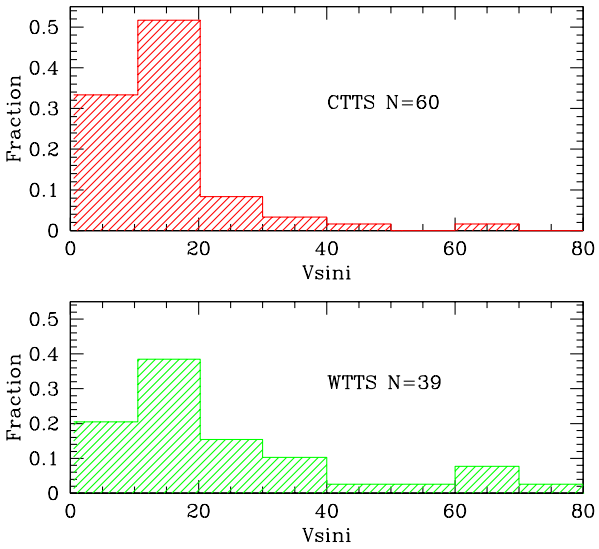

Figure 6.14 Rotational velocity distribution of CTTS and WTTS. We compare the rotational velocities in Rhode et al. (2001) for CTTS and WTTS, using their velocity values with our CTTS/WTTS classification based on Hα. We differ from the result stated there, since some differences are observed (i.e., the presence of a tail toward larger velocities for WTTS, which is scarcely populated by CTTS) as a result of the presence of an accretion disk. The two-sided KS test gives a probability of 0.4% for the two samples coming from the same distribution.

(1997) list as a K3-K7 proplyd. Shows strong Hα emission characterizing a CTTS, and Li absorption. Li absorption is particularly broad, which has been referred as a characteristic of proplyds by Henney & O'Dell (1999). Its 2MASS colors are consistent with the presence of an accretion disk.

205-330: Classified by O'Dell & Wong (1996) as an elongated and diffused object, described in Hillenbrand (1997) as a M0 proplyd. It shows strong Hα emission, and Li absorption, but no 2MASS counterpart was found.

184-427: Referred by O'Dell & Wen (1994) & O'Dell & Wong (1996) as an elongated, diffused irregular object. More references are given in Bally et al. (1998) and Hillenbrand (1997), and its spectral type is M2.5. We detect strong Hα of a CTTS. Li was not detectable in this faint star.

242-519: Described by O'Dell & Wong (1996) as a round object plus a tail, referred by Hillenbrand (1997) and classified as a K4-K5 star. We detect strong Hα that characterizes it as a classical T Tauri, but we cannot infer the presence of a disk from the 2MASS colors, rather consistent on the other side with some error in the spectral type and/or extinction. Li absorption is detected as well.

224-728: Described by O'Dell & Wong (1996) as a round object plus a tail, referred by Hillenbrand (1997) as a M4.5 star. We are able to detect strong Hα typical of a CTTS, but again Li absorption is not detectable for this very faint star. Nevertheless, the presence of an accretion disk stands clear from the 2MASS photometry, consistent with a very strong near-IR excess within the CTTS locus.

143-425: Described by O'Dell & Wen (1994) as an object with a round head, and by

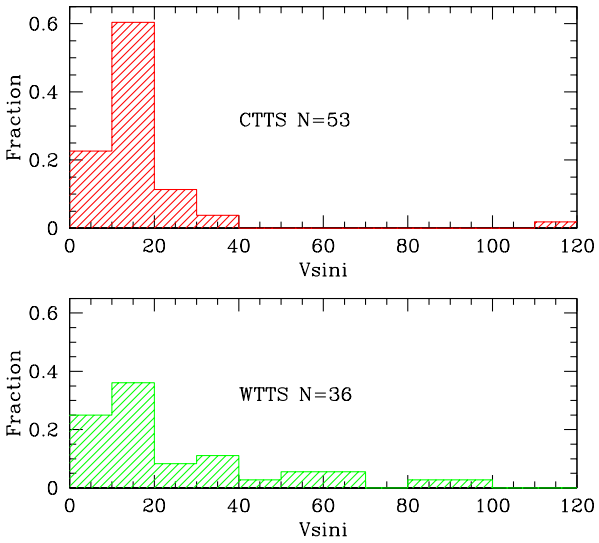

Figure 6.15 Rotational velocity distribution of CTTS and WTTS. The comparison of the rotational velocities of CTTS and WTTS using the velocities and classification inferred from Hectochelle spectra yields the same result than in Figure 6.14. The tail of the WTTS distribution toward larger velocities is present here as well, and although a substantial part of the WTTS population shows velocities similar to the CTTS ones, this tail is suggestive of some differences in the angular momentum evolution. The KS-test gives here a 3% probability for the two samples coming from the same distribution.

O'Dell & Wong (1996) as a round head plus tail. Hillenbrand (1997) classifies it as a K7 star, and according to its Hα, it is most likely a CTTS. No excess is detected in the 2MASS colors.

106-156: Cited by O'Dell & Wong (1996) to be a circularly symmetric proplyd, and it has a K3-K7 spectral type (Hillenbrand, 1997). It shows very strong Hα with a P-Cygni profile, and 2MASS excess consistent with the CTTS locus.

140-1952: Cited by O'Dell & Wong (1996) as a circularly symmetric object. Hillenbrand (1997) gives a late-G spectral type, and our observations reveal a CTTS showing inverse P-Cygni profile in Hα.

128-044: Described by O'Dell & Wong (1996) as a circularly symmetric object. The spectral type in Hillenbrand (1997) is M1, and we find very strong Hα emission, characteristic of a CTTS, with P-Cygni profile.

171-334: Described by O'Dell & Wen (1994) & O'Dell & Wong (1996) as a circularly symmetric object. According to Hillenbrand (1997), its spectral type is K0-K2, and our observations classify it as a CTTS, which is supported by the presence of an important 2MASS excess, consistent with the CTTS locus.

191-350: Classified by O'Dell & Wong (1996) as an irregular object. Hillenbrand (1997) gives a spectral type G8-K2, and our Hα spectra does not allow us to classify it as CTTS or WTTS.

218-324: Classified by O'Dell & Wong (1996) as an elongated object with a well-defined boundary. Hillenbrand (1997) gives a K3 spectral type, and its Hectochelle spectrum suggest it to be most likely a CTTS.

224-728: Described by O'Dell & Wong (1996) as an object with round head plus tail. Its

Table 6.1. Characteristics of the Proplyds in our sample

HST ID	Comments
064-705	blue-shifted wind, Li, CTTS locus
4596-400	no strong Hα nor near-IR excess
106-156	strong Hα, broad Li absorption, CTTS locus
205-330	strong Hα, Li absorption, no 2MASS counterpart found
184-427	strong Hα
242-519	strong Hα, Li absorption, no near-IR excess
224-728	strong Hα, CTTS locus
143-425	possible CTTS, no near-IR excess
106-156	very strong Hα with P-Cygni profile, CTTS locus
140-1952	strong Hα with inverse P-Cygni profile
128-044	very strong Hα with P-Cygni profile
171-334	strong near-IR excess, CTTS locus
191-350	Hα classification uncertain, CTTS or WTTS?
218-324	most likely CTTS
224-728	Hα classification uncertain, CTTS or WTTS?

Note. — Proplyds presented in our sample (according to the classification in O'Dell & Wen 1994 and in O'Dell & Wong 1996), and their characteristics derived from the Hectochelle spectra and 2MASS near-IR colors.

spectral type is M0.5, according to Hillenbrand (1997), and the classification according to Hα is uncertain, not showing any 2MASS excess.

One additional remark that we find in the seven proplyds from the 2003 run is that they all show very strong He 5876 Å emission line. The strength of the He 5876 Å line seems to be correlated with the nebular emission, being particularly strong in the cluster center, where all these proplyds are. These results are summarized in Table 6.1.

6.4 Summary and Conclusions

We presented the results of the first high-resolution spectra taken with the Hectochelle spectrograph during two engineering observing runs in December 2003 and March 2004. We obtained a set of 237 good signal to noise spectra of a sample of stars in the ONC, containing both previously studied cluster members (Hillenbrand, 1997) and additional stars from the 2MASS catalog. These spectra enabled us to identify accreting T Tauri stars using Hα profiles, complementing or improving upon other methods for detecting accretion. Despite the limitations in the available sky spectra, we were able to distinguish the presence of a broad Hα component and to subtract the narrow nebular background emission from the spectra with broad Hα. From the measurement of Hα lines, we find that approximately 65% of stars in ONC (within limits 40%-80%) are active accretors, consistent with the results of Hillenbrand et al. (1998). We also found 15 new members taken from the 2MASS catalog, 8 of them from the Li 6707 Å absorption line, and 7 from their strong Hα emission.

We obtained radial velocities for a subset of 79 stars, finding that the radial velocity dispersion is $\sim 1.8\,\mathrm{km\,s^{-1}}$ or smaller for the bright population. This is consistent with former studies of dispersion in proper motion for the ONC (Jones & Walker, 1988; Van Altena et al., 1988).

With our more accurate distinction between CTTS and WTTS, we have revisited the issue about differences in rotational velocities between CTTS and WTTS. Using the rotational velocities calculated by Rhode et al. (2001), and the Hα classification, and using the velocities calculated from the set of 2004 spectra, we made a KS test comparing the distribution of rotational velocities for the CTTS and WTTS, finding that there are important differences in the rotational properties of accreting and non-accreting stars. This could suggest disk locking reducing the velocities of the CTTS (Shu et al., 1994; Hartmann, 2002) and agrees with previous results in ONC (Choi & Herbst, 1996; Herbst et al., 2002).

This work, although based in a very limited data, shows the power of Hectochelle for the study of young clusters, both for the identification of young accreting and non accreting stars in different stages of their evolution, and for the studies of cluster kinematics and structure. Hectochelle spectra could be used in the future in order to settle down the remaining open questions about accretion in Tr 37 and NGC 7160, examining whether the "transition objects" are or not accreting. Stopping accretion while part of the disk remains around the star would be a clear indication of the formation of larger bodies in the inner disk. Moreover, Hectochelle could contribute as well to the study of the rotational velocities of the older CTTS and WTTS in Cep OB2, which would fill a gap in the history of angular momentum evolution.

6.5 Data Tables

Table 6.2. Results from 2003 December

JW	2MASS	Sp.Type	Type	EW(Li 6707 Å)	EW(Hα)	Comment
5	05342924-0523567	K1	W	0.38	—	fast:
11	05342999-0525173	M6-M6.5	C:	—	—	—
18	05343168-0528269	M2	C:	1.13:	-14	nIR
24	05343367-0514361	M1	W	0.44	—	(2004)
26	05343382-0527181	M6	—	—	—	lS/N
29	05343514-0532103	K2	W	0.41	—	fast:,(2004)
37	05343746-0534519	K2-K5	C	0.50	-34	PC,nIR
45	05343976-0524254	K4	W	0.52	—	—
46	05343988-0526420	K1	W	0.37	—	—
50	05344086-0522423	K1	C	0.17	-54	PC,very bHe,nIR,(2004)
60	05344241-0512186	K0-K1	W	0.43	-1	(2004)
62	05344286-0525163	early-K	W	—	-42	—
63	05344295-0520069	K6	W	0.59	—	(2004)
64	05344360-0518276	F1	W	—	—	—
74	05344518-0510476	M3	C	0.25	-62	(2004)
91	05344789-0530465	M4	C:	0.72	-32	(2004)
102	05344896-0528168	M3.5	C	—	—	nIR
106	05344929-0518555	M3	W:	0.71	—	(2004)
114	05345050-0523353	M1e	C	0.68:	-12	nIR
115	05345046-0532538	M5.5	—	—	-86	lS/N
118	05345099-0517565	M5.5	C:	—	—	—
122	05345143-0513295	M5	C:	—	-40	—
124	05345180-0521389	M3.5	W:	—	—	—
126	05345226-0512032	M3	W	0.63	—	—
127	05345203-0524429	M3.5e	C	0.38	-43	PC,nIR
133	05345259-0524037	M1.5	W:	0.51	—	—
145	05345411-0522265	M5.3	W:	—	—	—
149	05345464-0528182	M3	C	—	—	nIR
150	05345494-0517017	K4-K6	C	0.49	-28	nIR
158	05345597-0529264	M1.5	—	—	—	lS/N
162	05345636-0533404	M5-M6	C:	—	—	—
166	05345640-0538052	M5	W	0.73	—	—
168	05345675-0526372	M5.5	W:	—	—	—
170	05345719-0508238	late-G/early-K	W:	—	—	(2004)
177	05345802-0517376	M0	C	0.64	—	—
185	05345869-0512261	M5.5	C:	—	-12	IPC
191	05345955-0524002	M4-M2.5	W:	0.84	—	4596-400,nIR
194	05350039-0509441	M5.5	—	—	-10	lS/N
198	05350046-0525143	K6	C	0.45	-34	064-705,nIR
203	05350082-0538079	M0	C	0.40	-46	(2004),nIR
208	05350129-0520168	M2.5	W	0.57	—	—
211	05350148-0528207	M2.5	C:	0.68	-13	—
222	05350218-0529098	M2	C	1.60:	—	—
232	05350299-0530015	K1-K2	W:	0.49	—	(2004)
245	05350419-0526278	M2	C	0.95	—	IPC,nIR
248	05350437-0523138	M0.5-M2	C	0.55	—	IPC,nIR,(2004)
249	05350450-0523565	K2	C	0.41	—	IPC:
257	05350481-0522387	M4.5	C	—	—	—
273	05350563-0525195	K0	C	0.36	-30	IPC,nIR
295	05350644-0533351	M0.5	C	0.29	-91	PC,very bHe
301	05350753-0511145	—	C	0.48:	-30	—
321	05350822-0537047	MO	C	0.35	-34	bHe,nIR,(2004)
323	05350853-0525179	M2	C	0.80	—	IPC:
327	05350904-0520172	M4	W:	—	—	—
334	05350959-0528228	M1	C	0.31	—	nIR,(2004)
335	05350965-0526233	M1	C:	—	—	—
337	—	K8	W:	0.52	—	—

Table 6.2 (continued)

JW	2MASS	Sp.Type	Type	EW(Li 6707 Å)	EW(Hα)	Comment
347	05351058-0521562	K3-K7	C	0.45	—	106-156,nIR,(2004)
362	05351112-0534596	M4.5	W:	—	—	—
365	05351149-0526023	K2-K3	W:	0.50	—	(2004)
373	05351197-0520331	K2-K3	C	0.50	—	—
379	05351216-0530201	M5.4	C	—	—	bHe,nIR
388	05351281-0515240	K5	W:	0.66	—	(2004)
417	—	M0.5	C:	0.30	—	—
432	—	M3.1	W:	0.20	—	—
449	05351444-0533190	K5	C	—	—	nIR
460	05351467-0539108	K0-K3	C	0.36	-6	PC,nIR,(2004)
486	05351569-0528155	M4.5	W:	—	—	—
504b	05351606-0520363	K2-K4	C	0.34	—	—
527	—	M0.5	C:	0.55	—	—
567	05351794-0522454	late-G	W	0.44	—	—
608	05351913-0520387	A5	W	—	—	—
636	05352004-0525375	M0.3	C:	0.40	—	nIR
648a	—	M0	C	0.40	—	205-330
654	05352032-0536394	M5	C:	—	—	—
695	05352172-0526443	M2.8	C:	—	—	nIR
701	05352169-0534468	G8-K0	C	0.29	-100	very bHe,nIR,(2004)
706	05352226-0520292	K3	W	0.50	—	(2004)
716	05352237-0527283	M4.5	C	—	—	224-728
747	05352382-0530474	K0	W	0.38	—	—
750	05352425-0525186	K4-K5	C	0.38	—	242-519
753	05352424-0529571	M2	C	0.81	-23	nIR,(2004)
756	05352443-0524398	M0	C	0.25:	—	nIR,(2004)
779	05352573-0509494	K0	W	0.38	—	(2004)
792	05352600-0525477	K8	C	0.65:	—	—
804	05352698-0513145	G3	W:	—	—	—
815	05352749-0527259	M3	C:	0.58:	—	—
818	05352750-0535194	K8	W	0.56	—	(2004)
835	05352889-0535067	M3	W	0.82	—	—
836	05352909-0529103	M0	C	0.56	-26	—
839	05352958-0524568	M1	W	0.57	—	—
840	05352989-0512103	M5	C:	—	-30	—
842	05353009-0509094	M5.6	—	—	—	lS/N
860	05353066-0527167	M3.5	C:	0.98:	—	—
906	05353468-0534380	M3	W	0.58:	—	—
911	—	K4	C	0.59	-34	(2004)
912	05353522-0526550	M3	C:	0.89	—	—
927	05353679-0537464	M4	W	0.91	—	—
929	05353761-0519441	M5.5	—	—	—	lS/N
937	05353872-0516591	M6	C:	0.40:	—	—
938	05353885-0512419	K2	C	0.50	-12	IPC,(2004)
940	05353907-0508564	M2	C	0.56	-8	(2004)
942	05353907-0520257	M3	W:	—	—	—
960	05354229-0515079	M0.5	C:	—	-68	PC:
964	05354261-0526083	M5.5	C:	—	-28	nIR
967	—	F8	—	—	—	lS/N
968	05354324-0509171	K5	C	—	-5	IPC,(2004)
972	05354339-0532441	M1	W	0.70	-5	nIR,(2004)
973	05354359-0532118	M5	C:	—	—	IPC,nIR
980	05354484-0524344	M4	C	—	-26	(2004)
981	05354542-0520368	M0	C:	0.86	—	(2004)
982	05354537-0528107	M1	C	0.45	-46	bHe,nIR,(2004)
988	05354624-0515398	M2	C	—	-115	—
990	05354661-0522243	M4.5	C	—	—	—

Table 6.2 (continued)

JW	2MASS	Sp.Type	Type	EW(Li 6707 Å)	EW(Hα)	Comment
999	05354779-0510307	K2	C:	0.43	—	—
1002	05354764-0537388	M6	C	—	-80	PC
1011	05355011-0510294	M5	—	—	—	lS/N
1013	05355018-0521169	M3	—	—	—	lS/N
1016	05355077-0516291	K5	C	0.51	-11	IPC,(2004)
1017	05355105-0515090	K7	W	0.57	—	—
1026a	05355433-0526444	M0.5	C	0.54	-29	PC,nIR
1030	05355462-0527075	M2	C	0.65	-13	PC,(2004)
1032	05355498-0522355	M5.5	C:	—	—	—
1036	05355676-0519579	M6	C	—	-89	—
1037	05355672-0525263	K5	W	—	—	—
1042	05355894-0532538	M5.5	C	—	-51	—
1044	05355948-0537096	M4.5	—	—	—	lS/N
1046	05360055-0523298	K7	W	—	—	(2004)
3020	05342386-0515403	M0.5	W:	0.91:	—	—
3024	05341493-0515496	M1	W	0.62:	—	(2004)
3109	05342616-0526304	K2-K3	C	0.38	-82	IPC,bHe,nIR,(2004)
3118	05341447-0528168	G6-K0	W	0.35	—	—
3151	05341800-0533333	M1	C:	0.76	—	(2004)
3166	05350926-0516555	M2	C:	—	-96	bHe
5020	05361975-0514386	M1.5	—	—	—	lS/N,nIR
5022	05362890-0514434	M4.5	C	1.10	-20	—
5087	05360868-0521021	M4	—	—	—	lS/N
5093	05362838-0521421	—	—	—	—	lS/N
5116	05361459-0525498	M0	W:	—	—	(2004)
5146	05362753-0530555	M2.5	C:	0.59	-15	(2004)
5170	05362437-0534501	—	—	—	—	lS/N,nIR
9048	—	M3	W:	—	—	—
9124	—	M4	W:	—	—	—
9132	—	M3.5	C:	—	—	—
9224	—	M2.5	C	—	—	184-427
9316	05352411-0521556	M4.5	C:	—	—	—
—	05344751-0546300	—	W:	0.63	-8	new
—	05344587-0541097	—	C	0.60:	-73	new
—	05343856-0547350	—	W	0.70:	-2	—
—	05334545-0536323	—	C	—	—	nIR,new
—	05334765-0525485	—	C:	—	—	new:
—	05334668-0523256	—	C	—	-192	nIR,new
—	05334167-0524042	—	C:	0.63	-29	IPC,nIR,new
—	05333809-0514231	—	C:	—	—	new:
—	05334896-0517531	—	W	0.73	—	new
—	05334822-0513262	—	C	—	-84	nIR,new
—	05333571-0509235	—	C:	—	—	new:
—	05340358-0501568	—	—	—	—	lS/N
—	05341749-0510357	—	—	—	—	lS/N,nIR
—	05335414-0503401	—	—	—	—	lS/N
—	05342159-0510139	—	W	—	—	—
—	05350312-0509170	—	C:	—	—	nIR ,new:
—	05350333-0456430	—	C	0.66	-12	nIR,new
—	05350567-0458538	—	W:	0.54	—	—
—	05350945-0457117	—	C	—	-102	nIR,new
—	05351564-0457137	—	—	—	—	lS/N,nIR
—	05354885-0500285	—	C	—	-6	new
—	05353657-0504393	—	—	—	—	lS/N
—	05355506-0502372	—	—	—	—	lS/N
—	05364005-0512231	—	C:	—	-6	nIR,new:
—	05370321-0521361	—	—	—	—	lS/N,nIR

Table 6.2 (continued)

JW	2MASS	Sp.Type	Type	EW(Li 6707 Å)	EW(Hα)	Comment
—	05364605-0519013	—	—	—	—	lS/N,nIR
—	05365424-0532183	—	—	—	—	lS/N
—	05364760-0536312	—	C	0.62	-16	new
—	05363971-0540267	—	—	—	—	lS/N
—	05363813-0537102	—	—	—	—	lS/N,nIR
—	05355751-0539513	—	—	—	—	lS/N
—	05361703-0543144	—	—	—	—	lS/N
—	05362423-0544486	—	C	0.49	—	new
—	05355690-0545191	—	C	—	-43	IPC,nIR ,new
—	05360499-0548004	—	—	—	—	lS/N,nIR
—	05352281-0544428	—	W:	—	-10	—
—	05352617-0545084	—	C:	0.52	—	nIR,new
—	05351903-0546163	—	W	0.39	—	—
—	05351192-0545379	—	W	0.41	—	nIR,new

Note. — JW= Jones & Walker (1988) number if < 2000, otherwise from Hillenbrand (1997) and subsequent updates to electronically-available table; 2MASS identification number; type, C=CTTS, W=WTTS (see text); Hα EW in Å; Lithium 6707 Å EW in Å; spectral types from Hillenbrand et al. (1998); comments: Proplyds named using their HST ID number as given in Hillenbrand et al. (1998); Bally et al. (1998). Winds (denoted PC, or P-Cygni profiles) and infall (denoted IPC, or inverse P-Cygni profiles) detected by asymmetries in Hα profile. Broad or very broad He (written as bHe or very bHe) refers to the detection of the broad component of the He emission line at 5876Å. Low signal-to-noise spectra are marked with the label lS/N. Colons have been added to uncertain values. Stars with near-IR excess in 2MASS are labeled as nIR. An additional comment has been included to distinguish stars with systematically broad lines as possible fast rotators. The label "(2004)" indicate stars that were observed again in March 2004, which have the additional information corresponding to the 2004 run in Table 6.3.

Table 6.3. Results from March 2004

JW	2MASS	cz ($\mathrm{km\,s^{-1}}$)	R	v_r ($\mathrm{km\,s^{-1}}$)	Type	EW(Hα)	Sp. type	Comment
2	05342852-0524578	22.8 ± 0.2	23.0	5.4 ± 1.0	C	-8	K5Ve(D)	IPC,nIR
16	05343151-0512300	22.7 ± 0.2	24.0	—	W	—	G8-K2	—
22	05343266-0521074	25.4 ± 0.6	10.3	11.0 ± 1.3	C	-17	M1.5	IPC
23	05343359-0523099	32.7 ± 0.2	21.4	—	W:	—	G7V(S)	NM
24	05343367-0514361	25.2 ± 0.4	14.4	5.8 ± 1.5	W	-3	M1	—
29	05343514-0532103	28.5 ± 1.3	9.5	25.1 ± 1.6	W	—	K2IV(D)	—
50	05344086-0522423	29.7 ± 0.9	8.1	13.3 ± 1.9	C	-60	K1e	PC,SB2,nIR
60	05344241-0512186	26.7 ± 1.4	11.3	30.3 ± 1.5	W	-1	K0-1	—
61	05344273-0528375	21.6 ± 3.1	3.3	23.8 ± 3.9	C	—	—	NM,nIR
63	05344295-0520069	24.6 ± 0.8	13.8	22.1 ± 1.0	C	-6	K6	PC
65	05344340-0530070	24.4 ± 0.5	14.9	14.2 ± 1.1	W:	—	M0	—
72	05344437-0532187	8.5 ± 0.5	10.0	—	W	—	—	—
74	05344518-0510476	28.1 ± 1.2	4.4	8.8 ± 4.7	C	-94	M3e	PC
77	05344590-0524558	29.5 ± 3.5	6.2	41.8 ± 4.5	W:	—	M0	—
80	05344662-0510405	32.2 ± 0.8	6.1	5.4 ± 3.2	early	2	K2	NM
”	—	-14.4 ± 2	—	—	—	—	K2	—
81	05344639-0524318	24.6 ± 0.9	12.3	21.4 ± 1.1	W:	—	M0	—
82	05344629-0539077	25.1 ± 0.6	12.1	11.5 ± 1.2	C	-29	—	PC,nIR
91	05344789-0530465	25.0 ± 0.5	10.4	5.0 ± 2.0	C	-11	M4	—
95	05344830-0537228	24.5 ± 4.4	5.9	52.2 ± 7.0	W	—	K8	—
106	05344929-0518555	23.6 ± 1.7	6.3	22.6 ± 2.1	?	—	M3	—
111	05345049-0511105	26.8 ± 0.3	18.2	5.8 ± 1.2	W:	-3:	K8	—
113	05345044-0520203	21.8 ± 0.7	12.4	17.2 ± 1.1	C	-41	K6e	nIR
117	05345073-0527010	23.5 ± 0.4	16.9	7.7 ± 1.4	C	-40	M0e	nIR
128	05345216-0522319	24.2 ± 0.5	13.1	8.5 ± 1.8	?	—	M2.5	—
146	05345424-0521353	27.7 ± 0.7	8.6	9.2 ± 2.7	C	-22:	M2	—
163	05345681-0511330	21.3 ± 0.4	16.7	12.9 ± 0.9	C	-7	K5	IPC
165	05345648-0531361	29.6 ± 0.4	16.9	13.3 ± 0.9	W	-4	A7(?)	—
170	05345719-0508238	46.0 ± 8.0	1.9	—	early	3.6	lateG/earlyK	NM
176	05345776-0523522	25.6 ± 0.4	18.4	11.5 ± 0.8	C:	-9	K8	nIR
192	05345962-0525399	25.2 ± 0.6	12.0	12.1 ± 1.2	C	-25	M2	IPC,nIR
203	05350082-0538079	24.0 ± 1.0	7.0	13.7 ± 2.1	C	-39	MO	PC,nIR
204	05350142-0509326	30.8 ± 1.0	8.3	16.1 ± 1.5	W	-6	M1.5	—
220	05350208-0526362	30.0 ± 1.2	10.7	24.4 ± 1.4	C:	-4:	M1.5	nIR
221	05350238-0515479	23.5 ± 4.3	6.3	62.7 ± 6.9	W	0	K3	—
223a	05350243-0520465	25.7 ± 0.6	14.1	16.2 ± 1.0	?	—	K5	—
225	05350249-0533099	23.6 ± 2.5	5.0	26.5 ± 3.0	C	—	M1.5	IPC,nIR
232	05350299-0530015	25.1 ± 1.4	10.9	28.3 ± 1.6	W	-1:	K1-2(Sam)	—
239	05350392-0529033	-16.1 ± 1.0	10.0	19.7 ± 1.5	C	-13:	M1.5	nIR
”	—	94.1 ± 2	—	—	—	—	M1.5	—
248	05350437-0523138	25.1 ± 0.7	13.2	16.9 ± 1.0	C	—	M0.5-M2e	nIR
258	05350475-0526380	25.2 ± 0.5	14.4	10.4 ± 1.0	C	-20	M0.5	—
275a	05350568-0525058	14.4 ± 6.7	3.3	49.1 ± 8.6	?	—	M2	—
278	05350572-0524184	25.5 ± 0.8	8.4	11.0 ± 1.6	C	-59	K2-K7e	PC,nIR
291	05350651-0524414	19.4 ± 0.5	13.3	12.3 ± 1.1	?	—	M1	—
321	05350822-0537047	26.1 ± 0.8	8.5	12.5 ± 1.7	C	—	MOe	nIR
328	05350885-0531491	29.3 ± 1.3	4.8	12.3 ± 2.8	C	-54	K4	PC,nIR
330	05350905-0529591	25.3 ± 1.2	10.8	26.1 ± 1.5	W	-1	K1-K4	—
334	05350959-0528228	28.6 ± 2.4	4.4	27.6 ± 2.9	C	—	M1e	PC,nIR
343	05351031-0521130	25.6 ± 1.0	6.8	12.9 ± 2.1	?	—	K7	—
347	05351058-0521562	27.7 ± 0.4	17.5	10.0 ± 0.8	C	-40	K3-7	106-156,PC,nIR
363	05351113-0536511	-31.0 ± 1.9	4.7	—	W	-2:	M2	—
365	05351149-0526023	12.0 ± 3.7	6.3	67.6 ± 5.8	?	—	K2-3(Sam)	—
375	05351188-0531552	25.3 ± 0.7	13.7	18.4 ± 1.1	?	—	M0.5	nIR
378ab	05351227-0523479	26.5 ± 0.4	15.9	10.4 ± 0.9	?	—	K1/-	—
381	05351220-0530329	25.2 ± 0.7	11.5	15.9 ± 1.2	C	-51	M0.5	nIR
388	05351281-0515240	26.7 ± 0.4	17.7	13.1 ± 0.9	W:	—	K5	—

Table 6.3 (continued)

JW	2MASS	cz ($\mathrm{km\,s^{-1}}$)	R	v_r ($\mathrm{km\,s^{-1}}$)	Type	EW(Hα)	Sp. type	Comment
391	05351281-0520436	26.1 ± 0.7	9.1	10.6 ± 1.5	C	-90	M1e	128-044,PC
396	05351331-0509195	25.5 ± 0.5	12.2	7.3 ± 1.8	W	-4	M2.5	—
401	05351319-0524554	33.8 ± 2.6	1.1	—	—	—	K0-K2e	nIR
429	05351405-0519520	22.6 ± 0.4	18.1	10.2 ± 0.8	C	—	late-G	140-1952,IPC
437	05351427-0524246	34.7 ± 3.7	6.4	55.7 ± 5.9	C:	—	K7	143-425
456	05351494-0523392	29.3 ± 1.7	5.8	21.1 ± 2.1	?	—	K5-M2(LR)	nIR
460	05351467-0539108	22.4 ± 2.3	8.1	36.2 ± 2.5	C	-1	K0-3(P)	IPC,nIR
468	05351522-0522557	28.3 ± 1.5	4.4	12.7 ± 3.0	?	—	G6-G8	—
478	05351554-0525140	9.2 ± 3.3	6.0	43.6 ± 4.3	W:	—	M0.4(P)	—
487	05351595-0514590	26.0 ± 0.4	17.2	13.3 ± 0.9	C	-3	K6	IPC
501	05351579-0533123	24.9 ± 0.4	16.3	11.2 ± 0.9	C	-10:	M0	IPC,nIR
526ab	05351675-0524041	38.7 ± 3.9	1.4	18.6 ± 6.0	—	—	K6/-	—
538	05351705-0523341	23.0 ± 2.1	7.6	33.6 ± 2.3	C	-26:	K0-2	171-334,nIR
544	05351721-0521317	25.9 ± 4.7	6.2	84.7 ± 13.9	W:	—	K4-7	—
576	05351799-0529346	25.7 ± 2.8	6.2	35.3 ± 3.0	W	—	M1.5	—
601	05351889-0516140	22.0 ± 0.4	17.2	12.3 ± 0.9	W	-1	K3-4	nIR
607	05351906-0523495	32.4 ± 3.7	3.1	26.3 ± 4.4	?	—	G8-K2	191-350
613	05351930-0520078	22.5 ± 4.6	2.6	36.4 ± 4.9	early	—	K2(Sam)	nIR
614	05351898-0537367	27.8 ± 3.8	5.8	42.1 ± 4.8	C:	—	M1	—
641	05352016-0526390	26.3 ± 3.2	7.6	46.3 ± 4.1	?	—	midG/earlyK	—
655	05352074-0515492	30.4 ± 15.0	3.4	—	W	—	K0-5:	—
672	05352103-0528091	27.3 ± 0.6	11.6	12.9 ± 1.3	?	—	K8	—
673	05352098-0531216	26.8 ± 1.2	9.9	23.6 ± 1.5	C	-19	K5	IPC,nIR
678	05352128-0524572	24.8 ± 0.5	16.0	13.3 ± 1.0	W:	—	K1-2(Sam)	—
698	05352181-0523539	23.4 ± 3.6	6.8	50.3 ± 5.7	C:	—	K3	218-354
701	05352169-0534468	24.4 ± 0.6	11.6	10.8 ± 1.2	C	-105	G8-K0e	nIR
705	05352245-0509110	25.9 ± 0.5	16.4	16.6 ± 0.8	W	—	late-K::(H)	—
706	05352226-0520292	22.2 ± 0.4	19.3	11.7 ± 0.8	W:	—	K3(WSH)	—
709	05352219-0526373	27.4 ± 1.6	8.2	25.5 ± 1.9	?	—	M0.5	222-637
710	05352232-0524141	27.8 ± 5.7	1.9	29.3 ± 6.7	C:	—	M0.5-1.5	—
728	05352290-0532290	29.8 ± 0.4	13.5	5.8 ± 1.6	C	-12	M1	nIR
731	05352344-0510517	22.9 ± 0.5	16.4	16.4 ± 0.8	W	-1	K8	—
753	05352424-0529571	25.2 ± 0.7	9.8	11.7 ± 1.5	C	-6:	M2	nIR
756	05352443-0524398	22.7 ± 6.6	2.5	56.5 ± 10.5	?	—	M0e	nIR
766ab	05352505-0522585	26.3 ± 0.6	13.5	13.5 ± 1.2	?	—	K1-K4	nIR
779	05352573-0509494	22.3 ± 0.9	12.0	20.5 ± 1.1	?	—	K0IV-V(Par)	—
813	05352744-0526281	20.1 ± 1.7	9.4	33.9 ± 1.9	W:	—	K8	—
818	05352750-0535194	26.6 ± 0.7	13.6	17.5 ± 1.1	W	-1	K8V(D)	—
830	05352838-0525033	23.8 ± 0.7	10.5	12.5 ± 1.4	W:	—	M1.5	—
843	05352965-0531123	35.6 ± 6.7	2.1	80.0 ± 19.7	?	—	M2	—
850	05353042-0525385	25.1 ± 0.9	9.4	15.5 ± 1.3	C	—	K8e	PC,nIR
852	05353048-0524230	25.6 ± 7.1	4.1	74.4 ± 14.1	W:	—	—	—
855	05353048-0528305	21.8 ± 1.2	4.8	10.0 ± 2.5	C	-69	M2.5	PC,nIR
861	05353091-0518179	26.5 ± 4.7	3.1	34.9 ± 5.1	W:	-4:	M3.5	nIR
866	05353129-0515330	27.4 ± 1.2	11.6	27.3 ± 1.5	W:	—	K1IV(Ham)	—
867	05353126-0518559	26.2 ± 0.5	15.1	11.5 ± 1.0	C	-34	K8Ve(D)	nIR
868	05353124-0523400	23.5 ± 0.6	10.9	11.7 ± 1.3	HH	—	K3-K5	—
901	05353421-0527183	128.0 ± 0.0	0.0	—	?	—	—	—
907	05353490-0529144	22.1 ± 2.1	8.4	32.8 ± 2.2	W	—	K1-4	—
911	05353528-0521271	27.7 ± 0.4	17.5	10.2 ± 0.8	C	-62	K4(CK)	PC,nIR
923	05353644-0534111	25.4 ± 0.5	11.6	6.2 ± 1.9	C	-73	M1	—
926	05353670-0537415	24.6 ± 0.6	12.4	15.0 ± 1.0	W	-1:	K7	—
933	05353803-0528215	26.4 ± 0.6	8.6	7.3 ± 2.5	W:	—	M4	—
938	05353885-0512419	25.3 ± 0.7	14.1	18.3 ± 1.1	C:	—	K2	—
940	05353907-0508564	21.0 ± 5.9	6.1	98.6 ± 21.2	W	-1	M2II-III(?)	—
945	05354018-0517292	23.7 ± 5.6	1.7	—	early	4	B6	—
950	05354049-0527018	-2.5 ± 0.3	17.0	5.4 ± 1.3	W	—	G:	NM

Table 6.3 (continued)

JW	2MASS	cz ($km\,s^{-1}$)	R	v_r ($km\,s^{-1}$)	Type	EW(Hα)	Sp. type	Comment
961	05354276-0511547	33.3 ± 5.1	6.2	84.1 ± 15.0	W	-3	K6-7	SB2
968	05354324-0509171	27.2 ± 5.9	5.6	110.0 ± 0.0	C	-4	K5Ve(W)	—
971	05354322-0536274	29.9 ± 3.4	6.8	46.9 ± 4.3	W	-2	K6-8	nIR
972	05354339-0532441	27.4 ± 0.5	13.0	11.7 ± 1.1	W:	-4	M1	nIR
980	05354484-0524344	32.1 ± 2.4	2.3	13.7 ± 5.0	C	-24	M4	—
981	05354542-0520368	21.3 ± 6.1	5.0	64.0 ± 9.6	W	—	M0	—
982	05354537-0528107	26.2 ± 0.7	9.5	11.0 ± 1.4	C	-72:	M1e	nIR
992	05354700-0517569	32.4 ± 0.2	32.2	5.0 ± 0.7	W	1	K3-M0I	NM
994	05354741-0510284	27.0 ± 0.4	16.2	7.3 ± 1.4	C	-36	K5-7	nIR
995	05354739-0513185	26.0 ± 0.3	16.7	6.2 ± 1.3	W	-2	M1.5	—
998	05354747-0522495	28.2 ± 0.6	12.0	11.2 ± 1.2	W	-4:	M2.5	—
1004	05354816-0531556	25.5 ± 0.4	14.2	10.0 ± 0.9	W	-8	M1	—
1008	05354949-0535263	24.5 ± 0.4	15.6	10.6 ± 0.9	W	—	M0-0.5	—
1016	05355077-0516291	25.0 ± 0.6	15.1	16.1 ± 0.9	C	-16	K5	IPC
1020	05355202-0528471	24.3 ± 0.5	16.4	14.2 ± 1.0	W	-1	K6	—
1021	05355276-0512590	29.9 ± 0.9	8.5	14.0 ± 1.8	C	-13	K5-6	nIR
1030	05355462-0527075	27.8 ± 0.5	13.5	10.0 ± 1.0	C	-16	M2	IPC
1035	05355641-0516318	18.5 ± 6.0	2.6	58.6 ± 9.8	W	-3	M3	—
1040	05355771-0523092	26.5 ± 0.9	6.8	10.6 ± 1.9	C	-7:	M3.5	—
1041	05355807-0512547	37.2 ± 0.2	26.6	—	?	1.0	G0-5(Her)	NM
1046	05360055-0523298	16.2 ± 0.3	16.6	5.4 ± 1.3	W	—	K7	—
1049	05360185-0517365	33.6 ± 0.5	11.0	6.5 ± 2.0	W	-0.5	K6-7	—
”	—	4.0 ± 2	—	—	—	—	K6-7	—
3024	05341493-0515496	29.3 ± 0.3	15.8	—	W	—	M1	—
3067	05342477-0522104	19.1 ± 0.6	8.7	—	C	-23	M1	—
3085	05342617-0524190	17.5 ± 1.3	11.5	30.5 ± 1.4	W	-1	K7	—
3109	05342616-0526304	24.3 ± 2.1	4.5	21.0 ± 2.6	C	-74	K2-3e	nIR
3126	05341289-0528482	23.8 ± 0.4	16.5	8.5 ± 1.5	C	-12	K7	—
3143	05341748-0531586	25.2 ± 0.5	9.9	—	C:	-5	—	—
3151	05341800-0533333	21.5 ± 0.4	15.9	9.6 ± 1.5	C	-10	M1	—
3156	05341320-0533535	21.8 ± 0.9	6.7	9.6 ± 3.4	C	-100	—	nIR
3158	05341853-0534002	23.3 ± 0.5	15.6	12.5 ± 1.0	W	—	M0	—
5006	05362391-0513232	12.0 ± 1.7	3.6	12.1 ± 3.5	W:	—	—	—
5017	05362346-0514209	-8.3 ± 0.3	16.3	5.0 ± 1.3	W:	—	—	—
5073	05361049-0519449	24.4 ± 0.3	19.7	9.2 ± 1.2	C	-16	K3	IPC
5082	05362130-0520141	23.1 ± 0.6	10.1	6.9 ± 2.2	W	-3	M3	—
5094	05361010-0522050	24.5 ± 1.3	4.3	10.4 ± 2.8	W	-5	M4.5	—
5116	05361459-0525498	-9.1 ± 0.3	17.3	5.0 ± 1.2	W	—	M0	—
5146	05362753-0530555	24.9 ± 0.7	8.6	10.4 ± 1.5	C	-22	M2.5	—

Note. — JW= Jones & Walker (1988) number if < 2000, otherwise from Hillenbrand (1997) and subsequent updates to electronically-available table; 2MASS identification number; cz, heliocentric radial velocity; R, signal-to-noise value of cross-correlation peak (see text); v_r, v sin i; type, C= CTTS, W= WTTS, PC= P Cygni profile, IPC= inverse P Cygni profile (see text), NM = non-member from proper motions; EW, equivalent width of Hα in Å; Sp. type, spectral type from Hillenbrand (1997) and subsequent updates to electronically-available table except where noted: (P) = Prosser & Stauffer, unpublished; (Sam)= A.E. Samuel, 1993 unpublished PhD thesis, D= Duncan (1993); S = Strand (1958); Her = Herbig, quoted in Walker (1969); LR= Luhman et al. 2000; and “e” on spectral type indicates Ca II infrared triplet emission. Colons indicate uncertain values.

7 Summary and Conclusions

The objective of this work is to study the properties of young stars and their protoplanetary disks during the ages when most disks disappear (∼3-10 Myr), probably forming planets. This work contains the first comprehensive study of ∼4 and ∼10 Myr-old clusters, with enough statistics to look at disk frequencies more reliably than before. Thanks to the larger samples and the sensitivity of the Spitzer Space Telescope, the first real evidence for general and systematic differential evolution of inner versus outer disks among ∼3-4 Myr-old systems has been found. The isochronal ages for the low-mass stars in the two clusters in Cep OB2, Tr 37 and NGC 7160, confirm the estimates from upper Main Sequence turnoffs and gas expansion in the region. The effect of photoevaporation in a ∼4 Myr-old cluster is found to be less important for the disk removal than previously assumed. Some evidence of star formation triggered by the expansion of the IC 1396 H II region in Tr 37 is found as well. Studying the high- and intermediate-mass stars, some of the youngest debris disks have been detected, setting new important constraints on how disk frequency is much lower in the high- and intermediate-mass stars than in the low-mass stars. Finally, the technique of using high-resolution spectra for distinguishing accreting and non-accreting stars in heavily nebulous regions has been demonstrated in the ONC.

In addition to the identification and characterization of young stars, a sound method for the study of other similar regions is proposed, as well as other tools that could contribute to complete the questions which remain open after this research. The main achievements of this study can be summarized as follows:

- An optical study of two young clusters in Cep OB2 Association, Tr 37 and NGC 7160, located at 900 pc (Contreras et al., 2002), conduced to the first identification of large samples of low-mass stars with average ages 4 and 10 Myr, respectively, according to the Siess et al. (2000) isochrones. Using a combination of optical photometry and spectroscopy, 165 low-mass stars were identified in Tr 37, and 55 more in NGC 7160. The estimated ages are in good agreement with the dynamical and kinematical ages (Patel et al., 1998), and place these clusters in the epoch during which accretion disks dissipate forming planets (Strom et al., 1993). Using the Hectospec multifiber spectrograph in combination with the Hydra and FAST spectrographs, the member identification reached a completeness of ∼95% for the mid-G to M1 members in the central fields in Tr 37, and about 75% in the central fields in NGC 7160, The low-mass members were identified based on Li 6707 Å absorption and Hα emission. Spectral types and individual extinctions were also derived. The average extinction and standard deviation are $A_V = 1.56 \pm 0.55$ for Tr37, and $A_V = 1.17 \pm 0.45$ for NGC7160.

- The equivalent width of Hα was used to detect accreting stars, finding that a substantial fraction (∼40%) of the cluster members in Tr 37 is accreting, whereas only 1 out of 55 low-mass stars in NGC 7160 shows indication of active accretion. This large difference

suggest strong disk evolution during the intermediate age from 4 to 10 Myr. The fact that both clusters belong to the same region and are located at the same distance reinforces the idea that this important disk evolution occurs in a timescale comparable to the age difference between the two clusters. We observed clear evidences pointing to disk evolution, comparing Tr 37 with younger clusters and associations (i.e., Taurus, ONC), and Tr 37 with NGC 7160. The disk fraction drops from ∼60-80% in younger clusters, to about 40% in Tr 37 by the age of ∼4 Myr, and to few percent at the age of ∼10 Myr in NGC 7160.

- The spatial distribution of low-mass members in Tr 37 suggests a moderate asymmetry in the CTTS distribution as well as some spatial correlation of the younger members and the proximity of dust structures to the West of the O6 star HD 206267. The spatial location of the younger stars (∼1 Myr) suggests the presence of a second, maybe triggered, population associated with the dust structures on the western part of the cluster. The disk fraction is higher toward the West, as it would be expected in a younger region. The high disk fraction throughout the cluster suggests little disk removal due to photoevaporation. Further study of the CTTS depletion in the innermost part of the cluster (inside a projected radius of ∼1 pc), would be required in the future to reveal if photoevaporation by the O6 star HD 206267 could be responsible for the lack of CTTS in this region (which is not statistically significant due to the low density of the cluster).

- Mass accretion rates were obtained for some of the accreting stars in Tr 37, using U band photometry (Gullbring et al., 1998), deriving average values of $\sim 2\times10^{-8} M_{\odot} yr^{-1}$, consistent with those observed in other regions (Taurus, Chameleon, Ophiuchus). A comparison of the accretion rate versus the individual ages of the accreting stars reveals consistency with viscous disk evolutionary models (Hartmann et al., 1998), despite the individual errors in accretion rate and age (which can be a factor of 2). Separating the stars from the potential second population associated to the globule, from the bulk stars in the cluster, evolution of accretion rate during the ∼3 Myr interval, consistent with the evolution of a viscous disk, can be observed.

- Using spectral types and the average extinction in the cluster, together with photometric data from the literature, the membership of high- and intermediate-mass stars (spectral types OBAF) in Tr 37 and NGC 7160 was revised. The V vs. B-V colors of the high- and intermediate-mass members of NGC 7160 on the Main Sequence are consistent with this cluster being at the same distance than Tr 37, 900 pc, as it was obtained by Contreras et al. (2002).

- Both Tr 37 and NGC 7160 were included in a Spitzer GTO program to study the evolution of protoplanetary disks. Both clusters were observed with the IRAC and MIPS instruments on Spitzer, covering a wavelength range from 3.6 to 24 μm, which allows to study the characteristics of protoplanetary disks at distances from 0.1 to ∼20 AU from the central star.

- For the low-mass members, there is a good correlation between the presence of accretion disks and the strength of the Hα emission line. The Spitzer observations confirm that about 40-45% of the stars in Tr 37 have disks, whereas only 2 disks are detected in NGC 7160, of which only 1 is accreting.

- We find a total of 4 "transition objects" in Tr 37, and 1 in NGC 7160, defined as objects presenting an outer disk (detectable at 5.8 and/or 8.0 and 24.0 μm) but no excess emission at shorter wavelengths, and no indications of accretion (no strong Hα nor U band excess), suggesting very low (under $5 \times 10^{-10} M_{\odot} yr^{-1}$) or zero accretion. These objects would be the intermediate stage between accreting CTTS and non-accreting, diskless WTTS. High-resolution spectra would be required to determine any velocity wings in the Hα emission line due to very slow accretion, since zero accretion would suggest the existence of planetary-sized bodies blocking accretion from the outer disk. Statistically, the presence of these objects suggests timescales of the order of times 10^5yr for the dissipation or coagulation of the outer disk, once the inner disk has been removed or coagulated forming planets.

- A few of the accreting stars show "gaps" in the inner disk, or a very reduced or zero emission at the shorter IR wavelengths, indicating further grain growth without disruption of the accretion processes. The study of the gas content of these disks, as well as observations at longer wavelengths, would be the next step to characterize them. These objects, together with the "transition disks", suggest that the evolution in the disk (via dust settling and/or grain growth) starts in the inner part, propagating outward.

- Examining the high- and intermediate-mass stars (spectral types BAF), some differences between the two clusters are observed. Combining IRAC and MIPS data, we find 7 disks in Tr 37 (plus 1 possible disk), and 3 in NGC 7160 (plus another additional possible disk), out of samples of 58 and 68 cluster members, respectively. One of the disks in Tr 37 is associated to the B3 and B5 stars in the multiple system CCDM+5734Ae/w. A total of 3 disks in Tr 37 are optically thick, showing emission at IRAC wavelengths, whereas none of the disks in NGC 7160 presents IRAC emission, being detectable only at the 24 μm MIPS wavelength. These are one of the few thin disks around BAF-type stars with well-determined ages. The differences in disks properties and frequencies suggest that these disks could be either the remaining of protoplanetary accretion disks or re-processed debris disks resulting from the collision of planetesimals. The luminosity of the disks is comparable to the debris disk HR 4796 (Jayawardhana et al., 1998) and, in any case, this would indicate that a important degree of disk evolution and planetesimals or planet formation has occurred by the ages of 4 and 10 Myr.

- Comparison of the SEDs of stars with disks in Tr 37 and NGC 7160 with these of younger regions (Taurus, Hartmann et al. 2005), we find a systematic decrease in the emission from the disk, starting in the inner disk (tenths to few AU) and propagating outward with time. In the case of Tr 37, the emission is substantially lower than in Taurus at the shorter wavelengths (JHK, 3.6, 4.5, 5.8, 8.0 μm) and becomes comparable to Taurus at the longer wavelengths (24.0 μm). For the two disks in NGC 7160, the emission is significantly lower than in Taurus and than in Tr 37 at all the wavelengths, being comparable to the emission of a flat disk. The growth of the dust grains could be responsible, together with the dust settling, of the decrease in emission. This supports the idea that important dust settling/grain growth in the inner disk has occurred by the ages of 4 Myr, that the evolution of the disk proceeds from the inner part of the disk out, and that dust settling/grain growth produces nearly complete flattening over the whole disk by the age of 10 Myr. Comparison with accretion disk models (D'Alessio et al. 2004, 2005) suggests that including the effects of grain growth and dust settling

is necessary to account for the observed IR colors and SEDs.

- The study of the well-known, younger stars in the Orion Nebula Cluster (ONC) reveals the power of high resolution spectra (Hectochelle/MMT) for the detection of accretion processes in a H II region. A proper distinction between CTTS and WTTS is required for studying the evolution of angular momentum and the presence of star-disk locking during the accretion phase. The study of the stars in the ONC suggest that rotational velocities of CTTS are significantly slower than those of WTTS, suggesting that the CTTS are locked to their disks.

- The use of high-resolution spectra of the Hα and Li 6707 Å regions has revealed as well 15 new members of the ONC.

- Due to the fact that disks can be cleared in their inside before the accretion stops, the high-velocity wings of the Hα emission line are more reliable than the detection of accretion via near-IR (JHKL) excess. In addition, high-resolution optical spectra in the Hα region could be used to detect any signs of slow accretion in the "transition objects".

This work also opens a window for further research in the future, in order to study:

- The nature of the "transition objects": Are they accreting? High-resolution spectroscopy could answer this question. Is there any gas in the gap? Observations of the H_2 lines could help to sort this out. Is there coagulated dust accumulated in bigger (cm) grains? How far does the disk extend, and how does it evolve with time at very large distances from the star? Sub-mm and radio observations could be used for these purposes.

- The evolution of angular momentum: How is the rotation of CTTS and WTTS at the ages of 4-10 Myr? High-resolution spectra would be required for a detailed study.

- The presence of photoevaporation and its efficiency in the inner regions of the cluster: Are disks in the near HD 206267 being photoevaporated? Imaging in forbidden lines could help to answer this question.

- Study of other cluster with similar ages, following the same procedures described here. This would provide, in addition to more observations and statistics for the transitional disks, targets for the existing and coming instruments. In particular, the study of clusters in the southern hemisphere would be very interesting, since the new-generation radio interferometers (like ALMA) will be in the south.

Moreover, the study of Tr 37 and NGC 7160 provides the first large sample of young stars with ages in the epoch during which most disks dissipate, and should be taken into account in the modeling of accretion disks in the future.

8 Sumario y Conclusiones

El principal objetivo de este trabajo es estudiar las propiedades de las estrellas jóvenes y de sus discos protoplanetarios durante las etapas más relevantes para la formación de planetas: entre 3 y 10 millones de años, cuando la mayoría de los discos desaparece, probablemente tras aglomerarse en sistemas planetarios. Este trabajo comprende el primer estudio detallado de un número suficiente de objetos para obtener conclusiones estadísticas sobre la frecuencia de los discos y sus características en cúmulos jóvenes de $\sim$4 y $\sim$10 millones de años. Gracias a las muestras numerosas y a las capacidades del Telescopio Espacial Spitzer, se ha podido encontrar la primera evidencia concreta de evolución diferenciada en la parte interna y externa del disco a la edad de 3-4 millones de años. Las edades isocronales de los dos cúmulos de Cep OB2, Tr 37 y NGC 7160, confirman las predicciones a partir del punto de inflexión de la Secuencia Principal, y de la expansión del gas en la región. También se ha encontrado que el efecto de la fotoevaporación al cabo de 4 millones de años juega un papel menos importante de lo que se creía en la disipación de los discos. Se han hallado algunas evidencias que sugieren formación estelar desencadenada por la expansión de la región H II de Tr 37, IC 1396. El estudio de las estrellas de masa alta e intermedia ha conducido a la identificación de algunos de los discos residuales de escombros más jóvenes que se conocen, reafirmando la idea de que la frecuencia de los discos alrededor de estas estrellas es mucho menor que la encontrada para las estrellas de baja masa. Finalmente, empleando espectros de alta resolución, se ha probado la eficiencia de los mismos en la identificación de estrellas jóvenes en zonas con fuerte emisión nebular, como el Cúmulo de la Nebulosa de Orión.

Además de la identificación y caracterización de estos objetos, este trabajo propone un método muy eficiente para el estudio de regiones similares, así como las herramientas necesarias para la resolución de los interrogantes que aún quedan abiertos. Los principales logros de este estudio se pueden resumir como sigue:

- El estudio en el óptico de los dos cúmulos de la Asociación Cep OB2 (Tr 37 y NGC 7160), situada a 900 pc de distancia, ha conducido a la primera identificación de muestras numerosas de estrellas de baja masa con edades medias de 4 y 10 millones de años (de acuerdo con las isocronas de Siess et al. 2000), respectivamente, que permiten obtener resultados con significado estadístico. La combinación de fotometría y espectroscopía óptica ha permitido encontrar 165 miembros de baja masa en Tr 37, y 55 más en NGC 7160. Las edades estimadas concuerdan con las edades dinámicas y cinemáticas de la región (Patel et al., 1998), y sitúan a ambos cúmulos en la etapa más interesante para la formación de planetas (Strom et al., 1993). El uso del espectrógrafo multifibra Hectospec, combinado con otros espectrógrafos como Hydra y FAST, ha permitido cubrir la mayoría de las regiones centrales de los cúmulos, con un 95% de los candidatos de Tr 37 observados, y sobre el 75% en el caso de NGC 7160. Las identificaciones de nuevos miembros de baja masa se basan en la presencia de la línea de Li 6707 Å en absorción, y de la emisión en Hα. También se han obtenido tipos espectrales y

extinciones individuales para todos los miembros. La extinción promedio en los cúmulos es de $A_V = 1.56 \pm 0.55$ para Tr37, y $A_V = 1.17 \pm 0.45$ para NGC7160.

- La detección de los procesos de acrecimiento se ha llevado a cabo usando la emisión en Hα. El resultado del examen de los miembros de Tr 37 revela que un 40-45% de ellos está acretando activamente, mientras que sólo 1 de las 55 estrellas de baja masa en NGC 7160 presenta fuerte emisión en Hα, característica de los procesos de acrecimiento. Esta importante diferencia sugiere que hay un gran porcentaje de discos que desaparecen durante la etapa de 4 a 10 millones de años. Dado que ambos cúmulos están en la misma región y a la misma distancia aproximada, el resultado de la comparación es válido incluso si las edades presentaran algunos errores. También se puede observar la evolución comparando estos sistemas con regiones más jóvenes, como Tauro o el ONC. Las fracciones de discos pasan de ser un 60-80% a la edad de 1 millón de años, a ser del 40% a los 4 millones de años y sólo unas pocas estrellas de cada cien conservan sus discos tras 10 millones de años.

- La distribución espacial de los miembros de baja masa en Tr 37 sugiere una cierta asimetría en la localización de las CTTS comparadas con las WTTS, incluyendo el hecho de que las estrellas más jóvenes aparecen concentradas en las proximidades del glóbulo de gas y polvo al oeste de HD206267. El hecho de que las estrellas con edades inferiores a 1 millón de años están localizadas al oeste, sugiere que forman parte de una segunda población, posiblemente desencadenada por la influencia de la primera. La fracción de estrellas con discos es ligeramente más alta en el oeste del cúmulo, como cabría esperar en una región más joven. Dado el número de estrellas con discos, el efecto global de la fotoevaporación por parte de la estrella O6 HD 206267 no parece haber afectado a la mayoría de los discos. El estudio del defecto de discos en la parte más interna del cúmulo, en torno a 1 pc de la estrella O6, revela que la carencia de CTTS en esta región podría deberse a la fotoevaporación, aunque harían falta otras observaciones para probar esta hipótesis, puesto que el número de estrellas en la región central no tiene significado estadístico, debido a la baja densidad del cúmulo.

- Para algunas de las CTTS, se obtuvieron tasas de acrecimiento basadas en la fotometría en la banda U (Gullbring et al., 1998). Estas tasas son de $\sim 2 \times 10^{-8} M_{\odot} yr^{-1}$ en promedio, comparables a las observadas en otras regiones (Tauro, Serpentario, Camaleón). La evolución de la tasa de acrecimiento con la edad individual de las estrellas es consistente con una disminución del acrecimiento conforme aumenta la edad, consistente con los modelos de evolución viscosa del disco (Hartmann et al., 1998). Incluso si se tienen en cuenta los errores en la edad y en las tasas de acrecimiento (que pueden variar hasta un factor 2), la comparación de las estrellas más jóvenes (asociadas con el glóbulo y el resto del cúmulo muestra una concordancia con las predicciones para la evolución de un disco viscoso, revelando una evolución significativa durante este periodo de $\sim$3 millones de años.

- Los miembros de masa alta e intermedia (tipos BAF) de ambos cúmulos, estudiadas previamente en la literatura (Marschall & van Altena, 1987; Kun et al., 1987; De Graeve, 1983; Contreras et al., 2002), se han revisado, calculando sus tipos espectrales y extinciones, y comparando con la distribución de extinciones de las estrellas de baja masa. Los colores en el diagrama V vs. B-V de las estrellas en la secuencia principal de NGC

7160 confirman que este cúmulo se encuentra a la misma distancia de 900 pc que Tr 37 (Contreras et al., 2002).

- Tanto Tr 37 como NGC 7160 están incluidos en un proyecto con tiempo de observación garantizado (GTO) con Spitzer, destinado al estudio de la evolución de los discos protoplanetarios. Ambos cúmulos han sido observados con los instrumentos IRAC y MIPS a bordo del Spitzer, cubriéndose un rango de longitudes de onda entre 3.6 y 24 μm, lo cual permite trazar los discos y sus características a distancias entre 0.1 y 20 unidades astronómicas de la estrella central.

- En el caso de los miembros de baja masa, la correlación entre acrecimiento (derivado de Hα) y la presencia de un disco en el IR es muy buena. Spitzer confirma que el 40-45% de las estrellas en Tr 37 poseen discos de acrecimiento, mietras que sólo se detectan 2 discos entre las 55 estrellas de NGC 7160.

- Además de los objetos acretando, encontramos 4 WTTS con discos en Tr 37, y uno de los objetos con disco en NGC 7160 tampoco está acretando, o lo hace con una tasa muy baja. Éstos son los llamados "objetos de transición", no presentan emisión a longitudes de onda inferiores a 5.8 μm, y no tienen exceso en la banda U ni fuerte emisión en Hα, lo cual sugiere que no esán acretando, o lo hacen a tasas inferiores a $5 \times 10^{-10} M_{\odot} yr^{-1}$. Los "objetos de transición" se corresponderían con un estado intermedio entre CTTS acretando y WTTS sin disco. Sería interesante obtener espectros de alta resolución en la región de Hα para estos objetos, puesto que ello podría revelar si existe algún ensanchamiento de la línea por altas velocidades y, en definitiva, por acrecimiento. Si los "objetos de transición no estuvieran acretando, pese a tener un disco externo opticamente grueso, sería muy posible que se hayan formado cuerpos de tamaño planetario en la parte interna del disco, ya que se requieren objetos de grandes dimensiones para frenar el flujo de material del disco externo al disco interno, y del disco interno a la estrella. Estadísticamente, la escasez de "objetos de transición sugiere que sus tiempos de vida son del orden de algunos cientos de miles de años, lo que implica que el disco externo se disiparía rápidamente, una vez que el interior del disco se ha asentado o coagulado en forma de planetas.

- Unas pocas de las estrellas con acrecimiento activo muestran huecos en la parte interna del disco, caracterizados por un exceso de emisión nulo o muy pequeño en las longitudes de onda más cortas del IR. Esto indicaría que los procesos de coagulación o asentamiento del polvo pueden ser compatibles con el acrecimiento. Sería conveniente estudiar el contenido de gas de estos objetos, así como realizar observaciones en longitudes de onda más largas, para determinar la extensión de los discos. La presencia de huecos, junto con la existencia de los "objetos de transición, sugiere que la evolución de los discos (crecimiento y asentamiento del polvo) comienza en la parte más interna, propagándose hacia el exterior.

- El examen de las estrellas de tipos espectrales BAF en Tr 37 y en NGC 7160 revela diferencias entre los dos cúmulos, también en este rango de masas. Combinando IRAC y MIPS, se encuentran 7 discos en Tr 37 (más otro disco candidato), y 3 en NGC 7160 (más otro posible), de entre 58 y 68 estrellas, respectivamente. Uno de los discos en Tr 37 está asociado con las estrellas B3 y B5 del sistema múltiple CCDM+5734Ae/w. Tres de los discos en Tr 37 son ópticamente gruesos, y presentan emisión a las longitudes de

onda de IRAC, y el resto (incluyendo los de NGC 7160) sólo son detectables a 24 μm con MIPS. Las diferencias entre ambos cúmulos sugieren que los discos detectados podrían ser o bien los restos de discos protoplanetarios, o bien discos de polvo reprocesado o residuales (*debris disks*), producidos mediante las colisiones de planetesimales. La luminosidad de estos discos tenues es comparable a la del disco residual en torno a HR 4796 (Jayawardhana et al., 1998) y, en cualquier caso, ambas hipótesis indican que la formación de planetas y/o de planetesimales ha ocurrido de manera apreciable al cabo de 4 o 10 millones de años.

- Comparando las distribuciones espectrales de energía (SEDs) de las estrellas con discos en Tr 37 y NGC 7160 con las obtenidas en regiones más jóvenes (como Tauro, ver Hartmann et al. 2005), se encuentra un decremento sistemático en la emisión del disco, afectando principalmente a la parte más interna (décimas de UA, o unas pocas UA), y propagándose hacia afuera con el tiempo. En el caso de Tr 37, la emisión es substancialmente menor que en Tauro para longitudes de onda JHK, 3.6-8.0 μm, y es comparable a Tauro a 24 μm. En los dos discos de NGC 7160, la emisión decrece para todas las longitudes de onda, siendo comparable a la de un disco plano. Tanto el crecimiento de los granos, como el asentamiento de los mismos en el plano medio, podrían ser responsables de este fenómeno. Las observaciones están de acuerdo con la idea de que, a los 4 millones de años, ya ha ocurrido un grado importante de evolución en el disco, y esta evolución comienza en la parte más interna, y se propaga hacia afuera, de modo que los discos son prácticamente planos a la edad de 10 millones de años. La comparación con los modelos de los discos de acrecimiento (D'Alessio et al. 2004, 2005) sugiere que es necesario incluir los efectos de crecimiento de los granos y asentamiento (probablemente diferencial, es decir, dependiente de la distancia a la estrella) del polvo si se quieren reproducir las SEDs y colores observados.

- El estudio de las estrellas de la bien conocida región del Cúmulo de la Nebulosa de Orión (ONC) revela la idoneidad de los espectros de alta resolución (Hectochelle/MMT) para determinar si un objeto está acretando. Es necesario distinguir con claridad entre CTTS y WTTS si se pretenden examinar puntos como la evolución del momento angular en CTTS y WTTS, y el frenado de la rotación estelar por la conexión con el disco durante la fase de acrecimiento (*disk locking*). El estudio de las estrellas en el ONC revela que las CTTS tienden a rotar más lentamente que las WTTS, como sería de esperar si los discos frenan la rotación de la estrella.

- Usando espectros de alta resolución en las regiones de Hα y Li 6707 Å, se han podido identificar asimismo 15 nuevos miembros del ONC.

- Debido a que los discos pueden ser evacuados o aglomerados en su interior antes de que el acrecimiento cese, las alas de ensanchamiento por velocidad de la línea de Hα son indicadores de acrecimiento más efectivos que la presencia de excesos en el infrarrojo cercano (JHKL). De ahí que se proponga el uso de espectros de alta resolución para determinar si los "objetos de transición" están o no acretando.

El presente trabajo también ofrece nuevas perspectivas de estudio para el futuro, en particular:

- Investigar la naturaleza de los "objetos de transición": ¿Están acretando? Espectros de alta resolución podrían dar la respuesta. ¿Existe gas en el hueco? Observaciones de las líneas de H_2 podrían emplearse para averiguarlo. ¿Hay polvo acumulado y coagulado en gránulos de mayor tamaño (cm)? ¿Cual es la extensión del disco, y cómo evoluciona a mayores distancias de la estrella? Observaciones en el submilimétrico y radio podrían emplearse para este estudio.

- Estudiar la evolución del momento angular: ¿Cómo son las diferencias en rotación de las CTTS y WTTS de 4 y 10 millones de años de edad? Podría averiguarse mediante espectros de alta resolución.

- Estudiar la presencia y eficiencia de la fotoevaporación en las regiones internas del cúmulo: ¿Se están fotoevaporando los discos más cercanos a HD 206267? Observaciones en líneas prohibidas podrían contribuir a la respuesta.

- Observar y estudiar otros cúmulos de edades similares, siguiendo los procedimientos aquií descritos. Esto produciría, aparte de más objetos para la estadística de los discos, importantes muestras para ser estudiadas con los instrumentos que estarán disponibles en el futuro. En particular, la investigación de cúmulos en el hemisferio sur sería muy interesante, puesto que la mayoría de los interferómetros de nueva generación (como ALMA) estarán en el hemisferio sur.

Aparte de los puntos mencionados, el estudio de Tr 37 y NGC 7160 proporciona la primera muestra numerosa de estrellas jóvenes con edades comprendidas en la etapa durante la cual la mayoría de los discos se disipan, con lo cual estos resultados se deberían tener en cuenta en el futuro modelado de discos de acrecimiento.

9 Glossary

In order to clarify the meaning of several words and acronyms which are widely used in this text, and that may have a different meaning in other fields or situations, a list of the most important ones is presented here. The aim of this list is not to be complete, but to contribute to a better understanding of the terms used in this work and their implications.

Accretion Disk: The circumstellar protoplanetary disks, formed because of the conservation of angular momentum, during the collapse of a molecular cloud core that gives birth to a star. These disks are suffering magnetospheric accretion during the first stage of their life, as the magnetic field of the star disrupts the gaseous disk at a few stellar radii, channelizing the gas that falls onto the star.

BCD: Basic Calibrated Data. The Spitzer photometric data from IRAC and MIPS is provided from the standard pipeline with a basic reduction and calibration. The different coadds for a mosaic are provided separately, together with the corresponding "masks" to cover the bad pixels and other defects in the images. The coadds can be arranged in a mosaic using post-BCD tools like MOPEX or IDL Mosaickers.

Cep OB2 Association: OB Association, in the shape of a giant gas bubble of diameter $\sim$3 degrees (100 pc), and located at 900 pc distance. The bubble was originated by the stellar winds of the massive stars in the cluster NGC 7160 (located approximately in its center), and contains the cluster Tr 37 at its rim, and several dust and gas globules and embedded IRAS sources.

Class I Object: Protostar with infalling envelope.

Class II Object: CTTS or Classical T Tauri Star.

Class III Object: WTTS or Weak T Tauri Star.

CTTS: Classical T Tauri Star, or pre-main sequence stars with accretion disks.

Debris Disk: A circumstellar disk, optically thin, non-accreting, and evacuated in its inner part, formed from reprocessed material produced in the collision of planetesimals around a star.

EW: Equivalent width of a spectral line, measured as the ratio of the flux in the line to the normalized continuum. By agreement, EW values are positive when the line is in absorption, and negative for lines in emission, although in this work all the values are referred to as positive, indicating whether it is in absorption or emission.

FLWO: Fred Lawrence Whipple Observatory, located in Mount Hopkins, AZ. The 1.2m telescope used for the optical photometry, and the 1.5m telescope used for the spectroscopy with FAST, are located in FLWO.

GTO: Guaranteed Time Observing. A total of 15% of the Spitzer time was assigned to a certain number of projects directed by the groups which developed the different Spitzer instruments. The Spitzer data presented in this work belongs to the IRAC GTO program to study the evolution of protoplanetary disks. The P.I. of this program is Giovanni Fazio.

Hα: First line of the Balmer Series of the Hydrogen. It is produced in both the accretion columns and the chromosphere of the stars,and it is also one if the lines characteristic of H II regions. The emission in Hα from low-mass accreting stars is characterized for its large velocity wings (up to 200 km/s) and strong equivalent width (depending on the spectral type, but in general, larger than 10Å in emission). The chromospheric Hα emission is much weaker and does not present high velocity wings. The nebular emission from H II regions is usually very inhomogeneous and may present important velocity shifts due to the dynamics of the gas.

H II Region: Zone of ionized atomic hydrogen, created by the ionizing radiation of massive stars, inhomogeneous and in expansion.

High- and Intermediate-Mass Stars: We labeled this way the stars of spectral types OBAF. In case of Tr 37 and NGC 7160, this class comprises stars with masses from $\sim$10 to $\sim$1.5 $M_{\odot}$.

IRAC: Infra-Red Array Camera, on board of the Spitzer Space Telescope (Fazio et al., 2004). It possesses 4 different channels, allowing observations at 3.6, 4.5, 5.8 and 8.0 μm. The filters for each channel are wide, covering the spectral region from $\sim$2 to 10 μm continuously.

IRAF: Image Reduction and Analysis Facility. It is a general purpose software system for the reduction and analysis of astronomical data. IRAF is written and supported by the IRAF programming group at the National Optical Astronomy Observatories (NOAO) in Tucson, Arizona. In this work, IRAF was used for the reduction, calibration and identification of sources for the optical photometry and spectroscopy.

Li 6707Å: Absorption line produced by the Li I, which is found in the spectra of young low-mass stars of spectral types KM. It is used as an indicator of youth since Li is depleted in fully convective stars in timescales of less than $\sim$30 Myr (Randich et al., 2001; Hartmann, 2003). EW of Li I are usually $\sim$0.3-0.8Å and decrease with time.

Low-Mass Stars: In this work, we regarded as low-mass stars those stars with spectral types GKM, or masses from $\sim$1.5 to $\sim$0.3 $M_{\odot}$.

MIPS: Multi-Band Imaging Photometer for Spitzer (Rieke et al., 2004). It provides the Spitzer Space Telescope with capabilities for imaging and photometry in broad spectral bands centered nominally at 24, 70, and 160 microns, and for low-resolution spectroscopy between 55 and 95 microns.

MMT: 6.5 m Multiple Mirror Telescope and its Observatory, located in Mount Hopkins, AZ. The spectrographs Hectospec and Hectochelle operate on the MMT.

MOPEX: Post-BCD tool for the Spitzer data, containing routines for flat fielding correction, background matching, mosaicking, and source extraction, among others.

NGC 7160: Central cluster in the Cep OB2 OB Association. It is aged $\sim$10 Myr and contains multiple B stars and hundreds of low-mass stars. The winds of its massive stars (and maybe a supernova, occurred some Myr ago) have triggered the expansion of the Cep OB2 Bubble.

PhotVis: IDL routine developed by R. Gutermuth for the source detection, source extraction, and aperture photometry on the Spitzer mosaics.

ONC: Orion Nebula Cluster, very dense OB association aged $\sim$1 Myr.

SED: Spectral Energy Distribution. It is depicted as the λF_λ flux of the star versus the wavelength λ. Comparison with the photospheric emission of a star of a similar spectral type can reveal the presence and characteristics of the circumstellar disk.

Transition Object: We call transition objects the non-accreting stars presenting a circumstellar disk, which would be an intermediate stage between accreting CTTS and diskless WTTS. Typically, the disks of the "transition objects" present no emission at wavelengths shorter than $\sim$4.5 μm, suggesting that the gas in the inner AUs of the disk has been evacuated or/and accreted, and the dust is agglomerated into larger bodies. Since we find no accretion or extremely low accretion rates, it is possible that the bodies in the inner AU have planetary sizes. Only a few percent ($\sim$5%) of the objects in a $\sim$4 Myr age cluster are "transition objects", indicating that they have a very short life (of the order of several 10^5 years), and suggesting that the outer disk does not survive long once that the inner disk has been evacuated and/or agglomerated into planets.

WTTS: Weak T Tauri Star. These are pre-main sequence, low-mass stars, with no accretion disks. They are characterized for their weak Hα chromospheric emission.

Bibliography

Ábrahám, P, Balázs, L.G. & Kun, M. , 2000, A&A, 354,645

Allen, L., Strom, K., 1995, AJ, 109,1379

Allen, C.W. : Astrophysical Quantities. Springer Verlag, 2000.

Attridge, J., & Herbst, W., 1992, ApJ, 398, L61

Backman, D.E., & Paresce, F., 1993, Protostars and Planets III, ed. E.H. Levy and J.I Lunine, Tucson, University of Arizona Press, 1253

Balázs, L. & Kun, M., Astron. Nachr. 310, 385, 1989

Bally, J., Sutherland, R., Devine, D. & Johnstone, D., 1998, AJ, 116, 293

Bally, J., O'Dell, C.R. & McCaughrean, M., 2000, AJ, 119, 2919

Barden, S. & Armandroff, T., 1995: Hydra/WIYN users manual.

Bertout, C., Basri, G., & Bouvier, J., 1988, ApJ, 330, 350

Bessell, M.S. & Brett, J.M., 1988, PASP, 100, 113

Bevington, P.R. : Data Reduction and Error Analysis for the Physical Sciences. McGraw Hill, 1969.

Briceño, C., Hartmann, L, Stauffer, J., Gagné, M., Stern, R., & Caillault, J-P., 1997, AJ, 113, 2

Briceño, C., Hartmann, L, Stauffer, J., & Martín, E., 1998, AJ, 115, 2074

Briceño, C. and 10 coauthors, 2001, Science, 291, 93

Briceño, C., Calvet, N., Hernández, J., Vivas, A. K., Hartmann, L., Downes, J.J. & Berlind, P., 2005, AJ in press

Bonnell, I. A., Smith, K. W., Meyer, M. R., Tout, C. A., Folha, D. F. M., & Emerson, J. P. 1998, MNRAS, 299, 1013

Boss, A.P., 2003, ApJ, 599,577

Bouvier, J., Forestini, M., & Allain, S., 1997, A&A, 326, 1023

Buscombe, W. 2001, VizieR Online Data Catalog, III/222.

Caldwell, N. & Falco, E., 1993, Electronic 4Shooter/1.2m Manual

Calvet, N. & Hartmann, L. W. 1992, ApJ, 386, 239

Calvet, N. & Gullbring, E., 1998, ApJ, 509,802

Calvet, N., D'Alessio, P., Hartmann, L., Wilner, D., Walsh, A. & Sitko, M., 2002, ApJ, 568, 1008

Calvet, N., Briceño, C., Hernández, J., Hoyer, S., Hartmann, L., Sicilia-Aguilar, A., Megeath, S.T., D'Alessio, P., 2005, AJ139, 935

Cardelli,J.A., Clayton, G. C., Mathis, J.S. 1989, ApJ, 345, 245

Choi, P.I., & Herbst, W., 1996, AJ, 111, 283

Clayton, G.C. & Fitzpatrick, E. 1987, AJ, 92, 157

Codella, C., Bachiller, R., Nisiri, B., Saraceno, B. & Testi, L., 2001, A&A, 376, 271

Cohen, M. & Kuhi, L.V., 1979, ApJS, 41, 743

Contreras, M.E., Sicilia-Aguilar, A., Muzerolle, J., Calvet, N., Berlind, P., Hartmann, L. 2002, AJ, 124, 1585

Cutri R.M., Skrutskie, M.F., van Dyk, S. & 25 more coauthors, 2003yCat.2246, 0C, VizieR On-line Data Catalog: II/246

Daflon, S., Cunha, K., Becker, S.R., 1999, ApJ, 522, 950

D'Alessio, P., Merín, B., Calvet, N., Hartmann, L., & Montesinos, B., 2005, Rev. Mex. A. A., 41, 1

De Graeve, E., 1983, Vatican Obs. Publ., 2, 31

Duncan, D.K., 1993, ApJ, 406, 172

Dunkin, S.K., Barlow, M.J., & Ryan, S.G., 1997, MNRAS, 290,165

Dutrey, A., Guilloteau, S., & Simon, M., 2003, A&A, 402, 1003

Duvert, D., Cenicharo, J., Bachiller, R., Gómez-González, J., 1990, A&A, 233, 190

Duvert, G., Guilloteau, S., Ménard, F., Simon, M., Dutrey, A., 2000, A&A, 355, 165

Edwards, S., Strom, S., Hartigan, P., Strom, K., Hillenbrand, L., Herbst, W., Attreidge, J., Merril, K.M., Probst, R., & Gatley, I., 1993, AJ, 106, 372

Edwards, S., Hartigan, P., Ghandour, L. & Andrulis, C. 1994, AJ, 108, 3

Fabricant, D., 1994: FAST Manual.

Fabricant, D., Hertz, E., & Szentgyorgyi, A., 1994, SPIE, 2198, 251

Fabricant, D., Cheimets, P., Caldwell, N. & Geary, J., 1998, PASP, 110, 79

Fazio, G.G., Hora, J.L., Allen, L.E., & 62 more coauthors, 2004, ApJS, 154, 10

Forrest, W.J., Sargent, B., Furlan, E., & 18 more coauthors, 2004, ApJS, 154, 443

García, B. 1989, Bulletin d'Information du Centre de Donnees Stellaires,36, 27

Garrison, R.F. & Kormendy, J. 1976, PASP ,88,865

Goldreich, P. & Ward, W.R., 1973, ApJ183, 1051

Gray, R. O., Napier, M. G., & Winkler, L. I. 2001, AJ, 121, 2148

Gullbring, E., Hartmann, L., Briceño, C., Calvet, N., 1998, ApJ 492, 323

Gutermuth, R., Megeath, S.T., Muzerolle, J., Allen, L.E., Pipher, J., Myers, P., & Fazio, G., 2004, ApJS, 154,374

Haisch, K., Lada, E., & Lada, C., 2001, ApJ, 553,153

Hartigan, P., Raymond, J., & Hartmann, L. 1987, ApJ, 316, 323

Hartigan, P., Kenyon, S. J., Hartmann, L., Strom, S. E., Edwards, S., Welty, A. D., & Stauffer, J. 1991, ApJ, 382, 617

Hartmann, L., Hewett, R., Stahler, S., & Mathieu, R.D., 1986, ApJ, 309, 275

Hartmann, L., Hewett, R., & Calvet, N. 1994, ApJ, 426, 669

Hartmann, L.: Accretion Processes in Star Formation, Cambridge University Press, 1998.

Hartmann, L., Calvet, N., Gullbring, E. & D'Alessio, P, 1998, ApJ, 495, 385

Hartmann, L., 2001, AJ, 121, 1030

Hartmann, L., 2002, ApJ, 566, L29

Hartmann, L., 2003, ApJ, 585, 398

Hartmann, L., Megeath, S.T., Allen, L., Luhman, K., Calvet, N., D'Alessio, P., Franco-Hernández, R., Fazio, G., 2005, in press

Henney, W., & O'Dell, C.R., 1999, AJ, 118, 2350

Herbig, G.H. & Bell, K.R., 1988, Lick Observatory Bulletin, Santa Cruz

Herbst, W., Herbst, D., Grossman, E., & Weinstein, 1994, AJ, 108, 1906

Herbst, W., Rhode, K. L., Hillenbrand, L. A., & Curran, G. 2000, AJ, 119, 261

Herbst, W., Bailer-Jones, C. A. L., Mundt, R., Meisenheimer, K., & Wackermann, R. 2002, A&A, 396, 513

Hernández, J., Calvet, N., Briceño, C., Hartmann, L., & Berlind, P. 2004, AJ,127, 1682

Hernández, J., Calvet, N.,Hartmann, L., Briceño, C., Sicilia-Aguilar, A., & Berlind, P., 2005, AJin press

Hillenbrand, L. A. 1995, Ph.D. Thesis, Univ. Massachusetts

Hillenbrand, L.A., 1997, AJ, 113, 5

Hillenbrand, L.A., Strom, S., Calvet, N., Merrill, K.M., Gatley, I., Makidon, R., Meyer, M., Skrutskie, M., 1998, AJ, 116, 1816

Hueso, R., & Guillot, T., 2005 in preparation

Jaschek, M. 1978, Bulletin d'Information du Centre de Donnees Stellaires,15, 121

Jayawardhana, R., Fisher, S., Hartmann, L., Telesco, C., Piña, R., & Fazio, G., 1998, ApJ, 503, L79

Johnstone, D., Hollenbach, D. & Bally, J., 1998, ApJ, 499, 758

Jones, B.F., & Walker, M.F., 1988, AJ, 95,6

Keenan, P. C. & Barnbaum, C. 1999, ApJ, 518, 859

Kenyon, S.J. & Hartmann, L., 1995, ApJS , 101, 117

Kenyon, S.J., Yi, I. & Hartmann, L., 1996, ApJ, 462,439

Kirkpatrick, J.D., Henry, T.J.& McCarthy, D.W., 1991, ApJS,77,417

Kirkpatrick, J.D., McCarthy, D.W., 1994, AJ, 107, 333

Königl, A., 1991, ApJ, 370, L39

Kroupa, P., Tout, C.A., & Gilmore, G., 1990, MNRAS, 244, 76

Kun, M., Baláz, L.G. & Tóth, I., 1987 ApJS, 134,211

Lada, C.J., Muench, A.A., Haisch, K.E., Lada, E.A., Alves, J.F., Tollestrup, E.V. & Willner, S.P., 2000, AJ, 120, 3162

Landolt, A.U., 1992, AJ, 104, 1

Littlefair, S.P., Naylor, T., Harries, T., Retter, A., & O'Toole, S., 2004, MNRAS, 347, 937

Littlefair, S.P., Naylor, T., Jeffries, R.D., Devey, C.R., & Vine, S., 2003, MNRAS, 345, 1205

Luhman, K., Rieke, G., Young, E., Cotera, A., Chen, H., Rieke, M., Schneider, G., Thompson, R., 2000, ApJ, 540, 1016

Lynden-Bell, D. & Pringle, J., 1974, MNRAS, 168, 603

Mandel, G., & Herbst, W., 1991, ApJ, 383, L75

Marschall, L.A. & van Altena, W.F., 1987, AJ, 94,71

McCaughrean, M. & Stauffer, J.,AJ, 108, 4

Meyer, M., Calvet, N., Hillenbrand, L.A., 1997, AJ, 114, 288

Muench, A., Alves, J., Lada, C., & Lada, E., 2001, ApJ, 558, L51

Muzerolle, J., Calvet, N. & Hartmann, L. (Paper A), 1998, ApJ, 455, 468

Muzerolle, J., Calvet, N. & Hartmann, L., 1998, ApJ, 492, 743

Muzerolle, J., Calvet, N., Briceño, C., Hartmann, L. & Hillenbrand, L., 2000, ApJ, 535, L47

Muzerolle, J., Calvet, N. & Hartmann, L., 2001, ApJ, 550, 944

Muzerolle, J., Calvet, N., Hartmann, L., D'Alessio, P., Paper A, 2003, ApJ, 597, L149

Muzerolle, J., Hillenbrand, L., Calvet, N., Briceño, C., Hartmann, L., Paper B, 2003, ApJ, 592,266, Paper B

Muzerolle, J., Megeath, T.S., Gutermuth, R.A., and 15 more coauthors, 2004, ApJ, 154, 379

Natta, A., Prusti, T., Neri, R., Wooden, D., Grinin, V.P., & Mannings, V., 2001, A&A, 371,186

Patel, N.A., Heyer, M.H., Goldsmith, P.F., Snell, R.L., Hezel, T. & Pratap, P., 1998 ASP Conferences Series

Patel, N.A. , Goldsmith, P.F., Snell, R.L., Hezel, T. & Xie, T., 1995, ApJ , 447, 721

Patel, N.A., Goldsmith, P.F., Heyer, M.H. & Snell, R.L., 1998, ApJ , 507, 241

Perryman, M.A.C., Lindegren, L., Kovalevsky, J., & 16 more coauthors, 1997, A&A, 323,49

Platais, I, Kozhurina-Platais, V., van Leeuwen, F., 1998, AJ, 116, 2423

Podosek, F.A. & Cassen, P., 1994, Meteoritics 29, 6-25

Pollack, J., Hubickyj, O., Bodenheimer, P., Lissauer, J., Podolak, M. & Greenzweig, Y., 1996, Icarus 124,62

Przygodda, f., van Boekel, R., Ábrahám, P., Melikov, S., Waters, L., Leinert, C., A&A, 2003, 412, L43

O'Dell, C.R., & Wen, Z., 1994, ApJ, 436, 194

O'Dell, C.R., & Wong, S.K., 1996, AJ, 111, 2

Randich, S. Pallavicini, R., Meola, C.,. Stauffer, J.R., & Balachandran, S.C., 2001, A&A, 372, 862

Reach, W., Rho, J., Young, E., and 15 more coauthors, 2004, ApJS, 154, 385

Rhode, K., Herbst, W. & Mathieu, R., 2001, AJ, 122, 3258

Rieke, G., Young, E., Engelbracht, C., & 40 more coauthors, 2004, ApJS, 154, 25

Robberto, M., Song, J., Mora Carrillo, G., Beckwith, S.V.W., Makidon, R.B., & Panagia, N. 2004, ApJ, 606, 952

Scally, A. & Clarke, C. 2001, MNRAS325, 449

Schwartz, R.D., Gyulbudhagian, A.L. & Wilking, B.A., 1991, ApJ, 370, 263

Shu, F., Adams, F. & Lizano, S., 1987, ARAA, 25,23

Shu, F., Najita, J., Ostriker, E., Wilkin, F., Rudan, S. & Lizano, S., 1994, ApJ, 429, 781

Sicilia-Aguilar, A., Hartmann, L., Briceño, C., Muzerolle, J., & Calvet, N., 2004, AJ128, 805

Sicilia-Aguilar, A., Hartmann, L., Szentgyorgyi, A., Roll, J., Conroy, M., Calvet, N., Fabricant, D., & Hernández, J., Paper A, 2005, AJ, 129, 363 , Paper A

Sicilia-Aguilar, A., Hartmann, L., Hernández, J., Briceño, C., Calvet, N., 2005, AJin press, paper B

Simonson, S.C. & van Someren Greve, H.V.,1976, A&A, 46, 261

Siess, L., Dufour, E. & Forestini, M. 2000 A&A , 358, 593

Stassun, K. G., Mathieu, R. D., Mazeh, T., & Vrba, F. J. 1999, AJ, 117, 2941

Stauffer, J.R., Hartmann, L.W., & Barrado y Navascués, D., 1995, ApJ, 454, 910

Störzer, H., & Hollenbach, D., 1999, ApJ, 515, 669

Strand, K. Aa., 1958, AJ, 63, 1525

Strom, K., Wilkin, F., Strom, S., & Seaman, R., 1989, AJ, 98, 1444

Strom, S.E., Edwards, S. & Skrutskie, M., 1993, Protostars and Planets III, 837

Strom, S.E., 1994, Eight Cambridge Workshop, ASP Conference Series, Vol.64,

Szentgyorgyi, A. H., Cheimets, P., Eng, R., Fabricant, D. G., Geary, J. C., Hartmann, L., Pieri, M. R., & Roll, J. B., 1998, Proc. SPIE, 3355, 242

Tonry, J. & Davis, M., 1979, AJ, 84, 10

Uchida, K.I., Calvet, N., Hartmann, L., Kemper, F., & 16 more coauthors, 2004, ApJ, 154, 439

Van Altena, W.F., Lee, T.J., Lee, J.F., Lu, P.K., & Upgren, A.R., 1988, AJ95,6

Walker, M.F., ApJ, 155, 447

White, R., & Basri, G., 2003, ApJ, 582, 1109

Weidenschilling, S.J., 1977, MNRAS, 180, 57

Weidenschilling, S.J., & Cuzzi, J.N., 1993, Protostars and Planets III, 1031

Weidenschilling, S.J., 1997, Lunar and Planetary Science, 28, 1517

Weidenschilling, S.J., & Davis, R., 2001, Lunar and Planetary Science, 32, 1894

Wyatt, M.C., & Dent, W.R.F., 2002, MNRAS, 334, 589